TOPICAL CLEAR AQUEOUS NANOMICELLAR FORMULATIONS FOR ANTERIOR AND POSTERIOR OCULAR DRUG DELIVERY

A DISSERTATION IN
Pharmaceutical Sciences
and
Chemistry

Presented to the Faculty of the University
of Missouri - Kansas City in partial fulfillment of
requirements for the degree

DOCTOR OF PHILOSOPHY

by
KISHORE CHOLKAR

Master's in Chemistry
Western Illinois University, IL, USA 2008

Kansas City, Missouri
2015

TOPICAL CLEAR AQUEOUS NANOMICELLAR FORMULATIONS FOR ANTERIOR AND POSTERIOR OCULAR DRUG DELIVERY

Kishore Cholkar, Candidate for the Doctor of Philosophy Degree

University of Missouri – Kansas City, 2015

ABSTRACT

The objective of this study was to develop a clear, aqueous drug loaded nanomicellar formulation (NMF) for the back-of-the-eye delivery. Hydrophobic drugs such as cyclosporine, resolvin analog (RX-10045), dexamethasone, rapamycin were entrapped in the core of polymeric micelles and solubilized. Polymeric amphiphilic molecules (e.g., hydrogenated castor oil – 40 (HCO-40) and Vit. E TPGS) are known to generate nanomicellar constructs with hydrophobic core and hydrophilic corona. However, constructs prepared from a single polymer are unstable and easily fall apart at high temperature. Inclusion of a second polymer such as Oc-40 improves stability and prevents nanomicellar destabilization. Such stable nanomicellar constructs can encapsulate hydrophobic drugs in their lipophilic core while the hydrophilic corona helps solubility in aqueous solution. We screened resolvin for efflux pumps and prepared resolvin analog nanomicelles. Studies showed that NMFs were tolerable and delivered high drug concentrations to back-of-the-eye tissues with topical eye drop application to rabbits. Negligible drug levels were quantified in systemic circulation. These nanomicellar constructs efficiently utilize their hydrophilic corona and evade the wash-out into the systemic circulation from both the conjunctival and choroidal blood vessels and lymphatics,

thus overcoming the dynamic barrier. Moreover, this pathway might overcome the major drawback associated with steroid therapy (glaucoma and cataract), since a trans-scleral route of absorption is accessed.

In summary, for the first time we identified that resolvin analog was substrate/inhibitor for BCRP and MRP but not P-gp. Moreover, resolvin analog was identified as a strong inhibitor of influx transporter (OCT-1). Clear, aqueous NMF encapsulating hydrophobic drugs were successfully developed. Ocular bioavailability and pharmacokinetic studies demonstrated a very high drug levels in retina-choroid (place of drug action) with a negligible drug partitioning into lens and vitreous humor. These results suggest that drug and/or NMFs cannot reach back-of-the-eye tissues following corneal pathway. Alternatively, ~12 nm - 20 nm nanomicelles efficiently permeate through 20 nm to 80 nm scleral pores and reach back-of-the-eye tissues (retina-choroid) following conjunctival-scleral pathway. In the lipoidal posterior ocular tissues, these nano-constructs may release the cargo into Bruch's membrane/retina-choroid generating high drug levels.

APPROVAL PAGE

The undersigned, appointed by the Dean of School of Graduate Studies, have examined a dissertation titled "Topical Clear Aqueous Nanomicellar Formulations For Anterior And Posterior Ocular Drug Delivery", presented by Kishore Cholkar, candidate for the Doctor of Philosophy degree, and hereby certify that in their opinion it is worthy of acceptance.

Supervisory Committee

Ashim K. Mitra, Ph.D., Committee Chair
Division of Pharmaceutical Sciences

Chi Lee, Ph.D.
Division of Pharmaceutical Sciences

Kun Cheng, Ph.D.
Division of Pharmaceutical Sciences

Van Horn, J. David, Ph.D.
Division of Pharmaceutical Sciences

Andrew Holder, Ph.D.
Division of Pharmaceutical Sciences

CONTENTS

ILLUSTRATIONS

Figure Page

TABLES

Table Page

ACKNOWLEDGEMENTS

I am truly indebted and thankful to my advisor Prof. Ashim K. Mitra, for his constant support, encouragement, training and intellectual advice. I would like to thank my supervisory committee (Drs. Chi Lee, Kun Cheng, J. David Van Horn and Andrew Holder) for their critical review of my work. I feel privileged to have such extraordinary researchers in my supervisory committee. I am sincerely thankful to all my committee members for their technical support and motivation at various stages of my graduate studies. Also, I would like to extend my gratitude to Dr. Russell Melchert, Dean of School of Pharmacy for encouragement and all his support.

I would also like to thank Dr. Poonam Velagaleti, Mr. Sidney Weiss from Auven Therapeutics, New Jersey and Dr. Brian C. Gilger from North Carolina State University for helping me with *in vivo* ocular biocompatibility and pharmacokinetic studies in rabbits for nanomicellar cyclosporine-A and resolvin analog (RX-10045) formulations. I would like to extend my gratitude to Dr. Dhananjay Pal for his collaboration and support in my *in vitro* research. I would also like to thank Dr. Earla for his collaboration, support and help with LC-MS/MS in my research. I thank Drs. Sudharshan Hariharan and Sriram Gunda for their constructive criticism, help and collaboration in my research. A special thanks to Mrs. Ranjana Mitra for her constant support and encouragement in the lab.

It is my great pleasure to thank Mrs. Joyce Yolanda Johnson and Mrs. Sharon Self for their constant administrative support through my Ph.D program. I would also like to thank Dr. Netkal Made Gowda, Mrs. Bharathi Gowda, Drs.

Sandeep Putty, Aswani Dutt Vadlapudi, Ashaben Patel, Deep Kwatra, and Sulabh Patel for pursuing research, literary and educational work with me. I would also like to thank my colleagues at school of pharmacy Sujay Shah, Animikh Ray, Ravi Vaishya, Abhirup, Chandramouli, Mary Joseph, and Agrahari. A special thanks to Hoang M. Trinh for her collaboration and help. I also like to thank all my other pharmacy peers for their constant support and friendship.

I would also like to thank my dear friends at UMKC, Drs. Gayathri, Katakam, Mr. Jyothi Samuel Arapally, Mr. Kushal, Mr. Philip Melchert, Mr. Abhishek Goli, Mr. Arapally Ebenezer Anand, Mr. Omar Nazhat, Mr. Praveen Reddy Kaluvala, Mr. Ramsunil Veerubhotula and to all other friends whom I couldn't mention here.

I would also like to thank my younger brother & his wife, Surendar and Vyshnavi, my lovely sister & brother-in-law Santoshi & Dr. Bhagath, Mr. Bharath & Sruthi, Mrs. Saraswathi & Mr. Venkatesh, Mrs. Balamani Bai & Mr. Narsing Rao, Mrs. Aruna Bai & Mr. Satyanarayana Cholkar, brothers Kiran & Tarun, sisters Kavitha & Varsha, my uncle and aunts: Omprakash & Shoba, Amarnath & Surekha and my mother Mrs. Lata Bai and my father Mr. Madhusudhan Cholkar. I also like to thank my lovely and caring wife Shradha for her support and encouragement.My mother-in-law Vijayalakshmi Dounde, my father-in-law Dr. Mangesh Dounde, brother-in-law Mr. Amit Dounde for their nurture, support, encouragement and love. This wouldn't have been possible without them. Finally, I would thank to the God Almighty for his mercy and grace.

Dedicated to my family

Chapter 1

INTRODUCTION

Overview

The eyes are one of the most important and complex sensory organs that act as a gateway to collect external images and transmit them to brain as signals through the optic nerve. By this process they maintain a connection with body and our surroundings. Dry eye, ocular inflammation, surface injuries and diseases rank among the most painful eye conditions and are the leading cause of visit to ophthalmologists in United States. Anterior ocular tissues are exposed to external environment and, consequently, are subjected to inflammations (anterior uveitis) due to disease, dust, microbes such as but not limited to bacteria, virus, fungus and parasites(1, 2). In healthy eye, such ocular insults are normally prevented by blood aqueous barrier, while regulatory molecules and immune cells in the eye actively suppress immune response. Ocular inflammation and surgical trauma induce changes in blood aqueous barrier (3-5). This process causes entry and accumulation of immune cells and inflammatory mediators in ocular tissues and develops redness, pain, swelling and itching(6). Similarly, dry eye (keratoconjunctivitis sicca) is another commonly observed anterior ocular disease in United States population. Dry eye is a chronic disease condition that affects millions of people. Prevalence of this ocular disease in US increases with age, hypertension and benign prostatic hyperplasia. (7, 8). Traditionally, dry eye has been broadly classified depending on the recognized cause as aqueous-deficient or tear evaporative (9, 10).

Age-related macular degeneration (AMD), macular edema (ME), glaucoma, diabetic macular edema (DME), proliferative vitreoretinopathy (PVR), cytomegalo virus retinitis (CMV), non-infectious uveitis, endophthalmitis and diabetic vitreoretinopathies are some of the common posterior eye diseases which may lead to vision loss if not treated.

NIU affects patients of different age groups and it may be chronic and recurrent (11). However, management of NIU is far more challenging than anterior uveitis which leads to irreversible vision loss/impairment. Immediate and vigorous response (immunological and inflammatory) against ocular antigens is still unclear. Lymphocytes can stimulate ocular autoimmune activity in response to Th1 or Th17 (12). A major aim of NIU management includes suppression of inflammation and diminution of NIU intensity (13). Back-of-the-eye neovascularization diseases develop new leaky and fragile blood vessels which branches out from the choroid and then grows through the Bruch's membrane into sub-retinal pigment epithelia. Further, this new vasculature causes capillaries to leak causing blood and fluid accumulation in the retinal layers. During neovascularization, vascular endothelial growth factor (VEGF) is upregulated (14). Increased production of VEGF is induced by multiple cellular pathways: (i) hypoxia and (ii) pro-inflammatory cytokines such as TNF-α and β2 (15, 16).

DEX is a FDA approved drug as a first line of treatment for dry eye, uveitis and macular edema. Immunosuppressants (eg. cyclosporine (CsA) and rapamycin) are recommended as second line of treatment in steroid responders. Moreover, CsA is approved by FDA for the treatment of dry eye (keratoconjunctivitis sicca).

Rapamycin is in clinical trials for the treatment of posterior ocular neovascularization following sub-conjunctival and/or intravitreal injection. Resolvin analog is another novel investigational molecule which is currently in clinical trials for the treatment of dry eye syndrome and ocular inflammations.

Statement of the Problem

Oral and intravenous drug administrations have achieved limited success in treating ocular diseases due to sub-therapeutic levels of drug reaching ocular tissues. Moreover, conventional routes of drug administration are associated with development of systemic toxicities. To treat anterior ocular conditions topical applications of medications, preferably as eye drops, are usually indicated. Topically administered drugs have low probability of reaching anterior and posterior ocular tissues in therapeutic concentrations. Drug delivery to the anterior segment is important since 90% of the administered dose is lost due to excessive tear production, reflex blinking and drainage into the naso-lacrimal ducts. In order for a drug to reach therapeutic concentrations in the anterior segment, it has to pass through the anterior segment barriers. The precorneal pocket can accommodate a maximal fluid volume of 30 μL while draining 40% of drug solution (17). In order to achieve therapeutic levels in anterior ocular tissues highly concentrated drug solutions (~2 - 3% wt/v) is usually required. High rate of tear turnover also reduces drug residence in the pre-corneal and pre-conjunctival areas. Therefore, the tear film also acts as a barrier to topical drug absorption (17). On the other hand, the advent of diseases affecting posterior tissues of the eye, it is difficult to reach and

treat. Therefore, local invasive routes of drug administration (subconjunctival, intravitreal or periocular routes) have been developed for back-of-the-eye diseases. Though high drug concentrations may be achieved in posterior ocular tissues with intravitreal injection several route of administration based concerns limit its usage. However, intravitreal injection suffers from drawbacks such as development of toxicity due to dose dumping, interference with vision due to floating drug molecules, requires multiple intraocular injections, treatment is expensive, requires medical specialist to inject drug and is highly patient non-acceptable.

The first line of treatment for ocular diseases is with corticosteroids (eg. dexamethasone, DEX). Short-term treatment with topical corticosteroids may provide symptomatic improvement (18). However, chronic topical or intravitreal use of corticosteroids is often associated with side effects such as cataract, increased intraocular pressure (IOP), and other steroid related adverse effects(19-21). In such cases, a second line treatment of choice is immunosuppressants like CsA and rapamycin, which are not associated with steroid related ocular side effects. Another class of drugs (resolvin analog (RX-10045)) is under investigation for ocular disease treatment such as dry eye syndrome and inflammations.

Drug molecules (CsA, resolvin analog, DEX and rapamycin) suffer from two major barriers (i) sub-optimal physicochemical properties such as low aqueous solubility and (ii) ocular static and dynamic barriers. Ocular static barriers include corneal epithelium, corneal stroma, blood aqueous barrier sclera, and retinal pigment epithelium (RPE). The dynamic barriers include tear drainage, conjunctival and choroidal blood and lymph vessels that wash drug out of ocular

tissues into systemic circulation and metabolic barriers (22). Moreover, efflux pumps such as MDR1 (P-glycoprotein (P-gp)), multidrug resistance protein (MRP) and breast cancer resistance protein (BCRP) expressed on the cell membrane constitute another significant barrier to drug delivery. DEX, CsA and rapamycin are substrates of efflux transporter (23-25) that prevent drug accumulation into the target cells. Similarly, drug delivery to back-of-the-eye tissues (retina-choroid) is a challenging task. Various formulation strategies, including oil solutions, emulsions, nanoemulsions, ointments, and gels have been developed. These is still an unmet need for development of an aqueous, clear, topical formulation that could encapsulate drug and deliver the cargo to anterior and back-of-the-eye tissues with topical drop instillation. An aqueous clear nanomicellar formulation appears to be better candidate to improve aqueous solubility for drug and aid in drug delivery. Therefore, the following objectives were developed.

Objectives

Objectives of the project were:

To develop and optimize CsA, resolvin analog (RX-10045), DEX and rapamycin loaded nanomicellar formulations with blend of FDA approved amphiphilic polymers (hydrogenated castor oil-40 (HCO-40), vitamin E tocopherol polyethylene glycol succinate-1000 (Vit. E TPGS) and octoxynol-40 (Oc-40)). To characterize the above formulations with respect to their appearance, encapsulation efficiency, loading efficiency, dissociation temperature, regeneration time,

viscosity, size, polydispersity index, surface potential, surface morphology, proton NMR, critical micellar concentration, *in vitro* release and stability studies. To (i) evaluate *in vitro* cytotoxicity on corneal cell line (rabbit primary corneal epithelial (rPCEC) and human corneal epithelial cells (HCEC)) and retinal pigment epithelial cells (D407 and ARPE) with MTT (3-(4,5-dimethylthiazol-2-yl)-2,5-diphenyltetrazolium bromide) assay (ii) to evaluate membrane integrity of rPCEC/HCEC cells with lactate dehydrogenase (LDH) assays. To (i) study *in vivo* biocompatibility and ocular toxicity in rabbits post topical drop instillation with Hackett-McDonald ocular scoring (Microscopic Ocular Grading System) of inflammation (ii) study intraocular pressure development (iii) study retinal health with electroretinography (ERG) (iv) study histopathology of anterior and posterior ocular tissues after multiple topical dose treatment. To study drug (CsA, resolvin analog, DEX and rapamycin) ocular bio-distribution or tissue distribution pharmacokinetics post single topical drop administration to rabbit eye.

Chapter 2

LITERATURE REVIEW

Ocular Drug Delivery

Drug delivery to the eye is a challenging task for ocular pharmacologists. The eye can be broadly divided into two segments; the anterior segment and the posterior segment (**Figure 1**). The anterior segment consists of cornea, conjunctiva, aqueous humor, iris, ciliary body and crystalline lens. They occupy approximately one-third portion of front of the eye. The remaining portion *i.e.*, posterior segment, comprises sclera, choroid, Bruch's membrane, RPE, neural retina and vitreous humor (VH).

Anterior Segment

Cornea

The cornea is a thin, transparent, smooth, avascular, highly innervated and the most sensitive tissue in the body. It is convex, aspheric shaped, and directly exposed to external environment (**Figure 1**). The cornea is continuous with white part of the eye called sclera and the semi-transparent tissue called conjunctiva. Border of the cornea, where it continues with sclera, is called limbus (**Figure 1**). Limbus is highly vascularized and contains a reservoir of pluripotential stem cells (26). Corneal surface exposed to external environment is suffused by tear film and its inner surface is directly in contact with fluid called aqueous humor. Thickness of cornea gradually increases from center to periphery and *vice versa* (27). This is

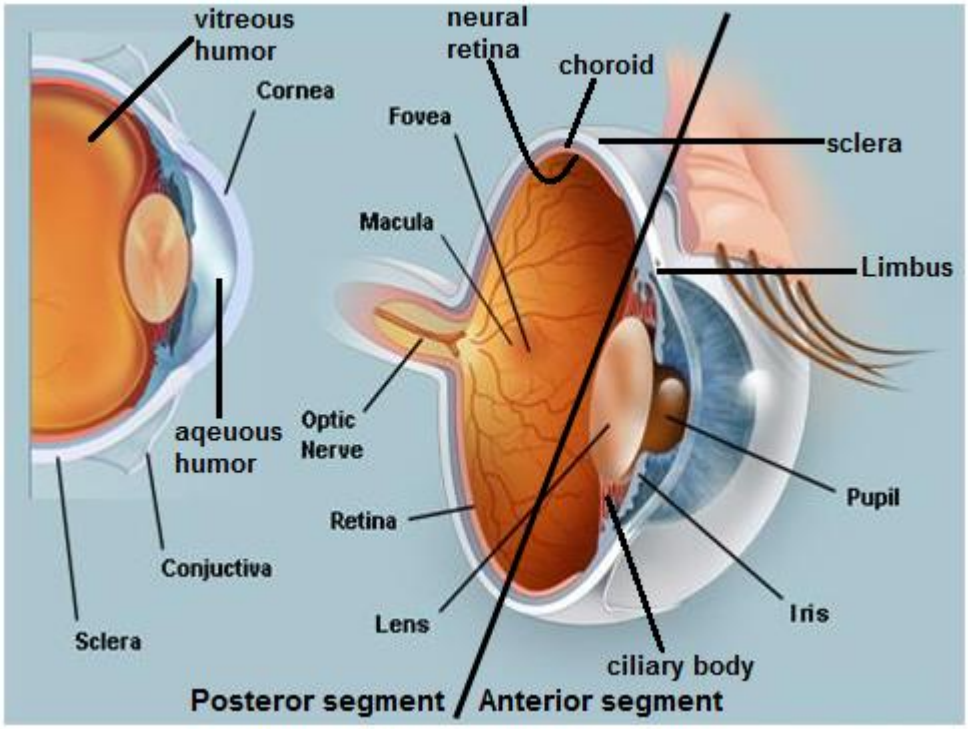

Figure 1. The structure of human eye

observed with corneal curvature which is greatest at the center and smallest at the limbus.

Corneal contour, surface smoothness, transparency and refractive index determine the optical properties of the cornea. The corneal stroma is embedded with relatively homogenous and uniform arrangement of collagen fibers (diameter 25 – 35 nm) (28). Such arrangement is thought to be responsible for preventing and cancelling scattered light interference from the incident ray of light on collagen. The precise arrangement and function of fibers allow the light rays to pass through cornea without any interference. Corneal smoothness is maintained by the corneal epithelium and tear film. Any deviation from normal architecture of corneal collagen fibers and the absence of tear film coverage causes dry eye, scattering of incident light ray and leads to loss of corneal contours, transparency and smoothness.

Corneal nerve fibers travel deeper into stroma radially and anteriorly to form subepithelial plexus (29). Any damage or loss of corneal epithelium exposes nerve endings to external environment causing severe ocular pain (30). Normal cornea does not have supply of blood vessels. So this tissue is considered as one of the avascular tissues in the body along with cartilage and lens. Despite being avascular, the epithelial and endothelial cells of cornea are metabolically active and actively involved in wound healing. Both cell layers get blood components and other requirements from the blood vessels of internal and external carotid arteries that form an arcade around the cornea in limbal region (27). The aqueous humor supplies glucose and small portion of oxygen required by cornea. Most oxygen

supply to the cornea comes from exposure to air, where oxygen absorbed into tear layer diffuses to corneal epithelial cells. This exposure of suffused tear layer on corneal surface is necessary for oxygen supply, maintenance of smoothness and integrity.

A histological section shows that the cornea is composed of six different layers namely, the corneal epithelium, Bowman's layer, the stroma, Dua's layer, Descemet's membrane and the endothelium (**Figure 2**). Corneal epithelium is made of 5 to 6 layers of stratified and squamous nonkeratinized epithelial cells. The different epithelial layers of cornea include two to three layers of superficial and wing cells and a single layer of basal cells. Epithelial cells are anchored to a 0.05μm thick basal lamina, made of columnar epithelium, approximately 20 μm tall. The presence of tight cell junctions between the cells and scaffolding make them highly impermeable (31)**.** Basal cells are only corneal epithelial cells which are capable of undergoing mitosis (32).

Bowman's layer is an 8 to 15 μm thick, amorphous band of fibrillar material present just below basal corneal epithelial cells. This layer is non-regenerative, forms a boundary between corneal stroma and epithelial cells, and maintains corneal shape. It is thought to be involved in re-epithelialization (33). Bowman's layer contains short type I collagen fibrils implanted in the proteoglycan matrix. Corneal stroma is sandwiched between Bowman's layer and Descemet's membrane and accounts for 95% of corneal thickness. Stroma consists of Keratocytes, fibroblastic cells, neural tissue and Schwann cells (27). Most of the stroma is occupied and made by collagen fibrils, mainly type I collagen (34).

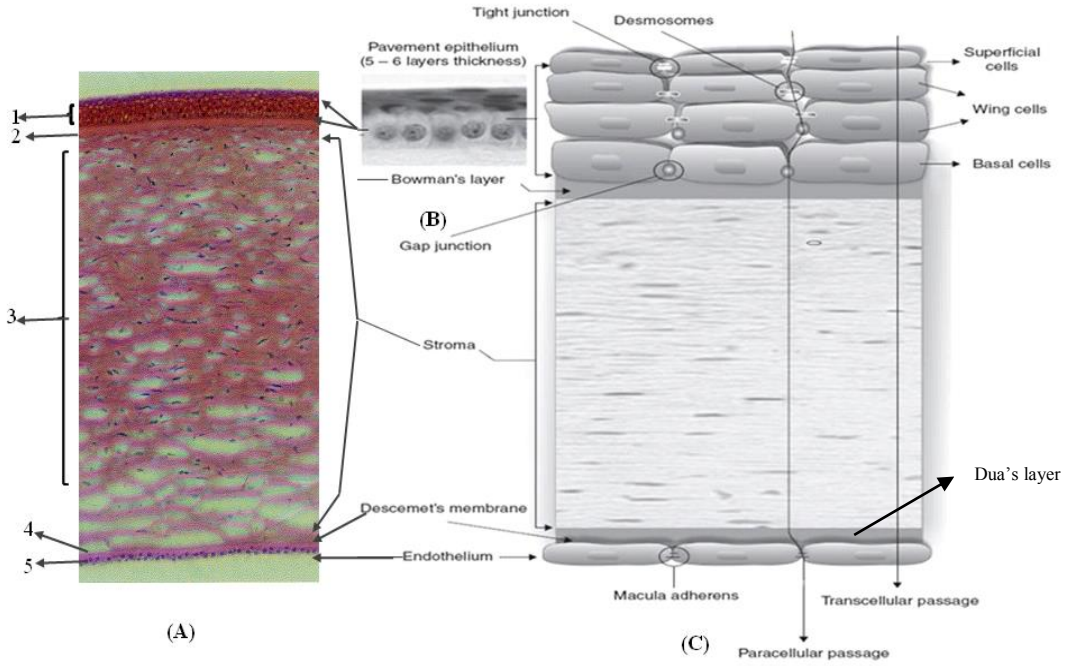

Figure 2. Corneal layers of the eye.

(1) corneal epithelium, (2) Bowman's layer, (3) Stroma, (4) Descemet's membrane and (5) endothelium. Figure A represents the corneal histological image. Figure B and C represent the expanded diagrammatic representation of corneal layers of the eye. Figure A represents the corneal histological image. Figure B and C represent the expanded diagrammatic representation of cornea. Reproduced and modified with permission from Journal of Ophthalmic Vision Research and Progress in Retinal and Eye Research (35, 36).

These fibrils extend from one end of the limbus to other end, angled at 90° in the anterior and orthogonally at posterior stroma. The collagen fibril provides mechanical strength to cornea. The fibrils at posterior stroma are more strictly organized than anterior, probably to contribute to mechanical strength and dioptric stability in cornea (37).

Descemet's membrane is 10 μm thick with an amorphous texture and is unbanded. During developing stage, this layer is discontinuous and homogenous acellular which gradually becomes Descemet's membrane (38, 39). This membrane is thrown into several folds, which appear as striae, due to asymmetric swelling of the posterior stroma, and structural restrictions imposed by limbus.

Corneal endothelium is the innermost monolayer of cells, which is non-mitotic and in direct contact with aqueous humor. While endothelium maintains itself, stroma remains in deturgescence state to provide corneal transparency (40). This monolayer has limitedly permeable to ion flux, which is necessary in establishing osmotic gradient. Generally endothelial cell numbers decrease with age. During diseased conditions, cells increase in their size (polymegathism) and show shape variation (polymorphism) to compensate the spaces formed from degenerated cells.

Conjunctiva

The conjunctiva is a thin, highly vascularized, semi-transparent, and mucous secreting tissue, which forms the inner lining of upper and lower eye lids (41). It is reflected onto the eye as a thin transparent tissue on sclera (**Figure 1)** and extending

up to the corneal limbus. This tissue is highly innervated with efferent, afferent and sensory nerves and is also supplied with lymphoid tissue. The total surface area of conjunctiva is approximately 17 times larger relative to cornea (42, 43). Due to its elastic nature, conjunctiva facilitates motion of the eye ball and eye lids. Mucous layer of tears in conjunction with small portion of aqueous humor protect the inner ocular tissues from external environment. Depending on location, thickness and vascularization, this tissue can be further divided into three types as palpebral, fornic and bulbar conjunctiva. Upper and lower eyelids are internally lined by palpebral conjunctiva. A relatively a small fraction of the conjunctiva, called bulbar conjunctiva, is present near to sclera. The Bulbar conjunctiva is very thin, continuous with cornea, and exposed to external environment with an air interface during the intervals of open-eye. The Palpebral and bulbar portions are connected with a small portion of tissue called fornicial conjunctiva. Fornicial and palpebral conjunctiva are richly supplied with blood vessels and composed of heterogenous tissue (41). Histologically, conjunctiva is mainly composed of superficial multilayered epithelium and an underlying stroma (44). Conjunctival stroma is sandwiched between the anterior epithelium and posterior sclera. This layer is supplied with blood and lymph vessels and innervated with nerve endings. This is intertwined with mature lymphocytes, predominantly with T-cells relative to B-cells. Mucous associated lymphoid tissue (MALT) plays an important role in immune response (45). MALT is composed of lymphatic cells present below the epithelium which induces immune response against the antigens by secreting

soluble antibodies. Lymphocytes are circulated through a specialized vascular system termed high endothelial venules (46-48).

Aqueous Humor

Aqueous humor is an optically clear, slightly alkaline ocular fluid that is continuously formed (~ 2.5 µL/min in humans) from plasma by epithelial cells of ciliary body (49). Three different processes namely, diffusion, ultrafiltration and active secretion contribute for its chemical composition and formation of aqueous humor. It is estimated that the entire aqueous humor is replaced within an approximate time of 100 mins (50). This fluid contains relatively fewer amounts of proteins, albumin and γ-globulins, than plasma. Additionally, glucose, lactic acid, ascorbic acid and immunoglobulin-G (Ig-G) are also present (51, 52). Aqueous humor supplies nutrients and some amount of oxygen to the ocular avascular tissue, namely cornea and lens. It removes waste products, macrophages, blood and other debris from the posterior of cornea and anterior of the lens. Also, it plays an important role in maintaining the shape and internal ailments of eye ball along with production of intraocular pressure. Aqueous humor is produced and secreted into the posterior eye segment and passes through the pupil into the anterior chamber. It is drained into venous blood circulation *via* trabecular meshwork and the canal of Schlemm. Approximately 5% to 10% of aqueous humor is drained following the uveo-scleral pathway (53, 54).

Iris-Ciliary Body

Iris and ciliary body (ICB) are two different tissues with different anatomical locations and physiological functions. For easy understanding and close anatomical localizations, their anatomy and physiology are described together. The iris is located at the posterior region of cornea and appears as a root of the ciliary body. Histologically, the iris is composed of three different layers, namely endothelium, stroma and epithelium. Iris makes a small circular opening or aperture in front of the lens called pupil that helps to regulate the amount of light passing through to the retina. Each ciliary body contains a ciliary process which in turn possesses fibrovascular core that appears to be continuous with the stroma of ciliary body. The blood flows from anterior to posterior choroidal veins. All the blood from the ciliary body of the eye is drained out *via* vortex vein. Ciliary body is anatomically located anterior to the iris and is involved in regulating three major functions in the eye: (i) it secretes aqueous humor, which passes in front of the lens and drains out of the eye *via* tubules called trabecular meshwork and canal of Schlemm near to the junction of cornea and the iris; (ii) this tissue also contains smooth muscles that act *via* zonular fibers on the crystalline lens to adjust focusing objects and; (iii) it can help in draining of aqueous humor from the eye into the adjacent trabecular meshwork by extending smooth muscle fibers and tendons.

Lens

The lens is a transparent, avascular, non-innervated and biconvex in structure. It is positioned behind the pupil and iris with the support of ciliary body's

zonular fibers (55). The anterior lens is covered with aqueous humor and the posterior with VH. The lens-membrane (also known as capsule) regulates passive exchange of metabolic substrates and waste through simple diffusion (56) regulated by their size and charge (57-60). The lens consists of four distinct parts: the capsule, epithelium, cortex (fiber cell mass) and the nucleus. Also, it controls the light entry into the eye and its refraction. The lens nucleus is highly protected by its location. It contains 63.4% water (61) and is formed by deposition of old fiber cells that translocate to the center from periphery. Due to accumulation of old cells in this region, it becomes very thick and denser.

Posterior Segment

Sclera

The sclera, commonly called the "white of the eye", is a tough, avascular, sieve-like elastic tissue present below the conjunctiva and continuous with cornea (**Figure 1**). The optic nerve exits posteriorly through this densely interwoven fibrous tissue network called lamina cribosa. The episclera (topmost layer of sclera) supplies required nutrients to the sclera. The sclera makes almost 80% of the eye's tunic and remainder is made by cornea anteriorly. Thickness of sclera depends on its anatomical location. Anterior sclera, near the limbus, is thick and as one moves towards the equator, thickness decreases (62). Further moving to posterior of the eye, near and around the optic nerve, it doubles in thickness. The sclera is composed of a disorderly arranged network of collagen fibers derived from dura matter of the central nervous system. This type of arrangement causes scattering of all visible

light wavelengths and appears brilliant white in color. At the junction of sclera and cornea this irregular arrangement abruptly changes to a regular and systematic arrangement. Such change brings opaque white sclera to transparent cornea. Same collagen fibers are present in cornea but are arranged in a regular pattern which provides transparency to the tissue. Being hydrated scleral fibers remain opaque while corneal fibers do not retain water, become transparent. The corneal endothelium helps to maintain its transparency by draining out water. Sclera being the outer coat of the eye ball is subjected to frequent changes of external environment as well as intra ocular pressure. Diameter of the scleral fibers in the equatorial region ranges from 25 to 230 nm and the aqueous pore diameter of the sclera ranges from 20-80 nm (28, 63).

Choroid

The choroid is present between peripheral sclera and inner retinal pigmented epithelium. It is a highly vascularized and innervated tissue containing melanocytes along with mucous like extracellular fluid. The choroid consists of three distinct parts: from outer to inner (i) suprachoroid (sc), (ii) vascular layer, and (iii) Bruch's membrane.

The suprachoroid is made of 6 to 10 layers, approximately 30µm in thickness, which form the interface between outer sclera and inner choroid (29). The suprachoroid continues anteriorly with supraciliary space and extends posteriorly up to the optic nerve. This region is highly innervated with nerve fibers and ganglion but no vasculature. Thin lamellar fibers, in apposition to each other

interconnect choroid (CH) and sclera. This arrangement causes development of small space between these tissues called suprachoroidal or perichoroidal space. This space is generally absent as one move posteriorly towards the macula.

The vascular layer underneath suprachoroid consists of three distinct vessel layers with gradually decreasing capillary and luminal diameters. These vessels are surrounded by pigmented melanocytes and non-pigmented fibrocytes and occupy the largest choroid volume. The vessels, fibrocytes and melanocytes are embedded in small amounts of choroidal stroma. The density of melanocytes increases from center to periphery. Choroidal vessels are named according to luminal diameter and location as: (i) Haller's layer with outer larger size vessels, (ii) intermediately located Sattler's layer with medium sized vessel, and (iii) deeply located choriocapillaries with vessel of small diameter. The blood circulation in choroid is relatively high compared to other ocular tissues and brain (64-66). Increased choroidal blood circulation allows nutrient supply and diffusion of high gradient oxygen into the inner neural retina. Retinal metabolic wastes are removed along with changing intraocular temperature generated by visual process. Also, this accelerated blood flow is appeared to play a role in regulating intraocular pressure (67-69).

Bruch's membrane is the last and innermost layer of choroid that lies above the RPE/PE (70). It is also called lamina vitrea. This is a thin, pentalamillar, elastic, and acellular membrane-like structure which is produced in collaboration of choriocapillaries and RPE. Bruch's membrane extends from the posterior segment of the eye, i.e. optic nerve, to ora serrata of iris where its thickness gradually

decreases from back-of-the-eye to periphery. This membrane separates RPE and choriocapillaries. The retinal cellular organization contains seven different types of cells, including RPE cells. They are photoreceptor cells (rods and cones), horizontal cells, amacrine cells, interplexiform cells, bipolar cells, ganglion and glial cells (**Figure 3**).

Retinal Pigment Epithelium

Each eye of an individual contains approximately 3.5 million RPE cells (71) which adhere together to form tight junctions (zonulae occludentes). The RPE is composed of non-dividing cells which forms a monolayered lining above the neural retina. Though these cells are non-dividing, under pathological conditions they may proliferate. It provides protection to inner ocular tissues and secretes large number of growth factors (vascular endothelial growth factor, ciliary neurotrophic factor and platelet derived growth factor). This monolayer maintains ocular immunity and protects from oxidative damage (72) with secretion of immunomodulatory cytokines (73). The RPE cells produce several enzymes such as superoxide dismutase, catalase, glutathione, and melanin pigment. RPE plays a vital role in providing support and survival of choriocapillaries and functioning of photoreceptors. Therefore, its presence is essential for maintaining the visual endothelial growth factor, ciliary neurotrophic factor and platelet derived growth factor). This monolayer maintains ocular immunity and protects from oxidative damage (72) with secretion of immunomodulatory cytokines (73). The RPE cells function (74). Its functions involve disposition of photoreceptor to outer segments,

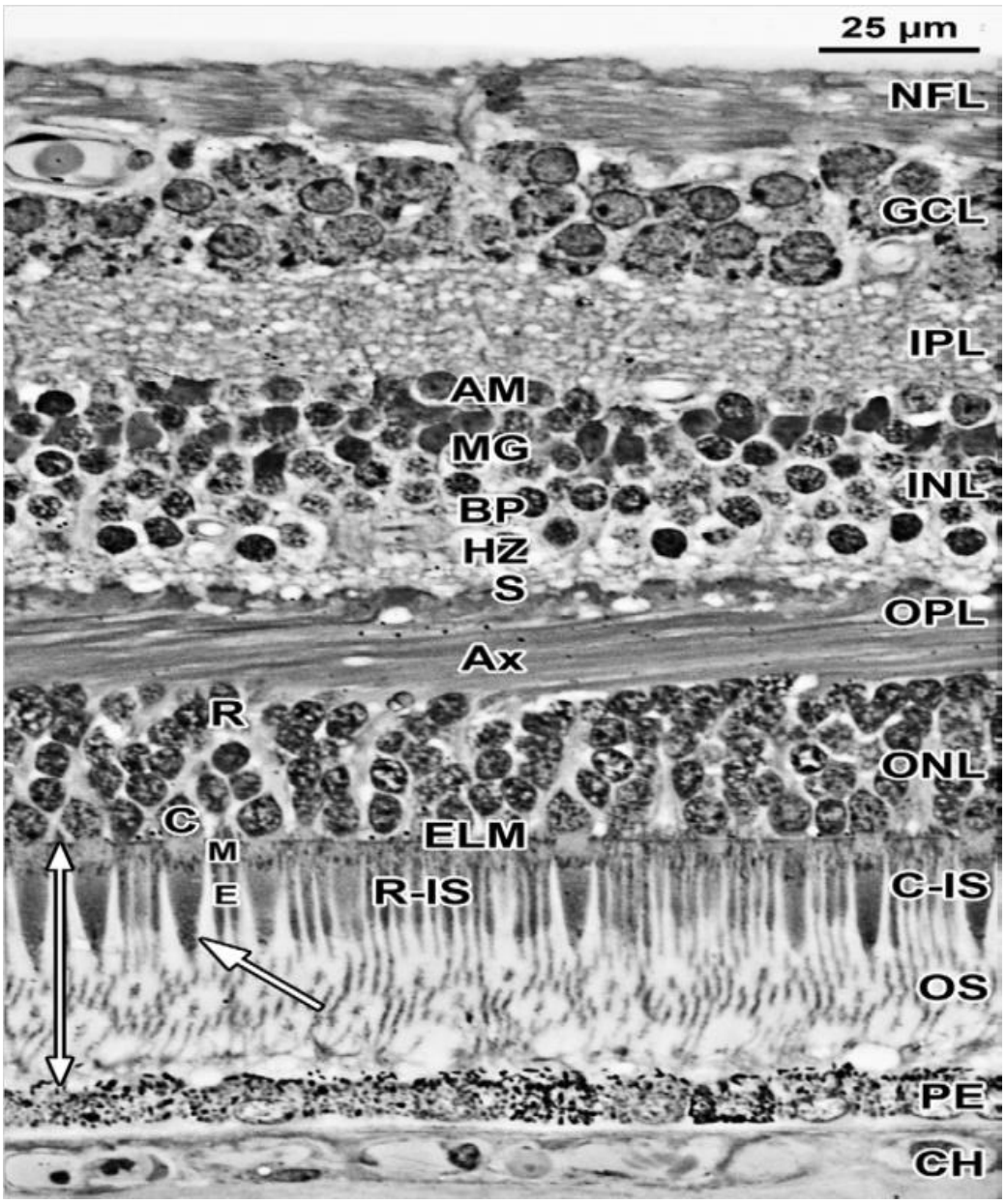

Figure 3. Layers and histology of normal adult human retina.

Adult human retina 2 mm nasal from the fovea center. The layers and their abbreviations used in this paper and in subsequent figures are choroid (CH); retinal pigment epithelium (PE); outer nuclear layer (ONL), which is subdivided into the photoreceptor outer segment (OS) and inner segment (IS) layers distal to the external limiting membrane (ELM); and the nuclear layer containing a single row

of cone (C) cell bodies near the ELM and multiple rows of deeper rod (R) cell bodies. The thin rod IS are indicated (R-IS). The rod OS are about half the thickness of the rod IS, are longer and reach the PE. The larger tapered cone IS have a shorter OS (arrow). The ELM marks the distal edge of the retina. IS myeloid (M) and ellipsoid (E) are indicated. The outer plexiform layer (OPL) contains a distal layer made up of the fibers of Henle or photoreceptor axons (Ax) and a proximal synaptic contact layer (S) containing cone pedicles and rod spherules. The inner nuclear layer (INL) contains the cell bodies of horizontal cells (HZ) lying most distal, bipolar cells (BP) in the middle, Müller glia (MG), and amacrine cells (AM) lying most proximal. The inner plexiform (IPL), ganglion cell (GCL), and nerve fiber (NFL) layers complete the inner retina (Reproduced with permission from American Journal of Ophthalmology (75)).

retinoid metabolism, maintaining visual cycle and regulation of subretinal chemical milieu (76-78).

Neural Retina

Topographically, the retina is organized into macula, optic disc, fovea and peripheral retina. The macula or area centralis is about 1.5mm in thickness and located approx. 3mm away from optic disc. The macula derives its name from the yellow carotenoid pigment, xanthophyll, as macula lutea. The center of the macula represents an important region of visual acuity (79) and is named fovea. The fovea has the highest density of narrow and elongated cone receptors to maximize light detection (80). The center of fovea is avascular up to 500 µm and the blood supply to this region comes from choriocapillaries. Retinal temporal blood vessels surround/enclose fovea. The outer layer of the fovea is thick and contains nuclei of photoreceptor cells. The remaining peripheral retina, anatomically one layer of ganglionic cells, is present outside the temporal retinal arteries. Most of the outer retina gets its blood supply from choroidal circulation whereas general retinal circulation fulfills inner retinal blood supply (81, 82)**.** The inner lining of the eye ball is composed of light sensitive neural cells, called the neural retina, which transmits sensory information to the brain and interacts with external environment. These sensory nerves are originated from central nervous system (83, 84)**.** Neural retina is made up of approximately 7.7 million rods and 5 million cones (85-87).

The photoreceptor cells consist of rods and cones. These cells mainly function to capture and convert the photons into a nerve signal (85). Retinal rod

cells are responsible for differentiating colors in bright light whereas cone cells take care in distinguishing black and white color in dim light. The highest amount of cones is found in fovea whereas the rods are distributed through the retina except the central fovea. The cones and rods are interconnected with inter-neurons called bipolar cells. The visual information is transmitted to ganglion cells through the bipolar cells, which act as a bridge. Ganglionic cells transmit information as electric signals to central nervous system, i.e. brain. During this process Müller's cells help in regulating local microenvironment for proper visual functioning.

Vitreous Humor (VH)

The posterior segment of the eye is mostly avascular and transparent thick gel-like fluid that covers the space between lens and retina. It is called vitreous humor or vitreous body. It aids in maintaining the structure of globe. This fluid is composed of 99.9% water and 0.01% collagen fibrils, hyaluronic acid and ions (76, 88, 89). The vitreous body and neural retina are separated from each other by an inner limiting membrane. The vitreous is firmly attached to anterior retinal layers at ora serrata which is present at the posterior segment of the iris ciliary body. It is loosely attached at optic nerve and posterior macula. In this way the anterior and posterior chamber fluids are separated. These connections around the optic nerve and macula help to hold the vitreous body against the retina.

Thickness of the fluid decreases with growing age. During this condition, anterior aqueous humor may permeate into posterior vitreous resulting in a tugging effect at the attachment point of retina and vitreous fluid. Additionally, this may

cause release of cells into the fluid, which appear as floaters and if significant tugging effect is developed it may pull away or detach retina.

Barriers to Ocular Drug Delivery

Ophthalmic drugs are available as solutions, suspensions, and ointments and are primarily administered topically. Other routes of drug delivery to the eye are oral, intravenous, intravitreal, subconjunctival and periocular injections or via implants (90). A challenging task in drug delivery is to overcome ocular barriers and deliver drugs efficiently to the targeted ocular tissue. Drugs are prevented from reaching targeted ocular tissues due to static and dynamic biological ocular barriers. These barriers can be classified depending on their anatomical location and their functional properties. In general, these barriers can be classified as anterior and posterior segment barriers.

Anterior Segment Barriers

There are two types of barriers i.e. static or dynamic barriers. Static barriers include cornea, conjunctiva, iris ciliary body, lens, blood aqueous barrier, and efflux pumps expressed on cell surface such as multidrug resistant (MDR) proteins: P-gp. Conjunctival lymph, blood flow, opposite directional flow of aqueous humor and tear production together make up the dynamic barriers. These barriers are described in detail below.

Anterior Segment Static Barriers

Cornea

The anatomy and physiology of the cornea has been described earlier in this chapter. Cornea behaves as a multilayered mechanical barrier to prevent exogenous substances, including topically applied drugs, from penetrating deeper into ocular tissues. In order to demonstrate corneal permeability, a comparative study was conducted with different molecular weights of hydrophilic polymer, polyethylene glycol (PEG) (average molecular wt. 200 to 1000) across the rabbit cornea, conjunctiva and sclera (91). Corneal tissue appears 15 and 25 times more resistant to PEG permeation in comparison to conjunctiva and sclera. Increasing molecular size affects the conjunctival permeability. Bulbar and palpebral conjunctiva does not show significant difference. Permeability comparison indicates that the conjunctiva is two times more permeable than the sclera, whereas the sclera is approximately ten times more permeable than cornea. The conjunctival epithelial pore size and density are two and sixteen times higher than sclera respectively. An estimated total paracellular space in conjunctiva is 230 times higher than that of cornea.

The outer corneal layer, with 90% epithelium cells, renders this membrane to be highly lipophilic. Mature corneal epithelial cells act as a barrier to drug absorption as they are tightly bound by cell adhesion proteins such as occludins, ZO-1 and ZO-2 (92). These proteins provide a continuous seal around the cells and form tight junctions to prevent paracellular drug transport across cornea. Drugs traverse the membrane by different mechanisms, namely (i) paracellular, (ii)

transcellular, (iii) active, (iv) carrier mediated and (v) receptor mediated transport**.** Paracellular diffusion of ionic (polar) molecules is prevented by the corneal tight junctions whereas lipophilic drugs may easily diffuse across lipophilic cornea by transcellular mechanism. Bowman's layer has no significant role in preventing drugs from deeper ocular diffusion. The hydrophilic stroma behaves as a rate limiting barrier for lipid soluble molecules and hinders their deeper ocular permeation. For highly lipophilic and relatively hydrophilic compounds, corneal epithelium and stroma act as depot. Descemet's membrane does not significantly participate in hindering drug absorption. The corneal monolayered endothelium forms a cellular barrier between stroma and aqueous humor. This barrier possesses leaky tight junctions which allow free movement of macromolecules between stroma and the aqueous humor (93). Mostly, transcorneal diffusion of drug absorption takes place into aqueous humor. Molecular size has no significant role in permeation across corneal epithelium but the ionization of compounds decreases transcellular diffusion. Therefore, the physicochemical properties of molecule, ionization constant and their pH of the ocular drug product play important roles in regulating and determining ocular drug permeability across corneal epithelium.

Vernal keratoconjunctivitis (VKC) is an allergic conjunctivitis that causes corneal epithelium to lose its integrity and barrier properties. During this condition eosinophils are activated to release cytotoxic proteins such as Myc promoter binding protein (MBP-1), eosinophil peroxidase, eosinophil-derived neurotoxin and eosinophil cationic protein in the tear fluid, which degrade the corneal epithelium (94-98).

Corneal ulceration develops due to corneal fibroblasts stimulation by neutrophils. These fibroblasts along with other factors such as TNF-α, IL-4, and IL-13 participate in corneal collagen breakdown (99-101). Thereby, cornea loses its precise collagen arrangement which may have an effect on corneal barrier properties to topically administered drugs. Corneal fibroblasts can participate in collagen degradation by altering components of the basement membrane to develop corneal ulcers. Tear fluid of VKC patients degrade type IV collagen and laminin, chief components of the basement membrane, and consequently allow to develop corneal ulcers (94, 102-105).

Conjunctiva

Conjunctival tissue acts as a permeability barrier to topically applied drugs. One of the barrier properties can be attributed to its trans-epithelial electric resistance (TEER) (106-108). Different routes of drug absorption such as paracellular, transcellular, active and endocytic routes play a key role in ocular drug delivery through conjunctiva for topically applied drug products. The paracellular route of drug permeation is highly restricted due to the presence of tight junctions at the epithelial surface, which is the rate limiting step for drug absorption (109). Presence of secretory glands embedded within the conjunctiva may have an impact on drug absorption (110, 111). Tear production is a protective response of the eye in response to topically applied xenobiotics. It is a barrier that reduces the drug concentration and bioavailability at the conjunctival apical surface. Physicochemical properties of the drugs such as hydrophilicity and molecular

weight were found to play a major role in drug permeation across conjunctiva. Experimental results demonstrate that hydrophilic drugs with molecular weights less than 20 kD are permeable (109, 112), but higher molecular weight drug molecules are restricted. Relatively conjunctiva has higher paracellular permeability than the cornea for proteins (insulin, molecular weight 5.8 kD) and peptides (p-aminoclonidine (molecular weight 245.1 D) because of its larger surface area and leaky vasculature. (113, 114). On the other hand, lipophilic drug absorption *via* transcellular route has significantly higher contribution relative to hydrophilic drugs. For example, propranolol (a lipophilic drug with logP of 3.21) has ten-fold higher absorption than sotalol (hydrophilic drug with log P of -0.62). Since, conjunctiva possesses esterase activity (115) it may act as an another barrier to drug delivery. During the diseased conditions the conjunctiva may grow larger and develop fibrosis, due to high amounts of collagen production (94).

Blood Aqueous Barrier

Endothelial cells of iris/ciliary blood vessels and the non-pigmented ciliary epithelium together form the blood aqueous barrier (BAB) in the anterior part of eye. This barrier forms tight junctions at the cellular level and regulates the exchange of solutes between the anterior and posterior ocular segments. Thereby, impedes some non-specific drug entry into deeper ocular tissues by functioning as a barrier. Cellular tight junctions impede non-specific drug entry into inner ocular tissues and act as barrier. BAB helps to maintain ocular transparency and regulate chemical composition (116, 117). An intact BAB possesses incomplete barrier

functionality; for example, 40 kD horse radish peroxide (HRP) reaches aqueous humor through fenestrated ciliary capillaries, which are engaged in regulating permeation of plasma proteins, into the aqueous humor. Most of the drugs reaching aqueous humor are eliminated into the systemic circulation through the iris blood capillaries. Hence, drugs in aqueous humor are absorbed by the iris pigments and eliminated into the iris blood circulation (118, 119). On the other hand, small lipophilic drug molecules that escape tight junctions and traverse BAB can be eliminated more rapidly than the larger hydrophilic molecules. As a result, drug penetration to deeper ocular tissues is prevented.

Efflux Pumps

Multidrug resistance in cells may be partially developed due to cell membrane anchored efflux transporter proteins. These efflux pumps belong to adenosine triphosphate (ATP) binding cassette (ABC) superfamily and are actively engaged in effluxing out exogenous xenobiotics and provide protection to the cell. Permeability glycoprotein (P-gp) and multidrug resistance associated protein (MRP) are two efflux proteins that majorly participate in drug efflux at cellular level, causing reduced intracellular drug concentration.

Anterior Segment Dynamic Barriers

Tear Drainage

Ophthalmic drug products are primarily administered by topical route into the cul-de-sac. A large fraction (~ 90%) of administered drug is lost due to pre-

corneal barrier - tear drainage into nasolacrimal ducts (**Figure 4**). Also, other factors that contribute to reduce drug concentrations in cul-de-sac include tear dilution, drug binding to tear proteins and accelerated clearance. Usually, commercially marketed droppers are adjusted to deliver a volume of topical drop from 20-50 µL. From the applied dose, the precorneal pocket holds only 7-10 µL by replacing tear which is already present in the precorneal pocket (120). Such excess administered dose may be lost due to spillage from the precorneal pocket or drainage through the nasolacrimal duct (120, 121). Precorneal tear drainage washes the topically instilled drops/solutions within the first 15-30 seconds, causing a significant reduction in drug contact time and ultimately reducing ocular bioavailability (< 5%) (122-124).

Conjunctival Lymph and Blood Flow

The conjunctiva is highly vascularized and supplied with lymph vessels. Topically applied drugs into the precorneal pocket may be primarily carried away into the systemic and lymph circulation while traversing the conjunctiva (125), resulting in lower drug permeation to deeper ocular tissues. Conjunctival blood and lymph considerably limit the transport of sodium fluorescein from reaching the inner retinal tissues (126, 127), indicating the dynamic role in drug elimination.

Aqueous Humor

Aqueous humor secreted by the ciliary body flows toward the cornea, i.e. in

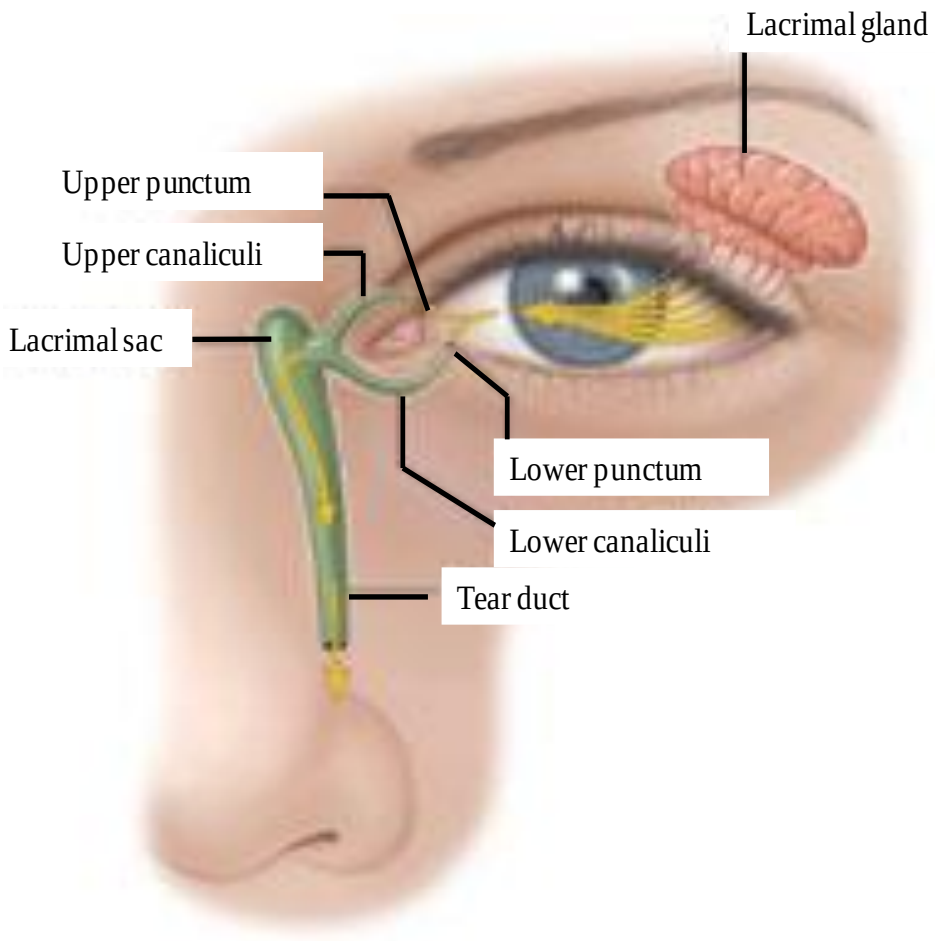

Figure 4. Picture showing the pathway for tear drainage.

opposite direction to the drug entry applied topically. Topically applied drugs, which traverse across the anterior corneal epithelial barrier, may be further limited by aqueous humor flow. Drugs may be drained out through trabecular meshwork into the canal of Schlemm. Larger hydrophilic drugs are found to be eliminated by aqueous humor causing sub-therapeutic levels in the inner ocular tissues (128).

Ocular BAB function may be compromised due to immunologically induced ocular inflammation and may prevent effective permeability of several agents. Intravitreally administered fluorescein labeled serum albumin (F-RSA) diffused into the anterior chamber after five mins in the inflamed eye but not in the control/non-inflamed eye (129). It is well known that only fluorescein sodium molecules easily traverse BAB but F-RSA does not. The F-RSA diffusion into the anterior chamber followed a biphasic pattern until it reached concentration maxima (Cmax) by 2 to 3 hours in the anterior chamber. Then there was a gradual decrease in the fluorescence. These experimental results indicate loss of BAB barrier function, and loss of drug into the anterior chamber through pupil (129). In another study, Xiangyun K, et al. showed that primary angle closure glaucoma damaged the BAB and developed inflammation in the anterior segment of the eye (130). A comparative study between the patients suffering from acute primary angle closure glaucoma (APACG) and chronic primary angle closure glaucoma (CPACG) revealed that patients suffering from APACG had highest BAB damage than CPACG (130). It was hypothesized that a dramatic increase in IOP may be the causative factor for the change of BAB in the eye of PACG patients.

Posterior Segment Barriers

Posterior Segment Static Barriers

Sclera

The sclera is one of the outermost layers of the eye which provides protection and prevents entry of exogenous substances to the posterior ocular tissues. Permeability across sclera mainly depends on certain parameters of the permeating molecule, such as molecular radius, physicochemical properties and surface charge. Drug permeability across sclera gradually recedes with increasing lipophilicity and molecular radius (

Figure **5**). Thus, molecules with higher lipophilicity and larger molecular radius may be prevented from permeation through aqueous scleral pores. The opposite surface charge of the molecule also limits its permeation across sclera. Drug molecules gets trapped in pores of sclera causing low permeability possibly due to interactions with negatively charged pores and proteoglycan matrix (131).

Scleral thickness varies with anatomical location. It is very thick at the posterior segment, near the optic nerve. Due to its thickness, here the posterior sclera has very low permeability for drug molecules.

Bruch's Membrane

The Bruch's membrane is partly involved in regulating the exchange of nutrients, fluids, metabolic waste, oxygen and biomolecules between choroidal blood circulation and retina (132). Thickness of Bruch's membrane increases with age, resulting in calcification, high collagen fiber crosslinking and glycosaminoglycan turnover (133-135). Changes in the thickness of this membrane may also affect permeability of molecules from the sclera into retinal tissues. Moreover, most of the drugs may be lost in the choroid before reaching Bruch's membrane. During diseased conditions such as age related macular degeneration, increased accumulation of extracellular debris causes oxidative stress and chronic inflammation to Bruch's membrane. Higher accumulation of extracellular debris reduces the transport of nutrients as well as drug molecules. This may contribute to the development of secondary metabolic stress (**Figure 6**) (136).

Blood Retinal Barrier

Blood retinal barrier (BRB) is composed of both inner and outer BRB. Outer BRB is composed of tight junctions of RPE cells whereas inner BRB by retinal capillary endothelial cells. Zonulae occludentes of outer BRB separates the retinal photoreceptors from RPE (137, 138). Both astrocytes and Müller cells provide

necessary functional support to these tight junctions. These two cells together regulate the exchange of substances between outer choroid and inner retina. Astrocytes help to maintain the integrity, enhance the barrier property of retinal endothelial capillaries (139, 140) and provide protection to inner retinal cells from circulating molecules in retinal circulation.

Similar to blood brain barrier, the lack of fenestrations in the RPE and retinal endothelial cells prevents passive drug diffusion. RPE allows diffusion of very small molecules such as CO_2, O_2 and lipophilic molecules to inner retinal tissues

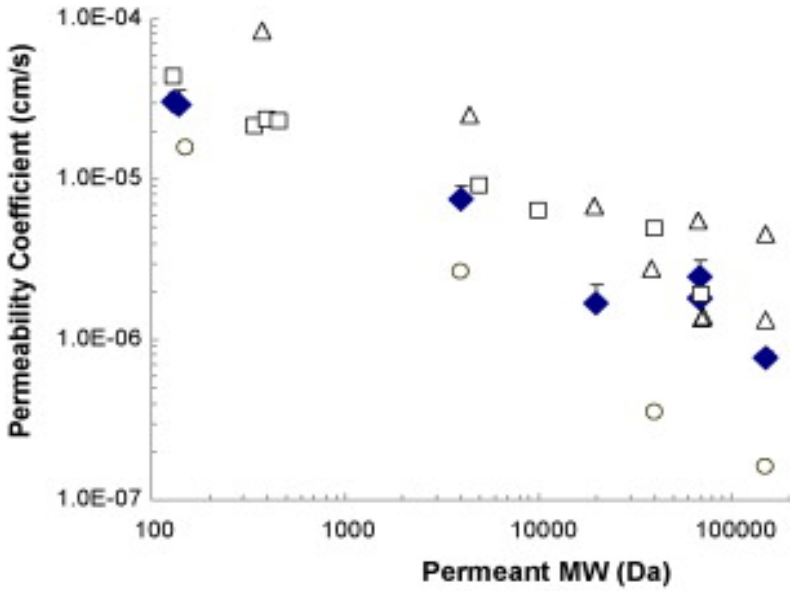

Figure 5. A comparative relationships between ^{14}C labeled permeants: tetraethyl ammonium bromide (130 Da), salicylic acid (138 Da), bovine serum albumin (~67 kDa), poly-(styrene sulfonic acid) (7 kDa), bevacizumab (149 kDa) molecular weight and passive permeability coefficients for human sclera (63).

Symbols: closed diamonds, experimental passive permeability with human sclera (mean and standard deviation, $n \geq 4$); open squares, previous published human passive permeability data (141), open triangles, rabbit passive permeability data (142), open circles, porcine passive permeability data (143). Reproduced with permission from International Journal of Pharmaceutics (63).

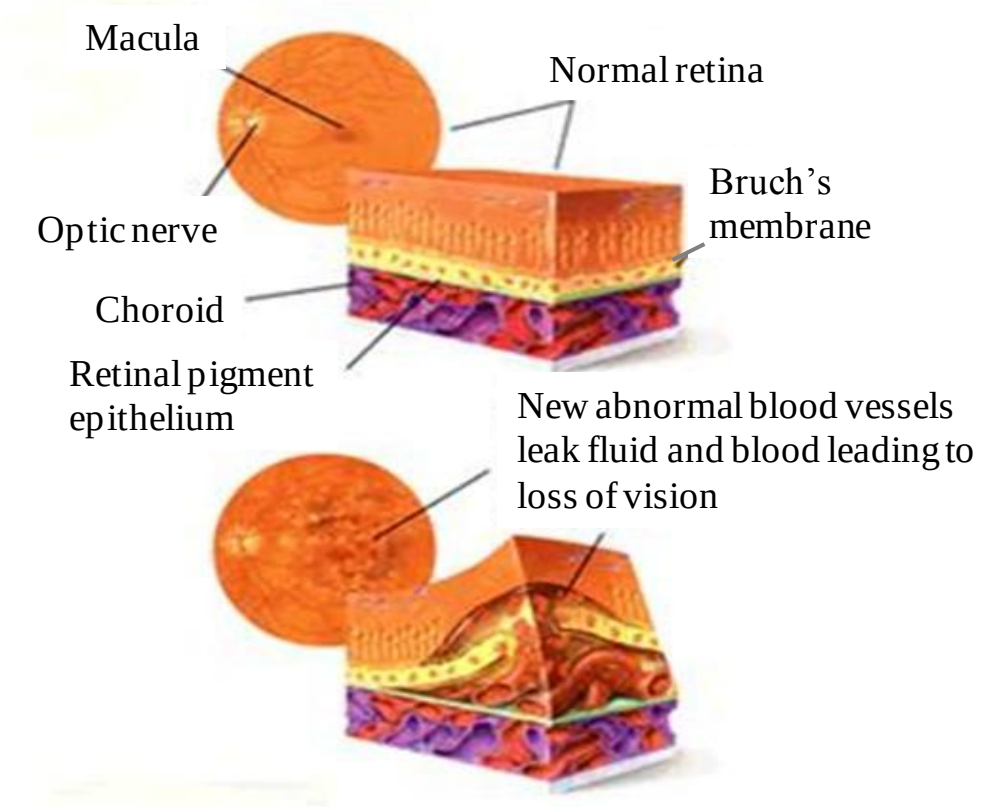

Figure 6. Extracellular accumulation of debris in Bruch's membrane (top) normal eye *versus* (bottom) diseased eye.

(*Source - http://www.decleeneoptometry.com/pages/diseases.htm*)

from the choroid. Thus, the transport of molecules may be mediated by receptor or energy/ATP dependent fluid phase pinocytosis. Therefore, drug entry is highly restricted due to the presence of tight junctions. Also, RPE works as a pump by dehydrating the subretinal space. This helps to maintain the normal neuroretinal apposition with RPE (144, 145). The pump function is necessary because there is no strong adhesion between the segments of external neural retina and RPE. The interphotoreceptor matrix, a gel-like viscous solution present between retinal cells, forms very weak bonds. During the ischemic conditions, retinal adhesive forces diminish within minutes (145).

Efflux Pumps

Trans-membrane efflux pumps such as P-gp or MRP expressed on apical and basal side of human RPE have been reported (146, 147). Expression of P-gp on rat retinal endothelial cells was also reported (148). Similarly the presence of P-gp, MRP4 and BCRP in retinal vasculature of postnatal mouse has been reported. The expression of P-gp in retinal astrocytes has also been reported (149). Recently, different expression levels of MRP1, MRP4 and MRP5 efflux proteins in human retinal pigment epithelial cells have also been indicated (150). At cellular level, these efflux pumps are actively involved in reducing the intracellular drug concentrations and act as a major barrier to drug delivery.

Posterior Segment Dynamic Barriers

Choroidal Blood and Lymph Circulation

The choroid is a highly vascularized tissue (see above) and supplied with lymph vessels. This tissue has the highest blood vasculature (~80%) of the total ocular blood supply relative to iris-ciliary body and retina (151). Drug molecules, lipophilic, may be actively drained in the choroidal and systemic circulation, preventing further entry into the inner ocular tissues. This restricted drug entry may lead to sub-therapeutic drug concentration in retinal tissues. Studies with hydrophilic drugs such as sodium fluorescein indicate very low elimination through choroid (127, 152).

Approaches to Ocular Drug Delivery

Topical instillation is the most widely preferred non-invasive route of drug administration to treat diseases affecting the anterior segment. Conventional dosage forms such as eye drops account for 90% of the marketed ophthalmic formulations. The reason may be attributed to ease of administration and patient compliance (153, 154). Nonetheless, the ocular bioavailability is very low with topical drop administration. Numerous anatomical and physiological constraints such as tear turnover, nasolachrymal drainage, reflex blinking, and ocular static and dynamic barriers pose a challenge and impede deeper ocular drug permeation (155). Hence, less than 5% of topically applied dose reaches to deeper ocular tissues (156). Also, it is difficult to achieve therapeutic drug concentration into posterior segment ocular tissues following topical eye drops instillation because of the above mentioned

barriers. The drug can be delivered to the posterior segment ocular tissues by different mode of administration such as intravitreal injections, periocular injections, and systemic administration. However, the small volume of eye compared to whole body and presence of blood retinal barriers; makes systemic administration an impractical approach. Intravitreal injection is the most common and widely recommended route of drug administration to treat posterior ocular diseases. Though, the need of repeated eye puncture with intravitreal injections causes several side effects such as endophthalmitis, hemorrhage, retinal detachment and poor patient tolerance (157). The transscleral drug delivery with periocular administration route is evolved as an alternative mode of drug delivery to the posterior ocular tissues. Although transscleral delivery is comparatively easy, less invasive and patient compliant, drug permeation is compromised by ocular static and dynamic barriers. Ocular barriers to transscleral drug delivery include: static barriers, i.e. sclera, choroid, RPE, and dynamic barriers, i.e., lymphatic flow in the conjunctiva and episclera, and the blood flow in conjunctiva and choroid (126, 158).

To overcome the ocular drug delivery barriers and improve ocular bioavailability, various conventional and novel drug delivery systems have been developed such as emulsion, ointments, suspension, aqueous gels, nanomicelles, nanoparticles, liposomes, dendrimers, implants, contact lenses, nanosuspensions, microneedles, and *in situ* thermosensitive gels for the earlier mention ocular diseases. This review will provide an overview on various conventional and novel

ophthalmic drug delivery systems developed to deliver drug to diseased ocular tissues for the treatment of ocular diseases.

Conventional Ocular Drug Delivery Systems

Topical drop instillation into the lower precorneal pocket is a patient compliant and widely recommended route of drug administration. However, most of the topically administered dose is lost due to reflux blinking and only 20% (~7 µL) of instilled dose is retained in the pre-corneal pocket (120). Concentration of drug available in the precorneal area acts as a driving force for its passive diffusion across cornea. However, for efficient ocular drug delivery with eye drops, high corneal permeation with longer drug cornea contact time is required. Several efforts have been made toward improving precorneal residence time and corneal penetration. To improve corneal permeation iontophoresis, prodrugs, ion-pair forming agents and cyclodextrins are employed (113, 159-162). There is a wide range of ophthalmic products available in the market of which about 70% of prescription include conventional eye drops. The reasons may be due to ease of bulk scale manufacturing, high patient acceptability, drug product efficacy, stability and cost effectiveness.

Topical liquid/solution eye drops

Topical drops are the most convenient, safe, immediately active, patient compliant and non-invasive mode of ocular drug administration. An eye drop solution provides a pulse drug permeation post topical drop instillation, after which its

concentration rapidly declines. The kinetics of drug concentration decline may follow an approximate first order. Therefore, to improve drug contact time, permeation and ocular bioavailability; various additives may be added to topical eye drops such as viscosity enhancers, permeation enhancers and cyclodextrins. Viscosity enhancers improve precorneal residence time and bioavailability upon topical drop administration by enhancing formulation viscosity. Examples of viscosity enhancers include hydroxy methyl cellulose, hydroxy ethyl cellulose, sodium carboxy methyl cellulose, hydroxypropyl methyl cellulose and polyalcohol (163-165).

Permeation enhancers improve corneal uptake by modifying the corneal integrity. Other additives such as chelating agents, preservatives, surface active agents and bile salts were studied as possible permeation enhancers. Benzalkonium chloride, polyoxyethylene glycol ethers (lauryl, stearyl and oleyl), ethylenediaminetetra acetic acid sodium salt, sodium taurocholate, saponins and cremophor EL are the examples of permeation enhancers investigated for improving ocular delivery (166-168). Addition of permeation enhancers to ocular solutions improves ocular drug bioavailability, but a few studies revealed a local toxicity with permeation enhancers (169). Hence, research is still being conducted to modify the effect of permeation enhancers and evaluate their safety on corneal tissues. Hornoff, et al. evidenced that polycarbophil-cysteine as an excipient did not damage the corneal tissue integrity and suggested that it could be safe for ocular formulations (170). Cyclodextrins act as carriers for hydrophobic drug molecules in aqueous solution. This helps to deliver drugs to the surface of

biological membrane. Highly lipophilic biological membrane has much lower affinity towards hydrophilic cyclodextrins. Therefore, cyclodextrins remain in aqueous solution and the hydrophobic drug is absorbed by the biological membrane. Optimal bioavailability was achieved for eye drops with cyclodextrins concentration of <15% (171). Other applications of cyclodextrins in eye drop formulation were recently reviewed elsewhere by Cholkar et al.(172).

Among these approaches, viscosity enhancers and cyclodextrins suffer from the disadvantage of precorneal loss. In the case of penetration enhancers, care should be taken in the selection due to high sensitivity of ocular tissues. Hence, it leads to development of other conventional formulations approaches with inert carrier systems for ocular delivery of therapeutics. Conventional ocular formulations such as emulsions, suspensions, and ointments have been developed to improve solubility, precorneal residence time and ocular bioavailability of drugs. In the current era of nanotechnology, these conventional formulations still retain their place, importance and capture the market at large. However, these formulations are associated with various side effects such as ocular irritation, redness, inflammation, vision interference and stability issues (119). Currently, research is being conducted to improve the *in vivo* performance of these carrier systems and to minimize their side effects (173). Several attempts are also being made to deliver the drugs to posterior ocular tissues with the conventional formulations. In the following sections, attempts have been made to describe the recent efforts made to improve *in vivo* performance of conventional ocular formulation and reduce their side effects.

Emulsions

An emulsion based formulation approach offers an advantage to improve both solubility and bioavailability of drugs. There are two types of emulsions which are commercially exploited as vehicles for active pharmaceuticals: oil in water (o/w) and water in oil (w/o) emulsion systems (174). For ophthalmic drug delivery, o/w emulsion is common and widely preferred over w/o system. The reasons include less irritation and better ocular tolerance of o/w emulsion. Restasis™, Refresh Endura® (a non-medicated emulsion for eye lubrication) and AzaSite® are the examples of currently marketed ocular emulsions in the USA. Several studies have demonstrated applicability of emulsions in improving pre-corneal residence time, drug corneal permeation, providing sustain drug release and thereby enhancing ocular bioavailability (175).

In a recent study, Tajika, et al. demonstrated improved anti-inflammatory activity with a prednisolone derivative, 0.05% [^{3}H] difluprednate, with an emulsion as vehicle (176). Results confirmed that in the rabbit eye, emulsion could deliver drug to the anterior ocular tissues with small amount of drug reaching posterior tissues following single and multiple topical drop instillation. Single and multiple topical drop instillation studies revealed highest radioactivity in cornea followed by iris-ciliary body > retina-choroid > conjunctiva > sclera > aqueous humor > lens > and vitreous humor. Post single drop administration, T_{max} for cornea, conjunctiva, lens, iris-ciliary body, aqueous and vitreous humor was 0.5 h while T_{max} for retina-choroid was 1 h. Negligible amount of drug was quantified in systemic circulation. With repeated dose instillation, T_{max} for lens and retina-choroid was 8 h and 0.5 h,

respectively. After 168 h, a total dose of approximately 99.5% of radioactivity was excreted in urine and feces. This study suggests difluprednate emulsion as a potential candidate for treating anterior ocular inflammations.

Emulsions with lipid additives such as soyabean lecithin, stearylamine were evaluated as carrier systems for azithromycin to demonstrate better ocular performance and bioavailability (177). A comparative study for azithromycin solution *vs* emulsion at different doses (3, 5 and 10 mg/mL azithromycin) was studied for tear elimination characteristics. *In vivo* studies were conducted in rabbits with topical drop administration. Emulsion, not only observed to behave as a vehicle for azithromycin but also slowed drug release, improved its chemical stability and precorneal residence time. Additionally, emulsion formulation improved the chemical stability ($t_{1/2}$) of azithromycin at pH 5.0 and 7.0 relative to aqueous solutions. Altogether, results suggest that lipid emulsion could be a promising vehicle for ocular drug delivery.

Similarly, another novel approach is to derivatize active pharmaceutical ingredients (API), and improve its ocular bioavailability with an emulsion as carrier system. This strategy may help to reduce ocular irritancy and improve the effect of API. To test this hypothesis Shen, et al. made attempts to improve emulsion biocompatibility for the flurbiprofen. In this study, a derivative of flurbiprofen, flurbiprofen axetil, with castor oil and Tween-80 was used to prepare emulsion (173, 178). Four different emulsions with varying ratios of castor oil (0.1 to 2.5 wt%) and Tween 80 (0.08 to 4 wt%) were prepared and labeled as F1, F2, F3 and F4) respectively.

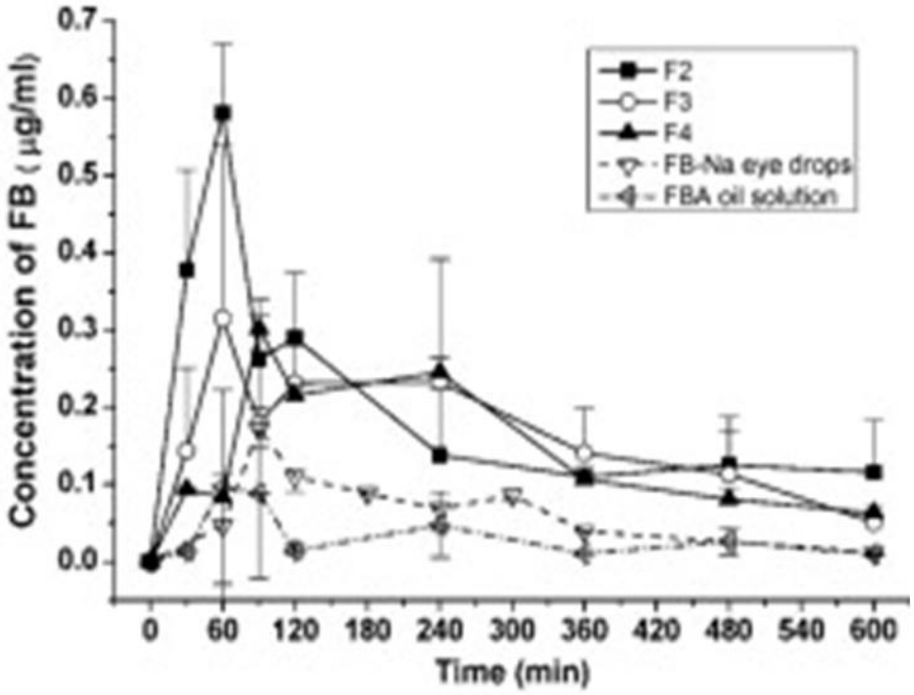

Figure 7. Concentration–time profiles of flurbiprofen (FB) in the aqueous humor after instillation of flurbiprofen axetil (FBA-EM) emulsion F2–F4, FB-Na eye drops and FBA-oil solution in rabbits. (F1 = 0.1 wt% of castor oil, 0.08 wt% of Tween-80; F2 = 0.5 wt% of castor oil, 0.4 wt% of tween-80; F3 = 1.0 wt% of castor oil, 0.8 wt% of tween-80 and F4 = 2.5 wt% of castor oil, 4.0 wt% of tween-80 with 2.2 and 0.1 wt% of glycerol and flurbiprofen respectively. Reproduced with permission from reference (173).

In vivo studies were conducted in male New Zealand albino rabbits with a topical drop instillation. Aqueous humor pharmacokinetic studies showed F2 emulsion (castor oil to tween 80 wt% ratio of 0.5:0.4) to be better relative to other emulsion formulations and solution. The F2 emulsion translocated high drug concentrations into aqueous humor post topical drop administration relative to 0.03% flurbiprofen sodium eye drops (**Figure 7**). Similarly, ocular irritation studies with F2 emulsion demonstrated better biocompatibility relative to other emulsions.

Several researchers have introduced mucoadhesive polymers such as chitosan and hydroxypropyl methyl cellulose ether (HPMCE) for emulsion coating. Studies concluded that chitosan surface coating improves pre-corneal residence time of API and thereby ocular bioavailability. Indomethacin loaded oil-in-water emulsion was prepared employing castor oil and polysorbate-80 and the resultant emulsion was surface coated by chitosan (179).

A comparative *in vivo* study for chitosan coated *vs* non-coated indomethacin emulsions were conducted in male albino rabbits with topical drop instillation. Tear fluid pharmacokinetic study showed that emulsion surface coating with chitosan improves emulsion mean residence time and also half-life by 1.5 and 1.8 times, respectively relative to non-coated emulsion. Indomethacin concentrations were quantified in cornea, conjunctiva and aqueous humor, post 1 h of emulsion instillation. Indomethacin concentrations with emulsion system were found to be~ 5.3 and 8.2 times higher in cornea relative to conjunctiva and aqueous humor.

Suspensions

Suspensions are another class of non-invasive ocular topical drop drug carrier system. Suspension may be defined as dispersion of finely divided insoluble API in an aqueous solvent consisting of a suitable suspending and dispersing agent. In other words, the carrier solvent system is a saturated solution of API. Suspension particles retain in pre-corneal pocket and thereby improve drug contact time and duration of action relative to drug solution. Duration of drug action for suspension is particle size dependent. Smaller size particle replenishes the drug absorbed into ocular tissues from pre-corneal pocket. While on the other hand, larger particle size helps retain particles for longer time and slow drug dissolution (156). Thus, an optimal particle size is expected to result in optimum drug activity. Several suspension formulations are marketed worldwide to treat ocular bacterial infections. TobraDex® suspension is one of the widely recommended commercial products for subjects responding to steroid therapy. TobraDex® is a combination product of antibiotic, tobramycin (0.3%), and steroid, dexamethasone (0.1%). The major drawback of this commercial product is high viscosity. Recently Scoper, et al. made attempts to reduce the viscosity of TobraDex® and to improve its *in vivo* pharmacokinetics along with bactericidal activity (180). The rationale behind developing this formulation was to improve the suspension formulation characteristics such as quality, tear film kinetics and tissue permeation. The new suspension consists of tobramycin (0.3%), and steroid, dexamethasone (0.05%) and called TobraDex ST®. Suspension settling studies showed that new formulation had very low settling over 24 h (~3%) relative to marketed TobraDex® (~ 66%).

Ocular distribution studies showed higher tissues concentrations of dexamethasone and tobramycin in rabbits treated with TobraDex ST® relative to TobraDex®. New suspension formulation was found to be more effective than TobraDex® against Staphylococcus aureus and Pseudomonas aeruginosa. Clinical studies in human subjects showed high dexamethasone concentrations in aqueous humor than TobraDex®. These results suggest that new suspension formulation to be an alternative to marketed suspension. This is because the new suspension possesses better formulation characteristics, pharmacokinetics, bactericidal characteristic and patient compliance than marketed TobraDex® suspension.

In another study to treat dry eye, 4 week, randomized, double masked, multicenter phase II clinical trials were conducted with rebamipide (OPC-12759) suspension (181). Two suspension formulations 1% and 2% rebamipide were employed for this study, where placebo served as control. The efficacy and safety of suspension formulation were determined in human subjects following topical instillation. A dose dependent response was observed for placebo, 1% and 2% rebamipide suspension for both FCS (fluorescein corneal staining) and Lissamine green conjunctival staining (LCGS) studies at 2 and 4 week. Tear production showed no significant difference from baseline from day 1 to week 4. But, the tear film break up time showed significant change in 1% and 2% rebamipide relative to placebo. All the subjects receiving treatment with suspension rebamipide formulation reported improvement of 64.1% and 54.9% respectively than subjects receiving placebo. Dysgeusia, ocular irritation and nasopharyngitis adverse events were frequently observed in 27.2%, 29.1% and 30.4% patients receiving placebo,

1% and 2% suspension, respectively. Drug induced adverse effects such as eye irritation was observed in 3.9%, 2.9% and 2.0% subjects receiving placebo, 1% rebamipide and 2% rebamipide respectively. All these adverse effects were found to recover without any additional treatment. This 4 week studies revealed that suspension formulations were well tolerated and both formulations were effective in treating dry eye. In some measures, of the two formulations, 2% rebamipide suspension was found to be more effective relative to 1% suspension.

Ointments

Ophthalmic ointments are another class of carrier systems developed for topical application. Ocular ointment comprises of mixture of semisolid and a solid hydrocarbon (paraffin) that has a melting point at physiological ocular temperature (34 ºC). The choice of hydrocarbon is dependent on biocompatibility. Ointments help to improve ocular bioavailability and sustain the drug release (182).

Vancomycin HCl (VCM) is a glycopeptides antibiotic with an excellent activity against aerobic and anaerobic gram positive bacteria and methicillin and cephem resistant Staphylococcus aureus (MRSA). Inspite of better activity of VCM, no appropriate topical formulation was available in the market. Better ocular tissue permeability of VCM was not expected in a normal eye but few clinical effects of VCM solution were reported in ocular disease treatment. The reason for the observed effects was hypothesized due to broken ocular barrier system, which might have improved drug permeation. Fukuda, et al. studied the intraocular dynamics of vancomycin hydrochloride ophthalmic ointments in rabbits (183).

Thus, authors made attempts to demonstrate ocular dynamics of VCM ophthalmic ointment (TN-011) with indications limited to extraocular MRSA infections. The minimum growth inhibitory concentration to treat MRSA bacterial infections was found to be 1.56 µg/g. *In vivo* studies were conducted in rabbits (normal *vs Bacillus subtilis* (BS) group). The BS group was developed in cornea by injecting BS solution into the central portion of parenchyma. Treatment was by topical ocular ointment (1% VCM) administration to normal and BS group rabbit eye. In normal group, after 15 mins, VCM concentration in cornea of 12.04 ± 4.73 µg/g was attained at 30 mins which was decreased to 0.49 ± 0.97 µg/g at 120 mins. On the other hand, VCM concentrations in BS group cornea was 25.60 ± 11.01 µg/g after 15 min and 3.68 ± 1.38 µg/g after 240 mins of administration. The concentrations of VCM were maintained above MIC levels, in MRSA infection induced BS group, a considerable benefit to the patients from TN-011 is expected.

In another study by Eguchi, et al. four different ointment formulation of vancomycin with varying concentrations (0.03%, 0.1%, 0.3% and 1.0%) were prepared in 1:4 mixtures of liquid paraffin and vaseline (184). The efficacy of formulations was evaluated in rabbit model of MRSA keratitis infection after topical application. It was observed that at low drug concentrations i.e., 0.03% and 0.1%, numerous infiltrates were found in corneas with abscesses. On the other hand, animals treated with 0.3% formulation showed no recurrence of keratitis in any eye over 14 day study period. Therefore, 0.3% vancomycin ointment was suggested to be adequate and effective to resolve corneal MRSA keratitis.

Though considerable effort is being put into research to improve efficacy, still there is a need to overcome certain drawbacks associated with conventional formulations. The above mentioned formulations: emulsion, suspension, and ointment are known to cause ocular adverse effects such as irritation, redness of eye and interference with vision. Also, chronic administration may increase systemic API availability which may lead to severe systemic complications (185-187). Formulations with preservatives also induce adverse reactions upon systemic absorption (188, 189). Therefore, to overcome formulation based adverse effects and to deliver therapeutic amounts of drug in ocular tissues, research is now being focused on exploring and developing other novel strategies of ocular drug delivery. In the following sections, we will discuss about the recent developments made in nanotechnology and controlled release devices in past decade for improving ocular drug delivery.

Novel Ocular Drug Delivery Systems

Nanotechnology based ocular drug delivery

In a last few decades, many approaches have been utilized for the treatment of ocular diseases. Nanotechnology based ophthalmic formulations are one of the approaches which is currently being pursued for both anterior, as well as posterior segment drug delivery. Nanotechnology based systems with an appropriate particle size can be designed to ensure low irritation, adequate bioavailability, and ocular tissue compatibility. Several nanocarriers, such as nanoparticles, nanosuspensions, liposomes, nanomicelles and dendrimers have been developed for ocular drug

delivery (**Figure 8**). Some of them have shown promising results for improving ocular bioavailability.

Nanomicelles

Nanomicelles are the most commonly used carrier systems to formulate therapeutic agents in to clear aqueous solutions. In general, these nanomicelles are made with amphiphilic molecules. These molecules may be surfactant or polymeric in nature. Recently, Cholkar et al. have reviewed in detail about ocular barriers and application of nanomicelles based technology in ocular drug delivery (190).

Currently, tremendous interest is being shown towards development of nanomicellar formulation based technology for ocular drug delivery. The reasons may be attributed due to their high drug encapsulation capability, ease of preparation, small size, and hydrophilic nanomicellar corona generating aqueous solution. In addition, micellar formulation can enhance the bioavailability of the therapeutic drugs in ocular tissues, suggesting better therapeutic outcomes. So far, several proofs of concept studies have been conducted to investigate the applicability of nanomicelles in ocular drug delivery. For instance, Civiale et al. developed dexamethasone loaded nanomicelles by employing copolymers of polyhydroxyethylaspartamide (PHEAC(16)) and pegylated PHEAC(16) for anterior segment delivery (191). *In vivo* dexamethasone concentration time profiles were studied and determined in rabbits with aqueous humor sampling. Results showed that dexamethasone loaded PHEA micelles have higher ocular bioavailabi-

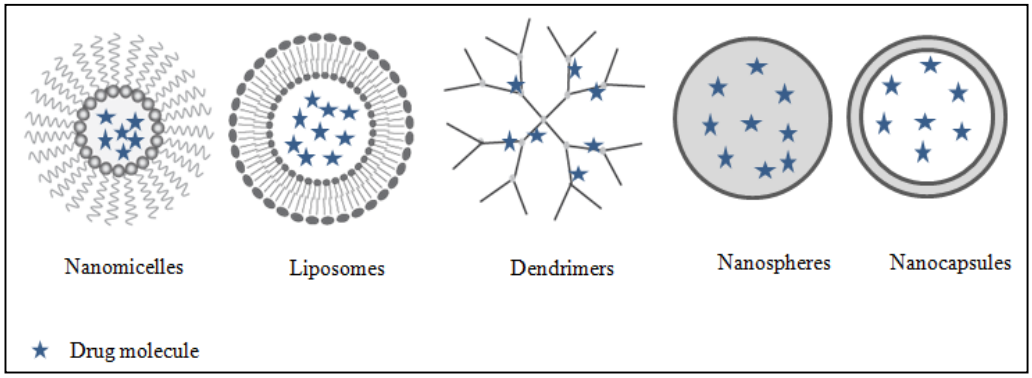

Figure 8. Nanocarriers for ocular drug delivery.

lity relative to dexamethasone suspension. The area under the curve for dexamethasone micellar formulation was 40% higher than that of control suspension. Results suggest that nanomicellar formulations are a viable option for topical ocular delivery of small molecules. Researchers have also utilized nanomicelles for ocular gene delivery. In a study, Liaw et al. made attempts to deliver genes by topical drop administration to cornea (192). Copolymer, poly(ethylene oxide)-poly(propylene oxide)-poly(ethylene oxide) (PEO-PPO-PEO) was used to develop micelles as a vehicle for gene delivery. This polymeric system efficiently transferred plasmid DNA with LacZ gene in rabbit and mice ocular tissues. Results were promising and indicated the potential application of copolymers in DNA transfer. Further studies were conducted with the copolymer to deliver two cornea specific promoters i.e. keratin 12 (K12) and keratocan. Transgene expression was quantified with β-Gal activity. Significant elevated levels of keratin 12 (K12) and keratocan were quantified following six doses of eye drop of pK12-Lac Z-PM three times a day in both mouse and rabbit corneas. The probable mechanism of transfection was endocytosis and particle size dependent paracellular transport of polymeric micelles (193).

Several attempts are also being made to utilize nanomicelles for the posterior ocular drug delivery. Recently, Mitra and co-workers have made a significant stride to deliver therapeutic drugs to the posterior ocular tissues with the aid of topical drops of nanomicellar formulations (194). To bolster the hypothesis that the nanomicelles can deliver the drug to the posterior ocular tissues, *in vivo* studies were carried out in rabbits using voclosporin loaded nanomicelles.

Interestingly, the nanomicelle formulations were able to efficiently traverse ocular tissues and deliver drug to back-of-the-eye tissues. Ocular tolerability of nanomicelles was evaluated against Restasis® as control in New Zealand White (NZW) rabbits. A detailed 72 h study with Hackett-McDonald scoring with microscopic ocular examination was included for two voclosporin (0.02 and 0.2%) micellar and Restasis® formulations. Post 1 hour topical drop administration of Restasis® highest ocular irritation was observed relative to two micellar voclosporin formulations. It was demonstrated that the novel nanomicellar formulations were well tolerated and induced markedly low irritation than Restasis®. Further, authors also prepared dexamethasone and rapamycin nanomicellar formulations at a concentration of 0.1 and 0.2 wt%, respectively. Ocular tissue distribution studies with single drop instillation showed that nanomicellar formulation encapsulating voclosporin, dexamethasone and rapamycin was able to deliver therapeutic concentrations of drug to back-of-the-eye tissues post topical drop instillation. These studies suggest that small size, hydrophilic nanomicellar corona help to evade ocular barriers and deliver drug cargo to posterior ocular tissues. A non-corneal pathway of drug delivery has been hypothesized for back-of-the-eye drug delivery. Ryuichi and co-workers made attempts to deliver FITC-P(Lys) to back-of-the-eye tissues *via* intravenous drug administration to treat back-of-the-eye tissue neovascularization (195). *In vivo* studies with unformulated FITC-P(Lys) resulted in death of animals post 1 h of administration. In contrast encapsulating the FITC-P(Lys) in polyehthylene glycol-block-poly-α,β-aspartic acid micelles resulted in no death. This indicates no free drug was available in nanomicellar

formulation. Micellar formulation showed a C_{max} at 4 h in retina-choroid and drug was detected up to 7 days following single intravenous administration. Prolonged micellar circulation was achieved by controlling polymer to drug charge ratios. Authors speculated that longer systemic micellar circulation may aid in enhanced permeation and retention (EPR) effect at neovascularization site. Micellar constructs were observed to selectively accumulate at the pathologic neovascular site to a greater extent than in normal tissues.

In another study, Ususi et al. made attempts to encapsulate dendritic photosensitizer (DP) in PEG-b-P(Lys) micellar construct for the treatment of exudative AMD with photodynamic therapy (196). *In vitro* cytotoxicity studies were performed under dark and light irradiation for DP alone and DP loaded polyionic complex (PIC) micelles to be more cytotoxic in light irradiated conditions. This higher cytotoxic effect of polymeric ion complex micelles under light irradiation was utilized for the treatment of exudative AMD. Photocoagulation was induced in rat eye. DP loaded PIC micelles were administered by intravenous injection and DP accumulation in choroidal neovascular site was observed. Application of mild laser light treatment destroyed/choked the abnormal vasculature. This new technology prevents further drug leakage. Histological studies revealed accumulation of PIC micelles at ocular lesion site. Reason may be attributed due to EPR effect. Administered free DP was eliminated within 24 h. On the other hand, PIC micelles encapsulated DP were detected after 24 h indicating micellar construct accumulation at lesion site with slow cell uptake. A reduction in fluorescence was

observed post 25 mins intravenous administration of DP loaded PIC micelles, due to chocking of abnormal vasculature. Hypofluorescence of DP micelles was increasing with time indicating increased vascular chocking. Normal endothelial cell destruction was not observed, possibly due to lower DP accumulation. Results suggest that small size and hydrophilic negatively charged micellar corona resulted in considerable EPR effect. This resulted in selective drug accumulation in the choroidal neovascular tissues with minimal/no drug induced adverse effects on normal cells.

Ocular research is currently focused to non-invasively deliver therapeutic levels of drugs to both anterior and posterior ocular segments. The advent of nanomicellar technology to delivery drugs in a non-invasive route i.e. topical drop is novel and patient acceptable. Due to their extremely small size and hydrophilic corona, nanomicelles may be retained in systemic circulation for longer time and accumulate at the diseased tissue *via* EPR effect. Thereby, non-specific drug accumulation in to normal tissues may be minimized. Proper selection of surfactant/polymer and engineering technique may aid in delivery of drugs to both anterior and posterior eye segments.

Nanoparticles

Nanoparticles are colloidal carriers with a size range of 10 to 1000 nm. For ophthalmic delivery, nanoparticles are generally composed of lipids, proteins, natural or synthetic polymers such as albumin, sodium alginate, chitosan, poly (lactide-co-glycolide) (PLGA), polylactic acid (PLA) and polycaprolactone. Drug

loaded nanoparticles can be nanocapsules or nanospheres (**Figure 8**). In nanocapsules, drug is enclosed inside the polymeric shell while in nanospheres; drug is uniformly distributed throughout polymeric matrix. From past few decades, nanoparticles have gained attention for ocular drug delivery and several researchers have made attempts to develop drug loaded nanoparticles for delivery to both anterior and posterior ocular tissues (Table 1).

Nanoparticles represents a promising candidate for ocular drug delivery because of small size leading to low irritation and sustained release property avoiding frequent administration. However, like aqueous solutions, nanoparticles could be eliminated rapidly from pre-corneal pocket. Hence, for topical administration nanoparticles with mucoadhesive properties have been developed to improve pre-corneal residence time (197). Polyethylene glycol (PEG), chitosan and hyaluronic acid are commonly employed to improve precorneal residence time of nanoparticles.

Chitosan coating is the most widely explored way of improving precorneal residence of nanoparticles. The chitosan is positively charged and hence it binds to negatively charged corneal surface and thereby improves precorneal residence and decreases clearance. For instance, natamycin loaded chitosan/lecithin nanoparticles exhibited high ocular bioavailability at reduced dose and dosing frequency in rabbit eye compared to marketed suspension. Following topical administration, the AUC (0-∞) was increased up to 1.47-fold and clearance was decreased up to 7.4-fold in case of chitosan/lecithin nanoparticles compared to marketed suspension (198). In another study, Teresa, et al. reported that melatonin

loaded PLGA-PEG nanoparticles were most effective and demonstrated significant intraocular pressure (IOP) lowering effect compared with melatonin loaded PLGA nanoparticles and aqueous solution of equivalent concentration in the rabbit eye (**Figure 9**) (199). It was speculated that the reduced zeta potential of nanoparticles fabricated from PLGA-PEG than the PLGA allowed better and longer interaction between the nanoparticles and eye surface leading to higher hypotensive effect for prolonged period.

Nanoparticles have also been successfully employed as an alternative strategy for long term drug delivery to the posterior segment ocular tissues. For posterior segment delivery, disposition of nanoparticles depends on the size and surface property. Following, periocular administration in to Sprague-Dawley rats, 20 nm particles were cleared rapidly from periocular tissues. The rapid clearance can be due to removal by conjunctival, episcleral or other periocular circulatory systems. On the other hand, particles in the range of 200–2000 nm were retained at the site of administration for at least two months. Moreover, due to the rapid clearance and fast drug release, small size nanoparticles could not sustain retinal drug level. Therefore, it can be concluded that for prolonged transscleral drug delivery to the back-of-the-eye, nanoparticles with slow drug release and low clearance by blood and lymphatic circulations are suitable drug delivery candidates (200, 201). Following intravitreal injection, nanoparticles migrate through the retinal layers and tend to accumulate in the RPE cells. The PLA nanoparticles were

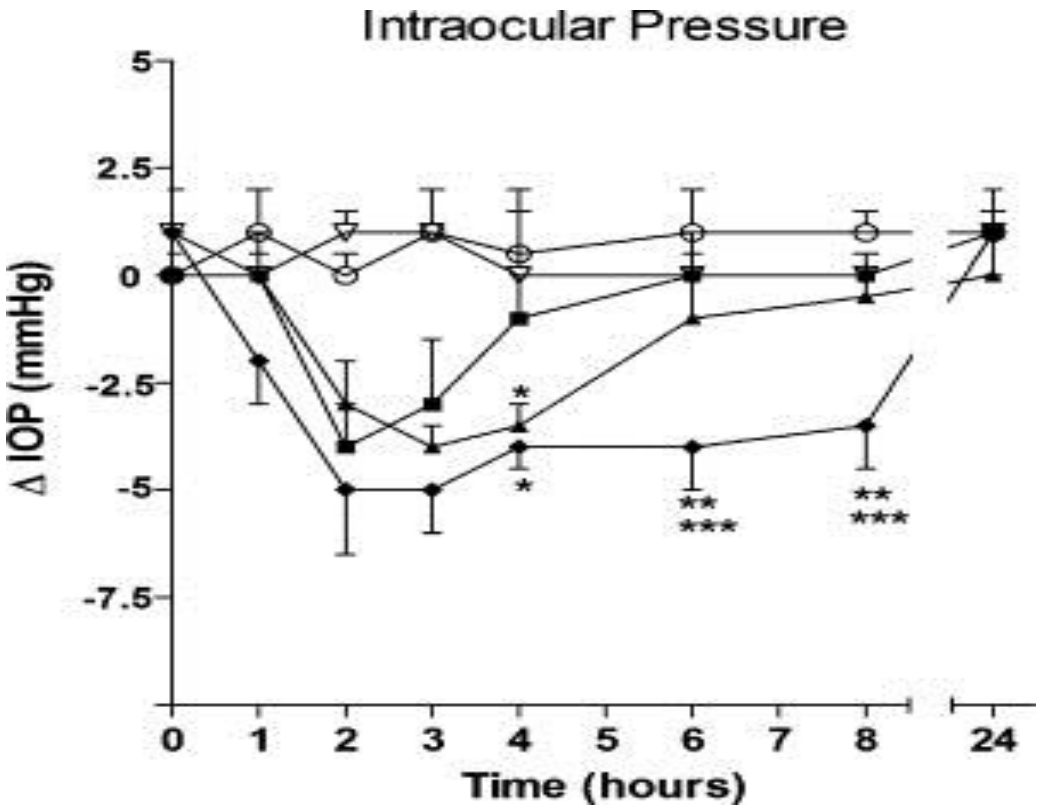

Figure 9. Intraocular pressure in normotensive rabbit eyes after topical instillation of melatonin (MEL) aqueous solution (■) or NPs: RG (O), RGP (Δ), RG-MEL1 (MEL loaded PLGA NPs) (▲), or RGP-MEL1(MEL loaded PLGA-PEG NPs) (♦). *p < 0.01, **p < 0.001 *vs*. melatonin; ***p < 0.001 *vs*. RGP-MEL1. Reproduced with permission from reference (199).

present in rat RPE tissues up to 4 months following single intravitreal injection which suggest that nanoparticles have great potential for achieving steady and continuous delivery to the back-of-the-eye. Zhang, et al. investigated the pharmacokinetics and tolerance of dexamethasone (DEX) loaded PLGA nanoparticles in rabbits following intravitreal injection (202). Authors concluded that DEX when encapsulated in nanoparticles exhibited sustained release for ~50 days. The constant DEX levels were maintained in vitreous over 30 days with a mean concentration of 3.85 mg/L. Contrary, only trace amounts of DEX being detected on the seventh day after injection of DEX solution. These results imply that intravitreal injection of dexamethasone nanoparticles may be employed for sustained delivery of drugs for the treatment of posterior segment eye diseases. The surface property of nanoparticles is a key factor affecting their distribution from vitreous humor to retinal layers (203). Heebeom et al. studied correlation between surface properties of the nanoparticles and their distribution in the vitreous and retina after intravitreal injection (204). Heterogeneous PEI (polyethyleneimine)/GC (glycol chitosan), HSA (human serum albumin)/GC, and HSA/HA (hyaluronic acid) nanoparticles were prepared by blending two polymers. The value of zeta potential of these nanoparticles were 20.7 ± 3.2, −1.9 ± 4.1 and −23.3± 4.4 for PEI/GC, HSA/GC, and HSA/HA nanoparticles, respectively. The nanoparticles were injected into vitreous cavity of Long Evans rats and vitreous/retinal distribution was evaluated by confocal microscopy. Fig 10 shows vitreal and retinal distribution of intravitreally administered heterogeneous nanoparticles. It can be depicted from the Fig 10 that PEI/GC nanoparticles easily penetrated the vitreal

barrier and reached at the inner limiting membrane. However, PEI/GC nanoparticles did not penetrate through the physical pores of inner limiting membrane into the deeper retinal layers and also some aggregates were observed in vitreous. Similar to PEI/GC nanoparticles, HSA/GC nanoparticles reached to inner limiting membrane but could not penetrate to the deeper retinal layers which might be due to inhibition of the interaction between HSA and the Müller cells in retina by GC. On the other hand, negatively charged HSA/HA nanoparticles, could penetrate the whole retina structures and reach the outer retinal layers such as the photoreceptor layer and RPE which was attributed to interaction between anionic surface and Müller cells. In another study, HSA-NPs penetrated the whole retina and localized inside the RPE of the normal retina after intravitreal injection in rat eyes. Furthermore, in the laser photocoagulated retina, HSA-NPs were observed to reach the choroid through the disruption site of the RPE and Bruch's membrane. Therefore, the anionic HSA-NP could be promising drug delivery carrier for the treatment of AMD which required drug distribution to the choroid region in order to inhibit choroidal neovascularization (205).

Nanosuspensions

Nanosuspensions are colloidal dispersion of submicron drug particles stabilized by polymer(s) or surfactant(s). It is emerged as promising strategy for delivery of hydrophobic drugs. For ocular delivery, it provides several advantages such as sterilization, ease of eye drop formulation, less irritation, increase precorneal residence time and enhancement in ocular bioavailability of drugs which

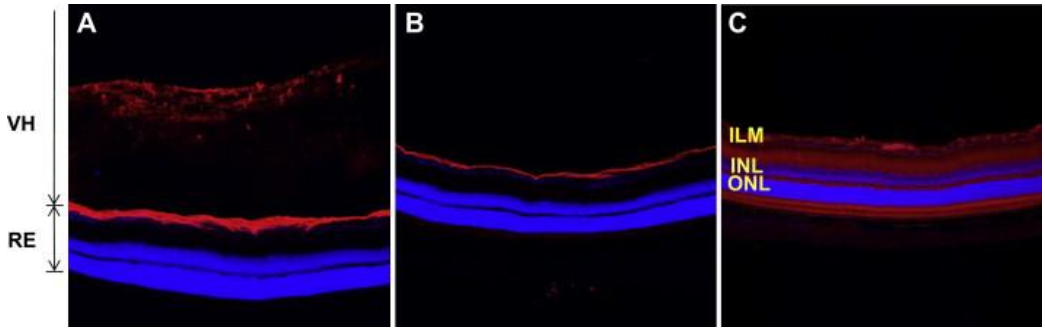

Figure 10. The vitreal and retinal distribution of intravitreally administered (A) PEI/GC heterogeneous nanoparticles, (B) HSA/GC heterogeneous nanoparticles, and (C) HSA/HA heterogeneous nanoparticles 6 h post-injection. (Red color = FPR-552 conjugated nanoparticles, blue color = DAPI staining of retinal cell nuclei). VH, RE, ILM, INL, and ONL represent the vitreous, retina, inner limiting membrane, inner nuclear layer, and outer nuclear layer, respectively. All images were captured at 10x magnification. Reproduced with permission from reference (204).

Table 1. Summary of recent developments with nanoparticles as ocular drug delivery vehicles

Drug	Polymer	Features	Ref.
Carboplatin	Chitosan, Sodium alginate	Carboplatin loaded NPs demonstrated elevated and sustained anti-proliferative activity in a retinoblastoma cell line (Y-79), with IC_{50} of 0.56 µg/ml and 0.004 µg/ml for free carboplatin and carboplatin loaded NPs, respectively.	(206)
5-Fluorouracil	Chitosan (CH), Sodium alginate (SA)	Chitosan (CH) coated sodium alginate (SA)-chitosan (CH) nanoparticles (CH-SA-CH NPs) loaded with 5-Fluorouracil (5-FU) showed significantly higher concentration of 5-FU in aqueous humor as compared to SA-CH 5-FU loaded NPs and 5-FU solution. The higher C_{max} was achieved in case of CH-SA-CH NPs (24.67 µg/ml) compared to 5-FU solution (6.14 µg/ml).	(207)
Sparfloxacin	PLGA	After topical application, sparfloxacin-loaded nanoparticles were retained for a longer duration on the corneal surface as compared to an aqueous solution, which was drained rapidly from the corneal surface. Also, *in vitro* release studies revealed an extended release of sparfloxacin.	(208)

Drug	Polymer	Features	Ref.
Brimonidine Tartrate (BT)	Sodium alginate	BT-loaded nanoparticles provided prolong drug release over a period of 8 h after topical instillation to albino rabbits.	(209)
Levofloxacin	PLGA	The nanosuspensions was retained for the longer time on rabbit eye surface and drained out slowly compared to marketed formulation. Results of ex-vivo transcorneal permeation study across excised goat cornea revealed that levofloxacin from the marketed formulation was permeated 36.9% in 4 h whereas levofloxacin from PLGA nanoparticles was permeated 47.43% in 4 h across cornea.	(210)
Diclofenac Sodium (DS)	PLGA	An extended DS release was observed from the nanoparticles under *in vitro* conditions. The developed polymer nanoparticles formulation was non-irritant to cornea, iris, and conjunctiva for as long as 24 h after application.	(211)
Pilocarpine	PLGA	The *in vivo* miosis studies showed that the duration of miotic response increased by 40% for the nanoparticles compared to the eye drops.	(212)

Drug	Polymer	Features	Ref.
Gatifloxacin/Prednisolone	Eudragit RS 100 and RL 100, coating with hyaluronic acid	*In vitro* release studies revealed prolonged drug release compared to the free drugs with no burst effect. Nanoparticles formulation showed better bioavailability of gatifloxacin in rabbit eye with 1.76 fold increase in C_{max} of gatifloxacin in the aqueous humor in comparison to the eye drops.	(213)
Cloricromene (AD6)	Eudragit	Nanosuspension enhanced stability of the ester drug for several months as compared to an AD6 aqueous solution.	(214)
Brimonidine Tartrate (BT)	Eudragit RS 100, Eudragit RL 100	The AUC (ΔIOP vs. time) for the selected nanoparticles formulations were about seven times higher than that of eye drop formulations in rabbit eye.	(215)

are insoluble in tear fluid (216). Efficacy of nanosuspensions in improving ocular bioavailability of glucocorticoids has been demonstrated in several studies.

Glucocorticoids such as prednisolone, dexamethasone and hydrocortisone are widely recommended for the treatment of inflammatory conditions affecting anterior segment ocular tissues. The current therapy with these drugs requires frequent administration at higher doses which induce cataract formation, glaucoma, and damage optic nerve. Efforts have been made toward improving ocular bioavailability of glucocorticoids by formulating as nanosuspensions. For instance, Kassem et al. compared ocular bioavailability of various glucocorticoids (prednisolone, dexamethasone and hydrocortisone) from nanosuspensions, solutions and microcrystalline suspensions. The formulations were instilled into the lower cul-de-sac of the rabbit eye and intraocular pressure (IOP) was measured at frequent time intervals up to 12 h. The area under percentage increase in IOP versus time curve (AUC) values for all the suspensions were higher than that for the respective drug solutions. In addition, higher extent of drug absorption and more intense drug effects were observed for all steroids form nanosuspensions compared with solutions (217). In another study, Ali et al. compared ocular bioavailability of hydrocortisone (HC) nanosuspensions prepared by precipitation and milling method with HC solution in rabbits post topical instillation (218). Nanosuspensions prepared by both the precipitation and milling method achieved significantly higher AUC (0-9 h) values of 28.06 ± 4.08 and 30.95 ± 2.2 than that of HC solution (15.86 ± 2.7). A sustained drug action which was represented in terms of changes in intraocular pressure was maintained up to 9 h for the nanosuspensions compared to

5 h for the drug solution (**Figure 11**). From the results of above research studies, it can be concluded that nanosuspensions could be an efficient ophthalmic drug delivery system for delivery of poorly soluble drugs. In addition, nanosuspension can also be incorporated into hydrogels or ocular inserts for achieving sustained drug release for stipulated time period.

Liposomes

Liposomes are lipid vesicles with one or more phospholipid bilayers enclosing an aqueous core (**Figure 8**). The size of liposomes usually range from 0.08 to 10 µm and based on the size and phospholipid bilayers, liposomes can be classified as small unilamellar vesicles (SUV) (10-100 nm), large unilamellar vesicles (LUV) (100-300 nm) and multilamellar vesicles (contains more than one bilayer) (219).

For ophthalmic applications, liposomes represent ideal delivery systems due to excellent biocompatibility, cell membrane like structure and ability to encapsulate both hydrophilic and hydrophobic drugs. Liposomes have demonstrated good effectiveness for both anterior and posterior segment ocular delivery in several research studies. Recent advancements in liposomal ocular drug delivery are summarized in **Table 2**. In a recent study, for delivery of latanoprost to anterior segment ocular tissues, a liposomal formulation was developed by Natarajan et al. (220). The single subconjunctival injection of latanoprost/liposomal formulation in rabbit eye produced sustained IOP lowering effect over a period of 50 days with IOP reduction comparable to daily eye drop administration. For drug delivery to

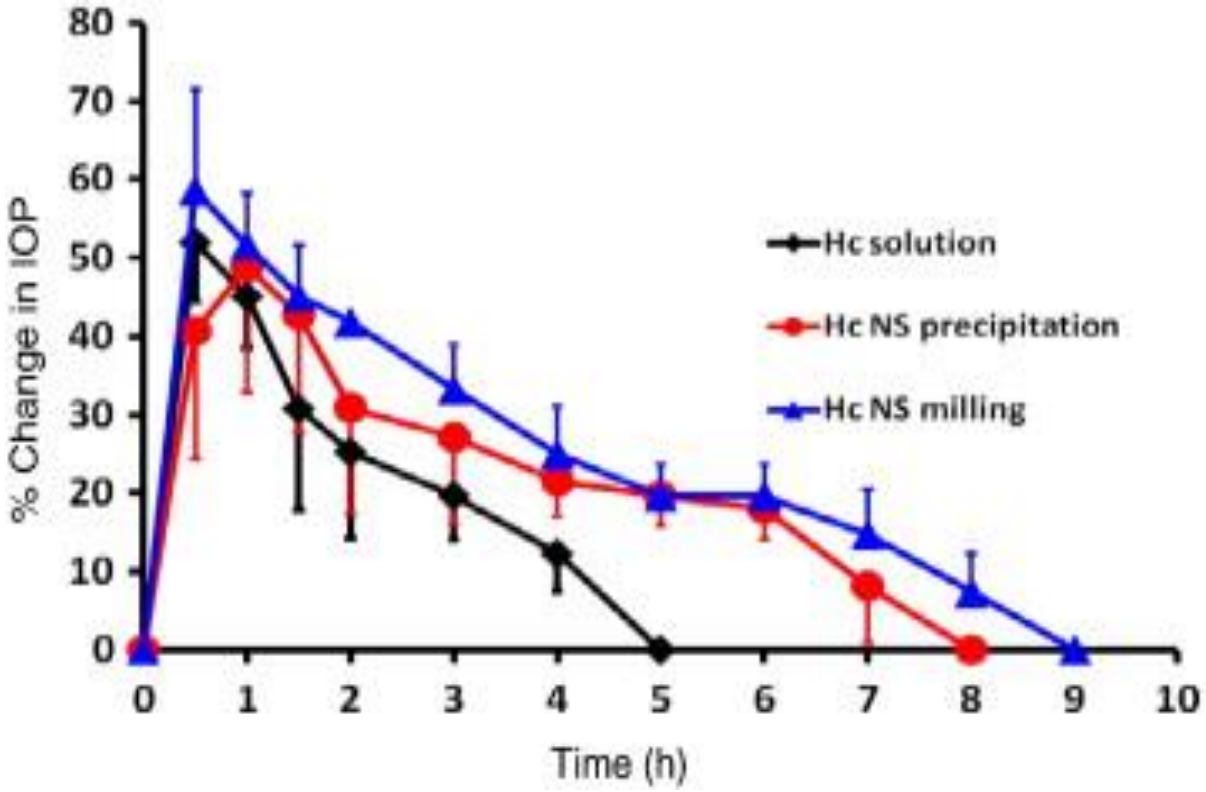

Figure 11. Changes in intraocular pressure (IOP) of rabbits eyes following administration of hydrocortisone solution and nanosuspensions produced by milling and precipitation. Reproduced with permission from reference (218).

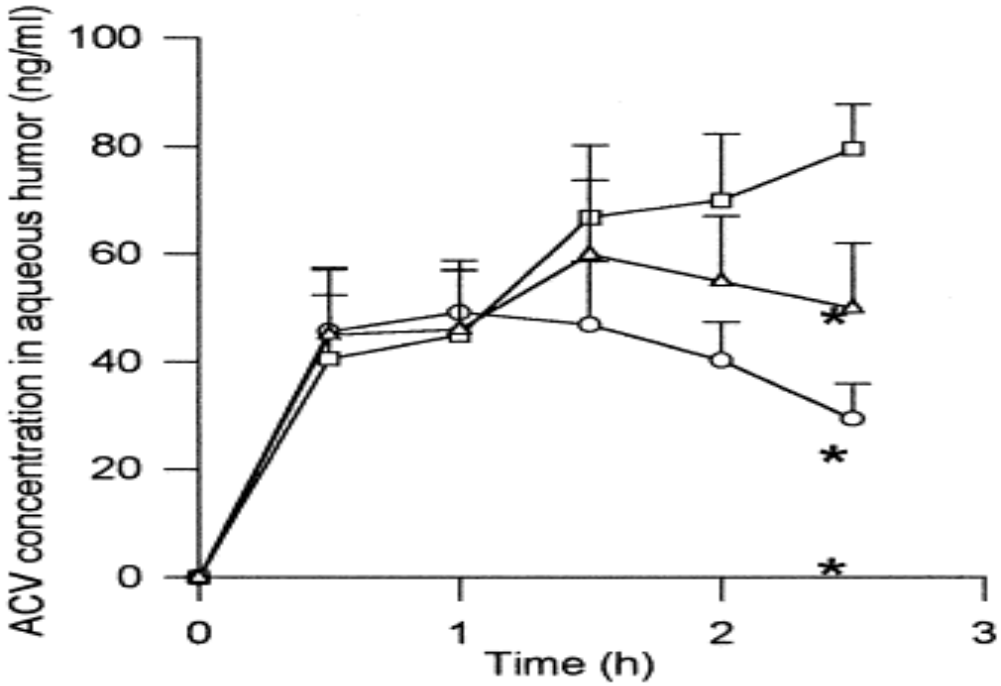

Figure 12. ACV concentrations in aqueous humor after topical administration of ACV solution and ACV-containing liposomes: ACV solution (circles), positively charged liposomes (squares), negatively charged liposomes (triangles). * represents significant difference; $p < 0.05$ ($n = 6$). Reproduced with permission from reference [73].

anterior segment of the eye, efforts are mainly put toward improving precorneal residence time by incorporating positively charged lipids or mucoadhesive polymer in liposomes. The positively charged liposomes, i.e. cationic liposomes have exhibited better efficacy in ocular delivery than negatively charged and neutral liposomes due to binding with negatively charges of corneal surface. Didodecyldimethylammonium bromide, stearylamine, and *N*-(1-(2,3-dioleoyloxy)propyl)-*N*,*N*,*N*-trimethylammonium chloride (DOTAP) are commonly employed for fabricating cationic liposomes.

Acyclovir loaded cationic and anionic liposomes were prepared by incorporating stearylamine and dicetylphosphate (DP), as cationic and anionic charge-inducing agents, respectively. In rabbit eyes, the acyclovir concentration in the cornea at 2.5 h after topical administration of positively charged liposomes was greater than those of negatively charged liposomes and free acyclovir. ACV concentrations in cornea were 253.3 ± 72.0 ng/g, 1093 ± 279 ng/g and 571 ± 105 ng/g for ACV solution, ACV loaded positively and negatively charged liposomes, respectively. Also, the extent of ACV absorption through cornea was higher from positively charged liposomes which can be observed from ACV concentrations in aqueous humor at 2.5 h after instillation (**Figure 12**). The suggested reason was the higher binding of positively charged liposomes with negatively charged corneal surface via electrostatic interaction which ultimately lead to an increase of residence time and increase in acyclovir absorption (221). In another study, when Coenzyme Q_{10} (CoQ_{10}) loaded liposomes was coated with mucoadhesive trimethyl

chitosan, there was a 4.8-fold increase in the precorneal residence time in the rabbit eye was observed (222).

For posterior segment delivery, liposomes development is more focused toward improving half-life of drug by lessening clearance from vitreous humor, protecting labile molecules such as peptides and oligonucleotides from degradation and providing sustained drug release (157, 223, 224). For instance, the vitreal half-life of fluconazole in rabbit eye was increased from 3.08 h to 23.40 h after formulating into liposomes (224). In another study, tacrolimus loaded liposomes were developed for the treatment of uveoretinitis. Following single intravitreous administration, tacrolimus vitreous level above 50 ng/mL was sustained for 14 days. The tacrolimus liposomal formulation demonstrated more effectiveness in suppressing uveoretinitis relative to drug alone and there was also reduced toxicity to inner retinal cells (225). Several liposomal formulations for ocular drug delivery are being exploited, few are in pre-clinical and clinical study stage and few are commercially available. Visudyne® and Tears Again® are the examples of commercially available liposomal formulations for the treatment of ocular diseases. Visudyne® (QLT Ophthalmics, Inc., Menlo Park, CA, U.S.) is a liposomal formulation containing photosensitizer, verteporfin. It is used in photodynamic therapy for subfoveal choroidal neovascularization in age related macular degeneration, presumed ocular histoplasmosis and pathological myopia (226). Tears again® (Optima Pharmaceutical GmbH, Germany) is a phospholipid liposomes spray approved for the treatment of the dry eye syndrome. In clinical

studies, this liposomal spray demonstrated significant advantages when compared with triglyceride-containing eye gel and a balanced salt solution (227, 228).

Dendrimers

Dendrimers are characterized as nanosized, highly branched, star shaped polymeric systems. These branched polymeric systems are available in different molecular weights with terminal end amine, hydroxyl or carboxyl functional group. The terminal functional group may be utilized to conjugate targeting moieties (229). Dendrimers are being employed as carrier systems in drug delivery. Selection of molecular weight, size, surface charge, molecular geometry and functional group are critical to deliver drugs. The highly branched structure of dendrimers allows incorporation of wide range of drugs, hydrophobic as well as hydrophilic. In ocular drug delivery, few promising results were reported with these branched polymeric systems (156, 230, 231). Poly (amidoamine) (PAMAM) dendrimers are widely employed in ocular drug delivery (230). Vandamme et al. demonstrated application of PAMAM dendrimers as ophthalmic vehicles for delivery of pilocarpine nitrate and tropicamide, for miotic and mydriatic activity (232). In this study, mean ocular residence time for fluorescein in saline and in PAMAM solutions was studied in rabbit eye. Fluorescein in 0.2% w/v Carbopol solution was used as reference bioadhesive polymer. The mean ocular residence time was significantly higher in case of PAMAM solutions and 0.2% w/v Carbopo1 solution compared to saline. Therefore, the use of dendrimers could be another option for increasing ocular

.

Table 2. Recent advancements in liposomal ocular drug delivery.

Drug	Type of Liposomes	Result	Ref.
Acetazolamide	Multilamellar, Unilamellar	Multilamellar liposomes produced a more significant lowering in IOP in comparison with REVs liposomes.	(233)
Ciprofloxacin (CPX)	Multilamellar	The mean residence time of ciprofloxacin was three fold higher for the CS-coated liposomes (3.85 h) compared to commercially available eye drops Ciprocin® (1.39 h).	(234)
Cytochrome C		The cytochrome C loaded freeze-dried liposomes exhibited significant efficacy in retarding the onset and progression of cataract formation in rat eye.	(235)
Vasoactive intestinal peptide (VIP)	Pegylated liposomes	After intravitreal injection, VIP concentration in ocular fluids was 15 times higher for liposomal formulation (155 ± 65 ng/ml) than the solution (10 ± 1 ng/mL), at 24 h.	(236)
Coumarin-6	Multilamellar	After topical administration in mice, the intensity of coumarin-6 in the retina was much higher with PLL (poly-L-lysine) modified liposomes.	(237)
Bevacizumab (Avastin)		Vitreous concentration of bevacizumab after 42 days of administration was 16 and 3.3 µg/mL in the eyes for	(238)

Drug	Type of Liposomes	Result	Ref.
Bevacizumab (Avastin)		liposomal and non-liposomal bevacizumab, respectively. The AUC (conc. Vs time) for liposomal bevacizumab was 1.5 fold higher compared with non-liposomal bevacizumab.	(238)
Fluorescence probe (Coumarin-6)	Submicron-sized liposomes(ssLips) and multilamellar	After topical instillation of submicron-sized liposomes (ssLips), drug was delivered to the posterior segment ocular tissues including retina.	(239)
Fluconazole		Antifungal activity of fluconazole in liposomal formulation was better than that of fluconazole solution.	(240)
Edaravone	Submicron-sized liposomes	Topical administration of edaravone-loaded ssLips protected retina against light-induced dysfunction in mice eye while there was no marked protection found in the group treated with free edaravone.	(241)
Diclofenac	Multilamellar	Topical administration of diclofenac loaded PVA-R modified liposomes lead to improved retinal delivery in rabbit eye. Concentration of diclofenac in the retina–choroid was enhanced by 1.8-fold in case of drug loaded PVA-R modified liposome compared to that of the diclofenac solution.	(242)

residence time and therapy enhancing ocular bioavailability and achieving better therapeutic outcomes. For instance, PAMAM dendrimers when co-administrated with pilocarpine nitrate and tropicamide showed higher miotic and mydriatic activity in albino rabbits (232).

In order to avoid scar tissue formation after glaucoma filtration surgery, conjugates of modified PAMAM dendrimers with glucosamine (DG) and glucosamine 6-sulfate (DGS) were synthesized to exert immunomodulatory and anti-angiogenic activities, respectively. The subconjunctival administration of these modified conjugates in rabbit model of glaucoma filtration surgery have shown significant inhibition of pro-inflammatory and pro-angiogenic responses and consequently reduced scar tissue formation. The results obtained from the experiment indicated that the ocular administration of DG and DGS might be effective and safe in clinical practice in avoiding scar tissue formation post glaucoma filtration surgery (243).

In-Situ Gelling Systems

In-situ hydrogels refer to the polymeric solutions which undergo sol-gel phase transition to form viscoelastic gel in response to environmental stimuli. Gelation can be elicited by changes in temperature, pH and ions or can also be induced by UV irradiation. For ocular delivery, research studies have been more focused toward development of thermosensitive gels which respond to changes in temperature (244). Several thermogelling polymers have been reported for ocular delivery which includes poloxamers, multiblock copolymers made of

polycaprolactone, polyethylene glycol, polylactide, polyglycolide, poly *N*-isopropylacrylamide, and chitosan. These thermosensitive polymers form temperature dependent micellar aggregates which gellify after a further temperature increment due to aggregation or packing (245, 246). For drug delivery, these polymers are mixed with drugs in the solution state and solution can be administered which forms an *in situ* gel depot at physiological temperature. These thermosensitive gels demonstrated promising results for enhancing ocular bioavailability for both anterior and posterior segment. Gao et al. have evaluated suitability of thermosensitive gel made of triblock polymer PLGA-PEG-PLGA (poly-(DL-lactic acid co-glycolic acid)–polyethylene glycol–poly-(DL-lactic acid co-glycolic acid) as a ocular delivery carrier for dexamethasone acetate (DXA) (247). It was formulated as either 0.1% w/v DXA solution or 0.1%, w/v DXA in 20% PLGA–PEG–PLGA *in situ* gel forming solution and administered topically in rabbit eye. Following topical administration, the C_{max} of DXA in the anterior chamber was significantly higher for the PLGA–PEG–PLGA solution (125.2 μg/mL) relative to the eye drop (17.6 ± 2.18 ng/mL) along with higher AUC values. The increment in both C_{max} and AUC was approximately 7- and 7.98-fold for PLGA–PEG–PLGA *in situ* gel compared to the solution eye drops. These results suggest potentiality of PLGA–PEG–PLGA thermosensitive gel forming solution in enhancing ocular bioavailability.

Rieke, et al. have reported applicability of ReGel™ (biodegradable and thermosensitive triblock copolymer consisting of poly(lactic-*co*-glycolic acid) (PLGA) and polyethylene glycol (PEG), in providing sustained release of a large

molecule ovalbumin to the choroid and retina following subconjunctival administration in the rat eye (248). The ovalbumin concentrations were maintained at measurable levels in the sclera, choroid, and retina of rats over a period of 14 days. These results suggest feasibility of thermosetting gel system in providing sustained delivery of macromolecules to the posterior segment ocular tissues such as choroid and retina. Cross linked polyN-isopropylacrylamide (PNIPAAm)-polyethylene glycol diacrylate hydrogels were also synthesized for sustained release of macromolecules such as bovine serum albumin (BSA) and immunoglobulin G (IgG) (249). The gel system has provided nearly 3 week of sustained BSA release under *in vitro* condition. The results of research studies clearly signify the advantages of thermosensitive gels in providing sustained drug release; prolong contact time of drugs with the cornea, less frequency of applications, reduced side effects and higher ocular bioavailability over aqueous drops. In conclusion, the thermosensitive gels may be a viable option for the delivery of drugs for treating chronic ocular diseases.

Contact lens

Contact lenses are thin, and curved shape plastic disks which are designed to cover the cornea (250). After application, contact lens adheres to the film of tears over the cornea due to the surface tension. Drug loaded contact lens have been developed for ocular delivery of numerous drugs such as β-blockers, antihistamines and antimicrobials. It is postulated that in presence of contact lens, drug molecules have longer residence time in the post-lens tear film which ultimately led to higher drug

flux through cornea with less drug inflow into the nasolacrimal duct. Usually, drug is loaded into contact lens by soaking them in drug solutions. These soaked contact lenses demonstrated higher efficiency in delivering drug compared to conventional eye drops. Jinah et al. observed much higher bioavailability of dexamethasone (DX) from poly hydroxyethyl methacrylate (PHEMA) contact lenses in comparison to eye drops (251). Indeed, efficient than topical drops, these soaked contact lenses suffers from disadvantages of inadequate drug loading and short term drug release. To overcome these obstacles, particle-laden contact lenses and molecularly imprinted contact lenses have been developed. In particle-laden contact lenses, drug is first entrapped in vesicles such as liposomes, nanoparticles or microemulsion and then these vesicles are dispersed in the contact lens material. Chauhan et al. developed particle-laden contact lenses for ocular delivery of lidocaine. In two different studies, they have prepared particle-laden contact lenses by dispersing lidocaine loaded microemulsion drops or liposome in poly-2-hydroxyethylmethacrylate (p-HEMA) hydrogels. Results of both the studies demonstrated the extended release of lidocaine over a period of eight days (252, 253). Indeed, particles-laden contact lenses look promising for extended ocular drug delivery; it needs to be stored in drug saturated solutions to avoid drug loss during storage. The designing of stimuli responsive such as pH or temperature sensitive 'smart' particles which can release drug only in the eye could eliminate this problem. The imprinted contact lenses have also showed benefit in terms of both drug loading and drug release (254). It has been demonstrated that soft contact lenses fabricated by the molecular imprinting method have 1.6 times higher timolol

loading capacity than the contact lenses prepared by a conventional method and also provided sustained timolol delivery (255). In another study, ketotifen fumarate loaded imprinted lenses have revealed higher tear fluid bioavailability compared to drug soaked lenses or ketotifen fumarate marketed eye drops. The relative bioavailability for the imprinted lenses was three times greater than that of non-imprinted lenses. The AUC value of ketotifen fumarate for imprinted lenses, non-imprinted lenses and eye drops were 4365 ± 1070 μg hr/mL, 493 ± 180 μg hr/mL, 46.6 ± 24.5 μg hr/mL, respectively (256). The results clearly demonstrate more effectiveness of imprinted lenses over non-imprinted lenses and eye drops.

Implants

Intraocular implants are specifically designed to provide localized controlled drug release over an extended period. These devices help in circumventing multiple intraocular injections and associated complications (257, 258). Usually for drug delivery to posterior ocular tissues, implants are placed intravitreally by making incision through minor surgery at pars plana which is located posterior to the lens and anterior to the retina. Though implantation is invasive procedure, these devices are gaining interest due to their associated advantages such as sustained drug release, local drug release to diseased ocular tissues in therapeutic levels, reduced side effects and ability to circumvent blood retina barrier (258, 259). Several implantable devices have been developed for ocular drug delivery especially for the treatment of chronic vitreoretinal diseases.

Ocular implants are available as biodegradable and non-biodegradable drug releasing devices. Non-biodegradable implants offer long-lasting release by achieving near zero order release kinetics (259). Polymers such as polyvinyl alcohol (PVA), ethylenevinyl acetate (EVA), and polysulfone capillary fiber (PCF) are being employed for fabricating non-biodegradable implants (257). Vitrasert® and Retisert® are the examples of marketed non-biodegradable implants.

Vitrasert® (Bausch & Lomb Inc., Rochester, NY, U.S.) is a controlled-release intraocular implant of ganciclovir approved by FDA for the treatment of AIDS associated CMV retinitis. It is composed of a ganciclovir tablet of 4.5 mg surrounded by PVA/EVA that slowly release the drug over an extended period of 5-8 months. The device provides long term sustained release without systemic toxicity at reduced cost (257, 259, 260).

Retisert® (Bausch & Lomb Inc., Rochester, NY, U.S.) is approved by FDA for the treatment of chronic uveitis which affects the posterior segment of the eye. It is the first marketed silicone laminated PVA implant. The implant provides sustained release of fluocinolone acetonide up to three years. The implant had effectively controlled inflammation, reduced uveitis recurrences and improved vision acuity. The associated side effects are cataracts and elevated IOP (259-262). Long term drug release may be achieved with these non-biodegradable implants but are associated with certain short comes. These devices have to be surgery implanted and removed after drug depletion, which makes the treatment expensive and patient non-compliance. Also, adverse events such as endophthalmitis,

pseudoendophthalmitis, vitreous haze and hemorrhage, cataract development and retinal detachment limit their applications.

Another category of ocular implant includes biodegradable implants. These implants are gaining much attention and are being studied at large due to their biocompatible property and sustained drug release properties. Because of biodegradable nature, these implants are not required to be surgically removed which signify a distinctive advantage over the non-biodegradable implants. Polylactic acid (PLA), polyglycolic acid (PGA), poly(lactide-co-glycolide) (PLGA), and polycaprolactones (PCL) are the most commonly used polymers for the fabrication of biodegradable implants (257). Examples of biodegradable implants for ocular delivery include Surodex™ and Ozurdex® which are designed for the sustained delivery of dexamethasone for the treatment of intraocular inflammation and macular edema (ME), respectively (259). Surodex™ (Allergan, Inc., Irvine, CA) composes PLGA and hydroxypropyl methylcellulose (HPMC) enclosing dexamethasone. The implant is inserted in the anterior chamber of eye to control postoperative inflammation in cataract patients. It provides sustained dexamethasone release for a period of 7–10 days with improved anti-inflammatory effect comparable to topical steroid administration (259).

Ozurdex® (Allergan Inc., Irvine, CA) is another biocompatible and biodegradable intravitreal implant. It was approved by FDA in June 2009 for the treatment of macular edema. It employs Allergan's NOVADUR® technology for delivering dexamethasone. The NOVADUR® system contains a PLGA polymer matrix which degrades slowly to lactic acid and glycolic acid allowing prolonged

release of dexamethasone up to six months. Randomized clinical trials have demonstrated its potency in reducing vision loss and improving vision acuity in eyes with macular edema associated with branch retinal vein occlusion (BRVO) or central retinal vein occlusion (CRVO). Also, clinical studies with Ozurdex® for treatment of diabetic retinopathy, and Irvine-Gass syndrome proved it as a promising treatment and drug delivery candidate (259).

Microneedles

Microneedle based technique is an emerging and minimally invasive mode of drug delivery to posterior ocular tissues. This technique may provide efficient treatment strategy for vision threatening posterior ocular diseases such as age related macular degeneration, diabetic retinopathy and posterior uveitis. This new microneedle based administration strategy may reduce the risk and complications associated with intravitreal injections such as retinal detachment, hemorrhage, cataract, endophthalmitis and pseudoendophthalmitis. Moreover, this strategy may help to circumvent blood retinal barrier (BRB) and deliver therapeutic drug levels to retina-choroid. Microneedles are custom designed to penetrate only hundreds of microns into sclera, so that damage to deeper ocular tissues may be avoided. These needles help to deposit drug or carrier system into sclera or into the narrow space present between sclera and choroid called "suprachoroidal space" (SCS). Puncturing of sclera and depositing drug solution or carrier systems in sclera or SCS may facilitate diffusion of drug into deeper ocular tissues, choroid and neural retina (263). For intraocular delivery of drugs, Jason, J et al. investigated the application of

microneedles surface coated with drugs. Cadaver eyes were used to evaluate the role and scleral penetration of microneedle and intrascleral dissolution of microneedle surface coated drug (sulforhodamine). Results demonstrated that surface coated drug was rapidly dissolved in scleral tissue indicating high scleral sulforhodamine deposition within microneedle hole. In another study, Jiang et al. made attempts to evaluate the performance of microneedles to infuse drug solutions, nanoparticles and microparticles into scleral tissues. By use of microneedles, authors were able to infuse approximately 10-35 μL of fluid in to tissues. Nanoparticle suspensions and microparticles were also delivered into sclera by microneedles however; microparticles were delivered only in the presence of collagenase spreading enzymes and hyaluronidase. Study demonstrated that hollow microneedles may be employed for scleral infusion of drug or micro/nanoparticles with minimal invasive route (264).

In another study Patel, et al. made attempts to deliver drug solution, nanoparticles and microparticles in the SCS of rabbit, pig, and cadaver eyes with microneedles. Authors hypothesized that microneedle based minimally invasive strategy may help to deliver high level of both drug and nanocarriers to retinal tissues from SCS. Parameters for suprachoroidal delivery with microneedles such as microneedle length, pressure, and particle size were studied and optimized. Results demonstrated the strategy to be safe, minimally invasive and may sustain drug release. But, the study did not provide any evidence of drug reaching the inner retinal tissues from SCS (265). Same group made further attempts to study *in vivo* pharmacokinetics of SCS deposited solution/suspension post microneedle infusion.

Results demonstrated that microneedle may provide a safe, reliable and targeted approach to chorio-retinal tissues (265).

Conclusion

Human eye is one of the most complex, sensitive and highly protected organs in the body after brain and testicles. Being direct contact with external environment this organ is highly vulnerable for injury and consequently impervious to exogenous chemicals. Moreover, excessive tear production, in response to external stimuli or therapeutic agents, increased blinking rate adds to its protection. These naturally developed protective functions act as a barrier to externally applied drugs, especially when these are targeted to back-of-the-eye tissues. Expression of drug efflux pumps at cellular level impedes drug entry into the diseased cell and therefore poses severe challenges to ocular drug delivery. The physico-chemical properties of the drug and delivery system can be modulated depending on the targeted eye tissue. For the back of eye delivery, various routes of drug administration such as periocular injections/implants are effectively employed to overcome ocular static and dynamic barriers. Administration of drug solutions as topical drop with conventional formulations was associated with certain drawbacks which initiated the introduction of different carrier systems for ocular delivery. Tremendous efforts are being put into ocular research toward the development of safe and patient compliant novel drug delivery strategies. Currently, researchers are thriving hard to improve *in vivo* performance of conventional formulations. On the other hand, advent of nanotechnology, new techniques, devices and their

applications in drug delivery is developing immense interest to ocular scientists. Drug molecules are being encapsulated into nanosized carrier systems or devices and are being delivered by invasive/non-invasive or minimally invasive mode of drug administration. Several nanotechnology based carrier systems are being developed and studied at large such as nanoparticles, liposomes, nanomicelles, nanosuspensions and dendrimers. Nanotechnology is benefiting the patient body by minimizing the drug induced toxicities and vision loss. Also, these nanocarriers/devices sustain drug release; improve specificity, when targeting moieties are used, and help to reduce the dosing frequency. However, there is still need of developing a carrier system which could reach targeted ocular tissue, including back-of-the-eye tissues, post non-invasive mode of drug administration. With the current pace of ocular research and efforts being made and put in, it is expected to result in a topical drop formulation that retains high pre-corneal residence time, avoids non-specific drug tissue accumulation and deliver therapeutic drug levels into targeted ocular tissue (both anterior and posterior). In near future, this delivery system may replace invasive mode of drug administration to back-of-the-eye such as periocular and intravitreal injection.

Chapter 3

TOPICAL AQUEOUS CLEAR CYCLOSPORINE NANOMICELLAR FORMULATION: OPTIMIZATION, IN VITRO & IN VIVO OCULAR TOXICITY EVALUATION AND PHARMACOKINETIC STUDY

Rationale

CsA is a fungus (*Tolypocladium inflatum)* derived cyclic decapeptide drug. It exerts its mechanism of action by inhibiting T-cell activation and thereby inhibits inflammatory cytokine production. Also, CsA blocks the opening of mitochondrial permeability transition pore and inhibits apoptosis (266). Additionally, CsA has been found to be important in treating allergic inflammation because of its direct inhibitory effects on eosinophil and mast cell activation and release of mediators (267). CsA is also shown to increase the conjunctival goblet cell density (268). However, CsA is a highly lipophilic drug with poor aqueous solubility of 12 ng/mL (269). Two decades ago, the potential of CsA in treating human dry eye (keratoconjunctivitis sicca) was evidenced in several small clinical trials (270, 271). In a dose ranging, randomized and multicenter efficacy and safety trial with topical CsA 0.05% emulsion (Restasis®; Allergan, Irvine, CA) was conducted. CsA emulsion has been shown to be an effective therapeutic agent to treat moderate to severe dry eye disease in clinical trials and leading to US Food and Drug Administration approval of the drug in 2003. The exact mechanism of enhanced tear production is not well delineated but, it is hypothesized that it may be related to CsA immunomodulatory activity, which reduces local inflammation (272).

However, in a recent study it was demonstrated that CsA has no stimulatory effect on lacrimal gland but, it increased reflex tear flow (273).

CsA 0.05% emulsion (Restasis®) has been studied for various other ocular conditions such as uveitis, vernal and atopic keratoconjunctivitis, and posterior blepharitis (274). However, Restasis® induces burning sensation and redness following topical instillation (275). Cationic, anionic and oily CsA emulsions were studied to reduce inflammation, stinging sensation and improve safety and tolerability (276). Cationic CsA emulsions were found to be more tolerable relative to anionic and CsA oil. But, inflammation was observed with topical application of cationic CsA emulsion in rabbits (276). Despite tremendous research in ocular drug delivery, only one topical formulation (Restasis®, Irvine, CA) has been commercialized in US. Since, the rationale of this chapter was to minimize local adverse effects and improve patient's acceptability; an aqueous, clear topical CsA nanomicellar formulation was optimized so that it overcomes ocular barriers and deliver high drug levels to anterior ocular tissues.

Materials and Methods

Critical micellar concentration (CMC) of the individual polymers i.e., HCO-40 (Barnet Product Corp, USA) and a blend of polymer surfactant selected for the preparation of NMF was determined following slight modification of a previously described procedure (277). CMC was determined with iodine as a probe by varying the ratios (wt%) of HCO-40 to Oc-40. Iodine solution (1:2 ratio of I_2 and KI) was added to each polymer solution and was incubated overnight.

Absorbance of hydrophobic iodine, I_2, entrapped in the core of nanomicelle was measured at 366 nm with the help of DDX 880, Beckman Coulter, and multimode detection software version 2.0.012.

HPLC analysis

In vitro analysis of CsA (Xenos Bioresources, CA) was performed by a reversed phase high performance liquid chromatography i.e., (RP-HPLC) method with a Shimadzu HPLC pump (Shimadzu, Shimadzu Scientific instruments, Columbia, MD). Alcott autosampler (model 718 AL), Shimadzu UV/Visible detector (Shimadzu, SPD-20A/20AV, USA), phenyl column (5 µm, 15 x 4.6 mm) thermostatted at 50 ± 1 ºC and Hewlett Packard HPLC integrator (Hewlett Packard, Palo Alto, CA) were assembled. The mobile phase was prepared with acetonitrile (ACN), water and trifluoroacetic acid (TFA) (75:25:0.1% v/v/v), which was set at a flow rate of 1.0 mL/min. Detection wavelength was set at 210 nm. The sample tray temperature was maintained at 4 °C. A volume of 50 µL was injected onto the HPLC column for analysis. All the standards and samples prepared were stored at 4 ºC before and during the analysis.

LC-MS/MS analysis

In vivo analysis of CsA was performed with a reversed phase liquid chromatography tandem mass spectroscopy (LC-MS/MS) method with CsA-d_4 as internal standard (IS). LC-MS/MS comprised a triple quadrupole mass spectrometer with SCIEX API 4000™ (API 4000; Applied Biosystems/MDI

SCIEX) coupled to a liquid chromatography system (Shimadzu LC-10 AD, USA) and reversed phase ACE 5 phenyl column, 50 x 2.1 mm × 5 µm (Advanced Chromatography Technologies, LTD) and a guard column (ACE 5 phenyl, 10 X 2.1 mm, 5 µm (Thermo-Hypersil Keystone). Column temperature was maintained at 70 °C (Eppendorf CH-30 column heater, USA). A gradient mobile phase comprising 20 mM NH_4COOH with 0.1% formic acid as mobile phase A and ACN:MeOH:0.4 M NH_4COOH (90:7.5:2.5, v/v/v, pH = 3.5) as mobile phase B was selected. The mobile phase was pumped at a flow rate of 0.75 mL/min. A sample volume of 25 µL was injected onto HPLC and the analysis run time was 6 min. Analyst® version 1.4.2 (Applied Biosystems-MDS Sciex) operated with Windows® was utilized for data acquisition and peak integrations.

Nanomicellar Formulation (NMF)

CsA loaded NMF was prepared following solvent evaporation and film rehydration method as described previously (278). Briefly, 0.025%, 0.050%, 0.075%, and 0.10% loaded CsA NMF (100 mL) was prepared in two steps: preparation of basic formulation and rehydration. In first step, CsA (0.025%, 0.050%, 0.075%, and 0.10%), HCO-40 (1.0 wt%) and Oc-40 (0.05 wt%) were dissolved separately in ethanol. HCO-40 solution was added with calculated volumes of Oc-40 (diluted in ethanol). This solution was stirred to generate a homogenous solution. To this solution, a calculated volume of CsA solution was added dropwise. The volumes were made up to 15 mL with ethanol. The solvent was removed with high speed vacuum (Genevac, UK); evaporation overnight (~10

h) to obtain a solid thin film. In step two, the resultant thin film was hydrated with 40 mL of double distilled deionized water (pH= 7.0) and resuspended. The rehydrated formulation was added with 10 mL of water and the volume was made up with 2X phosphate buffer solution containing 1.2% of povidone K90 (BASF, Aktiengesellschaft, Ludwigshafen, Germany). Finally, the formulation was filtered with 0.2 μm nylon filter membrane to remove unentrapped drug aggregates and other foreign particulates.

Characterization of Nanomicelles

Determination of critical micellar concentration

Critical micellar concentration (CMC) of the individual polymers i.e., HCO-40 and Oc-40, and a blend of polymer mixture used in the preparation of NMF was determined (N = 3) following a slight modification of previously described procedure (279, 280). CMC was determined with iodine as a probe. Earlier studies demonstrated that CMC values determined with iodine as probe were similar to other methods such as static surface tension and differential refractive index (281). Iodine, I_2, is fairly hydrophobic and particularly insoluble in water. The aqueous solubility of I_2 is improved by adding its salt, potassium iodide, which forms KI_3 solution. When this solution is added to the polymer solution and incubated for sufficient time, pure I_2 from KI_3 partitions into the hydrophobic core of nanomicelles. Iodine partitioning develops a donor-acceptor complex between polymer and I_2 (in aqueous medium) with electron donation by ether oxygen of polyoxyethylene group (281). The micelle entrapped I_2 shows a blue shift from

460 nm to 366 nm in the presence of polymeric surfactant medium. Shift in absorbance is due to the donation of electrons to the vacant σ* orbital of iodine by the ether oxygen of polyoxyethylene group of the polymer. Partitioning of the iodine into the hydrophobic microenvironment/core of nanomicelles causes a rise in iodine absorbance indicates increase in micelle concentration. As the concentration of monomers in the formulation increases, a sudden rise in absorbance will be observed. The point at which the constant absorbance values and the increased absorbance intersect is regarded as CMC. Briefly, thirty different concentrations of the polymer solutions ranging from 1 to $4.5x10^{-5}$ wt% were prepared. Similarly, other blend of polymers were diluted to determine their CMC. Iodine solution was prepared by dissolving 0.5:1 ratio of iodine and potassium iodide in distilled deionized water. Iodine solution was protected from light. The resulting solution was diluted to half of its original concentration with distilled deionized water for further experiments. Iodine solution (25 µL) was added to each polymer solution. All the solutions were incubated at room temperature for 15 hrs in dark. After allowing sufficient incubation time, samples (200 µL) were transferred to 96 well plates. Absorbance of hydrophobic iodine, I_2, entrapped in the core of nanomicelle was measured with the help of DDX 880, Beckman Coulter, and multimode detection software version 2.0.012.

Absorbance/Visual appearance

The optical clarity of all sample solutions was assessed by measuring absorbance at 400 nm with a UV-visible spectrophotometer, (Model: Biomate-3,

Thermo Spectronic, Waltham, MA). One mL of each sample was placed in a cuvette and absorbance was recorded. Distilled deionized water served as the blank/control.

Osmolality and pH

Osmolality was measured with osmometer (The advanced Osmometer Model 3D3, Two technology way, Norwood, Massachusetts, USA). A sample volume of 400 µL was used to measure osmolality. The pH of the samples was measured with Oakton pH meter (Model: pH 510 series, Oakton Instruments, Vernon Hills, IL).

Thermal dissociation temperature

Experiments were carried out to determine the thermal stability of nanomicellar formulations. Glass vials containing samples were kept in water bath with a thermometer inserted inside the vial. Formulations were observed for turbidity and temperature was recorded. A set of 3 samples (N = 3) were used for each experiment.

Nanomicellar regeneration time

After attaining the turbid temperature, samples were allowed to cool down to room temperature. Time taken by the turbid sample to become transparent or to original clear solution state, was recorded.

Nanomicellar size, polydispersity index and surface potential

Mean particle size, size distribution and polydispersity index of the nanomicellar formulations were measured by dynamic light scattering (DLS) (Malvern Zetasizer Nano, Westborough, MA, USA) at a wavelength of 630 nm and temperature of 25 °C. A sample volume of 1000 µL was used for determining the particle size, polydispersity index and surface potential.

Transmission Electron Microscopy

To determine the shapes and surface morphology of CsA loaded nanomicellar formulation transmission electron microscopy (TEM) (TEM: JEOL JEM 1200 EX II Electron Microscope) was utilized. Sample preparation included the grids (Ted pella Inc): glider grids center marked, 300 mesh copper G300. A layer of nitrocellulose and carbon using the evaporator was applied. To fix CsA nanomicelles on the grids, uranyl formate (UF) stain (Pfaltz and Bauer Inc, U01000 lot 115080-3) was used. To prepare a 1% stain, 5 mL of water was boiled and added 37.5 mg of UF. Further the solution was boiled for 5 min and 50 µL of 1 M NaOH was added and continued to boil for 5 mins. The solution was allowed to cool to room temperature and then filtered prior to use. To visualize nanomicelles with TEM, negative staining was applied. Preparation of negative staining is described below.

Negative stain

The grids were etched for 30 sec with SPI supplied Plasma Prep II, then added to 5 microliter of CsA nanomicellar sample on to the grid as a drop and

allowed 30 sec to adsorb onto the grid. It was rinsed 3 times with distilled deionized water and stain was applied for 30 sec. The stain was blotted with filter paper and dried.

Entrapment and Loading Efficiency

To determine CsA entrapment and loading efficiency of the nanomicellar formulation, all the prepared formulations were subjected to entrapment and loading efficiency tests. Briefly, formulations were vortex mixed for homogeneity and one mL was transferred to a fresh (15 mL) falcon tube (Midsci, USA). Each formulation was lyophilized to obtain a solid at the bottom of falcon tube. The solid was suspended in 1mL of organic solvent (dichloromethane) to generate reverse micelles which release the drug into the external organic phase. The organic solvent was evaporated for ~5 h in speed vacuum. The resultant reversed nanomicelles were resuspended in 1mL of HPLC mobile phase consisting of (acetonitrile:water, 1:1 v/v) (dilution factor was taken into account) and further diluted to determine the concentration of active pharmaceutical ingredient (CsA) entrapped in each nanomicellar preparation with RP-HPLC. The entrapment and loading efficiencies of the formulation was calculated with the following equations:

$$\text{Entrapment efficiency} = \frac{\text{(amount of CsA quantified in NMF)}}{\text{Amount of CsA added in the NMF}} \times 100 \qquad \textit{Eq 1.}$$

$$\text{Loading efficiency} = \frac{\text{(amount of CsA quantified in NMF)}}{\text{(Amount of CsA added+amount of polymers used)}} \times 100 \qquad \textit{Eq 2.}$$

(NMF= Nanomicellar Formulation)

Effect of dilution on nanomicellar size

To study the effect of dilution on the size of nanomicellar formulation (NMF), all the formulations were subjected to dilution test. NMF's were diluted with phosphate buffer and the effect on the nanomicelle size from no dilution to 500 times dilutions was studied. The NMF size and polydispersity indices were tested with Malvern Zetasizer and recorded as described earlier.

Proton NMR studies

Nuclear magnetic resonance (NMR) analysis was performed for CsA loaded HCO-40/Oc-40 nanomicelles, ^{1}H NMR spectra were recorded on a Varian 400 MHz spectrometer (Varian, USA) in deuterated water (D_2O) or deuterated chloroform ($CDCl_3$) at room temperature. The prepared placebo and 0.10 % CsA NMF (600 µL) was subjected to lyophylization to obtain dry pellets. The obtained pellets were resuspended in equal volumes (600 µL) of deuterated aqueous and organic solvents as follows: (i) placebo NMFs were resuspended in $CDCl_3$, (ii) 0.10 % CsA NMFs were resuspended in $CDCl_3$ and D_2O, and (iii) CsA drug was dissolved in $CDCl_3$.

Formulation viscosity

To determine the viscosity of all the solutions and formulations conventional glass Ostwald-Cannon-Fenske viscometer (Fisher Scientific, USA) was selected. Briefly, viscometer was filled from one end with sufficient volumes of water/buffer/placebo/CsA NMF with extreme care to avoid air bubble formation.

The solution was aspirated from the other end. The time taken by the solution to flow down under gravity was measured and density of the liquid was also determined. The following formula was used to calculate the viscosity.

$vis_{(liq)} = (density_{(liq)} * time_{(liq)} * vis_{(water)}) / (density_{(water)} * time_{(water)})$ *Eq 3.*

Where $vis_{(liq)}$ represents viscosity of the sample, $density_{(liq)}$ represents density of the sample, $time_{(liq)}$ denotes flow time for sample, $vis_{(water)}$ shows viscosity of water, 0.89 centipoise (25° C), $density_{(water)}$ represents density of water (1 g/mL), $time_{(water)}$ denotes flow time for water.

To improve the viscosity of NMF povidone K90 was selected. Earlier studies in our laboratory identified that povidone K90 improved NMF properties (small diameter of NMF and bio-adhesion) in comparison to other viscosity enhancers such as PVP-K-30, hydroxypropyl methyl cellulose, hydroxyethyl cellulose or polycarbophil (194).

Cell culture

Rabbit primary corneal epithelial cells (rPCEC) and human retinal pigment epithelial cells (D407) were cultured according to a previously published protocol from our laboratory (282, 283). In brief, rPCEC cells were grown with culture medium comprising MEM, 10% FBS, HEPES, sodium bicarbonate, penicillin, streptomycin sulfate, and 1% (v/v) nonessential amino acids, adjusted to pH 7.4. D407 cells were grown in a culture medium containing DMEM supplemented with 10% (v/v) FBS (heat inactivated), 29 mM $NaHCO_3$, 15 mM HEPES, 100 mg of

penicillin and streptomycin each, and 1% nonessential amino acids at pH 7.4. Cells in passage numbers between 75 and 80 were employed. Cells were grown at 37 °C, in a humidified atmosphere of 5% CO_2 and 90% relative humidity. Culture medium was replaced every alternate day. Both rPCEC and D407 cells were cultured in flasks, harvested at 80–90% confluency with TrypLE™ Express (a superior replacement for trypsin) (Invitrogen, Carlsbad, CA, USA). Cells were then plated in 96-well plates at a density of 10,000 cells/well and utilized for studies. NMFs (blank and CsA loaded) were resuspended in half the volume of endotoxin free cell culture water (Hyclone Inc, USA) and volume was made up with 2X DMEM medium.

Cytotoxicity studies

To evaluate the toxicity of NMFs, lactate dehydrogenase (LDH) release was conducted on rPCEC for 2h. Also, the toxicity was evaluated on rPCEC and D407 with WST-1 cell proliferation reagent assay. CsA loaded and blank NMF's have been prepared and evaluated for topical ocular delivery. Following topical drop administration, nanomicelles primarily comes in contact with corneal epithelial cells. Therefore, we aimed to test the effect of NMF on rPCEC cells.

Cell proliferation assay

Cell viability assay was performed to determine the toxicity of CsA NMF on rPCEC and D407 cells. Briefly, 10,000 cells/well were plated into 96-well plates. NMFs (blank and CsA loaded) were prepared in serum free cell culture

media and filtered with 0.2 µm sterile nylon membrane filters under laminar flow. Cells were exposed to 100 µL of placebo (blank/empty) and CsA (0.025%, 0.05%, 0.075% and 0.1%) loaded NMFs for 1h. In these experiments cell culture medium and 10% triton X-100 served as negative and positive controls, respectively. Percent viable cells were calculated using the Premixed WST-1 cell proliferation reagent according to manufacturer's protocol (Clontech, Mountain View, CA). Percent cytotoxicity of the placebo and CsA loaded NMF's was calculated.

Lactate Dehydrogenase (LDH) assay

In vitro plasma membrane damage assay for blank and CsA loaded NMFs was conducted on rPCEC cells and quantitatively measured with Takara LDH cytotoxicity detection Kit (Takara Bio Inc, CA, USA). rPCEC cells were grown on 96-well plates and added 100 µL of serum free cell culture medium, 100 µL of blank and CsA loaded NMFs. Cells were incubated for 2h at 37º C. In this assay, cell culture media and 10% Triton-X 100 served as negative and positive controls, respectively. After 2h incubation, the plate was centrifuged and the amount of formazan formed in supernatant was measured with a 96-well micro titer plate reader absorbance set at 490 nm.

$$\% \text{ Cytotoxicity} = \frac{\text{Observed experimental value - cell culture medium value}}{\text{TritonX-100 - cell culture medium value}} * 100 \qquad \textit{Eq. 4}$$

Stability of CsA NMF

Stability studies were conducted for 0.1% CsA NMF following international conference on harmonization (ICH) guide lines at 5 ºC, 25 ºC/60%

relative humidity (RH) and 40 ^{o}C/75% RH. Samples were withdrawn at predetermine time points for one months. Drug concentration, NMF size and polydispersity index were determined following the method described earlier. In these studies placebo or blank formulation served as control.

In vivo studies

Animals

Adult female New Zealand albino rabbits weighing between 2.0 and 3.0 kg were obtained from Charles River (Durham, North Carolina, USA). This research was conducted under aseptic conditions strictly under the regulation of ARVO statement for the use of animals in ophthalmic and vision research. Animals were acclaimed for 7 days under Photoperiod: 12 hrs light/12 hrs darkness and at a temperature of 68 ± 2 °F. Animals were allowed for *ad libitum via* water bottles with sipper tubes and were provided with Hi Fiber Rabbit Diet. Protocol for performing all the surgical procedure was also approved by Institutional Animal Care and Use Committee (IACUC) of the North Carolina State University.

Randomization and Study Identification

Animals were randomly assigned to four study groups by stratified body weight according to facility Standard Operating Procedures (SOPs). Animals were uniquely identified by an ear tattoo and a corresponding cage card number. Animal treatment and group assignment are presented in **Table 3**.

Table 3. Rabbit identification and groups

Treatment	Group #	Tissue Processing
0.1% CsA with HCO-40 pH 7.0 (OD); BSS (OS)	2	Histopathology
0.1% CsA with HCO-40 pH 7.0 (OD); BSS (OS)	2	Histopathology
0.1% CsA with HCO-40 pH 7.0 (OD); BSS (OS)	2	Drug levels
0.1% CsA with HCO-40 pH 7.0 (OD); BSS (OS)	2	Drug levels
Placebo HCO-40 pH 7.0 (OD); BSS (OS)	6	Histopathology
Placebo HCO-40 pH 7.0 (OD); BSS (OS)	6	Histopathology
Placebo HCO-40 pH 7.0 (OD); BSS (OS)	6	Drug levels

Animals

Studies were conducted in adult New Zealand White rabbits *(Oryctolagus cuniculus)* to determine ocular tissue drug concentrations, whole blood CsA levels and the *in vivo* performance of NMF after topical drop instillation into pre-corneal pocket. Placebo 0.05% CsA and 0.1% CsA loaded NMF were selected for *in vivo* studies. In these studies, Balanced Salt Solution (BSS, Alcon Laboratories, Fort Worth, TX) served as negative control. In another study Restasis® was used as control. Each treatment consisted of 35 µL of placebo/0.05% CsA NMF/0.1% CsA NMF/BSS applied with a calibrated micropipette to the ocular surface of each eye.

Ocular Examination and Irritation Scores

A complete ocular examination, using a slit lamp and indirect ophthalmoscope, was done to evaluate ocular surface morphology, anterior segment and posterior segment inflammation, cataract formation, and retinal changes. Hackett-McDonald ocular scoring (Microscopic Ocular Grading System) of inflammation was recorded. Ocular examination was conducted to determine pre-dose-(pre-study) baseline data for each rabbit, followed by a pre-dose (prior to first daily dose) each day and then 30 min after last dose daily. Ocular tolerability was assessed in BSS control, placebo, and 0.1% CsA NMF treated eyes.

Intraocular Pressure

Intraocular pressure (IOP) was measured in both eyes during the acclimation, then prior to initiation of treatment, and then every 24 hours for 5 days, an hour after the last treatment on each day. The measurement was done without use of topical anesthetic. The tip of the Tonovet tonometer probe was directed to contact the central cornea and 6 measurements were made consecutively. After the six measurements, IOP shown on the display was recorded. Prestudy IOPs were done at the same time of day that the post-treatment IOPs were conducted.

Electroretinography

Electroretinography (ERG) was performed prior to the study during acclimation and on day 4 of treatment, an hour after the last treatment. All animals were dark adapted for 15 minutes prior to ERG. Whole field ERGs were recorded from the right eye once during acclimation and on the day of euthanasia. A monopolar contact lens electrode (ERG-jet, La Chaux des Fonds, Switzerland) was placed on the cornea to serve as an active electrode. A subdermal electrode at the lateral canthus served as the indifferent electrode. A Barraquer eyelid speculum was placed to maintain open eyelids and a subdermal needle electrode was inserted dorsally as the ground electrode. ERGs were elicited by brief flashes at 0.33 Hz delivered with a mini-ganzfeld photostimulator (Roland Instruments, Wiesbaden, Germany) at maximal intensity. Twenty responses were amplified, filtered, and averaged (Retiport Electrophysiologic Diagnostic Systems, Roland Instruments, Wiesbaden, Germany).

Single dosing

To study CsA concentrations in the individual ocular tissues or fluids with single topical drop administration, animals were divided into three groups (BSS, placebo and 0.1% CsA NMF) with two animals per group. Rabbits were manually restrained and upper eyelid was gently elevated to expose the cornea. Both eyes were dosed with BSS, placebo, 0.1% CsA NMF (35 μL) without contacting the cornea. The rabbit was then allowed to blink several times to distribute the applied NMF/solution over the eye prior to returning the animal to the cage. After dosing, rabbits were left undisturbed in the cage for 60 mins. Post topical dosing (1h), approximately 3 mL of whole blood was collected. Following blood collection, animals were euthanized with intravenous injection of an AVMA-approved barbiturate-based euthanasia agent (Fatal-Plus™). Eyes were enucleated and were immediately frozen until further processing.

Multiple dosing

Animals were divided into two groups (placebo and 0.1% CsA NMF) with two animals per group. Right eye of the animal was treated with NMF (placebo or 0.1% CsA) and the contralateral eye with BSS. This procedure was repeated 4 x/ day at two hour interval for 5 days. After last dosing on day 5, rabbits were tranquilized and 3 mL of whole blood was collected from the jugular vein. Animals were sacrificed; eyes were enucleated and immediately frozen until further processing.

Ocular Pharmacokinetic studies

Single dose pharmacokinetic studies were conducted in female NZW rabbits. Animals were administered a formulation containing 0.05% or 0.1% CsA in nanomicellar formulation, or the formulation vehicle, or Restasis® (0.05% emulsion) to both eyes either as a single dose (single dose phase) or 4 times daily at approximately 2-hour intervals for 7 days (repeat dose phase) **(Table 4)**. An additional group of 3 female rabbits were not treated to serve as pre-dose controls for both study phases. In both phases, the rabbits were examined for clinical signs, specifically including ocular and peri-ocular effects. Intraocular pressure was measured daily (repeat dose phase), and ERGs were recorded during acclimation and then 1-hour post-treatment on Day 6.

Single Dose Phase

In this study phase, two rabbits were administered a single dose of nanomicellar formulation vehicle were euthanized at 0.25 hour post-dose, and 2 rabbits per time point in treated groups were euthanized at 0.25, 1, 4, and 12 h post-dose for assessment of CsA tissue distribution (**Table 4**). Whole blood and ocular tissues, including aqueous humor, vitreous humor, conjunctiva, cornea, lens, iris/ciliary body, retina-choroid, sclera, eyelid, lacrimal gland, and tears were obtained for analysis of CsA concentration.

Table 4. Formulation vehicle, or Restasis (0.05%) to both eyes either as a single dose (single dose phase) or 4 times daily at approximately 2-hour intervals for 7 days (repeat dose phase)

Group	No. of Animals Per Group	Formulation Administered (Bilateral)[a]	Matrices Collected	Sample Times
1b	3	None	Tear, blood, ocular tissues, histophathology samples	Pre-dose (both eyes/animal)
Single Dose			Tear, blood, ocular tissues	
2	2	Vehicle[c]		0.2 h post-dose
3	8	Restasis 0.05%		0.25, 1, 4, and 12 h post dose (both eyes/animal)
4	8	Cyclosporine 0.05%		
5	8	Cyclosporine 0.1%		
Repeat Dose (0, 2, 4, and 6 h each day x 7 days)				
6	4	Vehicle[c]	Tear, blood, ocular tisues (2 rabbits), histopathology samples (2 rabbits)	12 h after the last dose (both eyes/animal)
7	8	Restasis 0.05%	Tear, blood, ocular tissues	0.25, 1, 4 and 12 h after the last dose (both eyes/animal)
8	8	Cyclosporine 0.05%		
9	10	Cyclosporine 0.1%	Tear, blood, ocular tissues (8 rabbits), histopathology (2 rabbits)	

[a]All doses were 35 µL per eye (35 µL of Restasis 0.05%, cyclosporine 0.05% nanomicellar formulation and 0.1% nanomicellar formulation contained 17.5 µg, and 35 µg cyclosporine, respectively). [b]Group 1 served as the pre-dose samples for Groups 2 →9. [c]Vehicle without active contained all excipients but no drug (cyclosporine). [d]Cyclosporine in nanomicellar formulation.

Repeat Dose Phase

In the repeat dose phase, two rabbits per time point were euthanized at 0.25, 1, 4, and 12 hours after the last dose on Day 7 (**Table 4**) for assessment of CsA tissue distribution. Whole blood, ocular fluids/tissues (aqueous humor, vitreous humor, conjunctiva, cornea, lens, iris/ciliary body, retina-choroid, sclera, eyelid, lacrimal gland) and tears were obtained for analysis of CsA concentration. Ocular tissues were taken for histopathologic examination from the specified rabbits of the CsA-treated (0.1% CsA) and vehicle-treated groups.

Eyes were dissected while frozen to isolate ocular tissues and to minimize drug diffusion to adjacent tissues during dissection. Dissection was performed on a cooled ceramic tile that was placed on dry ice/isopentane bath to avoid any thawing of the eye during dissection. Care was taken to avoid cross contamination.

Rabbit ocular tissues (conjunctiva, cornea, eyelid, iris-ciliary body, lacrimal gland, lens, retina-choroid and sclera) were homogenized in extraction buffer (20:80 ACN: 50 mM NH_4OAc, pH 4.4). Tissue homogenates were subjected to protein precipitation extraction method with acetonitrile. The supernatant was further extracted using Waters Ostro 96-well plate. Similarly, aqueous and vitreous humors were subjected to protein precipitation CsA extraction method. Methanol was added to aqueous and vitreous humor samples (3:1) and vortex mixed. Samples were then centrifuged and supernatant was transferred to HPLC vials for analysis. Calibration curve was prepared in 3:1 methanol:rabbit aqueous or vitreous humor. CsA and internal standard were extracted from 250 μL of rabbit whole blood

(K_2EDTA) by liquid-liquid extraction using methyl-t-butyl ether (MTBE) after acidification with HCl. The organic extract was then washed with an alkaline solution. After evaporation to dryness and reconstitution, the extracts were analyzed by LC-MS/MS.

Euthanasia and Sample collection

Rabbits were euthanized 1 hour after single dosing and final treatment on day 5. Euthanasia was performed by intravenous injection of an AVMA-approved barbiturate-based euthanasia agent (e.g., Fatal-Plus™). Approximately 3 mL of whole blood was collected with the rabbits tranquilized from the jugular vein. Eyes were removed after euthanasia. Eyes from two animals per group were fixed in modified Davidson's solution, processed for histopathology, stained with H&E, and examined using light microscopy (see **Table 3**). Eyes were also stained with Ki-67 immunostaining as a standard marker of proliferation. Conjunctiva was collected from eyes from two animals from the drug treated groups and one animal from the placebo groups (see **Table 3**). Eyes from these animals were processed for drug levels and were removed and frozen immediately, tissues dissected while frozen (as described below), and stored at -80 ºC until processing. The list of ocular tissues collected included aqueous humor, vitreous humor, cornea, conjunctiva, lens, iris/ciliary body, choroid/retina, and sclera. Eyes were dissected while frozen to isolate ocular tissues and to minimize drug diffusion to adjacent tissues during dissection. Dissection was performed on a cooled ceramic tile that was placed on dry ice/isopentane bath to avoid thawing of the eye during dissection. In order to

prevent transfer of drugs between tissues of each eye, instruments were thoroughly rinsed with saline followed by methanol, followed by saline, and blotted dry. The globe was initially separated in half using a long razor blade (new blade was used for each eye) into a dorsal and ventral half. The frozen aqueous humor was removed first and placed into pre-weighed vials. The cornea sections were removed next, followed by lens, and vitreous. The iris and ciliary body were removed together, followed by the retina and choroid. The remaining sclera sections were then collected.

Rabbit ocular tissues (conjunctiva, cornea, eyelid, iris-ciliary body, lacrimal gland, lens, retina-choroid and sclera) were homogenized in extraction buffer (20:80 ACN: 50 mM NH_4OAc, pH 4.4). Tissue homogenates were subjected to protein precipitation extraction method with acetonitrile. The supernatant was further extracted using Waters Ostro 96-well plate. Similarly, aqueous and vitreous humors were subjected to protein precipitation CsA extraction method. Methanol was added to aqueous and vitreous humor samples (3:1) and vortex mixed. Samples were then centrifuged and supernatant was transferred to HPLC vials for analysis. Calibration curve was prepared in 3:1 methanol:rabbit aqueous or vitreous humor. CsA and internal standard were extracted from 250 μL of rabbit whole blood (K_2EDTA) by liquid-liquid extraction using methyl-t-butyl ether (MTBE) after acidification with HCl. The organic extract was then washed with an alkaline solution. After evaporation to dryness and reconstitution, the extracts were analyzed by LC-MS/MS.

Data and Statistical Analysis

Data for *in vitro* experiments were conducted at least in quadruplicate and the results were expressed as mean ± standard deviation (SD). Statistical comparison of mean values was performed with Student's t-test. A *p-value* of <0.05 was considered to be statistically significant. Parametric normally distributed data (i.e., IOP, ERG) were compared by time point for each group using one-way ANOVA models with Tukey-Kramer post-hoc analysis. For non-parametric data (i.e., clinical scores) Wilcoxon tests were conducted per animal by time point. Differences were considered significant at $P<0.05$. Results and probabilities were calculated using computerized statistical software (JMP 10, SAS Inc. Cary, NC).

Results

CMC

Critical micellar concentration was determined for HCO-40 and polymer blends with iodine as a probe. CMC of HCO-40 was found to be approximately 0.0303 wt%. The other surfactant, Oc-40, generated a CMC value of 0.107 wt% (278) which is greater than the CMC of HCO-40. A combination of the surfactants in varying ratios lowered the CMC value from 0.03 wt% to 0.00707 wt%. The results are presented in **Table 5**. A combination of HCO-40 and Oc-40 at 1.0 wt% and 0.05 wt% resulted in reduced CMC.

Size, polydispersity indices and surface charge

Placebo and CsA loaded nanomicelles presented a size range of 10 nm to 80 nm (**Figure 13A and B**) when measured with DLS. The average 0.1% CsA loaded nanomicellar size was around ~22.4 ± 0.411 nm. All the size determinations for increasing pay load of CsA are provided in **Table 6**. Similarly, all the NMF's were found to carry slight surface negative charge (**Table 6**).

Visual appearance

Visual appearance for all the formulations was found to be clear, transparent and devoid of any particulate matter. Absorbance at 400 nm was measured and results demonstrated that CsA loaded formulations have negligible absorbance.

Transmission Electron Microscopy

The prepared aqueous 0.10 % CsA nanomicellar formulation was clear, extremely small (**Figure 14A**), devoid of any visible particles to naked eye (**Figure 14A** right vial). The formulation appeared to be transparently clear similar to water (**Figure 14A left vial**) and free flowing. TEM images for 0.10% CsA nanomicelles appeared to show smooth surface morphology with spherical shape and no aggregation (**Figure 14B**). The size distribution was visualized at a scale bar of 500 nm (LS3600, 100.0KV, X60). The TEM image is in agreement with the particle size measurement and the size distribution is between 10 nm to 80 nm.

Table 5. Table showing critical micellar concentration for HCO-40, Oc-40 and blend of both in varying ratios. HCO-40 = hydrogenated castor oil-40; Oc-40 = octoxynol-40

HCO-40 and Oc-40 (wt% ratio)				
1.0 : 0	**1.0:0.05**	**0.5:0.5**	**0.05:1.0**	**0.0:1.0**
30.0×10^{-3}	7.07×10^{-3}	7.14×10^{-3}	88.0×10^{-3}	107.0×10^{-3}

Table 6. Nanomicellar average size (nm) and polydispersity indices.

Formulation (wt %)	Size (nm)			Average Nanomicelle size (nm)	St.dev	Polydispersity Index			Average	St.dev
	1	2	3			1	2	3		
Placebo	24.5	24.4	24.6	24.5	0.100	0.164	0.171	0.154	0.163	0.009
0.025	18.3	18.4	18.6	18.4	0.130	0.128	0.135	0.109	0.124	0.013
0.050	20.3	20.6	20.5	20.5	0.147	0.178	0.164	0.185	0.176	0.011
0.075	22.8	22.8	22.9	22.9	0.057	0.191	0.205	0.199	0.198	0.007
0.100	22.9	22.1	22.2	22.4	0.411	0.144	0.144	0.139	0.142	0.003

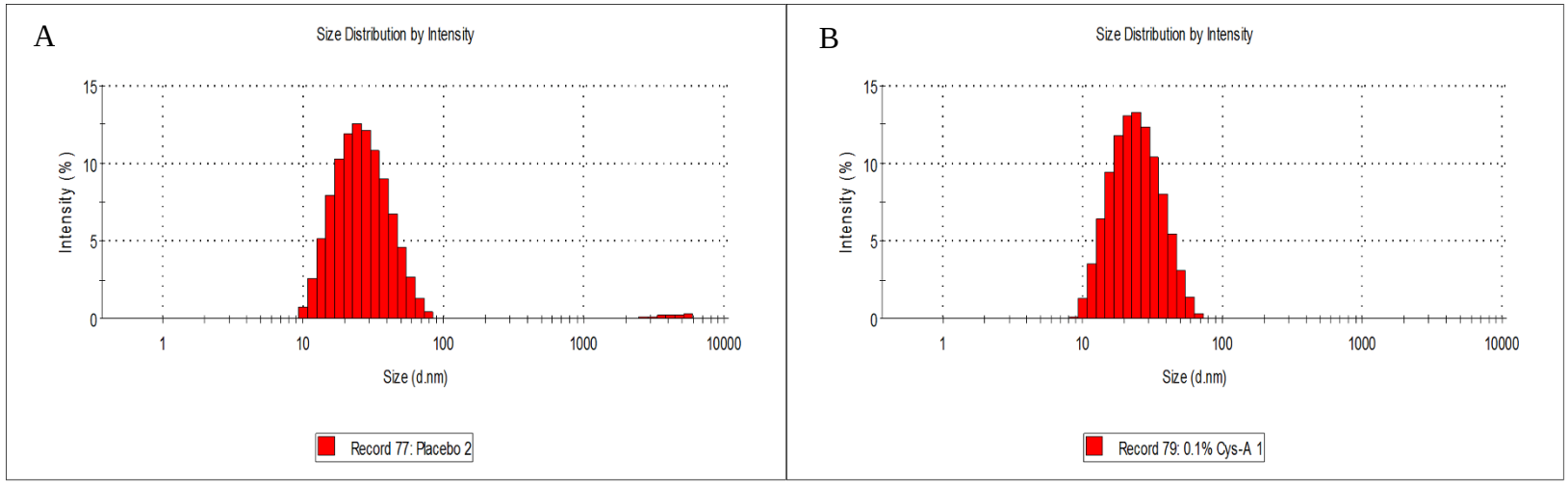

Figure 13. (A) Placebo nanomicellar formulation (B) Cyclosporine-A (CsA) (0.1%) loaded nanomicellar formulation.

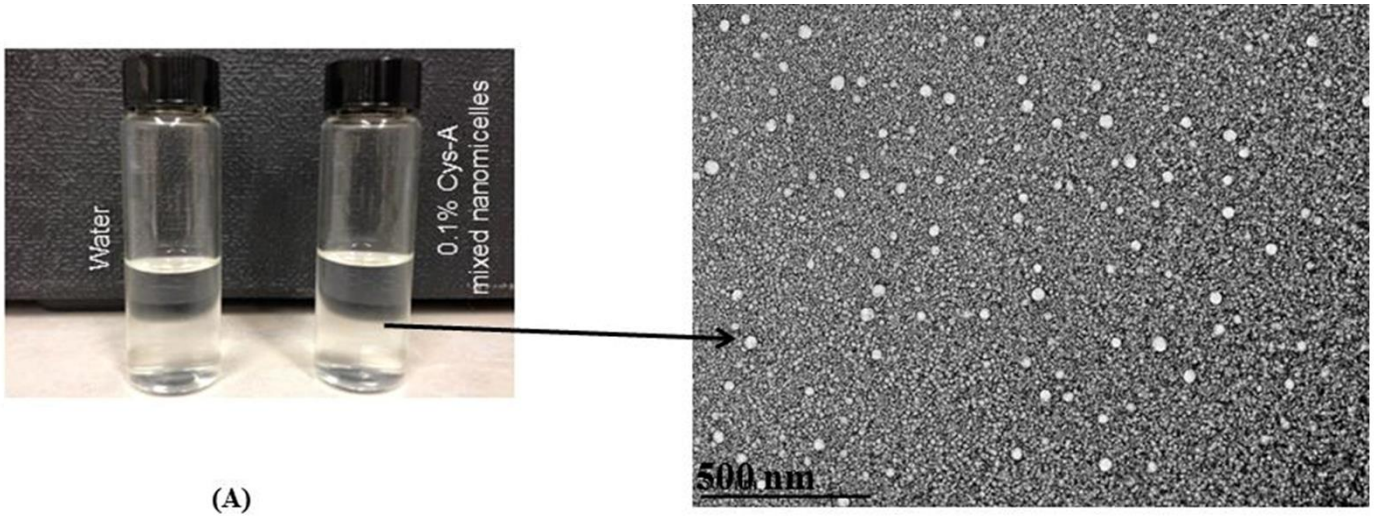

(A)

(B)

Figure 14. (A) Picture showing 0.1% cyclosporine-A (CsA) loaded nanomicellar formulation (right) in comparison to water (left); (B) Transmission Electron Microscopy image for 0.1% CsA loaded nanomicellar formulation.

Thermal dissociation

In general, thermal dissociation temperature (DT) of nanomicellar formulations is about 20-40 ^{o}C higher than formulation containing drug. Low DT of the drug-containing NMF's indicates that drug molecules are incorporated into nanomicelles, and thereby solubilized. With temperature rising above DT, nanomicelles appear to dissociate into individual monomer units. This disruption of nanomicelle structures causes drug release in surrounding aqueous medium. Such destabilization results in the formation of a cloudy or milky white solution. DT of the formulation appears to be high (> 45 °C) which provides stability to the formulation at room temperature (**Table 7**).

Nanomicelle regeneration time

NMF after attaining the DT are allowed to cool to room temperature under ambient room temperature. The time taken for the disappearance of the cloudiness and regeneration of transparent, clear formulation was recorded. This time was recorded as nanomicelle regeneration time (**Table 7**).

Nanomicelle entrapment and loading efficiency

The prepared NMF's were subjected to entrapment and loading efficiency tests by determining CsA concentrations in the nanomicelles after breaking or reverse opening the nanomicelles. The results demonstrated a high entrapment efficiency of > 95% and the loading CsA was improved to 8.85%. The results are summarized in **Table 7**.

Dilution effect

The effect of dilution on the NMF was studied following the size and polydispersity indices. There is no significant effect of size upon dilution with phosphate buffer. However, the polydispersity index was found to be increasing with dilution upto 500 times. Results indicate that the nanomicelles alter size distribution in the formulation. The results are summarized in **Table 8**.

Proton NMR studies

^{1}H NMR spectral analysis results are shown in **Figure 15** through **Figure 18.** In $CDCl_3$, the resonance peaks corresponding to CsA and nanomicelles are observed. However, in D_2O peaks corresponding to nanomicelles are only observed and no peaks for CsA were evident. These results clearly indicate, CsA was entrapped into the inner hydrophobic core of nanomicelles when CsA loaded nanomicelles are suspended in D_2O (**Figure 15 Figure 18**). These results are similar to the dexamethasone and paclitaxel loaded polymeric nanomicelles in D_2O (278, 284).

Formulation viscosity

The rehydrated NMF when resuspended in only 2X phosphate buffer generated viscosity nearly equal to water (0.9 cP). It was earlier reported that higher viscosity does not affect drainage rate unless viscosity exceeds a critical value of about 4.4 cP (285). Therefore, 0.6 wt% of povidone K-90 was added which raised NMF viscosity to 2.0 cP and maintained the viscosity well below critical value.

Addition of povidone K-90 improved the viscosity with negligible effect on flow property of the formulation.

In vitro cytotoxicity

Results with cell proliferation assay indicate that both, rPCEC and D407, cells displayed negligible cytotoxicity after NMF exposure (blank and CsA) and were comparable to negative control (culture medium) (**Figure 19**). On the other hand, triton X-100 exposure significantly reduced rPCEC and D407 cell number to 24% and 25%, respectively relative to blank culture medium. In another set of experiments (LDH assay) on rPCEC cells NMF did not generate any significant release of LDH. The results were again comparable to negative control (culture medium) with negligible effect on cell plasma membrane. The positive control (triton X-100) caused significant release of LDH by damaging the rPCEC cell membrane (**Figure 20**)

NMF stability

CsA loaded NMF were subjected to three different temperatures. Results indicate that NMF was stable for more than one month. No significant difference was observed in NMF size and polydispersity index **(Table 9**). Moreover, CsA concentration was >90% at all three temperatures.

Table 7. Characterization of cyclosporine-A nanomicellar formulations.

CsA formulations (wt%)	**Entrapment Efficiency (%)**	**Loading Efficiency (%)**	**Surface potential (mV)**	**Osmolality (mOsm/kg)**	**Dissociation Temperature (ºC)**	**Regeneration time**	**Absorbance (400 nm)**
Placebo	-	-	-0.039	290	79	33 sec	0.032
0.025	98.2	2.34	-0.251	289	78	30 sec	0.029
0.050	99.1	4.75	-0.157	312	70	3.7 min	0.042
0.075	100.5	6.97	-0.189	333	62	3.6 min	0.028
0.100	97.4	8.85	-0.179	305	47	9.0 min	0.035

Table 8. Effect of dilution on nanomicellar size.

Dilution factor (x)	Z average nanomicellar size (nm)	Polydispersity Index
0	20.80	0.147
10	21.77	0.159
20	23.39	0.215
50	21.81	0.213
100	22.65	0.226
200	26.11	0.329
500	24.52	0.360

Table 9. Cyclosporine-A (CsA) nanomicellar stability at 5 ◦C, 25 ◦C/60% relative humidity (RH) and 40 ◦C at 75% RH.

	Temperature/Relative humidity					
	5 °C		25 °C/60% RH		40 °C/ 75% RH	
Time point (Weeks)	**Average 0.1% CsA nanomicelle size (nm)**	**Polydispersity Index**	**Average 0.1% CsA nanomicelle size (nm)**	**Polydispersity Index**	**Average 0.1% CsA nanomicelle size (nm)**	**Polydispersity Index**
0	17.7	0.156	17.7	0.156	17.7	0.156
1	17.5	0.169	16.3	0.121	15.7	0.107
4	17.4	0.137	15.7	0.1245	15.3	0.082

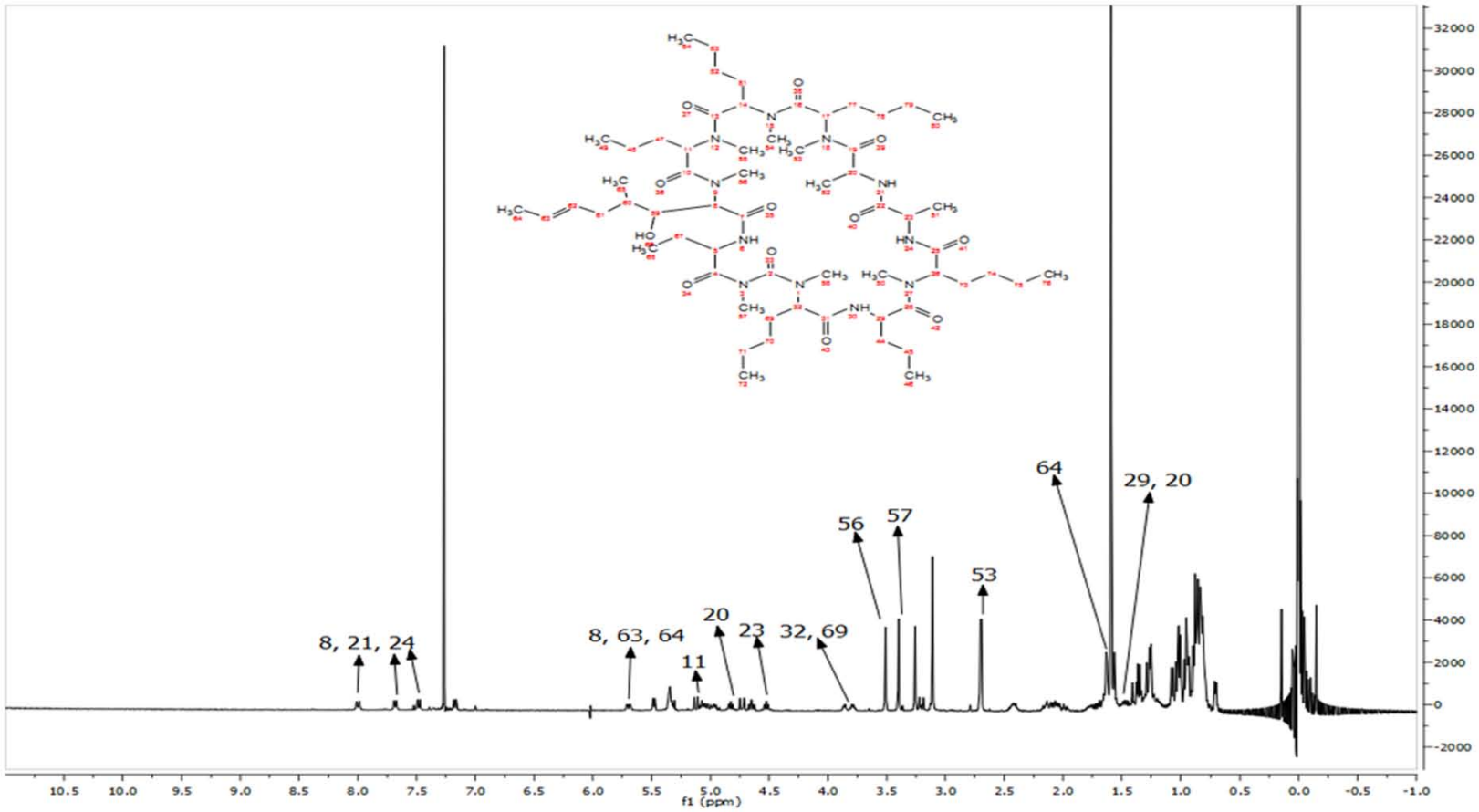

Figure 15. ^{1}H NMR for cyclosporine-A in $CDCl_3$

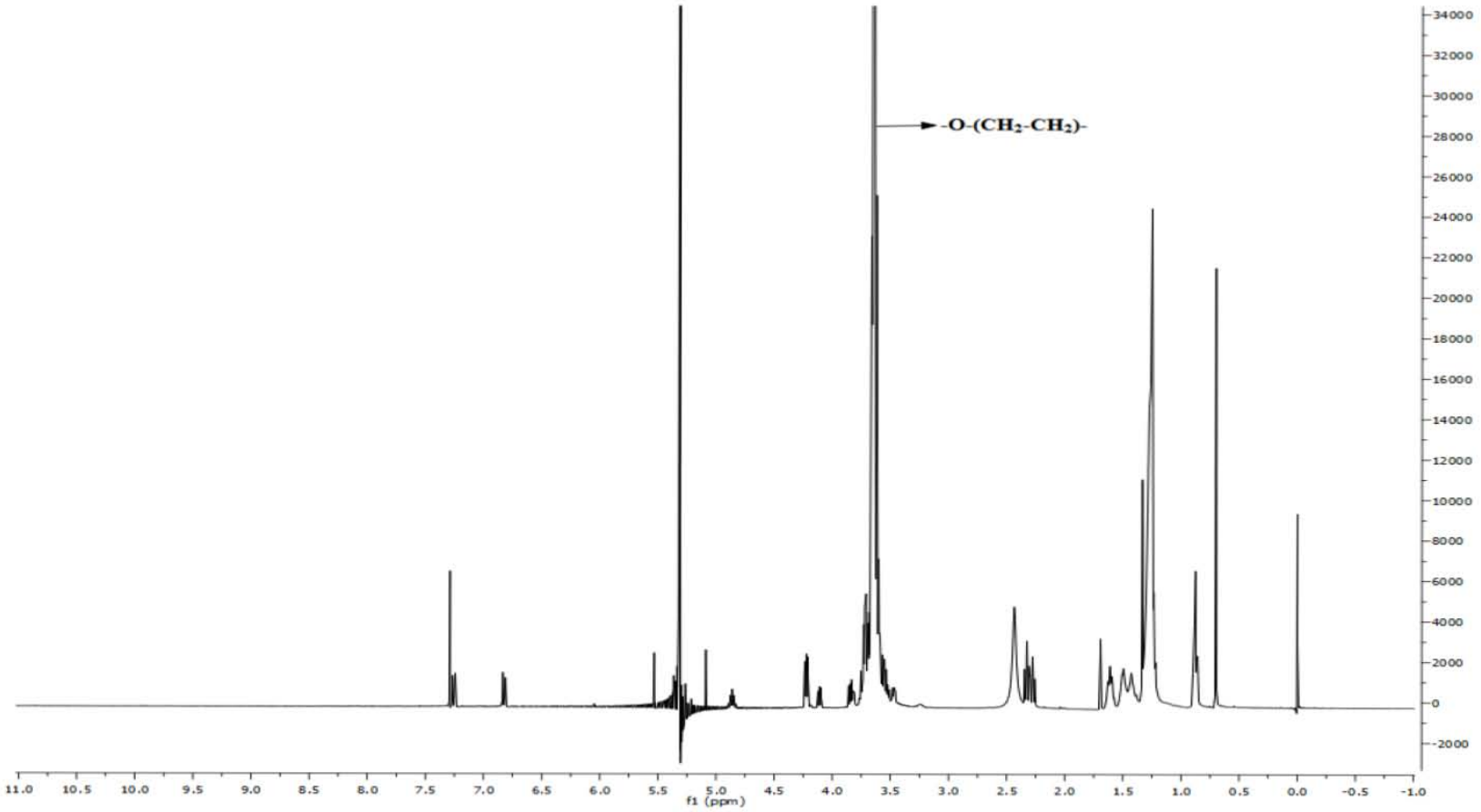

Figure 16. ^{1}H-NMR spectra for placebo or blank nanomicelles

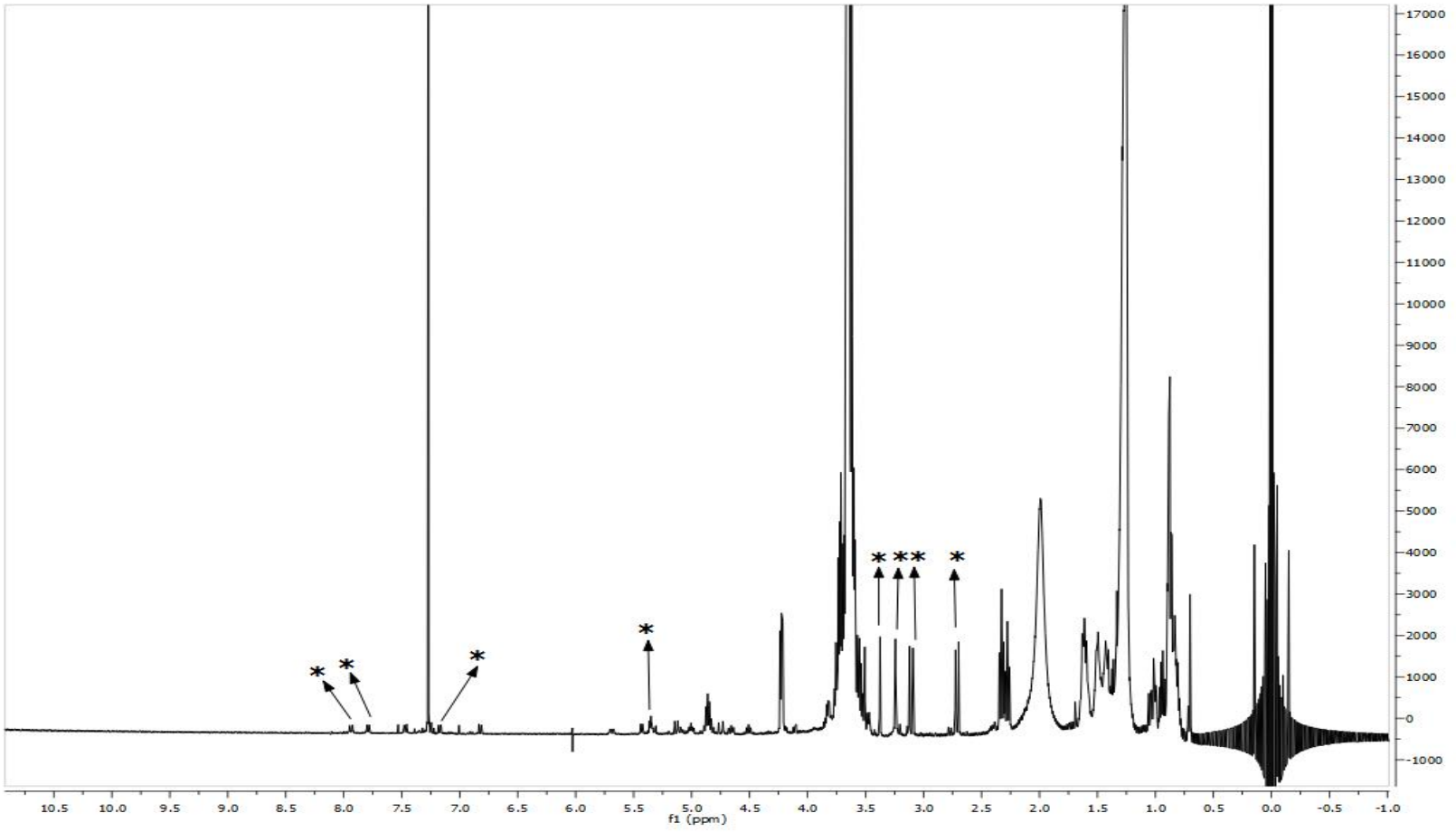

Figure 17. ^{1}H-NMR for cyclosporine-A loaded nanomicelles suspended in $CDCl_3$ (* = cyclosporine-A resonance peaks are evident)

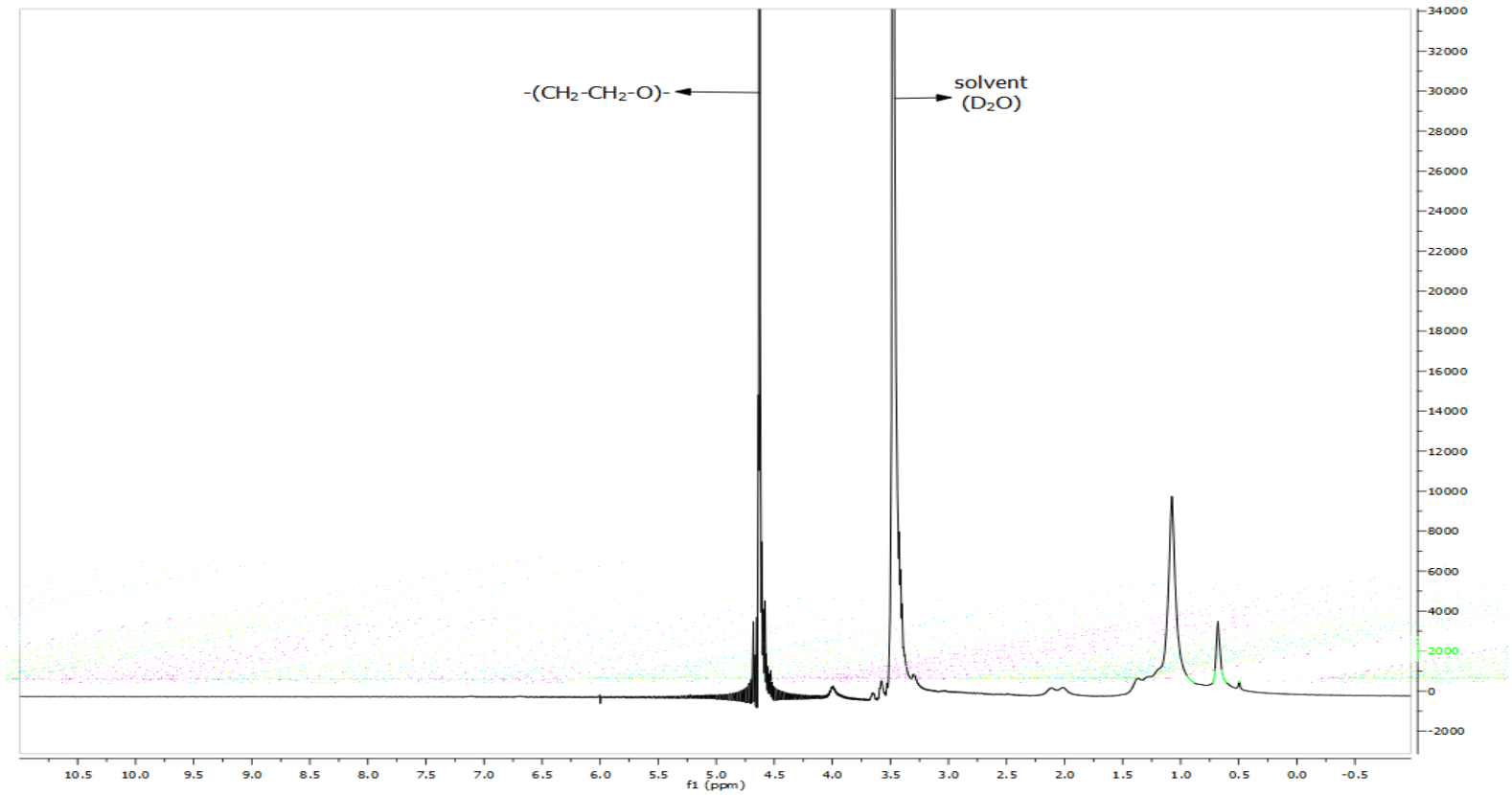

Figure 18. ^{1}H-NMR for cyclosporine-A loaded nanomicelles suspended in D_2O (no resonance peaks are observed/identified for cyclosporine-A).

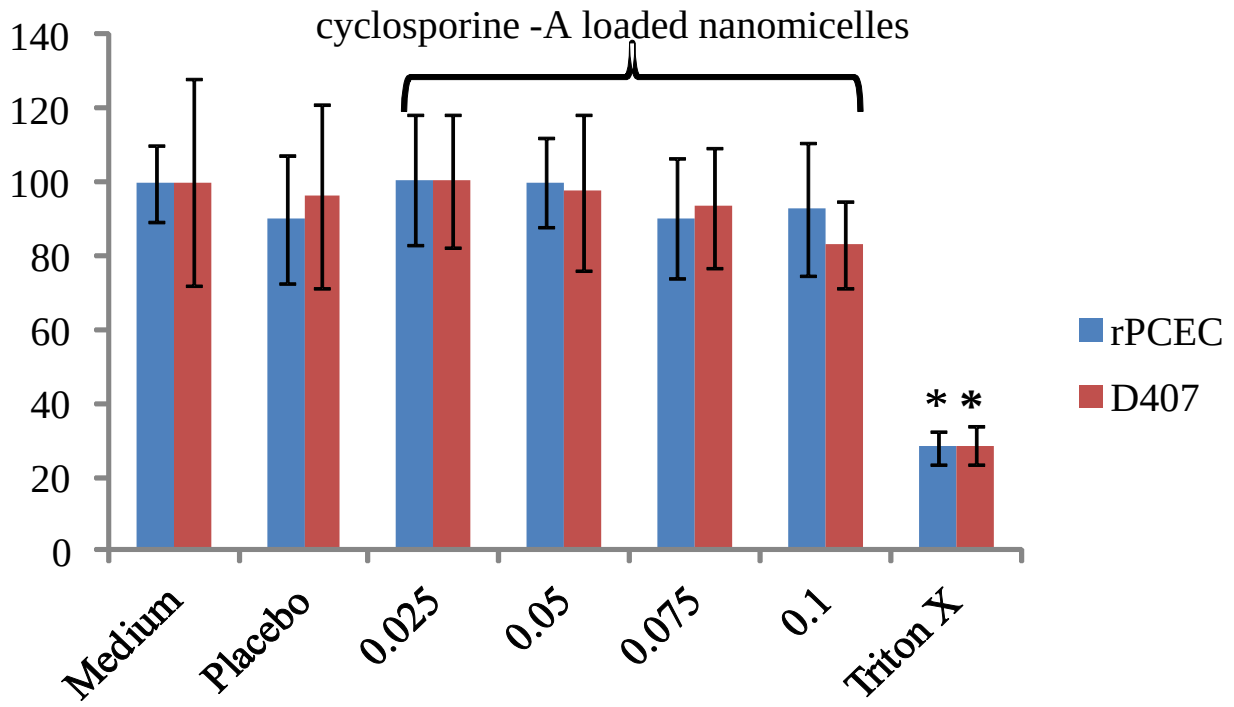

Figure 19. Cell proliferation assay for rPCEC and D407 cells incubated with NMF (placebo and CsA loaded) for a period of 1h. Values represent mean ± standard deviation (n= 4). A *p*-value of < 0.05 is considered to be statistically significant (*).

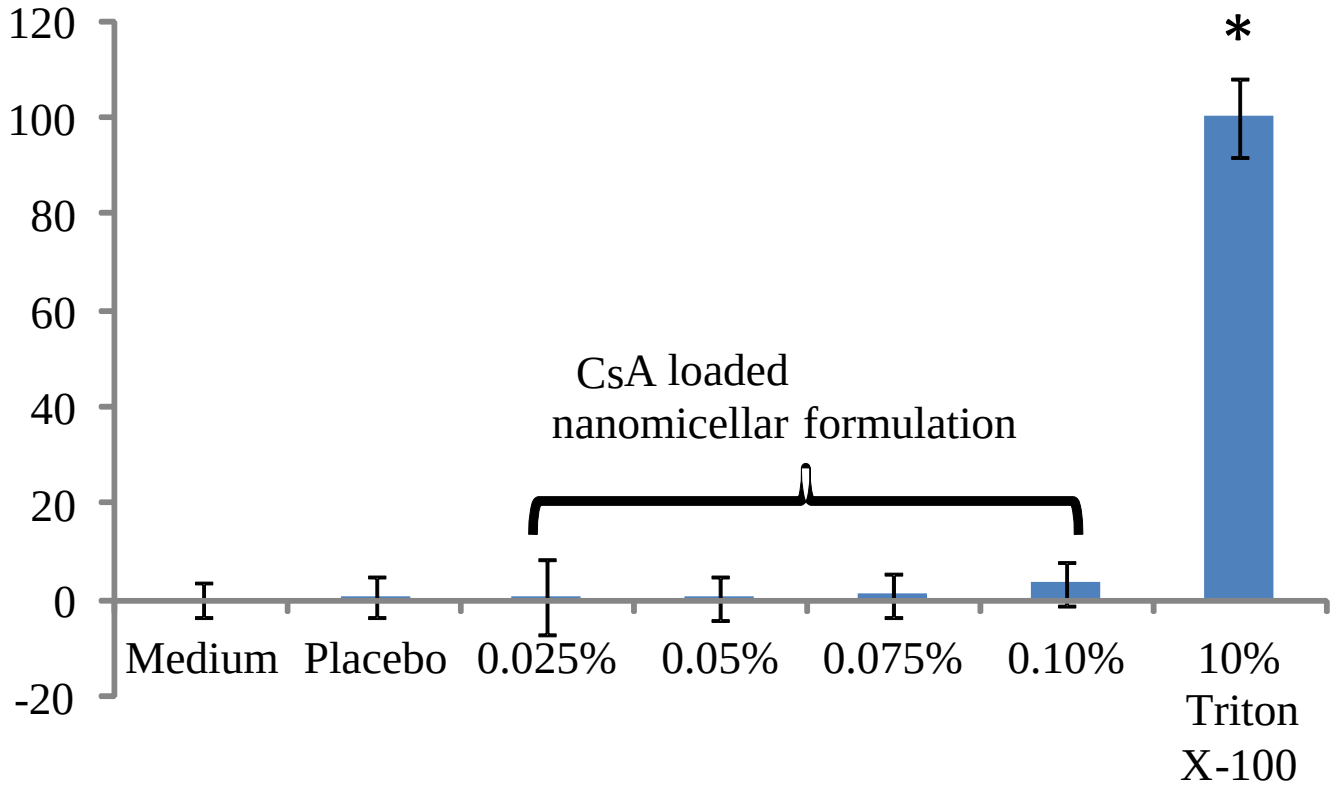

Figure 20. LDH assay for placebo and CsA loaded NMF for a period of 2h. Values represent mean ± standard deviation (n = 4). A *p*-value of < 0.05 is considered to be statistically significant (*).

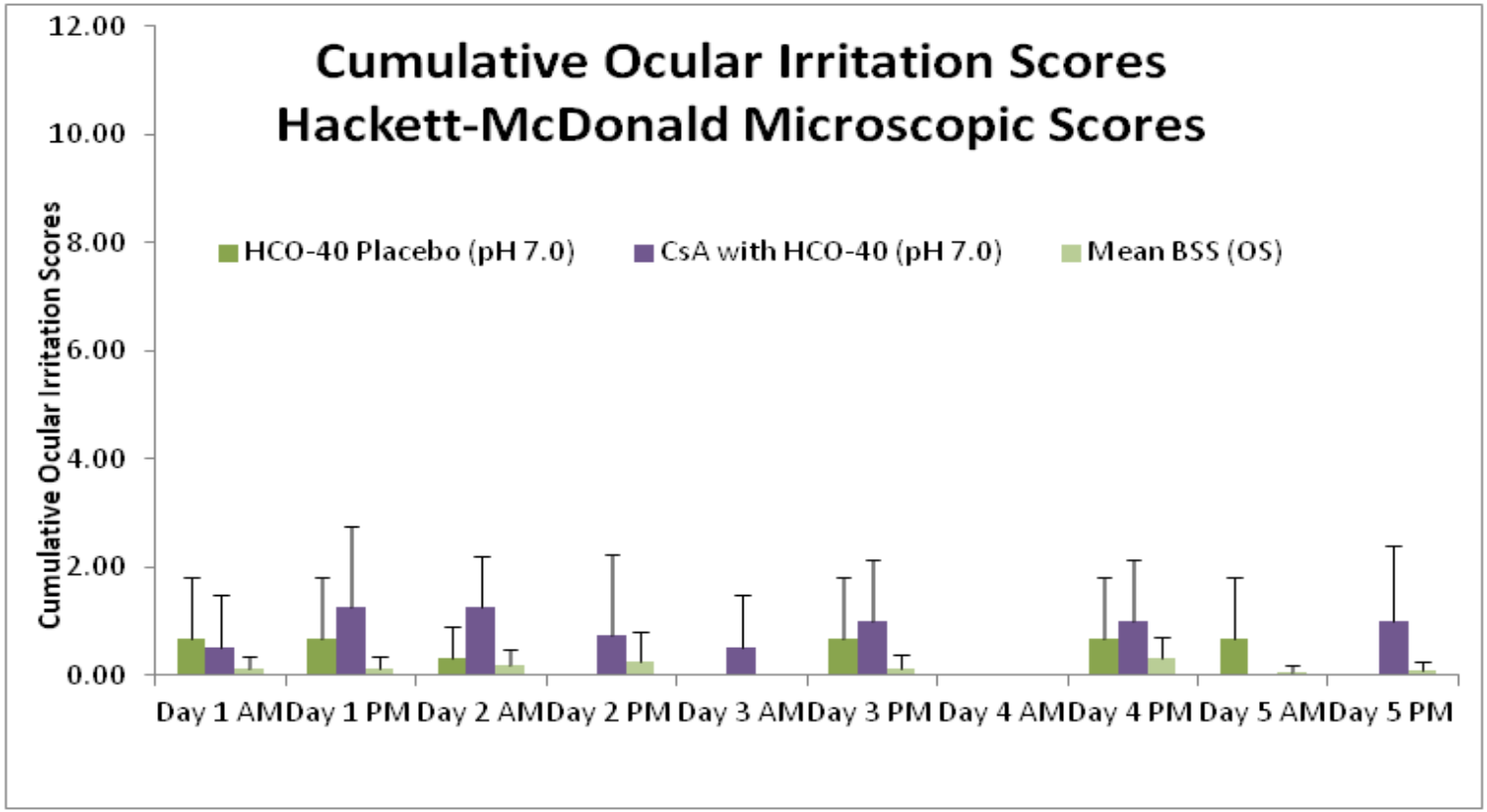

Figure 21. Cumulative Hackett-McDonald irritation scores. Values represent mean +/- standard deviation

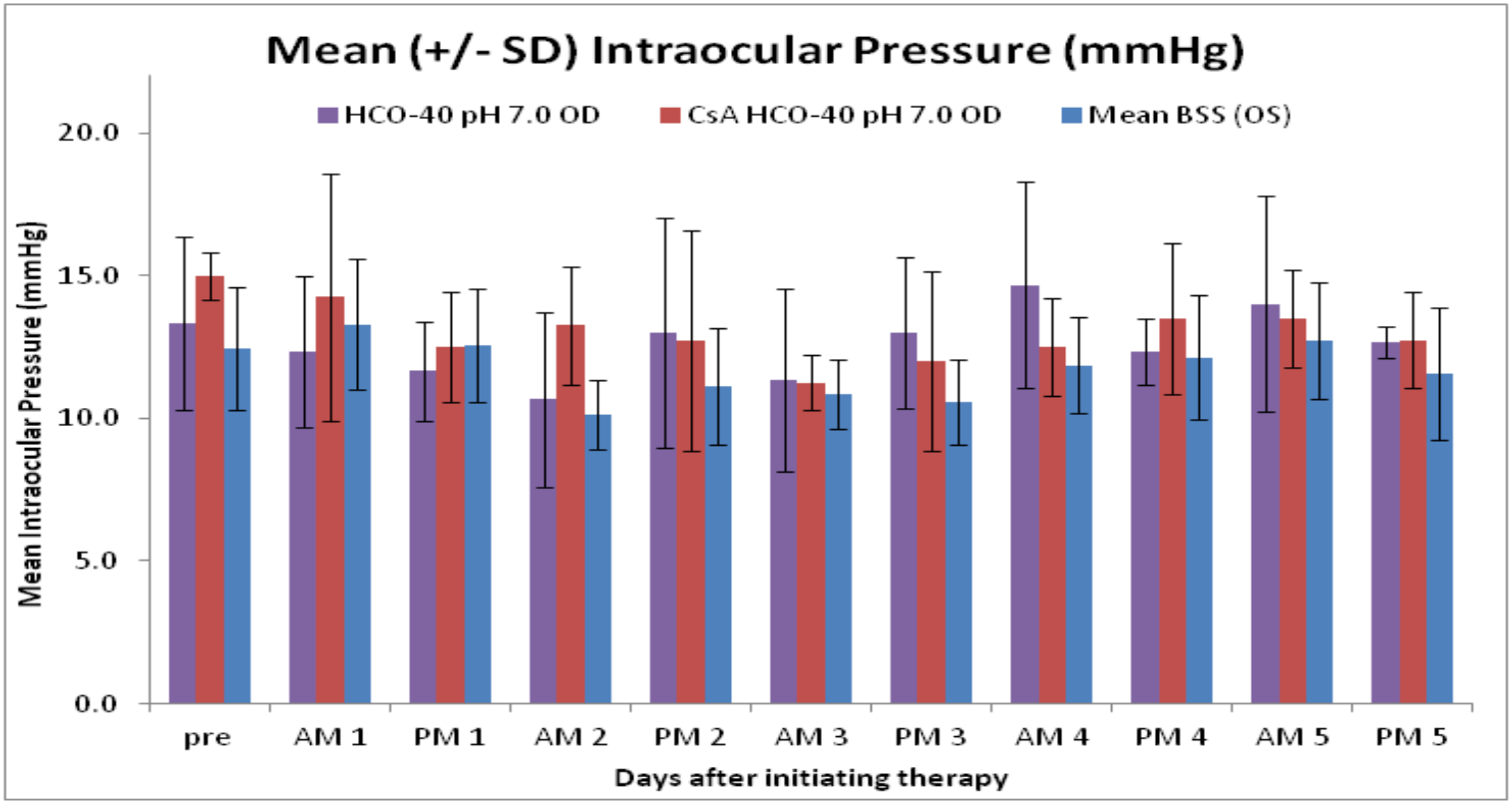

Figure 22. Intraocular pressure. Values represent mean +/- standard deviation

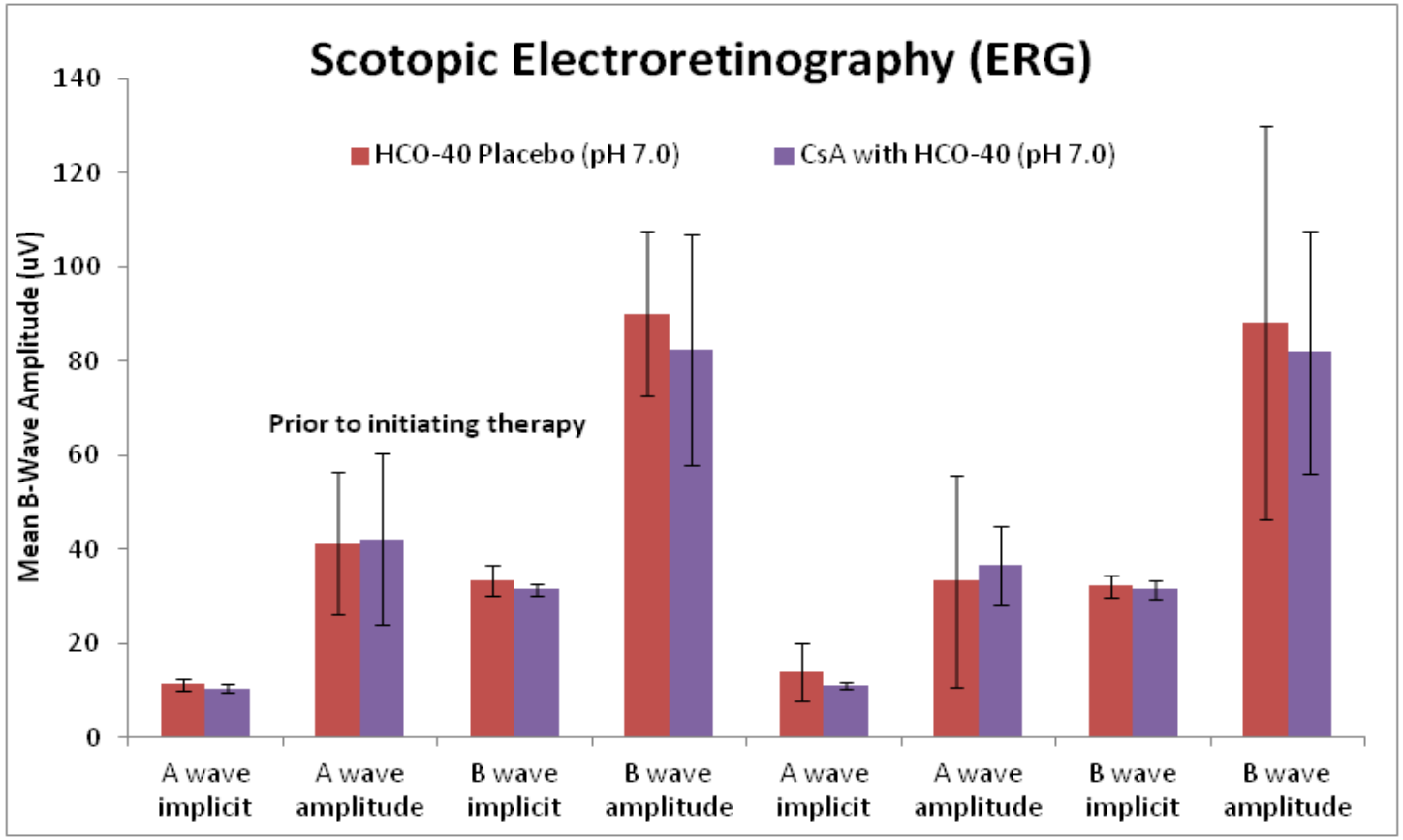

Figure 23. Scotopic electroretinography. Values represent mean +/- standard deviation

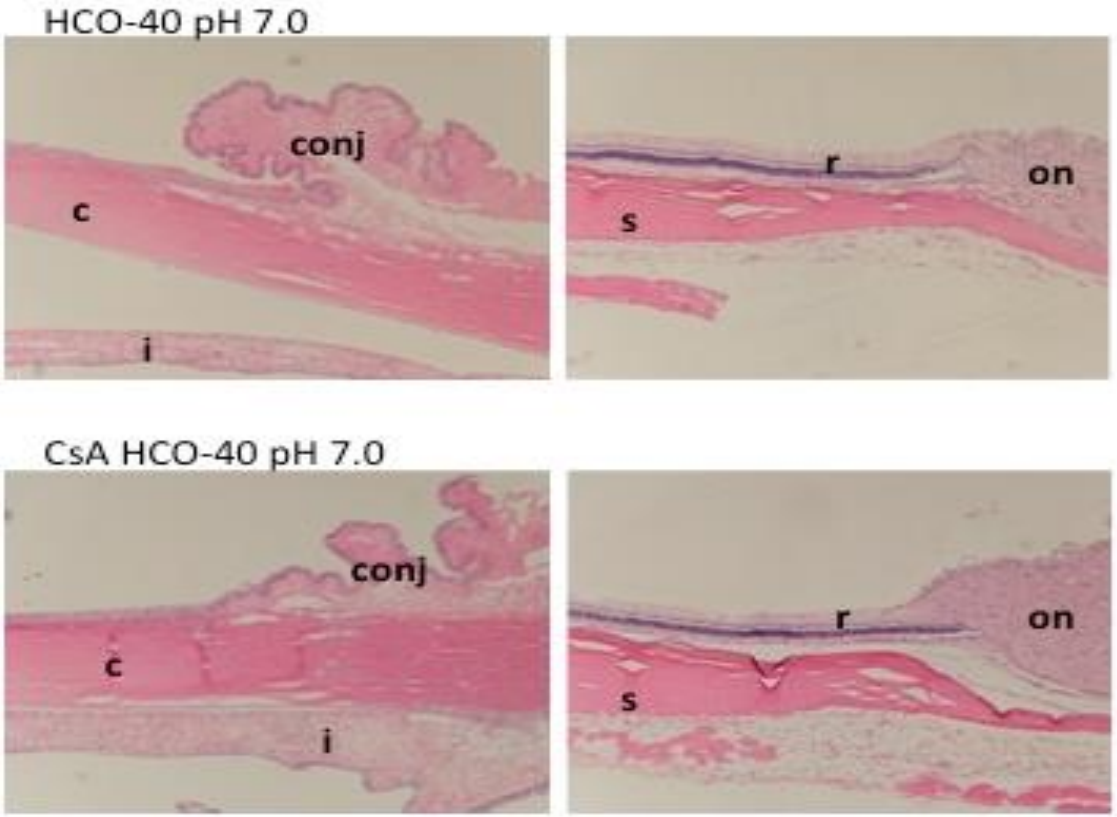

Figure 24.Ocular histopathology. Example of the ocular histopathology of the anterior segment of the eye (left) and the posterior segment (right). c=cornea; conj=conjunctiva, i=iris; s=sclera; on = outer nuclear layer; r=retina**.**

In vivo studies: LC-MS/MS method

A sensitive LC-MS/MS method was developed and applied to quantify CsA concentrations in ocular tissues, fluids and whole blood. The established analytical ranges for Cys-A were 0.100 ng/mL – 100 ng/mL for whole blood, and 2.00 ng/mL – 2000 ng/mL for aqueous humor and vitreous humor. The analytical ranges for the solid ocular tissues were 0.125 ng – 30 ng (low range) and 1.00 ng – 2500 ng (high range). Ocular tissue concentrations of CsA, collected one hour after single dosing and one hour following the last dose on Day-5 of multiple dosing are summarized in **Table 10** (**A and B**). The results of the tissue analyses were converted to ng/g by correcting for the amount of tissue analyzed. CsA ocular tissue distribution, post single topical dosing showed higher drug concentrations in the anterior ocular tissues (cornea and conjunctiva) and tears. With single topical dosing conjunctival CsA concentrations was 1.71 times higher than cornea. Also, higher CsA levels were observed in sclera. All other ocular tissues produced low CsA concentrations. Whole blood CsA concentration was found to be 0.73 ng/mL. With repeat dosing, highest average CsA concentrations were observed in the treated eye. CsA levels in ocular tissues were found to be in the order: cornea →conjunctiva → sclera → iris-ciliary body and →aqueous humor. Lower CsA concentrations were observed in the lens→ retina-choroid and → vitreous humor (Table **10B**). CsA concentrations in the contralateral eye treated with BSS were extremely low suggesting minimal systemic drug transfer. CsA whole blood concentration with repeated topical dosing was found to be only 0.718 ± 0.295 ng/mL.

Ocular Examination and Irritation Scores

Mean cumulative Hackett-McDonald ocular irritation scores demonstrated very minimal scores for both BSS-treated left eyes and CsA treated right eyes throughout the study, both for pre-treatment and post-treatment examination times. Mean cumulative inflammatory scores of less than 2 were observed in eyes treated with the placebo, 0.1% CsA NMF and BSS. These clinical scores represented mild conjunctival hyperemia (redness) and swelling. However, there were no significant differences in mean cumulative Hackett-McDonald ocular irritation scores between the groups (**Figure 21**) suggesting no differences in irritation from topical application of 0.1% CsA NMF, the placebo and BSS.

Intraocular Pressure

Although there was some variation in mean IOP between the groups on any given day, there was no consistent elevation or decrease in IOP in any group and all values were within normal ranges for all rabbits (**Figure 22**).

Electroretinography

Pre-study and post-study ERGs were normal in each rabbit. There were no significant differences in *a*- and *b*-wave implicit times or amplitudes before and after treatment (**Figure 23**).

Histopathology

No toxicologic or inflammatory changes were observed histologically in the anterior (conjunctiva / cornea / iris) or posterior segments (vitreous / retina) of the

Table 10. Summary of Ocular distribution of cyclosporine-A in Rabbits (A) After a Single Topical Drop Administration (35 µL) (N = 4 eyes) (B) Topical ocular administration of 0.1% CsA HCO-40 (pH 7.0) formulation or placebo to the eye four times a day at 2 hour intervals for five days to New Zealand White rabbits

Tissue/fluid	**CsA Concentration at 1 hr post dosing (N=4 eyes) (ng/mL or ng/g)[a] ± S.E.M**
Aqueous humor	1.5 ± 0.398
Conjunctiva	1417 ± 123
Cornea	828 ± 53.2
Eye lid	745 ± 190
Iris Ciliary Body	8.2 ± 1.9
Lacrimal gland	3.2 ± 0.4
lens	1.0 ± 0.06
Retina-Choroid	13 ± 2.4
Sclera	216 ± 15
Tears	800 ± 99
Vitreous Humor	2.0 ± 0.8

S.E.M = Standard Error of Mean

(B) Topical ocular administration of 0.1% CsA HCO-40 (pH 7.0) formulation or placebo to the eye four times a day at 2 hour intervals for five days to New Zealand White rabbits

Group No.	Treatment	Matrix	CsA Concentration at 1 hr post last dose (ng/mL or ng/g)[a]			
			OD[b]	Ave	OS[c]	Ave
2	0.1% CsA NMF administered 4 times a day (0, 2, 4, and 6 hr) for 5 days	Aqueous Humor	133 136	134.5	5.51 7.21	6.36
6	Placebo		BQL[d]	NA[e]	6.14	NA
2	0.1% CsA NMF administered 4 times a day (0, 2, 4, and 6 hr) for 5 days	Vitreous Humor	11.3 5.44	8.4	1.89 6.71	4.3
6	Placebo		BQL	NA	2.02	NA
2	0.1% CsA NMF administered 4 times a day (0, 2, 4, and 6 hr) for 5 days	Conjunctiva	2700 1550	2125	NC[f] NC	NC
6	Placebo		40.0	NA	NC	NA
2	0.1% CsA NMF administered 4 times a day (0, 2, 4, and 6 hr) for 5 days	Cornea	8130 7480	7805	NC NC	NC
6	Placebo		NC	NA	NC	NA
2	0.1% CsA NMF administered 4 times a day (0, 2, 4, and 6 hr) for 5 days	Lens	73.4 63.8	68.6	NC NC	NC
6	Placebo		NC	NA	NC	NA
2	0.1% CsA NMF administered 4 times a day (0, 2, 4, and 6 hr) for 5 days	Iris-Ciliary Body	274 134	204	NC 15.7	7.8[g]
6	Placebo		NC	NA	NC	NA
2	0.1% CsA NMF administered 4 times a day (0, 2, 4, and 6 hr) for 5 days	Retina / Choroid	85.0 22.4	53.7	NC 22.5	11.3[g]
6	Placebo		NC	NA	27.3	NA

Group No.	Treatment	Matrix	CsA Concentration at 1 hr post last dose (ng/mL or ng/g)[a]			
			OD[b]	Ave	OS[c]	Ave
2	0.1% CsA NMF administered 4 times a day (0, 2, 4, and 6 hr) for 5 days	Sclera	786	720	22.7	45.6
			655		68.6	
6	Placebo		12.2	NA	42.2	NA

[a]Aqueous humor and vitreous humor concentrations are expressed in ng/mL. All other tissue concentrations are expressed in ng/g; [b]OD = Right eye; [c]OS = Left eye; [d]BQL = Below quantitation limit; [e]NA = Not applicable; [f]NC = Not calculated. Concentration below quantitation limit; [g]Average value calculated by assuming NC = 0

Table 11. Group Mean Cyclosporine Toxicokinetic Parameters Whole Blood, Ocular Tissues and Tears Following Single Dose and Repeat Dose (7 Days) Topical Ocular Administration of Restasis (0.05%) or Cyclosporine Nanomicellar Formulations (0.05% or 0.1%) to Female New Zealand White Rabbits

Matrix	**Group**	**Dose**	**Treatments**	**Cmax[b]**	**Tmax**	**AUC$_{0-t}$ [c,d]**
Aqueous humor	3	Single dose	Restasis 0.05% Cyclosporine 0.05%	6.25	1	34.9
	4			18.2	12	91.6
	5		Cyclosporine 0.1%	11.0	12	63.7
	7	Repeat dose	Restasis 0.05% Cyclosporine 0.05%	30.8	12	359
	8			80.0	4	854
	9		Cyclosporine 0.1%	206	1	1596
Conjunctiva	3	Single dose	Restasis 0.05% Cyclosporine 0.05%	710	1	4564
	4			1553	0.25	7347
	5		Cyclosporine 0.1%	2665	0.25	8563
	7	Repeat dose	Restasis 0.05% Cyclosporine 0.05%	920	0.25	6391
	8			1883	0.25	8384
	9		Cyclosporine 0.1%	2630	0.25	12345

Matrix	Group	Dose	Treatments	Cmax[b]	Tmax	AUC0-t [c,d]
Cornea	3	Single dose	Restasis 0.05%	279	1	2468
	4		Cyclosporine 0.05%	738	12	7099
	5		Cyclosporine 0.1%	828	1	7771
	7	Repeat dose	Restasis 0.05%	1953	4	21096
	8		Cyclosporine 0.05%	4118	0.25	44325
	9		Cyclosporine 0.1%	6813	1	63978
Eyelid	3	Single dose	Restasis 0.05%	5925	12	30728
	4		Cyclosporine 0.05%	90	12	6721
	5		Cyclosporine 0.1%	845	0.25	4275
	7	Repeat dose	Restasis 0.05%	11093	1	119645
	8		Cyclosporine 0.05%	12093	4	95361
	9		Cyclosporine 0.1%	9193	0.25	100589
Iris/ciliary body	3	Single dose	Restasis 0.05%	6.2	1	21.42
	4		Cyclosporine 0.05%	9.3	12	72.32
	5		Cyclosporine 0.1%	15.7	0.25	8.77
	7	Repeat dose	Restasis 0.05%	62.0	1	607
	8		Cyclosporine 0.05%	165	4	1507
	9		Cyclosporine 0.1%	184	1	2106

Matrix	Group	Dose	Treatments	Cmax[b]	Tmax	AUC$_{0-t}$ [c,d]
Lacrimal gland	3	Single dose	Restasis 0.05% Cyclosporine	3.7	1	19.5
	4		0.05%	2.1	4	20.91
	5		Cyclosporine 0.1%	2.2	1	10.83
	7	Repeat dose	Restasis 0.05% Cyclosporine	53	4	472
	8		0.05%	24	1	230
	9		Cyclosporine 0.1%	26	4	266
Lens	3	Single dose	Restasis 0.05% Cyclosporine	0.3	12	2.7
	4		0.05%	1.9	0.25	5.74
	5		Cyclosporine 0.1%	2.1	4	16.65
	7	Repeat dose	Restasis 0.05% Cyclosporine	13	12	144
	8		0.05%	47.8	4	524
	9		Cyclosporine 0.1%	86.838	12	930
Retina-choroid	3	Single dose	Restasis 0.05% Cyclosporine	9	1	20.99
	4		0.05%	27	0.25	63.97
	5		Cyclosporine 0.1%	27	0.25	144
	7	Repeat dose	Restasis 0.05% Cyclosporine	50	1	372
	8		0.05%	56	4	517
	9		Cyclosporine 0.1%	59	4	628

Matrix	Group	Dose	Treatments	Cmax[b]	Tmax	AUC$_{0-t}$ [c,d]
Sclera	3	Single dose	Restasis 0.05%	111	1	762
	4		Cyclosporine 0.05%	205	0.25	1167
	5		Cyclosporine 0.1%	263	0.25	1344
	7	Repeat dose	Restasis 0.05%	315	4	2596
	8		Cyclosporine 0.05%	386	4	3435
	9		Cyclosporine 0.1%	701	0.25	4554
Tears	3	Single dose	Restasis 0.05%	10300	0.25	26135
	4		Cyclosporine 0.05%	958	12	8585
	5		Cyclosporine 0.1%	5833	0.25	8160
	7	Repeat dose	Restasis 0.05%	12815	1	78824
	8		Cyclosporine 0.05%	24278	1	118225
	9		Cyclosporine 0.1%	34950	1	134330
Vitreous Humor	3	Single dose	Restasis 0.05%	1.81	1	9.78
	4		Cyclosporine 0.05%	1.9	0.25	9.63
	5		Cyclosporine 0.1%	2.2	0.25	14.89
	7	Repeat dose	Restasis 0.05%	8.7	1	62.2
	8		Cyclosporine 0.05%	7.2	12	76
	9		Cyclosporine 0.1%	7.0	0.25	66

Matrix	Group	Dose	Treatments	Cmax[b]	Tmax	AUC_{0-t} [c,d]
Whole blood	3	Single dose	Restasis 0.05% Cyclosporine	0.15	1	0.44
	4		0.05%	0.52	0.25	1.64
	5		Cyclosporine 0.1%	0.77	0.25	3.4
	7	Repeat dose	Restasis 0.05% Cyclosporine	0.2	0.25	1.39
	8		0.05%	0.67	0.25	3.45
	9		Cyclosporine 0.1%	2.0	0.25	7.27

[a]Groups 2-5 received single doses and Group 6-9 received 4 doses/day at 4-hour intervals for 7 days.

[b]Units are ng/mL for whole blood, aqueous humor, and vitreous humor and ng/g for all other matrices.

[c]Units are h×ng/mL for whole blood, aqueous humor, and vitreous humor and h×ng/g for all other matrices.

[d]AUC_{0-t} = AUC_{0-12} except Group 3 Whole Blood AUC_{0-4}

eye of any groups (**Figure 24**). Eyes were also stained with Ki-67 immunostaining as a standard marker of proliferation. Ki-67 expression is usually estimated as the percentage of tumor cells positively stained by the antibody, with nuclear staining being the most common criterion of positivity. In corneal epithelium, but not in other tissues, Ki-67 was expressed at a very low level (< 1% of cells) with no difference among treatment groups.

CsA concentrations in whole blood and ocular tissues

Whole blood samples collected 1h following the last dose on Day-5 from all seven rabbits, and selected ocular tissues (aqueous humor, vitreous humor, conjunctiva, cornea, iris-ciliary body, lens, retina-choroid, and sclera) collected from two rabbits that received 0.1% CsA NMF (OD), and BSS (OS), and from one rabbit that received placebo NMF (OD) and BSS (OS), were assayed for CsA by liquid chromatography-tandem mass spectrometry (LC-MS/MS) as described earlier. CsA whole blood concentration was found to be 0.718 ± 0.295 ng/mL Concentrations of CsA in ocular tissues collected 1 hour following the single dose and last dose on Day-5 are summarized in **Table 10 (A and B).** The results of the solid tissue analyses were converted to ng/g by correcting for the amount of tissue analyzed. Following repeated administration of the 0.1% CsA NMF, the highest average CsA concentrations in the treated eye were observed in cornea (7805 ng/g), followed by.conjunctiva (2125 ng/g), sclera (720 ng/g), iris-ciliary body (204 ng/g), and aqueous humor (134 ng/mL). The lowest CsA concentrations were observed in the lens (68.6 ng/g), retina-choroid (54 ng/g), and vitreous humor (~8 ng/mL).

CsA concentrations in the collateral eye treated with BSS were quite low suggesting minimal systemic transfer of drug.

All the pharmacokinetic parameters for Restasis®, 0.05% and 0.1% CsA nanomicellar formulations were determined with Winnonlin®. Summary for pharmacokinetic parameters are summarized in **Table 11.** Group mean CsA PK parameters for whole blood, ocular tissues, and tears are presented in **Table 11**. In general, following either single or repeat (4 times per day at 2-hour intervals) dose administration of Restasis (0.05%) and CsA nanomicellar formulations (0.05% and 0.1%), the highest exposure to CsA was observed in the tears and eyelid, followed by the cornea and conjunctiva. Intermediate exposure was observed in the sclera, aqueous humor, and iris/ciliary body. Low exposure was observed in the lens, retina choroid, lacrimal gland, and vitreous humor. Systemic exposure, as measured by whole blood concentrations and AUC values, was substantially lower than exposure in ocular tissues.

In the repeat dose phase, CsA concentrations in the conjunctiva, cornea, aqueous humor, iris/ciliary body, sclera, lens, retina-choroid, and tears were highest after administration of CsA 0.1% in nanomicellar formulation followed by CsA 0.05% in nanomicellar formulation, with Restasis 0.05% having the lowest concentrations (**Table 11**).

Systemic exposure to CsA was also ranked in the same order (highest for the 0.1% nanomicellar formulation, followed by the 0.05% nanomicellar formulation and then Restasis), but systemic exposure to all three formulations was

substantially lower than exposure in ocular tissues (**Table 11**). In vitreous humor, CsA concentrations and AUC values were low but comparable after administration of both nanomicellar formulations and greater than those after administration of Restasis. CsA concentrations were reasonably comparable among all 3 CsA treatments for the eyelid. The CsA concentrations in lacrimal gland for all 3 treatments were low. However, CsA concentrations and AUC values after administration of Restasis® were higher than for either of the nanomicellar formulations.

Although CsA exposure in ocular tissues was lower after single doses compared to repeat doses, the rank orders of exposure between Restasis and the nanomicellar formulations after single dose administration were similar to those observed after repeat dose administration. Following both single and repeat dose administration, systemic exposure was substantially lower than exposure in ocular tissues.

Discussion

Therapeutic delivery with no ocular side effects after topical dosing, is a challenging task. Ocular static and dynamic barriers pose a challenge by impeding drug transport across cell membrane/tissues (286). After topical dosing, a large fraction of the dose is lost due to excessive tear production and/or drainage through nasolacrimal duct (14). Further sub-optimal physicochemical properties of drug will retard aqueous solubility thereby impeding drug delivery. In such a scenario,

clear aqueous nanomicellar formulations appear to be highly promising. Nanomicelles can encapsulate hydrophobic drugs inside the hydrophobic core improving aqueous solubility. Use of single polymer to encapsulate drug may result in clear aqueous nanomicelles, but may cause poor formulation stability. To improve the stability of micelles and lower their CMC a second polymer may be added. In our studies, we included Oc-40 as the second polymer. CMC is a point where the monomer surfactants start to aggregate and form micelles. Lower CMC indicates better stability of the nanomicelle formulation (14). For the blend of polymer surfactants CMC was determined. In the present study CMC for HCO-40 and blend of surfactants was determined with iodine as a probe. Pure I_2 is crystalline, fairly hydrophobic and particularly not soluble in water. Iodine solubility in an aqueous environment is improved by adding its salt, potassium iodide, to the solution. Addition of potassium iodide solubilizes water insoluble iodine by forming complexes, i.e., KI, KI_2, KI_3, KI_4. As the iodine solution is added to polymer solution the solubilized iodine prefers to partition into the hydrophobic core of the nanomicelles. It prefers to interact with hydrophobic nanoenvironment of nanomicelles causing conversion of I_3^- to I_2 from excess KI in the solution. The ether oxygen of PEG groups in the surfactant molecules donate electrons to the vacant σ^* orbital of I_2 resulting in the formation of a surfactant-iodine donor-acceptor type complex (287). A rise in absorbance for iodine entrapment indicates increase in micelle concentration. As the concentration of monomers in the formulation increases, a sudden rise in absorbance may be observed. Iodine intensity as a function of logarithm of surfactant mass concentration was plotted. A

combination of surfactants (HCO-40/Oc-40, 1.0:0.05) generated a lower CMC value, 0.00707 wt%, than the individual polymers (**Table 5**). Such low CMC value indicates that this combination of surfactants, at very low concentrations, will be able to entrap the hydrophobic drugs and can provide adequate solubility and stability.

To prepare CsA loaded NMF the blend of polymers (HCO-40/Oc-40, 1.0:0.05) were selected due to their low CMC. An aqueous clear nanomicellar CsA formulation was successfully prepared following novel solvent casting technique. In another set of experiments, we tried to encapsulate 1mg of CsA following direct dissolution method. Addition of CsA (0.1 wt%) to the blend of polymers in aqueous solution resulted in drug precipitation. Therefore, we selected solvent casting method to prepare CsA loaded NMF, which resulted in clear aqueous solution. NMF was devoid of any particulate matter. The prepared NMF needs to be maintained in the physiological range for osmolarity and pH. In general, to adjust tonicity; agents such as glucose, xylitol, glycerol, boric acid or sodium chloride is added. Tears have the tonicity equivalent to 0.9% solution of sodium chloride which produces osmolarity of ~305 mOsm/kg. Hypertonicity or hypotonicity of the topical drops may cause irritation to the eye. The pH of the eye ranges from 6.5 – 7.6. Therefore, osmolarity and pH was maintained at ~ 300 mOsm/Kg and ~7.0, respectively. NMF produced much higher drug entrapment (> 95%) and loading efficiencies (8.85%). This NMF demonstrated a small particle size ranging between 10 nm to ~80 nm. This data is also in agreement with real time TEM images. NMF after resuspending in phosphate buffer saline produced viscosity similar to that of

water (0.9 centipoise (cP)). Topical dosing results in immediate loss of drug due to tear drainage, spill on the cheeks, or by drainage through nasolacrimal duct (14). One method to improve viscosity is with addition of viscosity enhancer. Therefore NMF's (placebo and CsA loaded) contained viscosity enhancing agent, povidone K90. We selected povidone K-90 because povidone K90 imparts viscosity and bioadhesion to NMF (194). The dual nature of povidone K-90, viscosity improvement and bioadhesive property, may aid the formulation to improve viscosity and keep NMF in contact with pre-corneal pocket for longer time period. The surface potential for the formulations is slightly negative. This negligible charge may help to reduce repulsion of NMF with negative cell surface. Further, dilution studies of NMF were conducted to determine the stability of nanomicelles. In general, tears are produced at an average flow rate of 1.2 μL/min (14). An excessive tear production following NMF instillation should not cause NMF dissociation and drug release. Therefore, we examined the dilution effect on nanomicellar size and PDI up to 500 times (way above tear dilution that is expected *in vivo*). Dilution of NMF caused very small increase in mean micelle size. Similarly, PDI of NMF was slightly higher with dilution (up to 500x). The reason may be attributed to change in concentration of monomers in the NMF with dilution. The results obtained are similar and in agreement to the earlier results observed by Xu, et al. (288). Upon nanomicelle dilution, the outer hydrophilic polyethylene oxide segment may form large and loose complex clusters in aqueous solution. These new larger aggregates that are developed with dilution exhibit thermodynamically reversible association. Hydrophobic effect and hydrogen

bonding may be forcing the outer hydrophilic segment to cluster and form larger aggregates in aqueous solution. The clustering of outer hydrophilic segment may be the reason for increase in micelle size upon dilution. However, NMF sustained the dilution effect up to 500 times and produced negligible effect on their size and demonstrated high stability upon dilution. Thermal dissociation and regeneration time of NMFs suggest a fairly robust formulation. The results may help to select a formulation with a high thermal dissociation temperature. Following thermal dissociation when NMFs is allowed to cool to room temperature under ambient conditions, nanomicelles regenerated within minutes resulting in optically clear solution. In general nanomicelles are unstable structures possessing two characteristic relaxation times i.e., fast ($\tau 1$) and slow ($\tau 2$). The results suggest that time taken to regenerate the nanomicelles is in minutes, because both polymers are non-ionic in nature and display longer nanomicellar relaxation times ($\tau 2$). This peculiar behavior of the formulation indicates that hydrophobic CsA is entrapped in the nanomicellar core even after being subjected to harsh conditions.

CsA has poor aqueous solubility of 12 ng/mL at room temperature (25 °C) (269). There is a possibility that a small amount/concentration of CsA, due to its aqueous solubility, may be present in the outer aqueous solution of NMF. We conducted qualitative proton nuclear magnetic resonance (^{1}H-NMR) studies that may determine the presence of free/unentrapped CsA molecules in solution at parts per million (ppm) levels. Formulations were prepared in different media such as $CDCl_3$ and D_2O. ^{1}H NMR spectroscopy studies were conducted for CsA, mixture of HCO-40/OC40 in $CDCl_3$ and NMF with entrapped CsA in $CDCl_3$ and D_2O.

Excessive addition of CsA above its aqueous solubility results in drug precipitation. In NMF we did not observe any CsA precipitation indicating drug entrapment in NMF, at a level higher than its aqueous solubility. On the other hand, results show that in $CDCl_3$, the resonance peaks corresponding to CsA and nanomicelles are present as evidenced from the spectra. However, in D_2O peaks corresponding to nanomicelles are only detected whereas peaks for CsA were not evident (**Figure 18**). These results clearly indicate that CsA is entrapped in the inner hydrophobic core of nanomicelles in D_2O. Suspended nanomicelles when dried and resuspended in $CDCl_3$, resonance peaks corresponding to CsA were evident and the spectra was similar to **Figure 17**. These results indicate that the nanomicelles entrapped CsA in the inner core and when subjected to organic solvent as outer environment NMF reversed and released CsA. Therefore, ^{1}H-NMR identified peaks corresponding to CsA in $CDCl_3$. However, in aqueous solvent (D_2O) NMF entrapped CsA inside the core and the nuclear magnetic resonance signals are lost. *In vitro* stability studies for 0.1% NMF at three different temperatures (4 °C, 25 °C and 40 °C) at 60% and 75% RH **(Table 9**) indicated that the CsA loaded NMF were highly stable and retained their original characteristics. There was no significant change in NMF size, polydispersity index (**Table 9**) and most importantly CsA concentration remained >90% after one month of exposure to 40 °C. The NMF formulation did not show any drug precipitation at the bottom of the vial. The formulation was clear, transparent and was comparable to that of DI water.

An important aspect of topical ocular drug delivery is to evaluate drug delivery vehicles for biocompatibility. Formulation components are expected to be

safe, reliable, and effective for its intended use. Also, these components are to be biodegradable and biocompatible. *In vitro* toxicity evaluation and ocular tissue drug distribution are the primary requirements to determine the safety of the carrier systems and their ability to deliver therapeutic drug levels to ocular tissues. *In vitro* toxicity tests are often conducted in cells. Therefore, selection of a cell line is crucially important because it should reproduce any toxic response that is similar to what occurs *in vivo* (289, 290). Therefore, we selected rPCEC and D407 as *in vitro* cell culture models to study the toxicity of CsA NMF.

To evaluate the cytotoxic effect of NMFs (blank and CsA loaded), cell proliferation (rPCEC and D407) and LDH assays (rPCEC) were performed. Since eye drops are rapidly cleared from the pre-corneal pocket (291, 292) cell proliferation assay was performed for 1h. It was assumed that a 1 h incubation period would be sufficient to evaluate any toxicity. In the first set of experiments (cell viability assay), percent viable cells in NMFs was comparable to that of negative control (culture medium) (**Figure 19**). Triton-X 100 served as positive control and reduced the percent cell viability to ~25% of the total cell number (rPCEC and D407). In another set of studies, cell plasma membrane damage test (LDH assay) was conducted. A two hour incubation time is sufficient because these formulations are to be delivered as topical eye drops into the pre-corneal pocket. After topical drop instillation most of the formulation is lost within minutes (286). In these experiments, the amount of LDH released in the culture media directly correlates with cytotoxicity. Triton-X 100 caused significant toxicity/membrane damage and released high amounts of LDH. Percentage cytotoxicity to rPCEC cells

with exposure to NMF (blank and CsA loaded) appeared to be negligible (**Figure 20**). Even 2 h continuous exposure, the formulations did not cause any cell membrane damage. Results from these assays clearly suggest that NMFs does not cause cell death and/or damage to plasma membrane. NMF appears to be safe for topical ocular application. Therefore, *in vivo* studies with 0.1% CsA loaded NMF and placebo were conducted, where BSS served as negative control.

In vivo studies conducted in female New Zealand rabbits with single and multiple dosing (4 x / day, at an interval of 2 h, consecutively for five days) showed very high CsA levels in anterior ocular tissues. Whole blood concentrations of CsA were measurable (*albeit* at very low levels) in rabbits that received the 0.1% CsA NMF single and multiple doses for 5 days (**Table 10 A and B**). The mean CsA whole blood concentration (0.718 ng/mL) in this study was similar to the Cmax (0.745 ng-eq/mL) value reported following single dose administration of an Allergan 0.2% ^{3}H-CsA formulation in NZW albino rabbits (293). Anterior ocular CsA concentrations in the present study are higher than values reported following topical drop administration of CsA loaded MPEG-hexPLA copolymer micelles (294). High CsA concentrations were delivered in aqueous humor, iris-ciliary body when compared to MPEG-hexPLA micelles indicating the better carrier ability of NMF. Considering that only a single time point (1 hour after the last dose) was sampled for analysis, the data were remarkably consistent between the two treated animals. For instance, the CsA concentrations observed in the cornea were 8130 ng/g and 7480 ng/g (**Table 10B**). The ocular tissue concentrations of CsA observed in this study were similar to or higher than those observed following repeat dose

administration (bid for 7 days) of an Allergan 0.2% ^{3}H-CsA formulation to rabbits (293). From **Table 10 A and B**, it is evident that CsA loaded NMF is able to safely deliver high CsA concentrations in anterior and posterior ocular tissues.

Instillation of topical eye drops is the most preferred and convenient route of drug administration resulting in higher patient compliance. This novel CsA formulation was able to translocate across cornea and deliver high levels in the anterior ocular tissues. Interestingly, we also found high drug levels in the back-of-the-eye tissues (retina-choroid) with CsA aqueous topical drops. There are two potential pathways for a molecule to reach the back-of-the-eye, following topical administration: (i) intraocular route, through cornea → aqueous humor → lens → vitreous humor and finally → retina and (ii) trans-scleral or conjunctival-scleral route around the conjunctiva through sclera→choroid and to retina (295). The first pathway is often unsuccessful for hydrophobic molecules such as CsA with high hydrophobicity, since the hydrophilic stroma becomes the rate limiting barrier for transcorneal absorption (296). Moreover, fluids in the anterior and posterior segments flow in opposite directions hindering the passage of molecules from the aqueous humor to lens and through to the vitreous humor, thus making this an unfavorable pathway. The second pathway offers a viable strategy to reach the back-of-the-eye for hydrophilic molecules by passive diffusion through the scleral aqueous channels/pores. But again, CsA being highly hydrophobic drug will encounter aqueous sclera as a potential barrier for permeation through the conjunctival-scleral route. CsA hydrophobicity limits the feasibility of formulating it into a clear aqueous solution at sufficient concentration to achieve therapeutic

levels in the ocular tissues. Hence, CsA is currently marketed as ophthalmic emulsion (Restasis®), which on chronic use may cause side effects (*http://www.restasis.com/ accessed on 12/28/2013)*. For CsA to reach the back-of-the-eye following topical administration, it is imperative to utilize the aqueous channels/pores of sclera (**Figure 25**). Hence, highly hydrophobic CsA when entrapped inside nanomicelle with a hydrophilic exterior/corona resulting in highly hydrophilic outer corona. The scleral aqueous pore size ranges between 20 and 80 nm (63). Our CsA loaded NMF's have small size (10 nm – 80 nm) with hydrophilic corona. We hypothesize that these nanomicelles utilize the hydrophilic corona and carry the CsA payload to the back-of-the-eye tissues following conjunctival scleral pathway. Also, ocular tissue CsA concentrations (conjunctiva > sclera > retina-choroid) support our hypothesis of conjunctival-scleral route for CsA delivery. Moreover, these CsA nanomicelles upon reaching back-of-the-eye tissues such as Bruch's membrane, RPE, choroid and retinal (**Figure 25**) may release CsA cargo by nanomicellar reversal as shown in **Figure 26**. The lipid bilayer of RPE and Bruch's membrane may aid in lipid-lipid interactions of nanomicellar core and lipid bilayer causing CsA release into the cells. Further, CsA permeation into the hydrophilic or aqueous vitreous humor is prevented because of the hydrophobic nature of CsA, where it gets deposited into the highly lipophilic tissues (RPE, Retina).

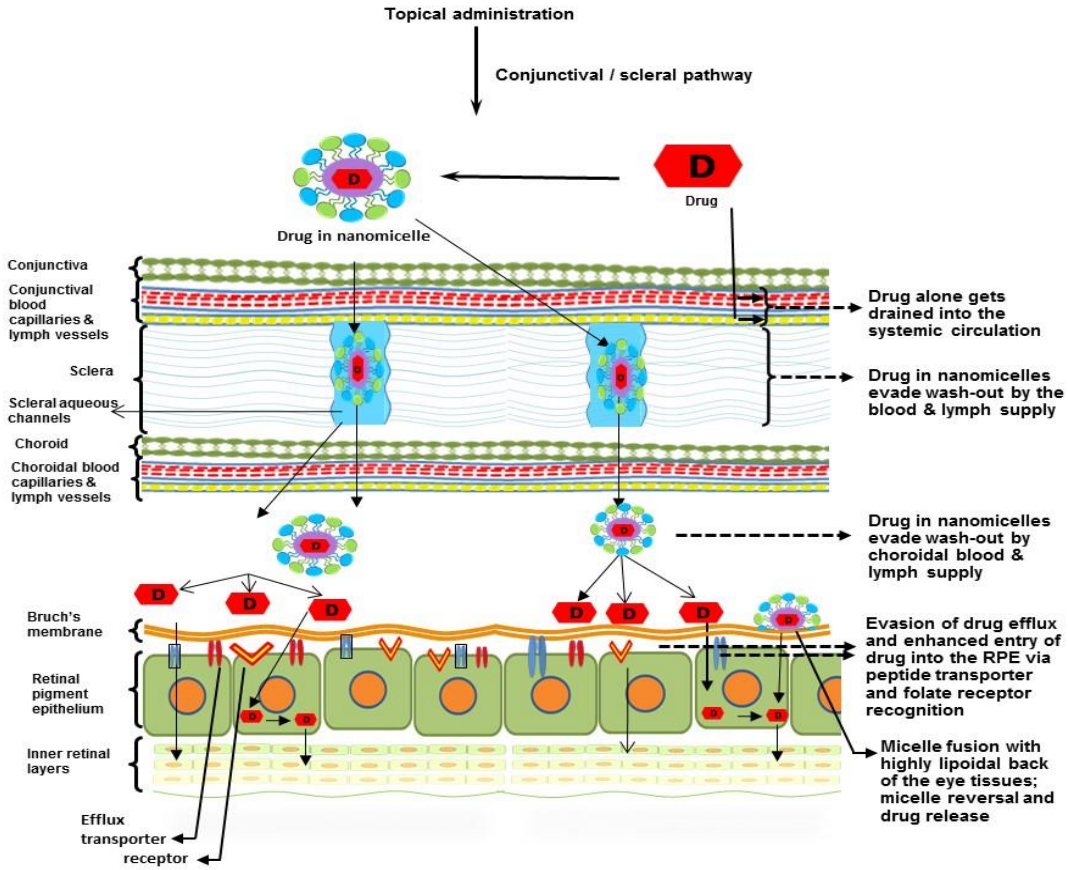

Figure 25. Hypothetical representation of cyclosporine A (CsA) loaded nanomicelles reaching back-of-the-eye (retina-choroid) following conjunctival scleral pathway after topical drop administration.

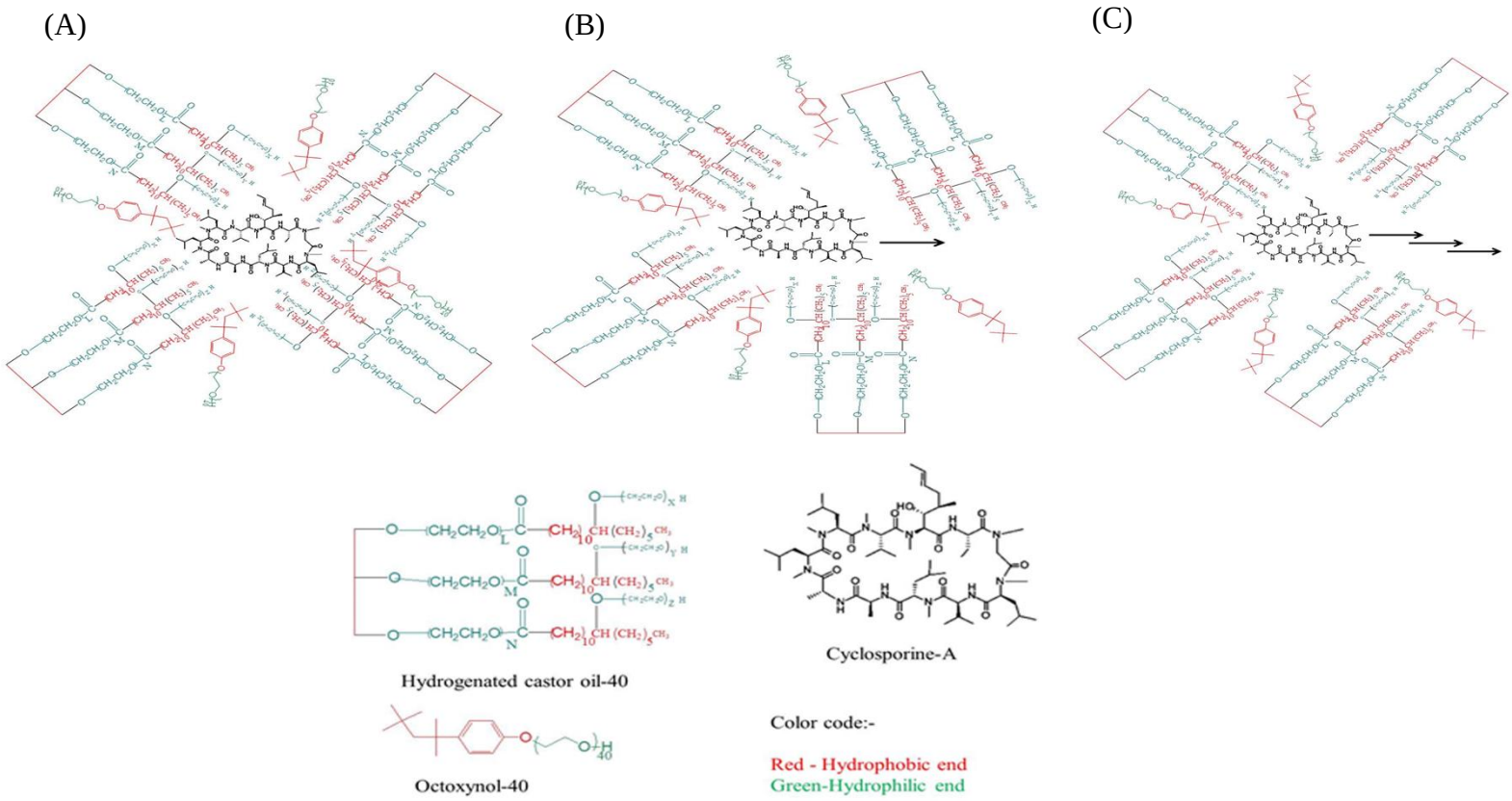

Figure 26. (A) Cyclosporine loaded nanomicelles composed of hydrogenated castor oil-40 and octoxynol-40 (Oc-40), (B) partial reversal of cyclosporine loaded nanomicelles. (C) complete reversal of nanomicelles and cyclosporine release upon contacting lipoidal ocular tissues.

Conclusion

In summary, an aqueous, clear nanomicellar CsA loaded formulation was successfully prepared and optimized with a blend of HCO-40/Oc-40 polymers. *In vitro* results indicate that these formulations are safe and well-tolerated. *In vivo* studies with topical drop application of BSS, placebo and 0.1% CsA loaded NMF showed very high CsA levels in anterior ocular tissues. Also, CsA concentrations in the back-of-the-eye tissues (retina-choroid) was much higher than the therapeutic level suggesting that NMF following the conjunctival-scleral pathway to reach retina-choroid. After application of 0.05% and 0.1% CsA nanomicellar formulation or Restasis (0.05% CsA), the concentration in tears and eyelids is very high and very variable, suggesting wash out from the ocular surface. After ocular administration of Restasis (0.05% CsA), 0.05% CsA in nanomicellar formulation, and 0.1% CsA in nanomicellar formulation 4 times daily at 2-hour intervals for 7 days, CsA exposures were highest after administration of 0.1% CsA in nanomicellar formulation followed by 0.05% CsA in nanomicellar formulation, with Restasis (0.05% CsA) having the lowest concentrations in the conjunctiva, cornea, aqueous humor, iris-ciliary body, sclera, retina-choroid, lens, and tears.In vitreous humor, exposures were low but comparable after administration of both nanomicellar formulations and greater than those after administration of Restasis.Exposures were reasonably comparable among all three CsA treatments for the eyelid. For the lacrimal gland, exposure after administration of Restasis® was low but higher than for either nanomicellar formulation. Systemic exposure, as

measured by whole blood concentrations, was substantially lower than exposure in ocular tissues. Maximum concentrations were less than 1 ng/mL after single applications and less than 2 ng/mL after application of 4 doses per day at 2-hour intervals for 7 days. Although exposures in ocular tissues were lower after single doses compared to repeat doses, in general, the rank orders of exposure among Restasis® (0.05% CsA), 0.05% CsA in nanomicellar formulation, and 0.1% CsA in nanomicellar formulation were comparable to those observed after repeat dosing. A blend of HCO-40 and Oc-40 are safe carrier to deliver drugs to anterior and back-of-the-eye tissues in therapeutic concentrations with aqueous topical drop instillation.

Chapter 4

TOPICAL AQUEOUS CLEAR RESOLVIN E1 ANALOG (RX-10045) NANOMICELLAR FORMULATION

PART A: INTERACTION STUDIES OF RESOLVIN E1 ANALOG WITH EFFLUX TRANSPORTERS

Rationale

Resolvins are small endogenous mediator molecules that are enzymatically biosynthesized from omega-3 polyunsaturated fatty acids i.e., eicosapentaenoic acid (EPA) and docosahexaenoic acid (DHA) (297). Other methods of biosynthesis include aspirin triggered and/or non-aspirin dependent pathways (298). Cyclooxygenase-2 (COX-2) dependent reactions in the presence of aspirin and microbial P450-initiated pathways are reported to facilitate production of resolvins (298). These compounds belong to a family of potent lipid mediators that causes reversal of the inflammatory response back to a non-inflamed state (299). Biosynthesized resolvins act by shielding tissues from leukocyte mediated injuries; dampen leukocyte response/trafficking to the site of inflammation and counter regulating proinflammatory gene expressions, thus reducing tissue inflammation (298). Resolvins are currently being studied to ameliorate the ocular pathological conditions such as dry eye (300), retinal diseases (301) and uveitis (302). This class of drugs opens up an entirely novel approach to treat inflammatory ocular conditions. RX-10045 (Resolvyx) **Figure 27** is a synthetic active pharmaceutical ingredient and an analog/derivative of naturally occurring resolvin E1(RvE1).

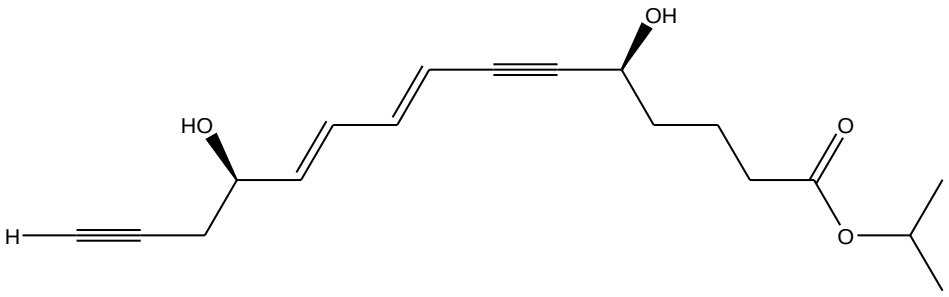

Figure 27. Structure of RX-10045 (resolvin E1 analog).

In vitro studies demonstrated a potent anti-inflammatory and cell survival benefits with RX-10045 (303). This novel molecule is highly effective against dry eye and goblet cell loss thereby accelerating tear production. Also, this compound can reduce corneal inflammation, epithelial damage and accelerate corneal tissue repair. In addition, RX-10045 can inhibit the release of several key pro-inflammatory mediators from corneal epithelial cells (304). This drug is originally formulated as an aqueous solution using propylene glycol as a solubilizing agent and tested for the treatment of dry eye with topical drop application. The drug was shown to be highly efficacious in murine models of dry eye syndrome. However, in Phase II clinical trials, RX-10045, though safe and well tolerated, produced equivocal efficacy results (303). A possible explanation is that, disposition across the human cornea and conjunctiva may be limited due to efflux transporters expressed on the ocular surface and poor aqueous solubility and stability. Therefore, the study was initiated to determine the interaction of RX-10045 with efflux transporters expressed on the ocular surface, improve drug stability and delivery. Therefore, the objectives of this study are (A) to assess the affinity of RX-10045 towards efflux transporters in polarized Madin-Darby canine kidney cells i.e., MDCKII-MDR1, MDCKII-MRP2 and MDCKII-BCRP and (B) development and optimization of RX-10045 nanomicellar formulation to improve drug solubility, stability and permeation across ocular tissues.

Materials and Methods

RX-10045 was prepared by PPD (Middleton, WI,, USA; lot# SYN-72799-05-11). GF and ketoconazole, a P-glycoprotein (P-gp) inhibitor, were acquired from Sigma Chemical Co, St. Louis, MO, USA. MK571, a specific inhibitor of MRP was obtained from Biomol International (Plymouth Meeting, PA). GF120918, a BCRP inhibitor was a generous gift from GlaxoSmithKline Ltd. Beta estradiol was purchased from Sigma-Aldrich, USA. [^{3}H] Digoxin (specific activity 35.4 Ci/mMol) was obtained from PerkinElmer Life and Analytical Sciences (Boston, MA), [^{3}H]Abacavir (specific activity 0.2 Ci/mMol) and [^{3}H]Vinblastine (specific activity 3.6 Ci/mmol) were obtained from Moravek chemical company, USA. [^{3}H] Digoxin, [^{3}H] Abacavir, and [^{3}H] vinblastine were used at 0.5 µCi/mL, 0.5 µCi/mL and 0.25 µCi/mL, respectively. Stock solution of the RX-10045 (1 mg/mL) was freshly prepared before an experiment. Briefly, RX-10045 (1 mg) was accurately measured and dissolved in 50 µL dimethyl sulfoxide (DMSO) (Thermo Scientific, Rockford, IL, USA) and the volume was made up with distilled deionized water. Further, aliquots of this stock solution were diluted in Dulbecco's phosphate-buffered saline (DPBS, composition: 130 mM NaCl, 7.5 mM Na_2HPO_4, 1.5 mM KH_2PO_4, 0.5 mM $MgSO_4$, 1 mM $CaCl_2$, 0.03 mM KCl and 5 mM glucose and pH 7.4) to achieve desired concentrations. Stock solutions of ketoconazole (10 mg/mL), GF120918 (1 mg/mL), beta-estradiol (1 mg/mL) and MK571 (25 mg/mL) were prepared in DMSO and aliquots were diluted in DPBS to achieve the desired concentration. Culture flasks (75 cm^2 growth area) were procured from MidSci (St. Louis, MO). Twelve well culture plates were purchased from Midwest Scientific,

St. Louis, MO. Twelve well transwell plates (Corning Incorporated, Corning, NY) with an insert membrane growth area of 1 cm^2 were selected for transport studies.

Cell Culture

Madin-Darby canine kidney (MDCK) cells transfected with the human MDR1 gene (MDCKII-MDR1), human MRP2 gene (MDCKII-MRP2), and human BCRP gene (MDCKII-BCRP) were generously provided by Drs. A. Schinkel and P. Borst (The Netherlands Cancer Institute, Amsterdam, Netherlands). Dulbecco's Modified Eagle's medium (DMEM) was procured from Caisson Laboratories Inc, UT. Tryple Express, nonessential amino acids, and fetal bovine serum were procured from Invitrogen (Carlsbad, CA). Penicillin, streptomycin, sodium bicarbonate, lactalbumin, HEPES, amphotericin B, and polymyxin B sulfate were supplied by Sigma-Aldrich. MDCKII-MDR1, MDCKII-MRP2 and MDCKII-BCRP cells were cultured as described previously (282). Cells were maintained in DMEM supplemented with 10% calf serum, 100 IU/mL penicillin, 100 mg/mL streptomycin and 20 mmol/L HEPES, pH 7.4. Cells were plated at a density of 250000/cm^2 in 12-well tissue culture treated plastic plates. Cells were incubated at 37^o C in an atmosphere of 5% CO_2 and 95% humidity in air and were allowed to grow for 5 - 8 days. Similarly, human corneal epithelial (HCEC) cell line was procured as a generous gift from Dr. Araki-Sasaki (Kinki Central Hospital, Japan). HCEC cells are SV-40 virus transfected human immortalized corneal cells. These cell were cultured and maintained as reported previously [18]. HCEC was cultured

in DMEM/F-12 media supplemented with 15% FBS (heat inactivated), penicillin and streptomycin, 22 mM sodium bicarbonate, 15 mM HEPES, 10 ng/mL of human epidermal growth factor and 5mg/mL insulin. The cells were grown at 37 °C in a cell culture incubator, which maintained 5% CO_2 and 90% relative humidity.

Uptake Experiments

Uptake studies were conducted according to previously published protocols (305). Briefly, cells (MDCKII-MDR1, MDCKII-MRP2, MDCKII-BCRP, and HCEC) were seeded in twelve well plate. After 5-7 days of seeding, the medium was aspirated and cells were rinsed three times with DPBS and then equilibrated with DPBS for 30 mins at 37 ^{o}C. Initial screening for uptake studies were conducted across MDCKII-MDR1, MDCKII-BCRP and MDCKII-MRP2 cells with a known concentration of RX-10045 (50 µM to 600 µM) solution containing [^{3}H] Digoxin (0.5 µCi/mL) for P-gp, [^{3}H] Abacavir (0.5 µCi/mL) for BCRP and [^{3}H] Vinblastine (0.25 µCi/mL) for MRP2. In these studies, efflux pump inhibitors such as GF120918 and ketoconazole for P-gp; beta-estradiol for BCRP and MK571 for MRP2 were selected. Cells were treated with drug solution. The experiment was conducted at 37 ^{o}C for 30 mins. At the end of an experiment, drug solution was aspirated. To terminate the uptake process, cells were rinsed three times with ice-cold stop solution (210 mM KCl, 20 mM HEPES [pH 7.4]). To determine the drug content, cell lysis was performed by adding 1 mL of lysis solution (0.3 M NaOH, 0.1% Triton X-100). Cells were left undisturbed overnight at room temperature.

Samples (500 µL) were transferred to scintillation vials containing 3 mL scintillation cocktail. The solutions were mixed and radioactivity was measured with a scintillation counter (Model LS 6500; Beckman Instruments Inc., Fullerton, CA). To normalize the uptake data cell protein content was measured by Bradford assay. A protein calibration curve was prepared with bovine serum albumin as standard and was used to determine the protein content in the samples. The amount of radioactive substrate accumulated inside the cell was determined using the following equation:

$$\text{Flux} = \frac{dM/dT}{A} \quad \text{or} \quad V = \frac{V_{max}[C]}{K_m + [C]} + K_d[C] \qquad \textit{Eq 5}$$

Concentrations of donor and samples are represented as C_{sample} and $C_{donor.}$ As represented in Eq.5, V is the total rate of uptake, V_{max} is the maximum uptake for carrier mediated process, K_d is the rate constant and K_m is the concentration at half saturation.

Following a similar procedure, dose dependent inhibition studies were performed. [^{3}H]-Digoxin, [^{3}H] Abacavir and [^{3}H] Vinblastine were spiked with various concentrations of RX-10045 ranging from 25 µM to 800 µM. Studies were performed as described before and data was obtained to determine the half maximal inhibitory concentration (IC_{50}) according to a previously published method (306, 307). IC_{50} was calculated according to Eq. 6.

$$Y = \min + \frac{(\max-\min)}{1+10^{(\text{Log } IC_{50}-X)H}} \qquad \textit{Eq. 6}$$

Y represents cellular accumulation of radioactive substrate, X denotes the logarithm of the RX-10045 concentration. Data was fitted to Eq. 6 with a transformed non-linear regression analysis program (Graphpad Prism version 4.0, San Diego, CA) to calculate IC_{50}. H is the Hill constant.

Permeability Studies

Transport studies were performed on MDCKII-MDR1, MDCKII-MRP2 and MDCKII-BCRP cells grown on transwell inserts. Cells were seeded on transwells at a density of 3 million cells/plate and allowed to grow for 5-7 days. Each day culture medium was removed and replaced with fresh medium. Apparent drug permeability from apical to basolateral (AP-BL) and vice versa (BL-AP) was examined indirectly by calculating the amount of radioactive substrate ([^{3}H] Digoxin for MDCKII-MDR1, [^{3}H] Abacavir for MDCKII-BCRP and [^{3}H] Vinblastine for MDCKII-MRP2) transported into the receiver chamber. The donor chamber contained test solution whereas the receiver chamber contained DPBS. The concentration of RX-10045 to be employed for permeability studies were identified and selected from the earlier dose dependent inhibition (IC_{50} value) studies. At predetermined time points (0, 15, 30, 45, 60, 90, 120, 150, and 180 mins), samples were withdrawn from the receiver chamber and was replaced with same volumes of DPBS to maintain sink condition. Further, the concentration of radioactive substrates transported across cell monolayer was determined by measuring radioactivity as described earlier. To determine apparent permeability

and efflux ratio, cumulative amount of radioactive substrate transported was plotted with time according to Eqs 7 – 9.

$$J = (dM/dt)/A \qquad \textit{Eq. 7}$$

J represents flux; (dM/dt) represents amount of radioactive substrate transported across the cell monolayer over a specific interval of time and A represents the cross section area of transwell.

$$P = J/C_{donor} \qquad \textit{Eq. 8}$$

P represents apparent radioactive permeability and C_{donor} represents concentration of radioactive substrate in the donor chamber

$$\text{Efflux ratio} = P_{(BL\text{-}AP)} / P_{(AP\text{-}BL)} \qquad \textit{Eq. 9}$$

Drug efflux ratio may be calculated by the ratio of apparent permeability from BL to AP and AP to BL directions.

Cytotoxicity Studies

To evaluate the cytotoxicity of RX-10045, cell titer 96® aqueous non-radioactive Cell Proliferation Assay Kit (Promega, Madison, WI) was utilized. *In vitro* cytotoxicity assays were conducted across MDCKII-MDR1, MDCKII-BCRP, MDCKII-MRP2, HCEC and human retinal pigment epithelial (D407) cells. In brief, cells were seeded at a density of 10,000 cells per well in 96 well plate. Since the permeability studies were conducted for 3 h, cells were treated with 100 µL of freshly prepared RX-10045 solutions and exposed for 3 h Cells treated with culture medium (containing no drug) served as negative control. Ten percent Triton-X100 served as positive control. After 3 h incubation, 20 µL of aqueous MTS and PMS

reagent (prepared following manufacture's protocol) were added to each well. The mixture was further incubated for 2.5h allowing tetrazolium compound ([3-(4,5-dimethylthiazol-2-yl)-5-(3-carboxymethoxyphenyl-2-(4-sulfophenyl)-2H-tetrazolium, inner salt; MTS] and an electron coupling phenazine methosulfate (PMS)) reaction to take place. The amount of formazan formed was measured with a 96-well micro titer plate reader (SpectraFluor Plus, Tecan, Maennedorf, Switzerland). Absorbance is measured at 490 nm which is directly proportional to the number of living cells in culture.

Statistical Analysis

All experiments were conducted at least in triplicate and results are expressed as mean ± S.D. For IC_{50}, data are expressed as the mean ± S.E.M difference between mean values was considered significant at $p \leq 0.05$. Fisher least-significance difference method was applied to discriminate among the means.

Results

Uptake Studies

Uptake of [^{3}H] Digoxin was conducted in MDCKII-MDR1 cells in the presence of GF120918, and ketoconazole, P-gp inhibitors. Intracellular accumulation of [^{3}H] Digoxin in MDCKII-MDR1 cells in presence of GF120918 and ketoconazole was higher by 1.25 and 1.47 times, respectively. We conducted initial screening uptake experiments for RX-10045 from 50 µM to 600 µM in

MDCK cells transfected with MDR1, MRP and BCRP genes. Since RX-10045 at lower concentrations did not inhibit any substrates of efflux transporter the concentration was increased upto 600 μM, to determine if there is any interaction occurs. In presence of RX-10045 (300 μM) [^{3}H] digoxin accumulation was ~2 times higher than the control ([^{3}H] digoxin) (**Figure 28**). Following similar protocol uptake of [^{3}H]-vinblastine was performed on MDCKII-MRP2 cells. Cellular accumulation of [^{3}H] vinblastine in presence of MK571 was increased by ~1.28 time. RX-10045 (400 μM) also elevated the uptake of [^{3}H] vinblastine to 1.31 times relative to control (**Figure 29**). In another set of experiments, similar results were observed in MDCKII-BCRP cells. Cellular accumulation of [^{3}H] abacavir increased by 1.77 fold in the presence of estradial-β (25 μM) and 1.62 fold in the presence of RX-10045 (300 μM) (**Figure 30**). These results indicate that intracellular accumulation of efflux transporter substrates increased significantly in the presence of RX-10045 relative to control.

Similarly, uptake studies were conducted in HCEC cells in the presence of MDCKII-MDR1, MDCKII-BCRP and MDCKII-MRP inhibitors. Results demonstrated that there was no significant difference in digoxin uptake in the presence of RX-10045. Uptake of [^{3}H] vinblastine was significantly enhanced by 3.43 times in the presence of RX-10045 relative to [^{3}H] vinblastine alone. However, uptake of [^{3}H] abacavir was inhibited in the presence of RX-10045. Cellular accumulation of [^{3}H] abacavir was 3.4 times lower than the control.

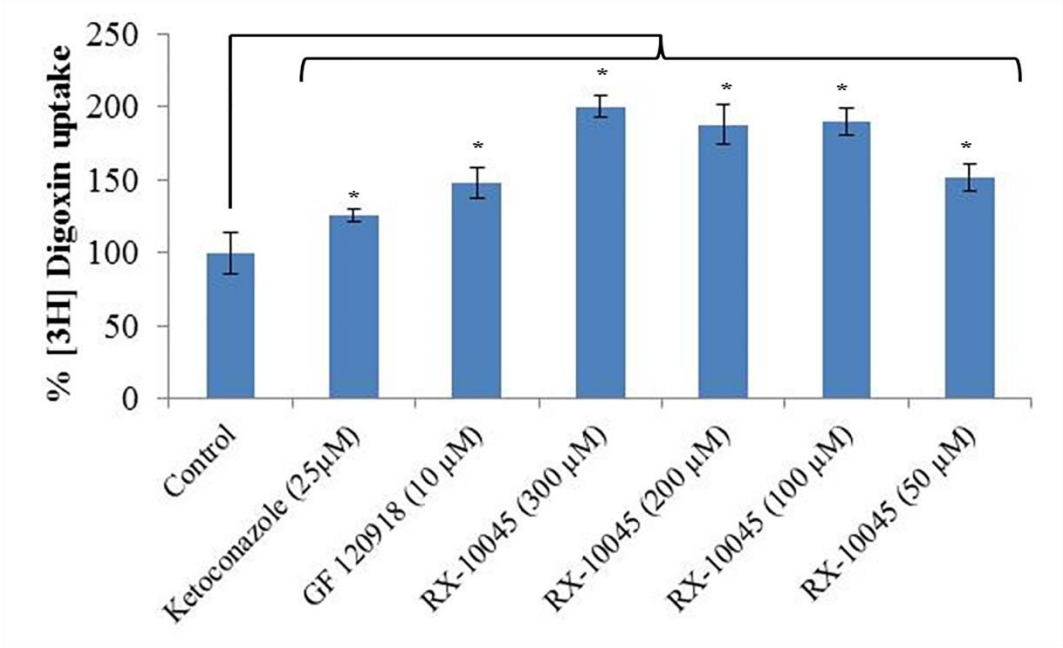

Figure 28. Uptake of [^{3}H] digoxin in presence of inhibitors (GF120918 and Ketoconazole) and increasing concentrations of RX-10045 on MDCKII-MDR1 cells, [^{3}H] Digoxin served as control. Data are shown as mean ± S.E.M (n = 4). *$p < 0.05$ versus control (paired t-test).

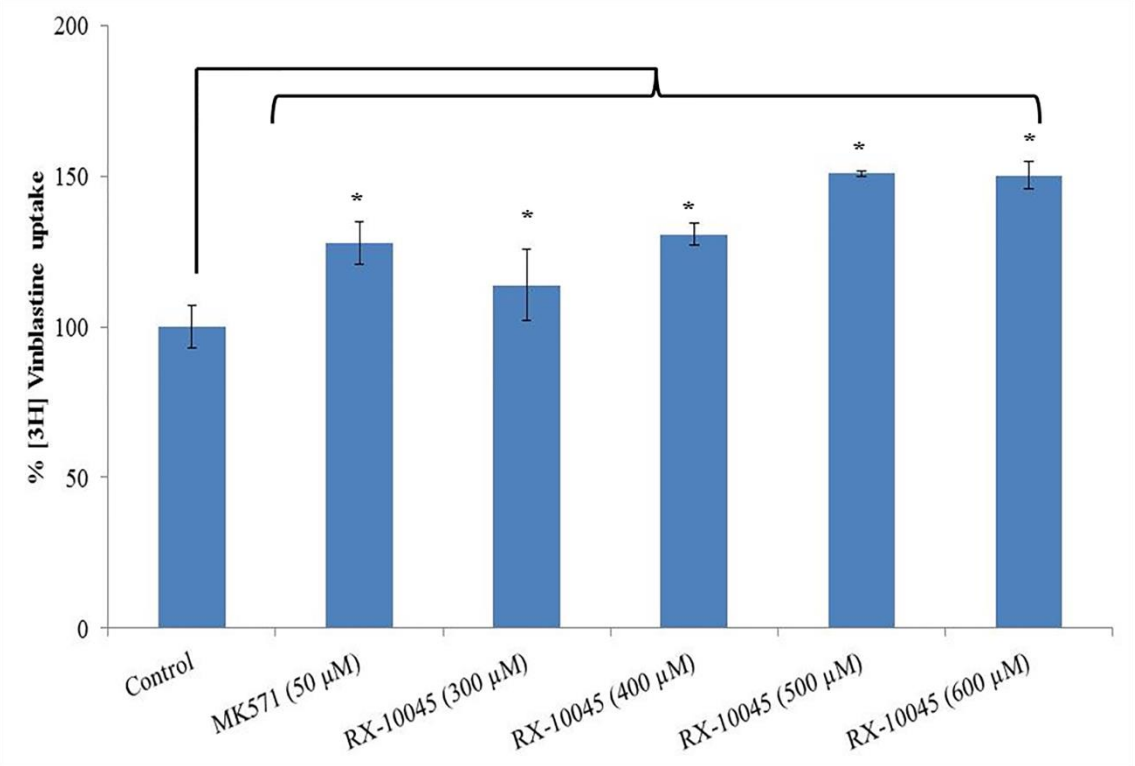

Figure 29. Uptake of [^{3}H] Vinblastine in presence of inhibitor (MK571) and increasing concentrations of RX-10045 on MDCKII-MRP2 cells, [^{3}H] Vinblastine served as control. Data are shown as mean ± S.E.M (n = 4). *$p < 0.05$ versus control (paired t-test).

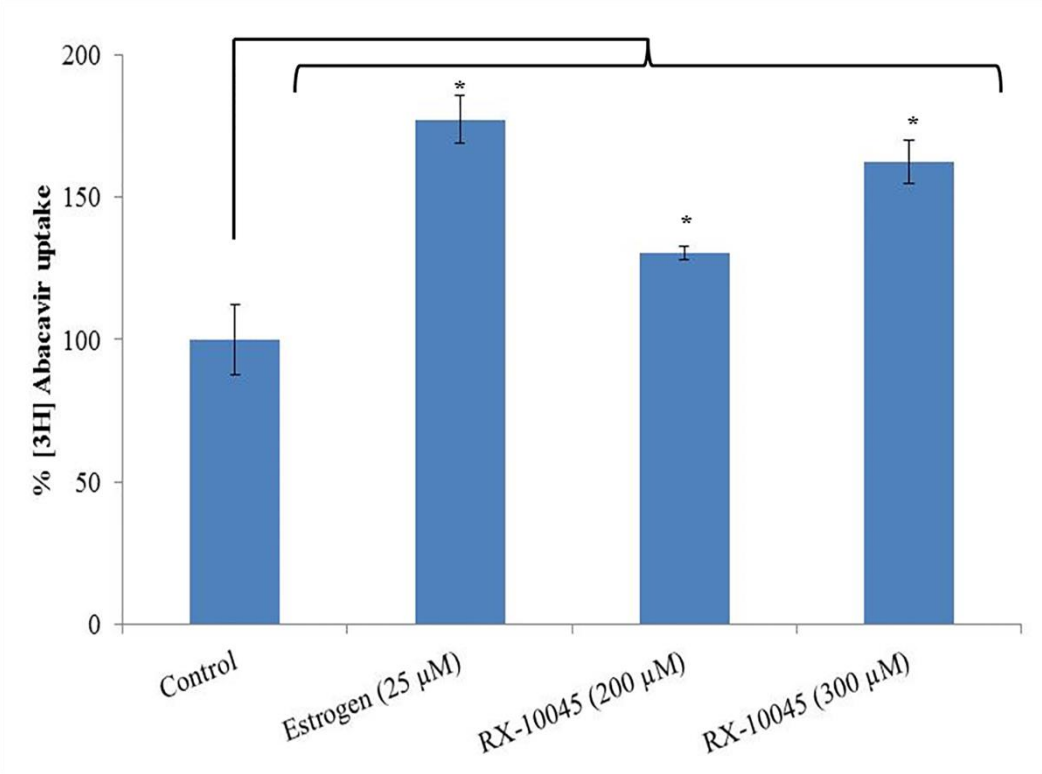

Figure 30. Uptake of [^{3}H] abacavir in presence of inhibitor (estrogen) and increasing concentrations of RX-10045 on MDCKII-BCRP cells, [^{3}H] abacavir served as control. Data are shown as mean ± S.E.M (n = 4). *$p < 0.05$ versus control (paired t-test).

Dose dependent inhibition studies

Half-maximal inhibitory concentrations of RX-10045 were calculated by indirect method using different efflux transporters substrates such as [3H] digoxin for MDCKII-MDR1, [3H] vinblastine for MDCKII-MRP2, and [3H] abacavir for MDCKII-BCRP. IC50 values for RX-10045 were calculated to be 239 ± 11.2 µM in MDCKII-MDR1, 291 ± 79.2 µM on MDCKII-MRP2, and 300 ± 42 µM in MDCKII-BCRP from dose response curves, respectively. **Figure 31** shows half maximal inhibitory concentration in MDCKII-BCRP cells. For further studies such as permeability and cytotoxicity studies, half-maximal inhibitory concentrations were selected and used.

Permeability studies

Transport experiments were conducted across three (MDCKII-MDR1, MDCKII-MRP2 and MDCKII-BCRP) cell lines in both AP-BL and BL-AP direction. These cells express efflux transporters on the apical side only. Apparent permeability of [3H] digoxin in AP-BL direction was not statistically significant in presence of RX-10045 relative to control [3H] digoxin 5.77 ± 0.379 x 10^{-6} cm/min. Similarly, transport of [3H] vinblastine across MDCKII-MRP2 cells was assessed in both AP-BL and BL-AP directions. Similar permeability values were observed as in earlier experiment. Apparent permeability from AP-BL direction for [3H] vinblastine rises in the presence of MK571 (1.66 times) and in the presence of RX-10045 (2.53 times) whereas, apparent apical to basal permeability of control [3H]

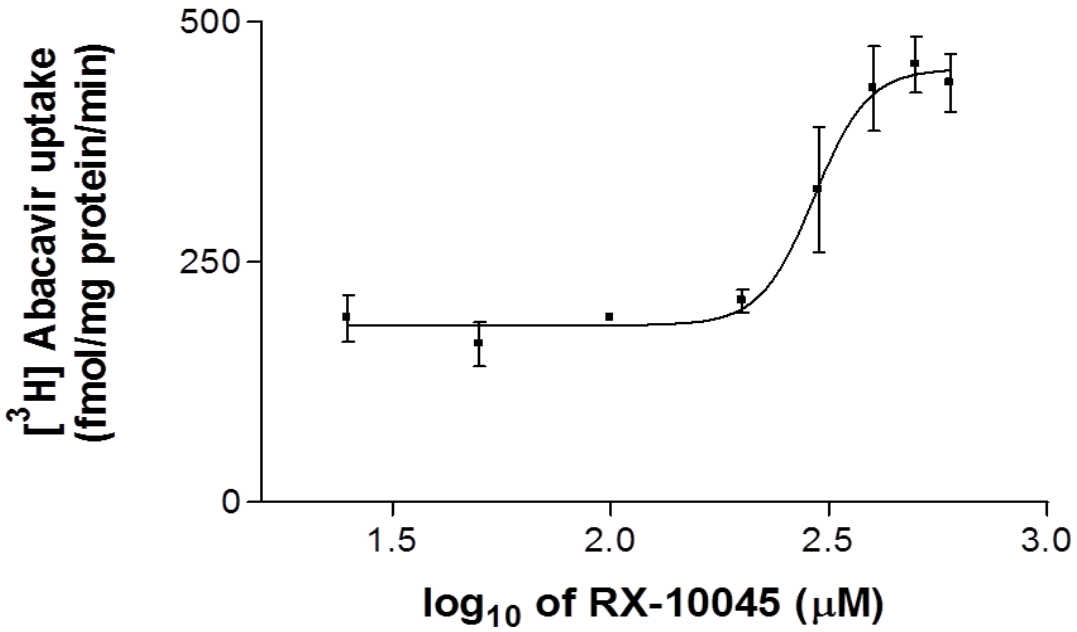

Figure 31. Half maximal inhibitory concentration (IC_{50}) for RX-10045 on MDCKII-BCRP cells. Data are shown as mean ± S.D (n = 4).

vinblastine was calculated to be 0.093 x 10^{-6} ± 0.79 cm/s (**Figure 32**) and *vice versa* and vice versa was 0.440 x 10^{-6} ± 0.0827 (**Figure 33**). In another set of experiments, transport of [3H] abacavir across MDCKII-BCRP cells was assessed in both AP-BL and BL-AP directions. Apparent AP-BL permeability of [3H] abacavir in presence of estradiol (inhibitor) and RX-10045 was enhanced by 2.36 time and 2.42 time, respectively. Apparent permeability of [3H] abacavir control was calculated to be 3.29 ± 1.26 x 10^{-6} cm/s. Cumulative transports of [3H] digoxin, [3H] vinblastine and [3H] abacavir in BL-AP direction in the presence of inhibitor or RX-10045 did not show significant difference.

Cytotoxicity Studies

Cytotoxicity of RX-10045 was evaluated in five cell lines (MDCKII-MDR1, MDCKII-MRP2, MDCKII-BCRP, HCEC and D407) over 3h with different concentrations of RX-10045 ranging from 1 µM to 350 µM. We conducted initial screening uptake experiments from 50 µM to 600 µM in MDCK cells transfected with MDR1, MRP and BCRP genes. Since RX-10045 at lower concentrations did not inhibit any substrate of efflux transporter we increased the concentration up to 600 µM to determine if there is any interaction occurs. However, uptake studies of RX-10045 were conducted at less than 350 µM concentration. Moreover, the IC_{50} value of RX-10045 for all the cell lines was found to be less than 350 µM. Therefore, we conducted cytotoxicity studies up to 350 µM. Cells (MDCK-MDR1, MDCKMRP2, MDCK-BCRP, HCEC and D407) were examined for their viability following manufacturer's protocol. Cells were

added with a dye solution containing MTS. Metabolically active cells in presence of dehydrogenase enzymes reduce MTS to a soluble formazan product. The amount of formazan formed is directly proportional to the number of live cells in culture. Percent cell viability was observed to be the same relative to positive control (culture medium without drug). Concentration range in the current study for RX-10045 appeared to have no effect on cell viability. In this study, 10% Triton-X 100 served as a positive control which significantly reduced cell viability (**Figure 34** - Figure **35**).

Discussion

RX-10045 is a resolvin E1 analog evaluated for the treatment of dry eye, ocular inflammation and ocular fibrosis. Interactions of resolvins with efflux transporters have not been previously investigated. This study therefore examined interactions between RX-10045 and efflux transporters P-gp, MRP2 and BCRP, whose expression and functional activity on corneal epithelium was previously reported (308-312). To evaluate drug interactions, MDCKII cell lines that are transfected with MDR1, MRP2 and BCRP human genes were selected for the current study. The rationale behind using MDCKII transfected cell lines which overexpress efflux transporters P-gp, MRP and BCRP was to delineate individual efflux transporter mediated interactions. These cell lines help in identification of the individual role of efflux transporters in reducing intracellular drug concentrations and permeability. Moreover results may help to modulate ocular

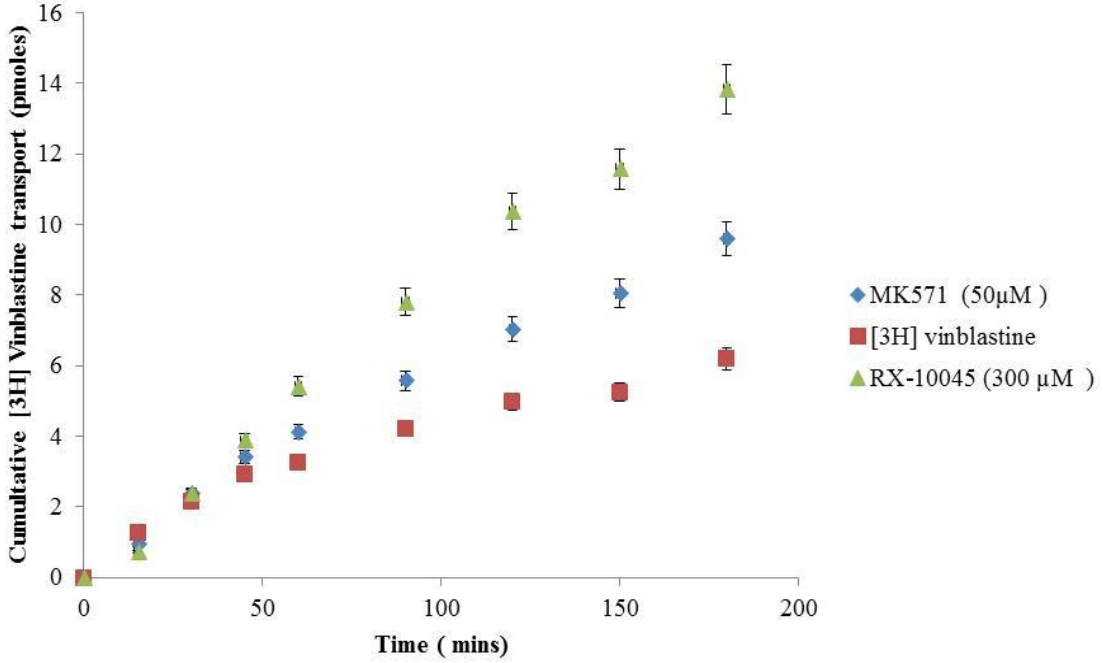

Figure 32. Apical to basal apparent permeability of [^{3}H] Vinblastine in presence of inhibitor (MK571) and RX-10045 with [^{3}H] Vinblastine alone as control. Data are shown as mean ± S.D (n = 4). *p < 0.05 versus control (paired t-test).

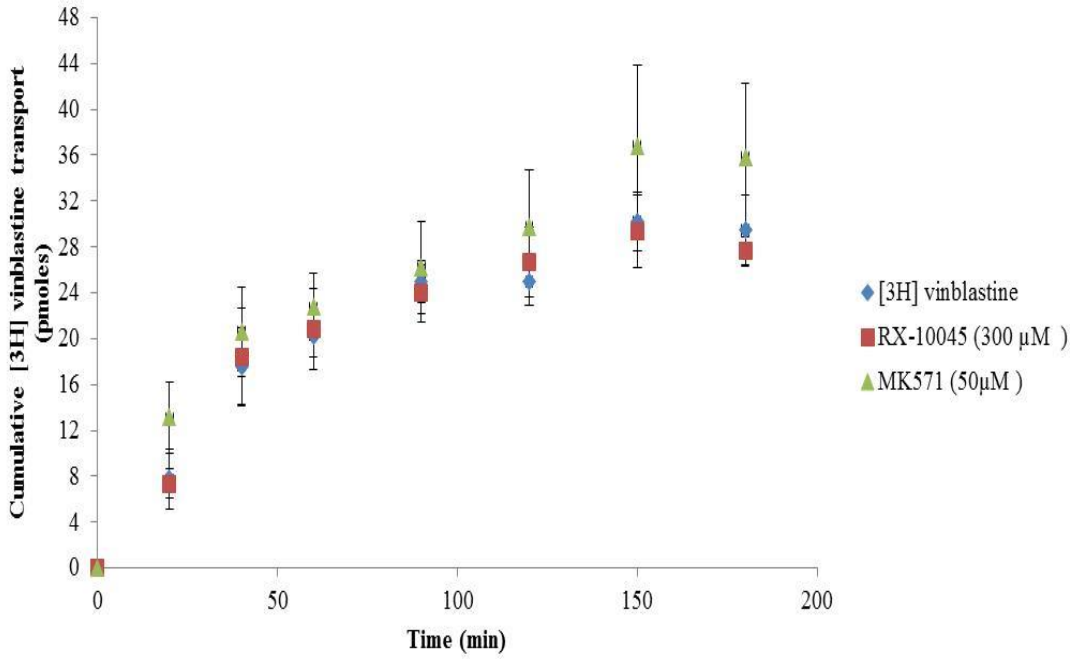

Figure 33. Basal to Apical apparent permeability of [^{3}H] Vinblastine in presence of inhibitor (MK571) and RX-10045 with [^{3}H] Vinblastine alone as control. Data are shown as mean ± S.D (n = 4). *$p < 0.05$ versus control (paired t-test).

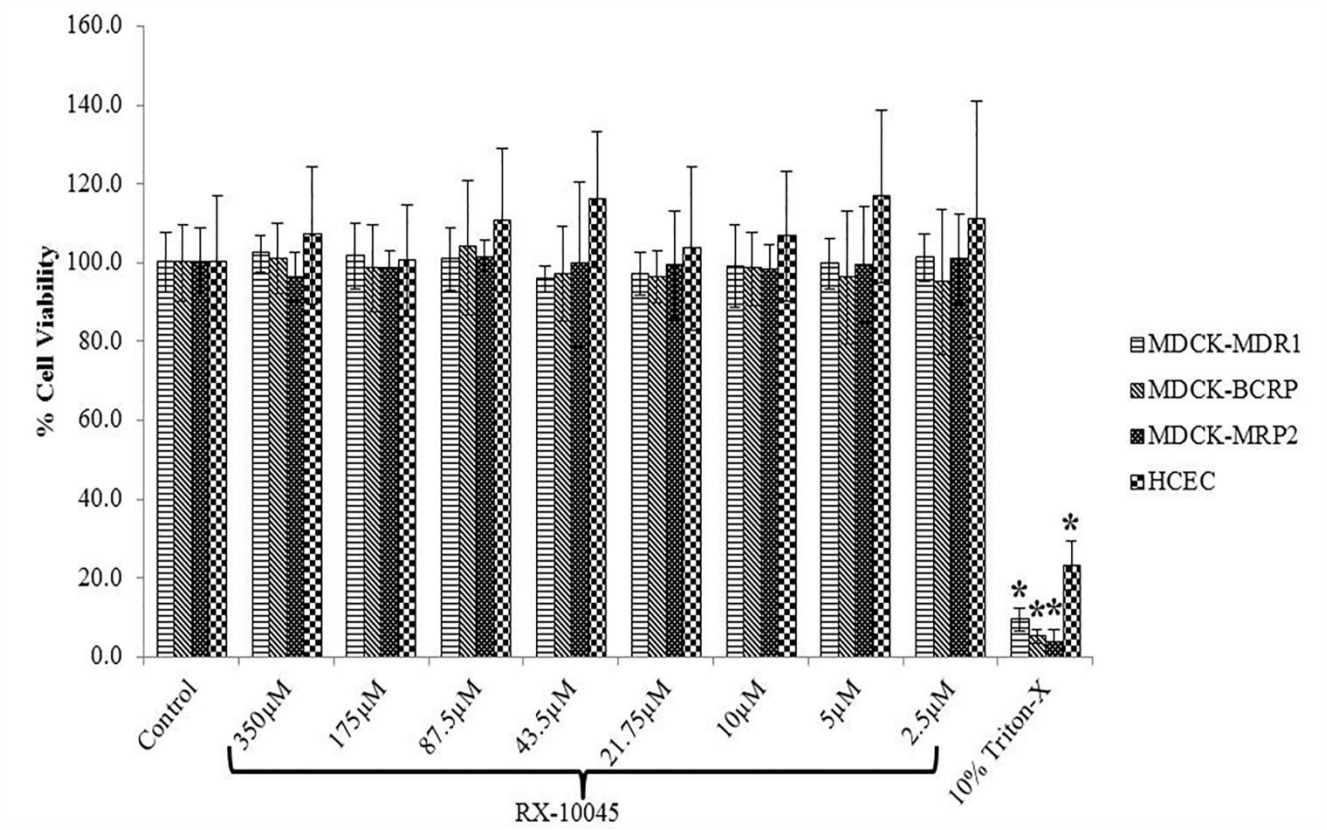

Figure 34. Cell viability studies with increasing concentrations of RX-10045. Cell culture medium served as positive control and Triton X-100 served as negative control. A p value of < 0.05 is considered significant. Data are shown as mean ± S.E.M (standard error of mean) (n = 8). *$p < 0.05$ versus control (paired t-test).

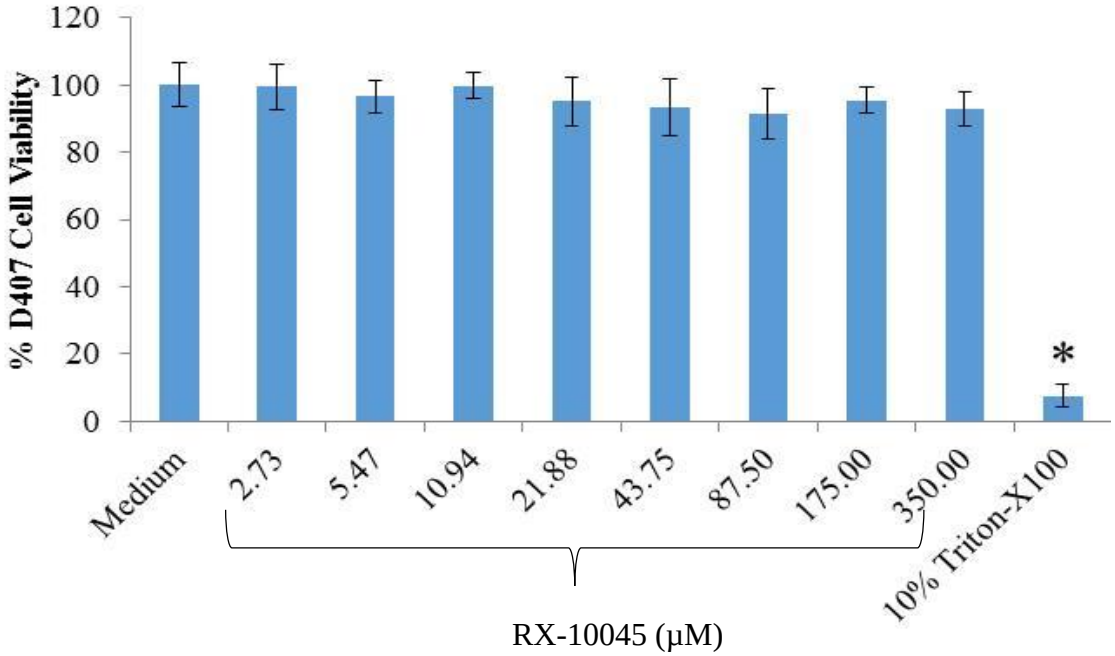

Figure 35. Cell viability studies with increasing concentrations of RX-10045 on D407 cells. Cell culture medium served as positive control and Triton X-100 served as negative control. A *p* value of < 0.05 is considered significant. Data are shown as mean ± S.E.M (standard error of mean) (n = 8). *$p < 0.05$ versus control (paired t-test).

drug delivery strategies for delivery of therapeutic amounts of RX-10045 to ocular tissues. Intracellular accumulation of [^{3}H] digoxin was significantly elevated in presence of P-gp inhibitors (GF 120918 and ketoconazole) and RX-10045 relative to [^{3}H] digoxin only (309, 313, 314). This result indicates that RX-10045 may interact with P-gp similar to other P-gp inhibitors. This interaction results in higher cellular accumulation of [^{3}H] digoxin. This observation suggests that RX-10045 may be a substrate for P-gp. In another set of experiments conducted on MDCKII–MRP2 cells with [^{3}H] vinblastine revealed higher accumulation in cells treated with inhibitor (MK571) and RX-10045. This suggests that RX-10045 may also interact with MRP2 as competitive inhibitor, resulting in higher [^{3}H] vinblastine uptake. Similarly, we conducted studies with MDCKII–BCRP cells with [^{3}H] abacavir. Higher accumulation of [^{3}H] abacavir in the presence of beta-estradiol and RX-10045 was observed relative to control suggesting that this resolvin analog may be a substrate or inhibitor of BCRP. A significant rise in [^{3}H] digoxin, [^{3}H] vinblastine and [^{3}H] abacavir uptake in the presence of GF120918, ketoconazole, MK571 and beta-estradiol indicates that P-gp, MRP2 and BCRP are highly expressed on MDCKII transfected cells and are functionally active. These results are consistent with our earlier results (307, 312, 315). Uptake experiments indicate that RX-10045 may be a substrate or inhibitor for all three efflux transporters (P-gp, MRP2 and BCRP). Dose dependent inhibition (IC_{50}) in uptake studies suggest affinity of RX-10045 towards P-gp, BCRP and MRP2. RX-10045 inhibited MDCKII-MRP2 and MDCKII-BCRP mediated efflux in a dose dependent manner.

Efflux transporters such as P-gp, MRP2 and BCRP are involved in the extrusion of a variety of therapeutic agents. Since the efflux transporters (P-gp, BCRP and MRP2) are localized on the apical surface, [^{3}H] digoxin, [^{3}H] vinblastine and [^{3}H] abacavir alone exhibited significantly lower transport in the AP-BL direction relative to BL-AP direction (**Table 12**). The efflux ratio (ratio of BL-AP *vs* AP-BL) is considered to be an indicator to identify efflux transporter (P-gp, MRP2 and BCRP) substrates (316). When the ratio of apparent permeability (BL-AP / AP-BL) approaches 1.0 then transport is equal in both directions. Efflux ratios of [^{3}H] digoxin, [^{3}H] vinblastine and [^{3}H] abacavir were found to be 2.07, 4.75 and 10.35 in MDCKII-MDR1, MDCKII-MRP2 and MDCKII-BCRP cells, respectively. A significant reduction in efflux ratio was evident in the presence of GF120918, MK-571 and beta-estradiol, confirming inhibition of P-gp, MRP2 and BCRP functional activities (**Table 12**). Furthermore, the presence of RX-10045 affected AP-BL permeability of [^{3}H] digoxin, [^{3}H] vinblastine and [^{3}H] abacavir. The efflux ratio is reduced in MDCKII-MDR1, MDCKII-BCRP and MDCKII-MRP2 cells (**Table 12**). This significant reduction in efflux ratio further confirms substrate specificity of RX-10045 towards P-gp, MRP2 and BCRP. There was no significant difference observed in permeability of [^{3}H] digoxin in presence of RX-10045 indicating non interaction with P-gp compared to other transmembrane efflux proteins (MRP2 and BCRP). A significant reduction in efflux ratio was evident in the presence of MK-571 and beta-estradiol, confirming inhibition of MRP2 and BCRP functional activities (**Table 12**). Furthermore, the presence of RX-10045 affected AP-BL permeability of [^{3}H] vinblastine and [^{3}H] abacavir. The

Table 12. Apparent permeability of [^{3}H] Digoxin, [^{3}H] Vinblastine and [^{3}H] Abacavir in presence of inhibitors and RX-10045.

Cell type		Apical to Basolateral (X 10^{-6})	Basolateral to Apical (X 10^{-6})	Efflux ratio
MDCKII-MDR1	[^{3}H] Digoxin	5.77 ± 0.38	11.96 ± 2.59	2.07
	GF (5μM)	6.07 ± 0.39	10.95 ± 1.57	1.80
	RX-10045 (350 μM)	5.86 ± 0.30	11.13 ± 0.95	1.90
MDCKII-MRP2	[^{3}H] Vinblastine	0.093 ± 0.028	0.440 ± 0.083	4.75
	MK571 (50μM)	0.154 ± 0.050	0.389 ± 0.005	2.53
	RX-10045 (300 μM)	0.235 ± 0.079	0.430 ± 0.190	1.83
MDCKII-BCRP	[^{3}H] Abacavir	3.29 ± 1.26	34.09 ± 2.73	10.35
	Estradiol-2 (25μM)	7.77 ± 0.883	27.61 ± 3.24	3.56
	RX-10045 (350 μM)	7.95 ± 1.38	31.96 ± 0.62	4.02

efflux ratio is reduced in MDCKII-BCRP and MDCKII-MRP2 cells, but not much in MDCKMDR1 cells (**Table 12**). This significant reduction in efflux ratio further confirms substrate specificity of RX-10045 towards MRP2 and BCRP. Uptake studies in HCEC cells demonstrated no effect of MDR1 (P-gp) on digoxin efflux in the presence of RX-10045. Results were comparable to MDCKII-MDR1 cells. However, uptake of MRP2 substrate ([^{3}H] vinblastine) was significantly improved. We observed that the uptake of [^{3}H] vinblastine was approximately 5 times higher in HCEC cells relative to MDCK-MRP2 cells possibly due to differences in isoforms expression in HCEC/MDCK-MRP2 cells. Tang F. Horie et al. reported that different isoforms of MRP2 are overexpressed in MDCK-MRP2 cells (150 kD) and Caco2 cells (190 kD) with a different kinetic profile (317).Therefore, these isoforms also make the difference in substrate specificity i.e, percent [^{3}H] vinblastine uptake resulting in higher cellular accumulation. The uptake of [^{3}H] abacavir along with RX-10045 was significantly reduced demonstrating reversal in drug accumulation relative to control [^{3}H] abacavir alone (**Figure 36**). This surprising result prompted us to investigate the cause of inhibition of [^{3}H] abacavir uptake in presence of RX-10045. Abacavir is a known substrate for organic cation transporter-1 (OCT), and HCEC cells highly express OCT-1 (318, 319). Therefore increase in HCEC cell uptake of [^{3}H] abacavir may be due to uptake by the OCT-1 transporter. The presence of RX-10045 inhibited the [^{3}H] abacavir uptake because this resolvin can cause inhibition of OCT-1 transporter. To determine its inhibitory effect, uptake and inhibition studies of [^{3}H] abacavir were performed in presence of 100 µM quinine (an OCT-1 inhibitor). Uptake of [^{3}H] abacavir was significantly

reduced in presence of quinine and RX-10045 is a strong inhibitor of OCT-1 (**Figure 36**).

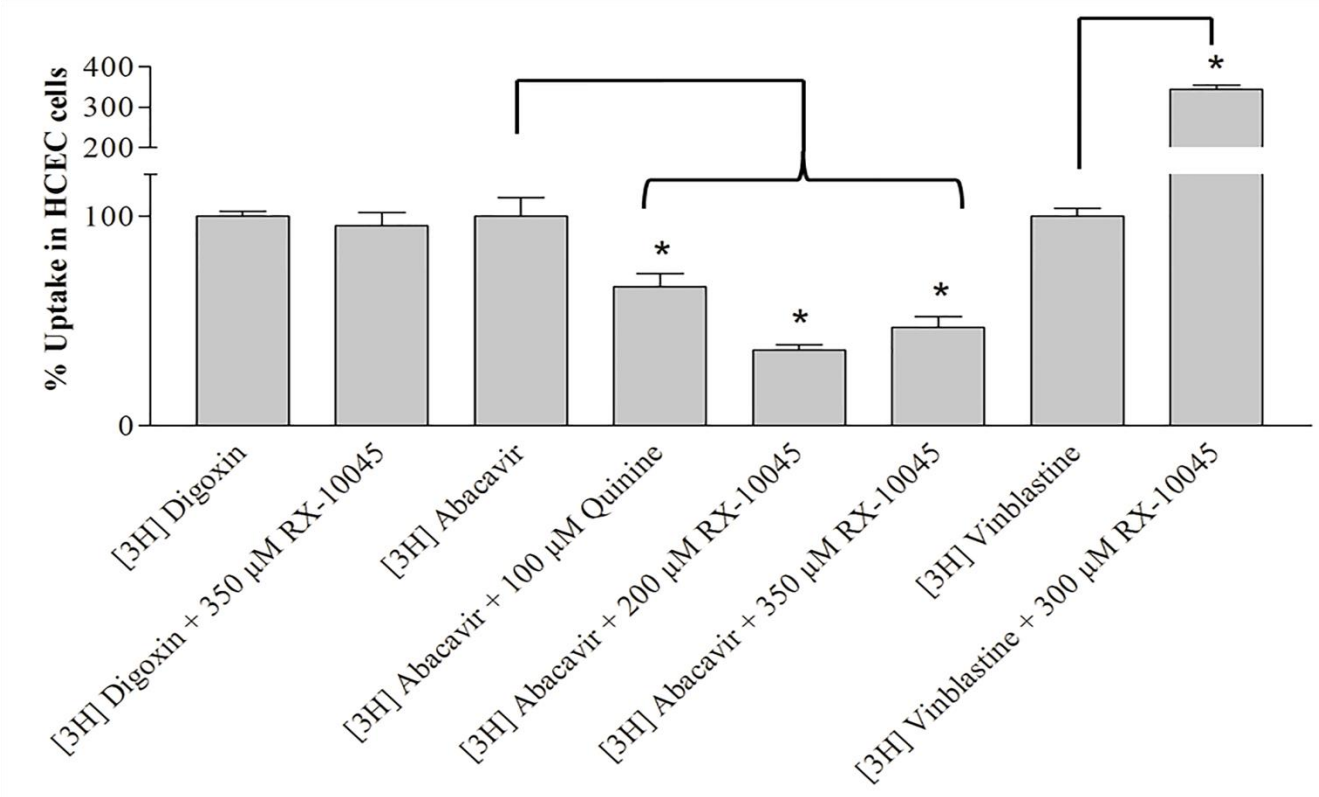

Figure 36. Uptake studies in human corneal epithelial cells (HCEC) for tritiated digoxin, abacavir and vinblastine in presence of RX-10045 at IC50 concentrations. A *p* value of < 0.05 is considered significant. Data are shown as mean ± S.E.M (n = 4). *p < 0.05 versus control (paired t-test).

PART B: FORMULATION OPTIMIZATION AND IN VIVO EVALUATION

Materials and Methods

Purified RX-10045 (physical state- solid; lot number: NR13799-969-143) was obtained from PPD. Hydrogenated castor oil-40 (HCO-40) of pharmaceutical grade was procured from Barnet Products, USA and Octoxynol-40 (Oc-40 or Igepal CA-897) was purchased from Rohdio Inc, New Jersey, USA. Ethyl acetate (HPLC grade) was purchased from Fischer Scientific, USA. PVP-K90 (lot # 56943447G0) was obtained from BASF Aktiengesellschaft 67056 Ludwigshafen Germany. Benzalkonium chloride was obtained from Sigma chemical Co. St. Louis, Missouri, USA. Disodium EDTA, sodium chloride and sodium citrate were purchased from Fischer Chemicals, USA. Citric acid was purchased from Sigma Chemical Co., USA. For buffer and formulation preparation double distilled deionized water was used. Water was degassed for 20 minutes prior to preparation.

Methods

Nanomicelle preparation

To prepare 100 mL of nanomicellar formulation of RX-10045 the experimental procedure was divided into two steps (i) basic formulation preparation and (ii) rehydration step.

(i) *Basic formulation preparation*: Briefly, 0.05 g and 0.1 g of RX-10045 (0.05% and 0.1%) was accurately weighed in an Eppendorf tube, HCO-

40 (1.0 %) and octoxynol-40 (0.05 %), were accurately weighed and dissolved separately in ethyl acetate. All the solutions, in calculated amounts were mixed together to prepare a homogenized solution. Organic solvent was evaporated under high vacuum overnight to obtain a homogenized thin film. The film was resuspended in 40 mL of 0.1 M citrate buffer (pH 5.5) (see below). This resulted in a homogenous clear aqueous solution. The volume of the mixture was made upto 50 mL with 0.1 M citrate buffer.

(ii) *Rehydration*: The above obtained clear solution was divided equally (25 mL each) into two round bottom flasks. To first flask, 25 mL of preservative free 2x citrate buffer (pH 5.5) was added and mixed thoroughly to obtain a homogenous clear aqueous solution. Similarly, the second round bottom flask (containing 25 mL of basic formulation of RX-10045) was mixed with 25 mL of 2x citrate buffer (pH 5.5) (see below for preparation) containing preservatives and was stirred for homogeneity. Both formulations i.e., with and without preservatives were filtered through 0.2 µm nylon filter.

Following similar procedure as described above placebo formulations for the RX-10045 were prepared. For the placebo formulation preparation RX-10045 was not added/used.

Citrate buffer (pH 5.5) preparation

Citric acid monohydrate 21.01 g was dissolved in one liter of water (0.1M citric acid). Similarly, 29.41 g of trisodium citrate dehydrate was dissolved separately in water (0.1 M sodium citrate). To prepare 100 mL of 0.1 M citrate buffer 21.0 mL of citric acid (0.1 M) was transferred to a 250mL flask and the volume was made up with 0.1M sodium citrate (79 mL). The mixture was mixed by stirring to get a homogenous buffer solution. The pH of the buffer was adjusted to 5.5 with 0.1 N HCl or 0.1 N NaOH.

Preparation of 2x Preservative free buffer

To prepare 2x citrate buffer 40 mL of 0.1 M citrate buffer (pH 5.5) was added with 0.1 wt% of sodium chloride and dissolved under constant stirring. PVP-K90 (0.6%) was accurately weighed and slowly dissolved under constant stirring until a clear homogenous solution is obtained. The pH of the buffer was measured and adjusted, if required, to 5.5 with 0.1 N HCl or 0.1 N NaOH. Finally, the volume was made upto 50 mL with 0.1 M citrate buffer.

Preparation of 2x buffer with preservatives

To prepare 2x citrate buffer 40 mL of 0.1 M citrate buffer (pH 5.5) was added with 0.1 wt% of sodium chloride and dissolved under constant stirring. Disodium EDTA (0.05%) was added and dissolved. Similarly, benzalkonium chloride (0.003%) was added and dissolved. Further, PVP-K90 (0.6%) was weighed and slowly dissolved under constant stirring until a clear homogenous solution is obtained. The pH of the buffer was measured and adjusted to 5.5 with

0.1 N HCl or 0.1 N NaOH, if required. Finally, the volume was made upto 50 mL with 0.1 M citrate buffer.

HPLC Analysis

In vitro analysis of RX-10045 was performed by a reversed phase RP-HPLC method with a Shimadzu HPLC pump (Shimadzu, Shimadzu Scientific instruments, Columbia, MD), Alcott autosampler (model 718 AL), Shimadzu UV/Visible detector (Shimadzu, SPD-20A/20AV, USA), ODS column (5 µm, 150 x 4.6 mm) thermostated at 40 ± 1 ºC and Hewlett Packard HPLC integrator (Hewlett Packard, Palo Alto, CA). The mobile phase was comprised of methanol (MeOH), water and trifluoroacetic acid (TFA) (70:30:0.05% v/v) which was set at a flow rate of 0.5 mL/min. Detection wavelength was set at 272 nm. The sample tray temperature was maintained at 4 ºC. Calibration curve (0.5 µg/mL to 5 µg/mL) for RX-10045 (injection volume 10 µL) was prepared by making appropriate dilutions from stock solution in 2-propanol.

UPLC Analysis

UPLC System consisted of Waters UPLC Acquity H Class with UPLC TUV& PDA Detector (230 nm) and data system: Waters Empower 2. Waters Acquity CSHTM C18 (1.7 µM, 2.1 × 50 mm) column was used for separation. Column temperature was maintained at 50 °C and autosampler temperature was set at 4 °C. The mobile phase was composed of phase A: 0.1% formic acid in water and Phase B: 0.1% formic acid in methanol and UPLC TUV Detector set at 230

nm. Injection volume was 2 µL. A gradient solvent system (see **Table 13**) was employed for separation and analysis.

LC-MS/MS Analysis

All *in vivo* ocular tissues, fluids and blood samples were analyzed with LC-MS/MS described in Chapter 3 (Pg# 89). Selected ocular fluids/tissues (aqueous humor, vitreous humor, conjunctiva, cornea, iris-ciliary body, lens, retina/ choroid, and sclera) collected from rabbits in the RX-10045 (0.1% in HCO-40) treatment groups, and from one rabbit in each of the matching placebo groups, were assayed for compound RX-1001 and another resolvin by liquid chromatography-tandem mass spectrometry (LC-MS/MS) with gradient mobile phase system (**Table 13**). Warfarin-d5 and 5-HDA were used as internal standards for the analysis of RX-10045 and its active metabolite, RX-10008, respectively, in aqueous humor and vitreous humor. For other ocular tissues, Warfarin-d_5 and phenyl acetic acid-d_5 (PAA-d_5) were used as the internal standards for compound 1001 and RX-10008, respectively. The analytical range for ocular tissues ranged between 0.125-100 ng. The results of the ocular tissue analyses were converted to ng/g by correcting for the amount of tissue analyzed.

Formulation Characterization

The prepared RX-10045 nanomicellar formulations (with and without preservatives) were subjected to characterization following procedures described in Chapter 3 for entrapment efficiency, loading efficiency, size,

Table 13. UPLC gradient mobile phase composition for RX-10045 sample stability analysis.

Time (min)	Flow Rate	A (%)	B (%)
0	0.5	70	30
9	0.5	52	48
10	0.5	70	30
15	0.5	70	30

Table 14. Storage Conditions of RX-10045 Formulation Samples

RX-10045 Mixed Nanomicellar Formulation (inert gas, time point, temperature (°C))			
Preservative	**Preservative**	**Preservative**	**Preservative**
N2, amber, 0 Day, 4°C	No N2, amber, 0 Day, 4°C	N2, clear, 0 Day, 4°C	No N2, clear, 0 Day, 4°C
N2, amber, 1 Day, 4°C	No N2, amber, 1 Day, 4°C	N2, clear, 1 Day, 4°C	No N2, clear, 1 Day, 4°C
N2, amber, 9 Days, 4°C	No N2, amber, 9 Days, 4°C	N2, clear, 9 Days, 4°C	No N2, clear, 9 Days, 4°C
N2, amber, 30 Days, 4°C	No N2, amber, 30 Days, 4°C	N2, clear, 30 Days, 4°C	No N2, clear, 30 Days, 4°C
N2, amber, 2 Mo, 4°C	No N2, amber, 2 Mo, 4°C	N2, clear, 2 Mo, 4°C	No N2, clear, 2 Mo, 4°C
N2, amber, 3 Mo, 4°C	No N2, amber, 3 Mo, 4°C	N2, clear, 3 Mo, 4°C	No N2, clear, 3 Mo, 4°C
N2, amber, 4 Mo, 4°C	No N2, amber, 4 Mo, 4°C	N2, clear, 4 Mo, 4°C	No N2, clear, 4 Mo, 4°C
N2, amber, 6 Mo, 4°C	No N2, amber, 6 Mo, 4°C	N2, clear, 6 Mo, 4°C	No N2, clear, 6 Mo, 4°C
N2, amber, 0 Day, 25°C	No N2, amber, 0 Day, 25°C	N2, clear, 0 Day, 25°C	No N2, clear, 0 Day, 25°C
N2, amber, 1 Day, 25°C	No N2, amber, 1 Day, 25°C	N2, clear, 1 Day, 25°C	No N2, clear, 1 Day, 25°C
N2, amber, 9 Days, 25°C	No N2, amber, 9 Days, 25°C	N2, clear, 9 Days, 25°C	No N2, clear, 9 Days, 25°C
N2, amber, 30 Days, 25°C	No N2, amber, 30 Days, 25°C	N2, clear, 30 Days, 25°C	No N2, clear, 30 Days, 25°C
N2, amber, 2 Mo, 25°C	No N2, amber, 2 Mo, 25°C	N2, clear, 2 Mo, 25°C	No N2, clear, 2 Mo, 25°C
N2, amber, 3 Mo, 25°C	No N2, amber, 3 Mo, 25°C	N2, clear, 3 Mo, 25°C	No N2, clear, 3 Mo, 25°C
N2, amber, 4 Mo, 25°C	No N2, amber, 4 Mo, 25°C	N2, clear, 4 Mo, 25°C	No N2, clear, 4 Mo, 25°C
N2, amber, 6 Mo, 25°C	No N2, amber, 6 Mo, 25°C	N2, clear, 6 Mo, 25°C	No N2, clear, 6 Mo, 25°C
N2, amber, 0 Day, 40°C	No N2, amber, 0 Day, 40°C	N2, clear, 0 Day, 40°C	No N2, clear, 0 Day, 40°C
N2, amber, 1 Day, 40°C	No N2, amber, 1 Day, 40°C	N2, clear, 1 Day, 40°C	No N2, clear, 1 Day, 40°C
N2, amber, 9 Days, 40°C	No N2, amber, 9 Days, 40°C	N2, clear, 9 Days, 40°C	No N2, clear, 9 Days, 40°C
N2, amber, 30 Days, 40°C	No N2, amber, 30 Days, 40°C	N2, clear, 30 Days, 40°C	No N2, clear, 30 Days, 40°C
N2, amber, 2 Mo, 40°C	No N2, amber, 2 Mo, 40°C	N2, clear, 2 Mo, 40°C	No N2, clear, 2 Mo, 40°C
N2, amber, 3 Mo, 40°C	No N2, amber, 3 Mo, 40°C	N2, clear, 3 Mo, 40°C	No N2, clear, 3 Mo, 40°C
N2, amber, 4 Mo, 40°C	No N2, amber, 4 Mo, 40°C	N2, clear, 4 Mo, 40°C	No N2, clear, 4 Mo, 40°C
N2, amber, 6 Mo, 40°C	No N2, amber, 6 Mo, 40°C	N2, clear, 6 Mo, 40°C	No N2, clear, 6 Mo, 40°C
No preservative	**No preservative**	**No preservative**	**No preservative**
N2, amber, 0 Day, 4°C	No N2, amber, 0 Day, 4°C	N2, clear, 0 Day, 4°C	No N2, clear, 0 Day, 4°C
N2, amber, 1 Day, 4°C	No N2, amber, 1 Day, 4°C	N2, clear, 1 Day, 4°C	No N2, clear, 1 Day, 4°C
N2, amber, 9 Days, 4°C	No N2, amber, 9 Days, 4°C	N2, clear, 9 Days, 4°C	No N2, clear, 9 Days, 4°C
N2, amber, 30 Days, 4°C	No N2, amber, 30 Days, 4°C	N2, clear, 30 Days, 4°C	No N2, clear, 30 Days, 4°C
N2, amber, 2 Mo, 4°C	No No N2, amber, 2 Mo, 4°C	N2, clear, 2 Mo, 4°C	No N2, clear, 2 Mo, 4°C
N2, amber, 3 Mo, 4°C	No N2, amber, 3 Mo, 4°C	N2, clear, 3 Mo, 4°C	No N2, clear, 3 Mo, 4°C
N2, amber, 4 Mo, 4°C	No N2, amber, 4 Mo, 4°C	N2, clear, 4 Mo, 4°C	No N2, clear, 4 Mo, 4°C
N2, amber, 6 Mo, 4°C	No N2, amber, 6 Mo, 4°C	N2, clear, 6 Mo, 4°C	No N2, clear, 6 Mo, 4°C
N2, amber, 0 Day, 25°C	No N2, amber, 0 Day, 25°C	N2, clear, 0 Day, 25°C	No N2, clear, 0 Day, 25°C
N2, amber, 1 Day, 25°C	No N2, amber, 1 Day, 25°C	N2, clear, 1 Day, 25°C	No N2, clear, 1 Day, 25°C
N2, amber, 9 Days, 25°C	No N2, amber, 9 Days, 25°C	N2, clear, 9 Days, 25°C	No N2, clear, 9 Days, 25°C
N2, amber, 30 Days, 25°C	No N2, amber, 30 Days, 25°C	N2, clear, 30 Days, 25°C	No N2, clear, 30 Days, 25°C
N2, amber, 2 Mo, 25°C	No No N2, amber, 2 Mo, 25°C	N2, clear, 2 Mo, 25°C	No N2, clear, 2 Mo, 25°C
N2, amber, 3 Mo, 25°C	No N2, amber, 3 Mo, 25°C	N2, clear, 3 Mo, 25°C	No N2, clear, 3 Mo, 25°C
N2, amber, 4 Mo, 25°C	No N2, amber, 4 Mo, 25°C	N2, clear, 4 Mo, 25°C	No N2, clear, 4 Mo, 25°C
N2, amber, 6 Mo, 25°C	No N2, amber, 6 Mo, 25°C	N2, clear, 6 Mo, 25°C	No N2, clear, 6 Mo, 25°C
N2, amber, 0 Day, 40°C	No N2, amber, 0 Day, 40°C	N2, clear, 0 Day, 40°C	No N2, clear, 0 Day, 40°C
N2, amber, 1 Day, 40°C	No N2, amber, 1 Day, 40°C	N2, clear, 1 Day, 40°C	No N2, clear, 1 Day, 40°C
N2, amber, 9 Days, 40°C	No N2, amber, 9 Days, 40°C	N2, clear, 9 Days, 40°C	No N2, clear, 9 Days, 40°C
N2, amber, 30 Days, 40°C	No N2, amber, 30 Days, 40°C	N2, clear, 30 Days, 40°C	No N2, clear, 30 Days, 40°C
N2, amber, 2 Mo, 40°C	No No N2, amber, 2 Mo, 40°C	N2, clear, 2 Mo, 40°C	No N2, clear, 2 Mo, 40°C
N2, amber, 3 Mo, 40°C	No N2, amber, 3 Mo, 40°C	N2, clear, 3 Mo, 40°C	No N2, clear, 3 Mo, 40°C
N2, amber, 4 Mo, 40°C	No N2, amber, 4 Mo, 40°C	N2, clear, 4 Mo, 40°C	No N2, clear, 4 Mo, 40°C
N2, amber, 6 Mo, 40°C	No N2, amber, 6 Mo, 40°C	N2, clear, 6 Mo, 40°C	No N2, clear, 6 Mo, 40°C

Table 15. Storage Conditions of Placebo Formulation Samples

Mixed Nanomicellar Formulation without RX-10045 (inert gas, time point, temperature (°C))			
Preservative	**Preservative**	**Preservative**	**Preservative**
N2, amber, 0 Day, 25°C	No N2, amber, 0 Day, 25°C	N2, clear, 0 Day, 25°C	No N2, clear, 0 Day, 25°C
N2, amber, 30 Day, 25°C	No N2, amber, 30 Day, 25°C	N2, clear, 30 Day, 25°C	No N2, clear, 30 Day, 25°C
N2, amber, 4 Mo, 25°C	No N2, amber, 4 Mo, 25°C	N2, clear, 4 Mo, 25°C	No N2, clear, 4 Mo, 25°C
N2, amber, 4 Mo, 40°C	No N2, amber, 4 Mo, 40°C	N2, clear, 4 Mo, 40°C	No N2, clear, 4 Mo, 40°C
N2, amber, 6 Mo, 4°C	No N2, amber, 6 Mo, 4°C	N2, clear, 6 Mo, 4°C	No N2, clear, 6 Mo, 4°C
N2, amber, 6 Mo, 25°C	No N2, amber, 6 Mo, 25°C	N2, clear, 6 Mo, 25°C	No N2, clear, 6 Mo, 25°C
N2, amber, 6 Mo, 40°C	No N2, amber, 6 Mo, 40°C	N2, clear, 6 Mo, 40°C	No N2, clear, 6 Mo, 40°C
No preservative	**No preservative**	**No preservative**	**No preservative**
N2, amber, 0 Day, 25°C	No N2, amber, 0 Day, 25°C	N2, clear, 0 Day, 25°C	No N2, clear, 0 Day, 25°C
N2, amber, 30 Day, 25°C	No N2, amber, 30 Day, 25°C	N2, clear, 30 Day, 25°C	No N2, clear, 30 Day, 25°C
N2, amber, 4 Mo, 25°C	No N2, amber, 4 Mo, 25°C	N2, clear, 4 Mo, 25°C	No N2, clear, 4 Mo, 25°C
N2, amber, 4 Mo, 40°C	No N2, amber, 4 Mo, 40°C	N2, clear, 4 Mo, 40°C	No N2, clear, 4 Mo, 40°C
N2, amber, 6 Mo, 4°C	No N2, amber, 6 Mo, 4°C	N2, clear, 6 Mo, 4°C	No N2, clear, 6 Mo, 4°C
N2, amber, 6 Mo, 25°C	No N2, amber, 6 Mo, 25°C	N2, clear, 6 Mo, 25°C	No N2, clear, 6 Mo, 25°C
N2, amber, 6 Mo, 40°C	No N2, amber, 6 Mo, 40°C	N2, clear, 6 Mo, 40°C	No N2, clear, 6 Mo, 40°C

polydispersity index, surface potential, and proton NMR studies. HPLC-UV was used for determining entrapment and drug loading.

Formulation stability studies were conducted at three different temperatures (4 ^{o}C, 25 ^{o}C and 40 ^{o}C) by dividing the formulations into different sub-groups and subjecting them to various conditions (**Table 14** and **Table 15**). At predetermined time points (0 day, 1 day, 9days, 30 days, 2 month, 3 month, 4 month and 6 month) both placebo and RX-10045 loaded nanomicellar formulation samples were collected into 200 µL HPLC inserts/vials and immediately stored at -80 ºC until further analysis with Ultra performance liquid chromatography (UPLC). After collecting samples the nitrogen gas labeled/containing formulation vials were filled with nitrogen gas, immediately sealed and the cap was wrapped with paraffin to prevent any leaks.

In vivo studies

A study was conducted in New Zealand White rabbits (2-3 kg) following the protocol described in Chapter # 3 to test the tolerance and ocular tissue distribution of 0.1% nanomicellar for formulations of compound 1001 (RX10045) (containing preservatives) against matching placebo and balanced saline solution (BSS). One topical drop (approximately 35 µL) of formulation (placebo/RX-10045 loaded) was applied o.d. 4X/day at two hour intervals for 5 days. One drop of BSS was applied to the contralateral eye. The tolerance parameters evaluated were physical examination (acclimation study release); viability (daily); clinical observations (daily); Hackett-McDonald Ocular Irritation scores (pre-dose)

baseline data for each rabbit and then a pre-dose (prior to first daily dose) each day and then 30 min after last dose daily, intraocular pressure (IOP) pre-dose base line data for each rabbit and then 30 minutes after the evening examinations each day, electroretinography (ERG) pre-dose (pre-study) baseline data for each rabbit and then one hour after the last treatment, and ocular histopathology at euthanasia. Ocular tissues, fluids (vitreous and aqueous humor) and blood samples were collected following similar protocol described previously in Chapter # 3.

Results

RX-10045 is a yellow oily viscous resolvin analog. It is highly unstable at room temperature and easily susceptible to degradation upon exposure to light and air. Therefore, pure yellow oily RX-10045 is stored at -80 ^{o}C with nitrogen atmosphere in dark. Nanomicellar formulations of RX-10045 (0.05% and 0.1%) were successfully prepared with the blend of HCO-40 and Oc-40 (**Figure 37**). The ratio of HCO-40/Oc-40 was set at 1.0:0.05 due to its low critical micellar concentrations relative to individual polymers. The size of placebo and RX-10045 (0.05% and 0.1%) loaded nanomicellar formulation was 10.37 ± 0.3 nm, 11.7 ± 1.2 nm and 11.2. ± 1.3 nm, respectively. The surface potential was slightly negative or negligible (-0.0237 mV). Proton nuclear magnetic resonance studies clearly demonstrated the absence of free RX-10045 in nanomicellar formulation (**Figure 38 - Figure 41**). Drug peaks were evident in organic solvent ($CDCl_3$) while the same drug peaks disappeared when resuspended in aqueous (D_2O) solution.

Stability studies for RX-10045 (0.1%) loaded nanomicellar formulation was conducted at different temperatures. Samples pulled/collected at predetermined time points appear clear/transparent to the naked eye (no yellow color development observed). Further the concentration of RX-10045 remaining in the formulation was quantified. The drug RX-10045 if degraded it is converted to its active parent molecule RX-10008. Both, resolvin E1 analog and the RX-10008 were quantified in long term stability studies. **Figure 42** through **Figure 46** represents, respective chromatograms for stability studies. Below description is provided for stability evaluation of RX-10045. All the results for RX-10045 stability for 6 months are summarized in **Table 16**.

Stability evaluation

The stability of RX-10045 in the various formulations under the storage conditions employed was evaluated by comparing RX-10045 peak area percent of the storage samples relative to that of the corresponding Day-0 sample.

For Example: Day-30 Stability by

RX-10045 Peak Area %: = RX-10045 Area % (Day-30)/RX-10045 Area % (Day-0) x 100 *Eq 10*

In vivo studies

Tolerability studies for placebo and RX-10045 nanomicellar formulations indicated that the formulations were safe and well tolerated. No IOP increase was observed with multiple topical drop administration of RX-10045 formulation. Results for tolerability studies are presented in **Table 17**. Mean ocular tissue and

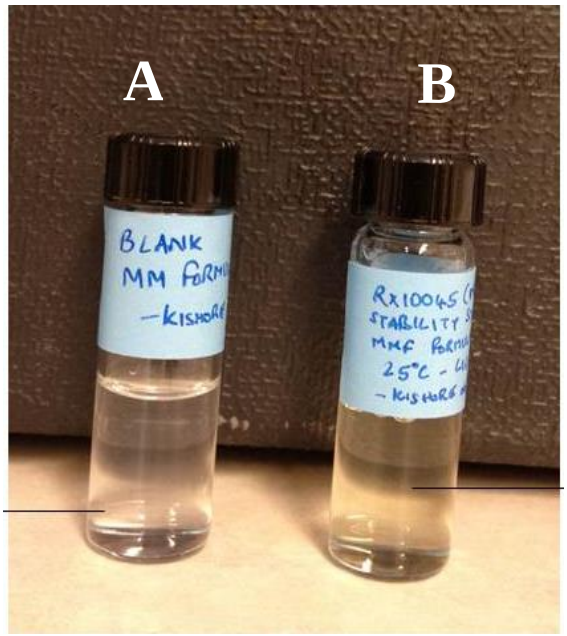

Figure 37. Image showing nanomicellar formulation (A) blank/placebo formulation and (B) RX-10045 (0.1%) loaded nanomicellar formulation.

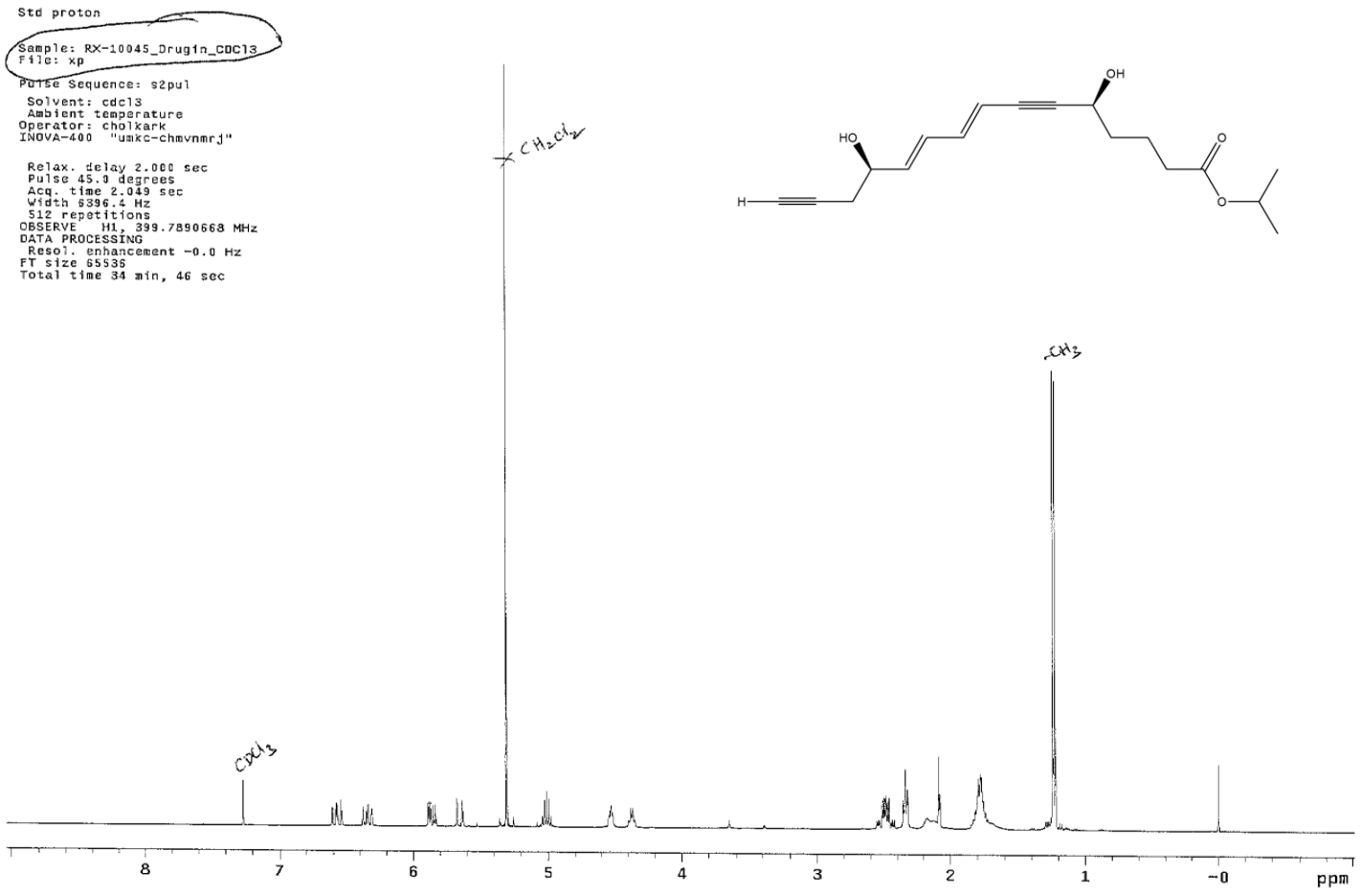

Figure 38. ^{1}H NMR spectrum for RX-10045 oily pure drug in $CDCl_3$

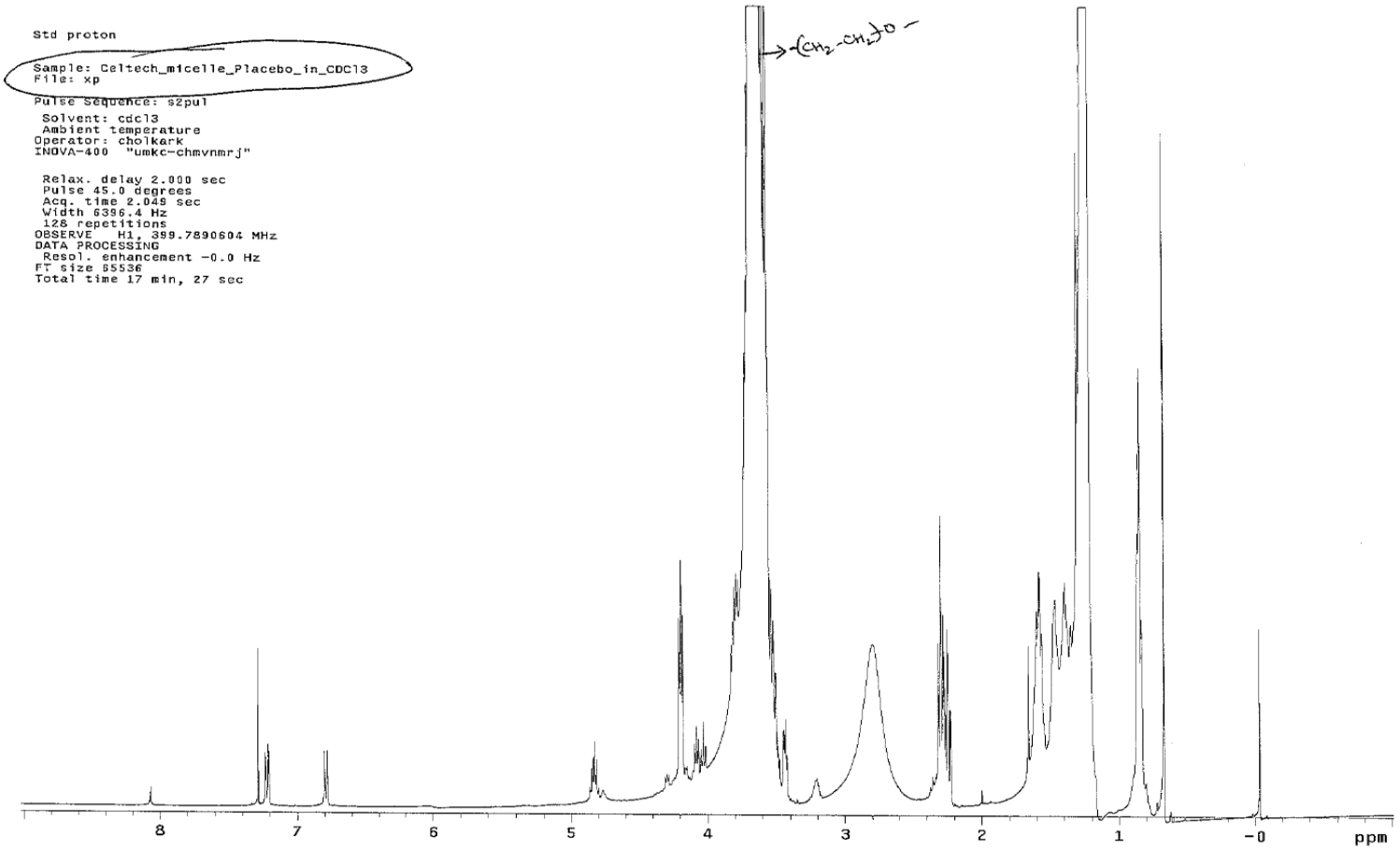

Figure 39. ^{1}H NMR spectrum for placebo HCO-40 polymer micelles in $CDCl_3$

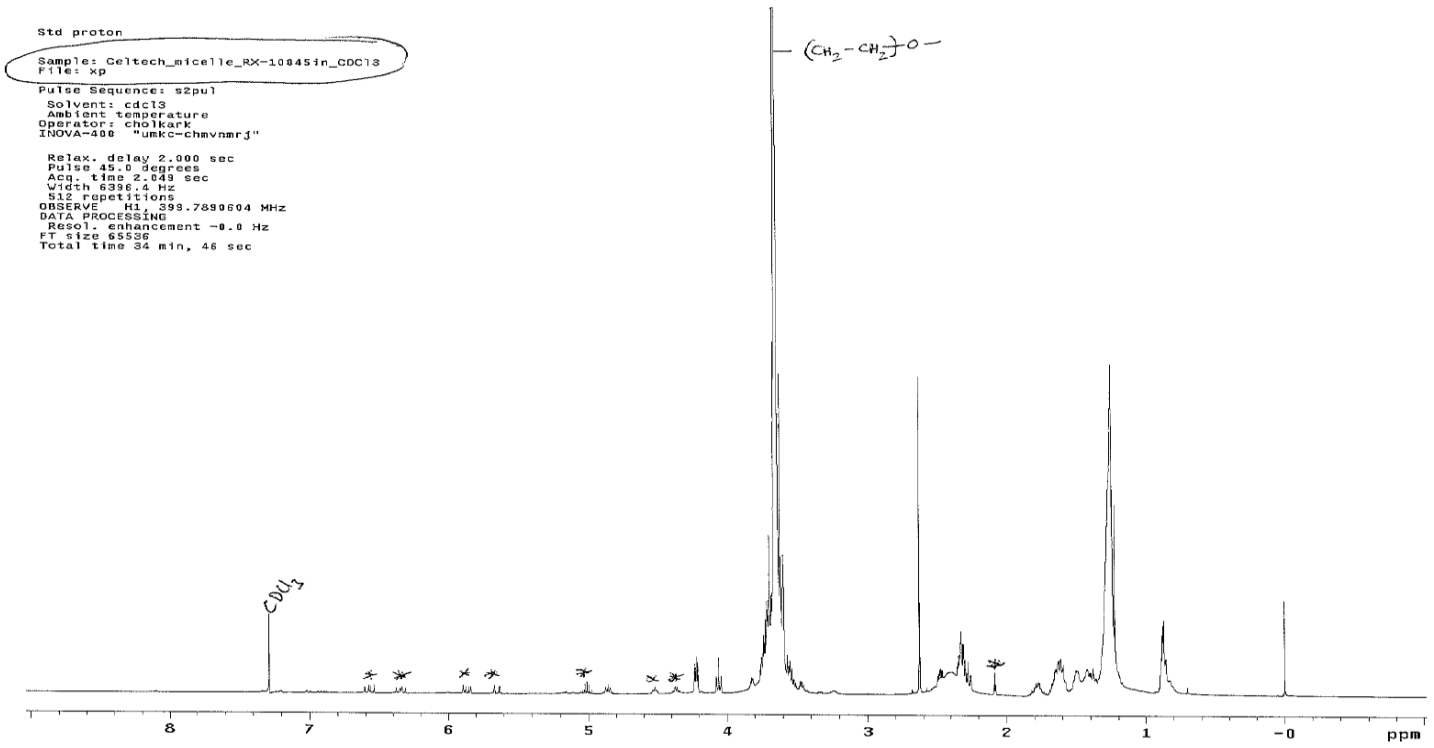

Figure 40. ^{1}H NMR spectrum for nanomicellar formulation of 0.1% RX-10045 resuspended in $CDCl_3$. Symbol (*) represents RX-10045 drug peaks evident in the formulation along with HCO-40 polymeric peaks

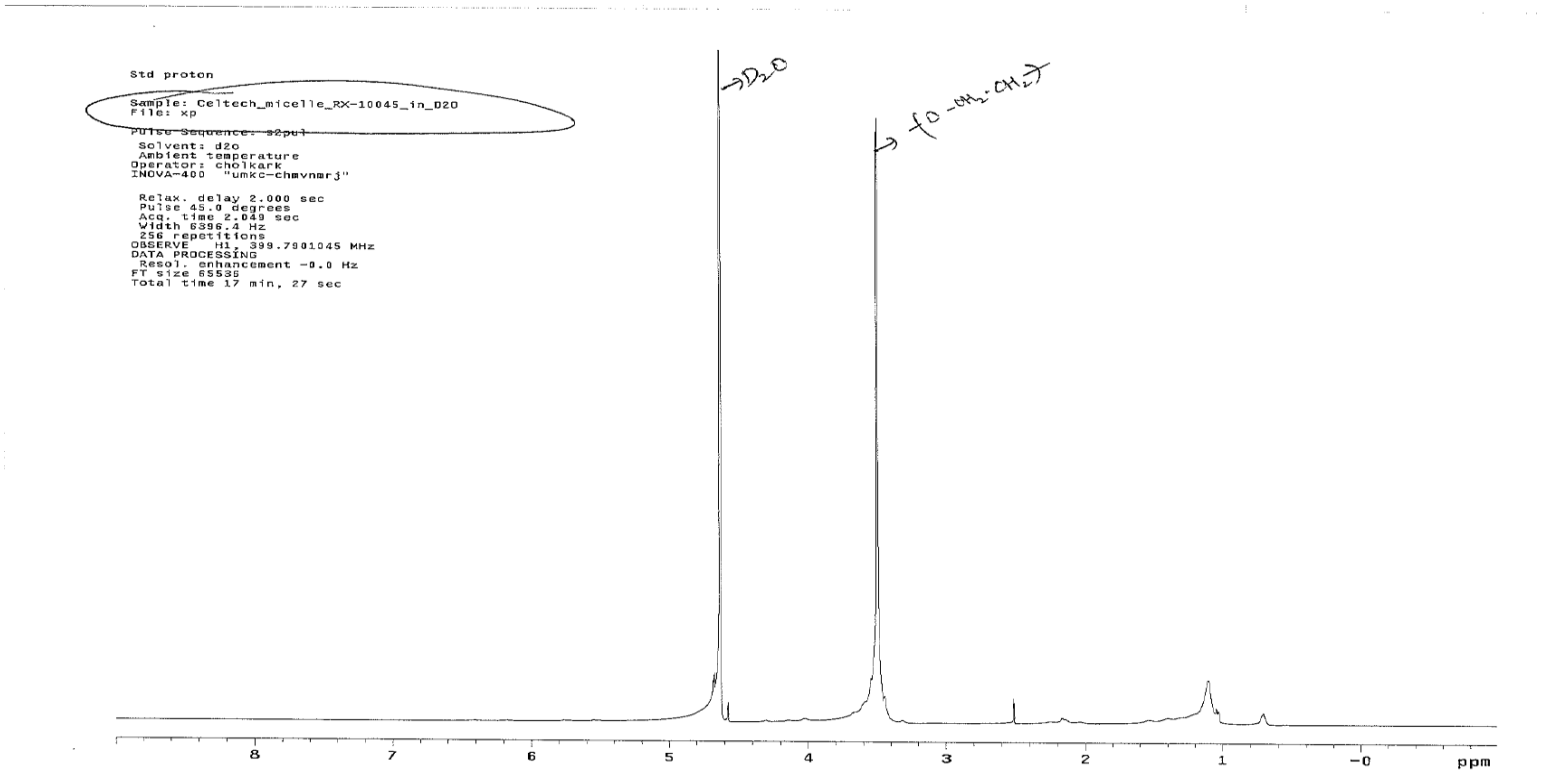

Figure 41. ^{1}H NMR spectrum for nanomicellar formulation of RX-10045 (0.1%) resuspended in D_2O.

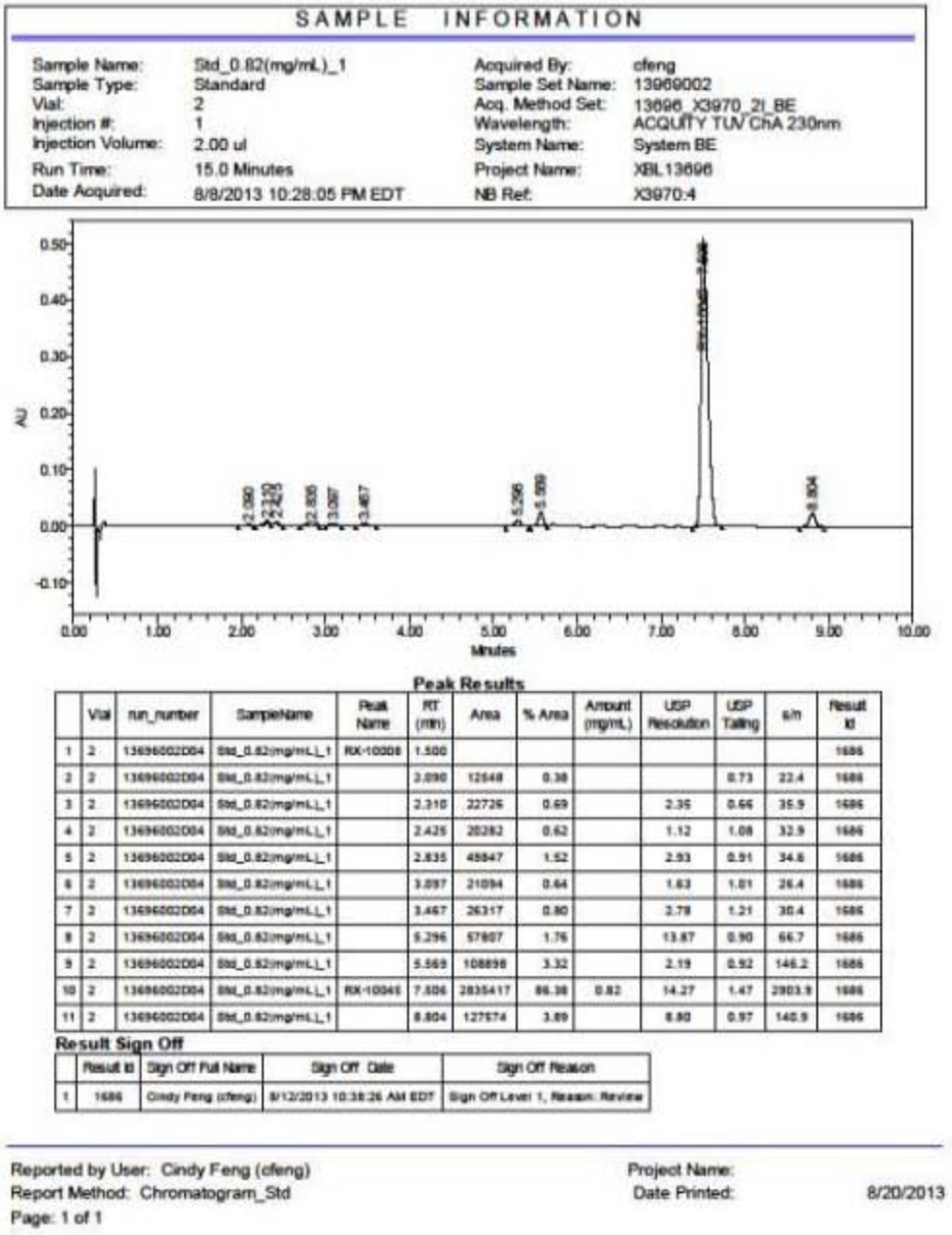

SAMPLE INFORMATION

Sample Name:	Std_0.82(mg/mL)_1	Acquired By:	cfeng
Sample Type:	Standard	Sample Set Name:	13969002
Vial:	2	Acq. Method Set:	13696_X3970_2I_BE
Injection #:	1	Wavelength:	ACQUITY TUV ChA 230nm
Injection Volume:	2.00 ul	System Name:	System BE
Run Time:	15.0 Minutes	Project Name:	XBL13696
Date Acquired:	8/8/2013 10:28:05 PM EDT	NB Ref:	X3970:4

Peak Results

	Vial	run_number	SampleName	Peak Name	RT (min)	Area	% Area	Amount (mg/mL)	USP Resolution	USP Tailing	s/n	Result Id
1	2	13696002D04	Std_0.82(mg/mL)_1	RX-10008	1.500							1686
2	2	13696002D04	Std_0.82(mg/mL)_1		2.090	12548	0.38			0.73	22.4	1686
3	2	13696002D04	Std_0.82(mg/mL)_1		2.310	22726	0.69		2.35	0.66	35.9	1686
4	2	13696002D04	Std_0.82(mg/mL)_1		2.425	20282	0.62		1.12	1.08	32.9	1686
5	2	13696002D04	Std_0.82(mg/mL)_1		2.835	45847	1.52		2.93	0.91	34.6	1686
6	2	13696002D04	Std_0.82(mg/mL)_1		3.097	21094	0.64		1.63	1.01	26.4	1686
7	2	13696002D04	Std_0.82(mg/mL)_1		3.467	26317	0.80		2.78	1.21	30.4	1686
8	2	13696002D04	Std_0.82(mg/mL)_1		5.296	57807	1.76		13.87	0.90	66.7	1686
9	2	13696002D04	Std_0.82(mg/mL)_1		5.569	108898	3.32		2.19	0.92	146.2	1686
10	2	13696002D04	Std_0.82(mg/mL)_1	RX-10045	7.506	2835417	86.38	0.82	14.27	1.47	2903.9	1686
11	2	13696002D04	Std_0.82(mg/mL)_1		8.804	127574	3.89		8.80	0.97	140.9	1686

Result Sign Off

	Result Id	Sign Off Full Name	Sign Off Date	Sign Off Reason
1	1686	Cindy Feng (cfeng)	8/12/2013 10:38:26 AM EDT	Sign Off Level 1, Reason: Review

Reported by User: Cindy Feng (cfeng)
Report Method: Chromatogram_Std
Page: 1 of 1

Project Name:
Date Printed: 8/20/2013

Figure 42. Representative UPLC-UV Chromatogram of RX-10045 Standard.

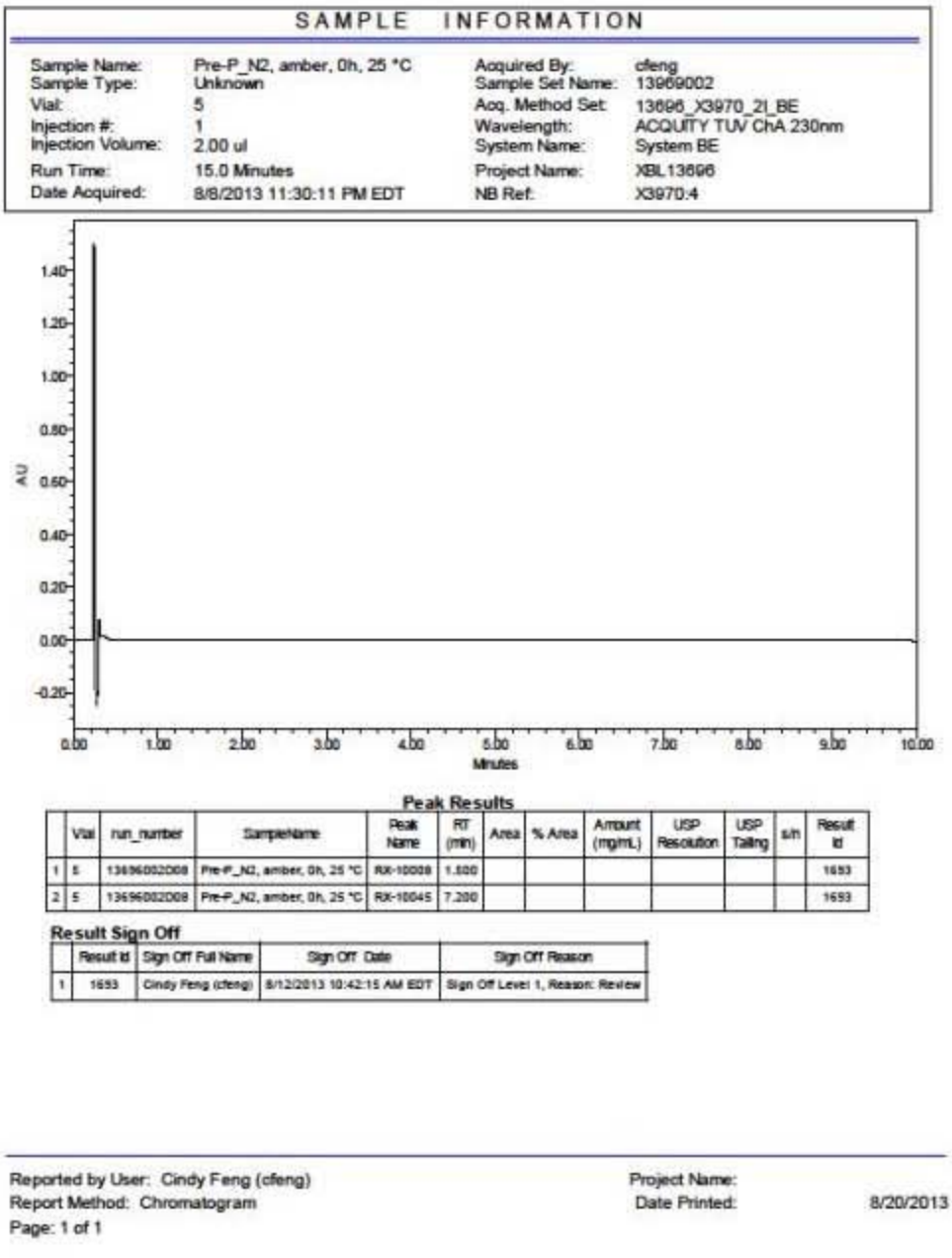

SAMPLE INFORMATION

Sample Name:	Pre-P_N2, amber, 0h, 25 °C	Acquired By:	cfeng
Sample Type:	Unknown	Sample Set Name:	13969002
Vial:	5	Acq. Method Set:	13696_X3970_2I_BE
Injection #:	1	Wavelength:	ACQUITY TUV ChA 230nm
Injection Volume:	2.00 ul	System Name:	System BE
Run Time:	15.0 Minutes	Project Name:	XBL13696
Date Acquired:	8/8/2013 11:30:11 PM EDT	NB Ref:	X3970:4

Peak Results

	Vial	run_number	SampleName	Peak Name	RT (min)	Area	% Area	Amount (mg/mL)	USP Resolution	USP Tailing	s/n	Result Id
1	5	13696002D08	Pre-P_N2, amber, 0h, 25 °C	RX-10008	1.500							1693
2	5	13696002D08	Pre-P_N2, amber, 0h, 25 °C	RX-10045	7.200							1693

Result Sign Off

	Result Id	Sign Off Full Name	Sign Off Date	Sign Off Reason
1	1693	Cindy Feng (cfeng)	8/12/2013 10:42:15 AM EDT	Sign Off Level 1, Reason: Review

Reported by User: Cindy Feng (cfeng)
Report Method: Chromatogram
Page: 1 of 1

Project Name:
Date Printed: 8/20/2013

Figure 43. Representative UPLC-UV Chromatogram of Placebo Formulation.

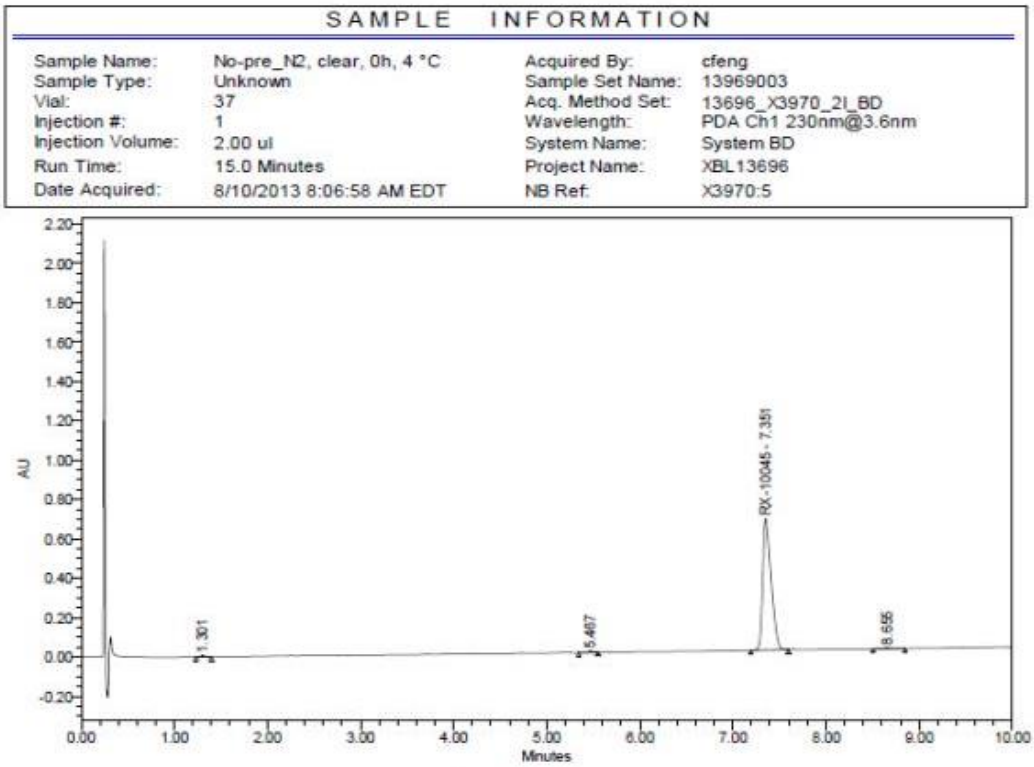

Peak Results

	Vial	run_number	SampleName	Peak Name	RT (min)	Area	% Area	Amount (mg/mL)	USP Resolution	USP Tailing	s/n	Result Id
1	37	13696003D46	No-pre_N2, clear, 0h, 4 °C		1.301	22981	0.55			1.03	2.3	2076
2	37	13696003D46	No-pre_N2, clear, 0h, 4 °C	RX-10008	1.500							2076
3	37	13696003D46	No-pre_N2, clear, 0h, 4 °C		5.467	26204	0.62		39.03	0.86	2.0	2076
4	37	13696003D46	No-pre_N2, clear, 0h, 4 °C	RX-10045	7.351	4135770	98.19	1.17	12.54	1.52	231.2	2076
5	37	13696003D46	No-pre_N2, clear, 0h, 4 °C		8.655	27246	0.65		8.05	0.76	1.7	2076

Result Sign Off

	Result Id	Sign Off Full Name	Sign Off Date	Sign Off Reason
1	2076	Cindy Feng (cfeng)	8/12/2013 11:11:12 AM EDT	Sign Off Level 1, Reason: Review

Reported by User: Cindy Feng (cfeng)
Report Method: Chromatogram
Page: 1 of 1
Project Name:
Date Printed: 8/12/201

Figure 44. UPLC-UV Chromatogram of Day-0 RX-10045 Formulation, No Preservative, No N_2, Clear, 4 °C Sample.

SAMPLE INFORMATION

Sample Name:	No-Pre_N2, clear, 6M, 4 °C	Acquired By:	cfeng
Sample Type:	Unknown	Sample Set Name:	13969005
Vial:	70	Acq. Method Set:	13696_X3970_2I_BD
Injection #:	1	Wavelength:	PDA Ch1 230nm@3.6nm
Injection Volume:	2.00 ul	System Name:	System BD
Run Time:	15.0 Minutes	Project Name:	XBL13696
Date Acquired:	1/25/2014 10:23:19 PM EST	NB Ref:	X3970:9

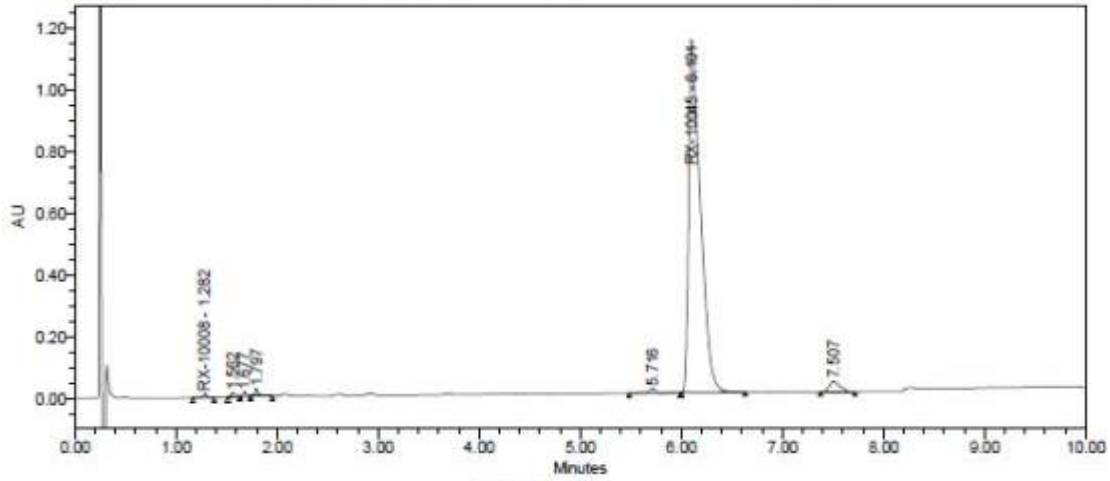

Peak Results

	Vial	run_number	SampleName	Peak Name	RT (min)	Area	% Area	Amount (mg/mL)	USP Resolution	USP Tailing	s/n	Result Id
1	70	13696005D085	No-Pre_N2, clear, 6M, 4 °C	RX-10008	1.282	32704	0.34			1.09	0.0	4695
2	70	13696005D085	No-Pre_N2, clear, 6M, 4 °C		1.562	45887	0.48		3.10	1.26	0.0	4695
3	70	13696005D085	No-Pre_N2, clear, 6M, 4 °C		1.677	35480	0.37		1.25	1.18	0.0	4695
4	70	13696005D085	No-Pre_N2, clear, 6M, 4 °C		1.797	62904	0.65		1.54	1.68	0.0	4695
5	70	13696005D085	No-Pre_N2, clear, 6M, 4 °C		5.716	50465	0.52		55.21	0.65	0.0	4695
6	70	13696005D085	No-Pre_N2, clear, 6M, 4 °C	RX-10045	6.101	9155566	95.20	0.92	2.58	2.14	1.0	4695
7	70	13696005D085	No-Pre_N2, clear, 6M, 4 °C		7.507	234659	2.44		6.16	1.31	0.0	4695

Result Sign Off

	Result Id	Sign Off Full Name	Sign Off Date	Sign Off Reason
1	4695	Cindy Feng (cfeng)	1/27/2014 12:36:17 PM EST	Sign Off Level 1, Reason: Review

Reported by User: Cindy Feng (cfeng) Project Name:
Report Method: Chromatogram Date Printed: 1/27/2014
Page: 1 of 1

Figure 45. UPLC-UV Chromatogram of Month-6, RX-10045 Formulation, No Preservative, No N_2, Clear, 4 °C Sample.

SAMPLE INFORMATION

Sample Name:	Pre_No N2, clear, 6M, 40 °C	Acquired By:	cfeng
Sample Type:	Unknown	Sample Set Name:	13969005
Vial:	44	Acq. Method Set:	13696_X3970_2I_BD
Injection #:	1	Wavelength:	PDA Ch1 230nm@3.6nm
Injection Volume:	2.00 ul	System Name:	System BD
Run Time:	15.0 Minutes	Project Name:	XBL13696
Date Acquired:	1/25/2014 2:05:53 PM EST	NB Ref:	X3970:9

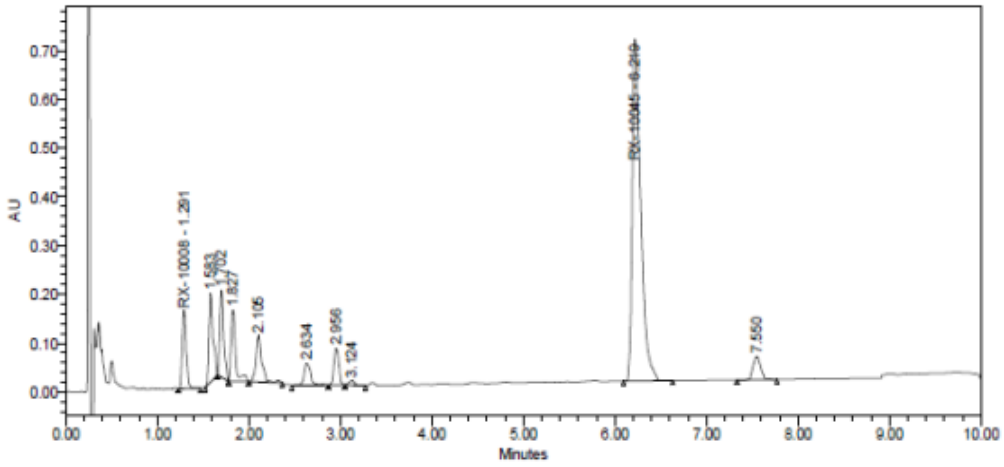

Peak Results

	Vial	run_number	SampleName	Peak Name	RT (min)	Area	% Area	Amount (mg/mL)	USP Resolution	USP Tailing	s/n	Result Id
1	44	13696005D053	Pre_No N2, clear, 6M, 40 °C	RX-10008	1.291	477554	6.11			1.27	0.2	4666
2	44	13696005D053	Pre_No N2, clear, 6M, 40 °C		1.583	572511	7.32		3.38	1.33	0.3	4666
3	44	13696005D053	Pre_No N2, clear, 6M, 40 °C		1.702	519313	6.64		1.44	1.38	0.3	4666
4	44	13696005D053	Pre_No N2, clear, 6M, 40 °C		1.827	493968	6.32		1.52	2.34	0.2	4666
5	44	13696005D053	Pre_No N2, clear, 6M, 40 °C		2.105	434734	5.56		3.07	1.24	0.1	4666
6	44	13696005D053	Pre_No N2, clear, 6M, 40 °C		2.634	234775	3.00		4.88	1.26	0.1	4666
7	44	13696005D053	Pre_No N2, clear, 6M, 40 °C		2.956	282024	3.61		2.81	1.07	0.1	4666
8	44	13696005D053	Pre_No N2, clear, 6M, 40 °C		3.124	40754	0.52		1.53	1.60	0.0	4666
9	44	13696005D053	Pre_No N2, clear, 6M, 40 °C	RX-10045	6.219	4490321	57.44	0.41	21.49	1.77	1.0	4666
10	44	13696005D053	Pre_No N2, clear, 6M, 40 °C		7.550	271614	3.47		8.15	1.09	0.1	4666

Result Sign Off

	Result Id	Sign Off Full Name	Sign Off Date	Sign Off Reason
1	4666	Cindy Feng (cfeng)	1/27/2014 12:33:51 PM EST	Sign Off Level 1, Reason: Review

Reported by User: Cindy Feng (cfeng)
Report Method: Chromatogram
Page: 1 of 1

Project Name:
Date Printed: 1/27/2014

Figure 46. UPLC-UV Chromatogram of Month-6, RX-10045 Formulation, Preservative, No N_2, Clear, 40 °C Sample.

Table 16. RX-10045 Formulation Stability Analysis

Preservative	Stability (% day 0)	Preservative	Stability (% day 0)	Preservative	Stability (% day 0)	Preservative	Stability (% day 0)
N2, amber, 0 Day, 4 °C	100	No N2, amber, 0 Day, 4 °C	100	N2, clear, 0 Day, 4 °C	100	No N2, clear, 0 Day, 4 °C	100
N2, amber, 1 Day, 4 °C	99.9	No N2, amber, 1 Day, 4 °C	100	N2, clear, 1 Day, 4 °C	100	No N2, clear, 1 Day, 4 °C	100
N2, amber, 9 Days, 4 °C	100	No N2, amber, 9 Days, 4 °C	100	N2, clear, 9 Days, 4 °C	101	No N2, clear, 9 Days, 4 °C	101
N2, amber, 30 Days, 4 °C	99.8	No N2, amber, 30 Days, 4 °C	99.7	N2, clear, 30 Days, 4 °C	100	No N2, clear, 30 Days, 4 °C	100
N2, amber, 2 Mo, 4 °C	97.2	No N2, amber, 2 Mo, 4 °C	97.0	N2, clear, 2 Mo, 4 °C	98.7	No N2, clear, 2 Mo, 4 °C	98.9
N2, amber, 3 Mo, 4 °C	96.8	No N2, amber, 3 Mo, 4 °C	96.0	N2, clear, 3 Mo, 4 °C	98.2	No N2, clear, 3 Mo, 4 °C	98.2
N2, amber, 4 Mo, 4 °C	96.5	No N2, amber, 4 Mo, 4 °C	95.4	N2, clear, 4 Mo, 4 °C	98.3	No N2, clear, 4 Mo, 4 °C	97.5
N2, amber, 6 Mo, 4 °C	95.3	No N2, amber, 6 Mo, 4 °C	91.8	N2, clear, 6 Mo, 4 °C	96.2	No N2, clear, 6 Mo, 4 °C	94.3
N2, amber, 0 Day, 25 °C	100	No N2, amber, 0 Day, 25 °C	100	N2, clear, 0 Day, 25 °C	100	No N2, clear, 0 Day, 25 °C	100
N2, amber, 1 Day, 25 °C	99.9	No N2, amber, 1 Day, 25 °C	100	N2, clear, 1 Day, 25 °C	100	No N2, clear, 1 Day, 25 °C	101
N2, amber, 9 Days, 25 °C	98.6	No N2, amber, 9 Days, 25°C	98.6	N2, clear, 9 Days,25 °C	99.8	No N2, clear, 9 Days, 25 °C	99.6
N2, amber, 30 Days, 25 °C	96.9	No N2, amber, 30 Days, 25 °C	96.6	N2, clear, 30 Days, 25 °C	97.4	No N2, clear, 30 Days, 25 °C	96.8
N2, amber, 2 Mo, 25 °C	95.7	No N2, amber, 2 Mo, 25 °C	94.0	N2, clear, 2 Mo, 25 °C	95.6	No N2, clear, 2 Mo, 25 °C	93.9
N2, amber, 3 Mo, 25 °C	95.2	No N2, amber, 3 Mo, 25 °C	93.2	N2, clear, 3 Mo, 25 °C	95.0	No N2, clear, 3 Mo, 25 °C	92.3
N2, amber, 4 Mo, 25 °C	94.3	No N2, amber, 4 Mo, 25 °C	92.4	N2, clear, 4 Mo, 25 °C	94.6	No N2, clear, 4 Mo, 25 °C	91.1
N2, amber, 6 Mo, 25 °C	89.9	No N2, amber, 6 Mo, 25 °C	83.6	N2, clear, 6 Mo, 25 °C	89.0	No N2, clear, 6 Mo, 25 °C	79.7
N2, amber, 0 Day, 40 °C	100	No N2, amber, 0 Day, 40 °C	100	N2, clear, 0 Day, 40 °C	100	No N2, clear, 0 Day, 40 °C	100
N2, amber, 1Day, 40 °C	99.6	No N2, amber, 1 Day, 40 °C	99.3	N2, clear, 1 Day, 40 °C	100	No N2, clear, 1 Day, 40 °C	99.9
N2, amber, 9Days, 40 °C	97.2	No N2, amber, 9 Days, 40°C	96.3	N2, clear, 9 Days,40 °C	98.0	No N2, clear, 9 Days, 40 °C	97.7
N2, amber, 30 Days, 40 °C	94.1	No N2, amber, 30 Days, 40 °C	92.5	N2, clear, 30 Days, 40 °C	96.0	No N2, clear, 30 Days, 40 °C	94.2
N2, amber, 2 Mo, 40 °C	90.6	No N2, amber, 2 Mo, 40 °C	86.7	N2, clear, 2 Mo, 40 °C	90.7	No N2, clear, 2 Mo, 40 °C	88.7
N2, amber, 3 Mo, 40 °C	86.3	No N2, amber, 3 Mo, 40 °C	82.6	N2, clear, 3 Mo, 40 °C	85.9	No N2, clear, 3 Mo, 40 °C	83.6
N2, amber, 4 Mo, 40 °C	84.3	No N2, amber, 4 Mo, 40 °C	78.5	N2, clear, 4 Mo, 40 °C	82.9	No N2, clear, 4 Mo, 40 °C	78.7
N2, amber, 6 Mo, 40 °C	74.9	No N2, amber, 6 Mo, 40 °C	62.9	N2, clear, 6 Mo, 40 °C	67.6	No N2, clear, 6 Mo, 40 °C	60.3
No preservative	Stability (% day 0)	No preservative	Stability (% day 0)	No preservative	Stability (% day 0)	No preservative	Stability (% day 0)
N2, amber, 0 Day, 4 °C	100	No N2, amber, 0 Day, 4 °C	100	N2, clear, 0 Day, 4 °C	100	No N2, clear, 0 Day, 4 °C	100
N2, amber, 1 Day, 4 °C	100	No N2, amber, 1 Day, 4 °C	100	N2, clear, 1 Day, 4 °C	101	No N2, clear, 1 Day, 4 °C	100
N2, amber, 9 Days, 4 °C	101	No N2, amber, 9 Days, 4 °C	101	N2, clear, 9 Days, 4 °C	101	No N2, clear, 9 Days, 4 °C	101
N2, amber, 30 Days, 4 °C	101	No N2, amber, 30 Days, 4 °C	101	N2, clear, 30 Days, 4 °C	101	No N2, clear, 30 Days, 4 °C	101
N2, amber, 2 Mo, 4 °C	99.6	No N2, amber, 2 Mo, 4 °C	100	N2, clear, 2 Mo, 4 °C	101	No N2, clear, 2 Mo, 4 °C	100
N2, amber, 3 Mo, 4 °C	99.9	No N2, amber, 3 Mo, 4 °C	100	N2, clear, 3 Mo, 4 °C	101	No N2, clear, 3 Mo, 4 °C	100
N2, amber, 4 Mo, 4 °C	99.8	No N2, amber, 4 Mo, 4 °C	99.6	N2, clear, 4 Mo, 4 °C	100	No N2, clear, 4 Mo, 4 °C	100
N2, amber, 6 Mo, 4 °C	98.2	No N2, amber, 6 Mo, 4 °C	97.8	N2, clear, 6 Mo, 4 °C	99.0	No N2, clear, 6 Mo, 4 °C	98.6
N2, amber, 0 Day, 25 °C	100	No N2, amber, 0 Day, 25 °C	100	N2, clear, 0 Day, 25 °C	100	No N2, clear, 0 Day, 25 °C	100
N2, amber, 1 Day, 25 °C	101	No N2, amber, 1 Day, 25 °C	101	N2, clear, 1 Day, 25 °C	101	No N2, clear, 1 Day, 25 °C	101
N2, amber, 9 Days, 25 °C	101	No N2, amber, 9 Days, 25°C	101	N2, clear, 9 Days,25 °C	100	No N2, clear, 9 Days, 25 °C	101
N2, amber, 30 Days, 25 °C	100	No N2, amber, 30 Days, 25 °C	99.9	N2, clear, 30 Days, 25 °C	98.7	No N2, clear, 30 Days, 25 °C	99.1
N2, amber, 2 Mo, 25 °C	99.2	No N2, amber, 2 Mo, 25 °C	97.4	N2, clear, 2 Mo, 25 °C	97.5	No N2, clear, 2 Mo, 25 °C	96.3
N2, amber, 3 Mo, 25 °C	98.1	No N2, amber, 3 Mo, 25 °C	96.9	N2, clear, 3 Mo, 25 °C	96.4	No N2, clear, 3 Mo, 25 °C	94.6
N2, amber, 4 Mo, 25 °C	97.8	No N2, amber, 4 Mo, 25 °C	96.1	N2, clear, 4 Mo, 25 °C	95.8	No N2, clear, 4 Mo, 25 °C	93.4
N2, amber, 6 Mo, 25 °C	93.6	No N2, amber, 6 Mo, 25 °C	89.9	N2, clear, 6 Mo, 25 °C	87.6	No N2, clear, 6 Mo, 25 °C	83.1
N2, amber, 0 Day, 40 °C	100	No N2, amber, 0 Day, 40 °C	100	N2, clear, 0 Day, 40 °C	100	No N2, clear, 0 Day, 40 °C	100
N2, amber, 1Day, 40 °C	101	No N2, amber, 1 Day, 40 °C	101	N2, clear, 1 Day, 40 °C	101	No N2, clear, 1 Day, 40 °C	101
N2, amber, 9Days, 40 °C	99.1	No N2, amber, 9 Days, 40°C	100	N2, clear, 9 Days,40 °C	99.9	No N2, clear, 9 Days, 40 °C	99.8
N2, amber, 30 Days, 40 °C	97.4	No N2, amber, 30 Days, 40 °C	96.1	N2, clear, 30 Days, 40 °C	98.0	No N2, clear, 30 Days, 40 °C	97.4
N2, amber, 2 Mo, 40 °C	95.3	No N2, amber, 2 Mo, 40 °C	92.9	N2, clear, 2 Mo, 40 °C	95.8	No N2, clear, 2 Mo, 40 °C	94.0
N2, amber, 3 Mo, 40 °C	94.0	No N2, amber, 3 Mo, 40 °C	90.4	N2, clear, 3 Mo, 40 °C	93.5	No N2, clear, 3 Mo, 40 °C	90.9
N2, amber, 4 Mo, 40 °C	93.0	No N2, amber, 4 Mo, 40 °C	87.7	N2, clear, 4 Mo, 40 °C	91.8	No N2, clear, 4 Mo, 40 °C	88.2
N2, amber, 6 Mo, 40 °C	85.3	No N2, amber, 6 Mo, 40 °C	75.6	N2, clear, 6 Mo, 40 °C	82.2	No N2, clear, 6 Mo, 40 °C	75.6

Table 17. Ocular tolerability study results in New Zealand White rabbits for RX-10045 (0.1%) nanomicellar formulation.

Hackett-McDonald Composite Scores (mean ± s.d).		
Dose	Placebo nanomicellar formulation	RX-10045 (0.1%) nanomicellar formulation
Day 1 Predispose	0.0 – 0.0	0.0 – 0.0
Day 1 Postdispose	1.75 – 1.5	0.5 – 0.1
Day 2 Predispose	0.0 – 0.0	0.0 – 0.0
Day 2 Postdispose	2.0 – 0.0	0.0 – 0.0
Day 3 Predispose	0.0 – 0.0	0.0 – 0.0
Day 3 Postdispose	1.3 – 1.2	0.0 – 0.0
Day 4 Predispose	1.3 – 1.2	0.0 – 0.0
Day 4 Postdispose	1.3 – 1.2	0.0 – 0.0
Day 5 Predispose	0.0 – 0.0	0.5 – 1.0
Day 5 Postdispose	1.3 – 2.3	0.0 – 0.0

Table 18. Comparison of mean ocular distribution of RX-10008 (active metabolite of RX-10045) after four times a day at 2 hour intervals for 5 days to New Zealand White Rabbits with topical drop administration

Ocular tissue or fluid	Treatment with 0.1% RX-10045 nanomicellar formulation (RX-10008) (N = 2) ng/g or ng/mL
Cornea	17725
Conjunctiva	879
Iris-Ciliary body	2655
Sclera	701
Lens	165
Aqueous Humor	3205
Vitreous Humor	16
Retina-Choroid	323

fluid (vitreous and aqueous humors) RX-10008 concentrations are presented in **Table 18**. The reason for RX-10008 quantification instead of RX-10045 is due to rapid hydrolysis of RX-10045 to RX-10008 in ocular tissues in fluids. The trend for drug concentration followed the same that was observed with CsA nanomicellar formulation. The highest drug concentrations of RX-10008 were found in the cornea, followed by iris-ciliary body, conjunctiva, and sclera. Moreover, high concentrations of RX-10008 were quantified in aqueous humor. Lower amounts were found in retina-choroid and lens. The lowest levels of RX-10008 were found in the vitreous humor. However, very low/sporadic concentrations of RX-1001 ester prodrug were observed in the sclera and conjunctiva. Compound RX-1001 was either not detected or was below quantitation limit of the assay. The results suggest that RX-10045 rapidly hydrolyzed to its active metabolite (RX-10008).

Discussion

The resolvin E1 analog suffers from poor aqueous solubility and stability (data not shown from Auven Therapeutics). Encapsulation of RX-10045 in nanomicellar formulation resulted in higher stability. But, for topical drop application formulation pH should be regulated. Therefore, to improve the stability and maintain the pH of the solution citrate buffer was used. Stability studies at different concentration of citrate buffer were conducted. All the stability studies are conducted at higher temperatures i.e., under accelerated conditions to save time and determine the shelf-life for the drug/formulation. These accelerated stability studies i.e, studies at higher temperatures (40 ^{o}C, 50 ^{o}C, 60 ^{o}C and so on) cause drug

degradation to be faster and help to determine the shelf life. In other words, drug is supposed to be degraded at higher temperatures which help to determine the shelf life in less time.

Results from stability studies indicate that at 25 ^{o}C, 0.05 M and 0.1 M citrate buffer concentration was very high and caused catalysis and degradation of the drug in the formulation. On the other hand, 0.005 M citrate buffer was not sufficient enough to maintain the pH for the entire length of time and therefore was prone to Rx-10045 degradation. Similar effects were observed at 40 ^{o}C. Citrate buffer at a concentration of 0.01 M provided sufficient pH stability, which is evident from the HPLC results. Data reveals that at 25 ^{o}C RX-10045 was ~ 100% and at 40 ^{o}C RX-10045 was ~ 97% remaining in the formulation at pH 6.0 i.e, only 3.2% of RX-10045 was degraded in one month. However, when the citrate buffer concentration was increased to 0.05 M, degradation of RX-10045 was observed because the citrate buffer itself was causing catalysis and showed drug degradation. In other words, at 0.05 M and 0.1 M citrate buffer (pH = 6.0 and 5.5) RX-10045 is more pronounced to degradation because of citrate buffer. While at concentration of citrate buffer less than 0.01 M i.e., 0.005 M was not effective in maintaining the pH and this led to drug degradation.

In vivo studies revealed no significant IOP changes in eyes treated with BSS or RX-10045 nanomicelles. No toxicological response or changes in retinal function were noted with ERG after 5 days of treatment with RX-10045 nanomicellar formulation. Moreover, no toxicological or inflammatory responses were observed histologically in the anterior (conjunctiva/cornea/iris) or posterior

segments (vitreous/retina) of the eye indicating the formulations are safe and well-tolerated. Ocular tissue distribution studies reveal high drug concentrations in the anterior tissues (cornea and conjunctiva). Moreover, results suggests that nanomicelles utilized conjunctival-scleral pathway to reach posterior ocular tissues and deliver RX-10045 into retina-choroid.

Conclusion

The delivery of drug into ocular cells may be inhibited due to the presence of membrane bound functional efflux transporters. For the first time, we have demonstrated a resolvin E1 analog (RX-10045) to be a substrate/inhibitor for efflux transporters (MRP2 and BCRP). It is observed that permeability of [^{3}H] digoxin was not affected in presence of RX-10045 indicating there may be negligible interaction with P-gp. It remains to be determined whether this is a class property of the resolvins; however, this report suggests that efflux transporters may impede the translocation of RX-10045 across some target cell membranes. A significantly reduced uptake of [^{3}H] abacavir in presence of RX-10045, compared to quinine (a known inhibitor of OCT-1), clearly suggests that RX-10045 is a strong substrate/inhibitor of OCT-1. Knowledge of resolvin interaction with efflux transporters can allow pharmaceutical scientists to develop new strategies and formulations (278, 320) to circumvent efflux barrier and deliver therapeutic concentrations of resolvin into target ocular tissues. A clear, aqueous nanomicellar RX-10045 formulation was successfully developed and optimized. Stability of the formulation was significantly improved when incorporated in nanomicellar

formulation with optimized citrate buffer. *In vivo* tolerability studies suggest that formulations are safe and well-tolerated. Ocular tissue distribution in New Zealand White rabbits suggest that RX-10045 was rapidly hydrolyzed to RX-10008 which was quantified in anterior and posterior ocular tissues. A trans-scleral pathway is hypothesized for nanomicellar formulation to reach and deliver the cargo to back-of-the-eye tissues.

Chapter 5

TOPICAL AQUEOUS CLEAR DEXAMETHASONE NANOMICELLAR FORMULATION: OPTIMIZATION AND IN VIVO TISSUE DISTRIBUTION

Rationale

Dexamethasone (DEX), a glucocorticoid, is widely indicated as an anti-inflammatory and immunosuppressive drug (321) following cataract surgery or corneal procedure (322, 323). DEX is also used in the treatment of posterior segment eye diseases such as uveitis and macular edema (324, 325). DEX has a poor aqueous solubility (0.159 mg/mL) (326) and is a substrate for efflux proteins (327). Moreover, efflux pumps expressed on corneal epithelial cells (328) may pose a barrier for DEX permeation and lower intracellular DEX concentrations. Encapsulating DEX inside the core of nanomicellar formulation may improve its solubility and drug delivery. Amphiphilic molecules such as Vitamin E TPGS and Oc-40 may aid in developing a stable, clear, aqueous DEX nanomicellar formulation.

Vitamin E TPGS is a safe and FDA approved water-soluble derivative of vitamin E. It is a non-ionic polymer with a hydrophilic lipophilic balance (HLB index) of about 13 (329). It is generally added to lipid based drug delivery systems as a stabilizer. Oc-40 is a non-ionic surfactant approved by FDA as a food additive and other pharmaceutical applications. Oc-40 (IGEPAL CA-897) has HLB index of about 18. Polymeric hydrophilic corona interacts with the external aqueous phase and prevents drug interaction with aqueous solution resulting in a stable aqueous

solution. Also, the interaction between encapsulated drug and polymers may sustain drug release. Additionally, these polymer combinations may lower critical micellar concentration. This perfect blend of polymers is optimal to formulate concentrated aqueous DEX solution. The steroid is not very soluble in aqueous medium (159 µg/mL) with partition coefficient (log $K_{o/w}$) of 1.72 (326).

Amphiphilic nature of Vit. E TPGS and Oc-40 allows spontaneous formation of spherical nanomicelles with a hydrophobic interior and hydrophilic corona in aqueous milieu. It allows high concentrations of hydrophobic DEX to be incorporated into the micellar core. Therefore, the objective of this study was to optimize and develop a clear, stable, aqueous DEX loaded nanomicellar formulation (NMF) with full factorial statistical design of experiments (DOE). Standard least square fit analysis was performed to identify the ideal polymeric blend to encapsulate DEX. Our method of DEX formulation preparation is simple, reproducible, easy to scale up for large scale production (330) and most importantly minimizes drug loss in the manufacturing process.

Materials and Methods

Dexamethasone and prednisolone (PD) were obtained from Tokyo chemical industry Co., Ltd, Japan. Vitamin E TPGS was purchased from Peboc division of Eastman Company, UK. Oc-40 (Igepal) was obtained from Rhodio Inc., New Jersey, USA. HPLC grade methanol, acetonitrile, and dichloromethane were procured from Fisher Scientific, USA. Ethanol was purchased from Aaper alcohol and chemical Co., Shelbyville, Kentucky, USA. Sodium phosphate monobasic and

Sodium phosphate dibasic were purchased from Mallinckrodt, USA. Povidone K 90 (PVP-K-90, Kollidon® 90 F, Ph.Eur., USP) was purchased from Mutchler, Inc. Pharmaceutical ingredients, Harrington Park, New Jersey, USA.

Methods

HPLC analysis

Analysis of DEX were performed by a reversed phase RP-HPLC method with a Waters 515 HPLC pump (Waters corporation, Milford, MA), Alcott autosampler (model 718 AL), Alcott 795 UV-visible detector, Zorbax SB-phenyl column (5 µm, 25 x 4.6 mm) (Agilent Technologies, Santa Clara, CA) and Hewlett Packard HPLC integrator (Hewlett Packard, Palo Alto, CA). The mobile phase was comprised of ACN, water and trifluoroacetic acid (TFA) (40:60:0.1% v/v), which was set at a flow rate of 1 mL/min. Detection wavelength was set at 254 nm. Calibration curve (0.5 to 1.5 µg/mL) for DEX was prepared by making appropriate dilutions from the stock solution. Prednisolone (1 mg/mL) was appropriately diluted and used as internal standard. An injection volume of 50 µL was injected into the HPLC column for analysis.

Sensitivity of the method was established with limit of detection (LOD) and limit of quantification for DEX with signal to noise ratio of 5:1. LOD and LOQ were determined by injecting a series of known concentrations of DEX. Precision was carried out at the LOQ level by injecting six replicates of DEX preparations at LOQ concentration by calculating relative standard deviation for each peak area.

Intra-day and inter-day (three different days) RSD of < 2.0 % was considered to be acceptable for analytical method sensitivity.

LC-MS/MS Analysis

For quantitative determination of DEX in ocular tissues a selective and sensitive LC-MS/MS method was developed. Chromatographic analysis was carried out on API 2000 triple quadruple linear ion QTrap mass spectrometer. High performance liquid chromatographic system consists of Agilent 1100 LC Quaternary pump, Agilent 1100 well plate, autosampler (Agilent technologies, Wilmington, DE) with a reversed phase gemini C18 column (50 mm × 4.6 mm i.d., 5 m, Phenomenex, Torrance, CA). Isocratic mobile phase composed of 30% of acetonitrile in water, containing 0.1% of formic acid, was at a flow rate of 0.2 mL/min.

Mass spectrometer operating conditions

MDS Sciex API 2000 Triple Quadrupole linear QTrap mass spectrometry (Applied Biosystems/MDS Sciex, Faster City, CA) system interfaced by turbo ion spray (TIS) with positive ion source in MRM mode was applied for detection. Ultra high pure nitrogen served as collisionally activated dissociation (CAD) at 4 psi and curtain gas at 20 psi. Nebulizer and turbo gas were optimized at 40 and 50 psi respectively. The TIS temperature was maintained at 200 ^{o}C, with source voltage and dwell time optimized at 5200 V and 400 ms respectively. Mass dependent parameters were tuned and optimized for DEX, and PD. Parent and daughter ions

obtained by direct infusion mode (10 µL min^{-1}) was injected with built-in Harvard infusion syringe pump and were optimized.

Experimental design

As a preliminary study to screen the weight percent of polymers, effects of formulation variables on DEX entrapment, NMF size and polydispersity index (PDI) were evaluated based on statistical design of experimental (DOE) protocol. Student version of JMP® 9.0 software (SAS institute, USA) was used to develop the experimental design and analyze the data. Two independent (X1 and X2) and three dependent variables (Y1, Y2, and Y3) were identified. Independent variables X1 and X2 are Vit. E TPGS and Oc-40, respectively. Dependent variables Y1, Y2 and Y3 represent percent entrapment efficiency, micellar size and polydispersity index, respectively. "Screening design" option in JMP® was selected to create a design that included the categorical variables that cannot be quantified. In the same way, other continuous variables (polymer concentration in weight percent (wt%)) were selected. A three level full factorial design with 9 runs was chosen from the "design list" (**Table 19**). Coded values -1, 0, +1 were assigned to the weight percent levels for the two polymers.

Preparation of DEX-loaded nanomicelles

Nanomicellar formulation of DEX was prepared by solvent evaporation method. The interactions between the hydrophobic core of polymers and the drug (0.1 wt%) improve the drug entrapment. Direct addition of the drug to the aqueous

polymeric solution leaves most of the added drug unentrapped. Therefore, the novel DEX loaded formulations were prepared following similar protocol described in Chapter 3 with minor modifications in step 2. In step 2, the resultant thin film was hydrated with 50 mL of double distilled deionized water and kept under sonication for 20 minutes in a water bath sonicator (50/60 Hz, 125 W). The volume of the rehydrated formulation was made up with 2X phosphate buffer solution, (pH 6.8). Further to improve the viscosity of the NMF povidone K 90 (solution viscosity enhancer) was added and mixed to obtain a clear solution. The solution was filtered through 0.2 μm nylon filter membrane to remove the unentrapped drug aggregates and other foreign particulates.

Characterization of nanomicelle formulation

The prepared DEX loaded nanomicellar formulations were subjected to characterization following procedures described in Chapter 3 for entrapment efficiency, loading efficiency, size, polydispersity index, surface potential, CMC and proton NMR studies. CMC for the blend of polymers (Vit. E TPGS and Oc-40) was determined following procedure described previously. HPLC-UV was used for determining entrapment and drug loading. Formulation stability studies were conducted at three different temperatures (4 ^{o}C, 25 ^{o}C and 40 ^{o}C). At predetermined time points both placebo and DEX loaded nanomicellar formulation samples were collected into 200 μL HPLC inserts/vials and immediately stored at -80 ^{o}C until further analysis with HPLC.

Nanomicelle stability

Stability studies were conducted for F1 NMFs. DEX-loaded and blank nanomicelles, were stored at 40 °C, room temperature and 4 °C. To avoid microbial growth during long term storage sodium azide, 0.025% w/v, was added. At predetermined time intervals, each sample was collected, centrifuged at 10,000 g for 5 min. The supernatant was collected and DEX was extracted from NMF following the procedure described for entrapment efficiency. The concentration of DEX remaining in solution was measured using RP-HPLC. Also, the size of nanomicelles was determined at each time point following the previously described procedure.

In vitro cytotoxicity

Cell viability and plasma membrane damage studies were conducted following the manufacturer's protocol described in Chapter 3 on rPCEC cell lines. For cell viability studies triton X-100 served as positive control and serum free cell culture medium with no NMF served as negative control. However, in LDH assay the control were triton X-100 as positive control and cell culture medium served as negative control.

In vivo Studies

New Zealand albino adult male rabbits, weighed between 2.0 and 2.5 kg, were obtained from Myrtle's Rabbittry (Thompson Station, TN) and housed in accordance with US Department of Agricultural and Association for Assessment

and Accreditation of Laboratory Animal Care international guidelines. All protocols were reviewed and approved by Animal Care and Use Committee of University of Missouri Kansas City. Studies performed were in accordance with the Association for Research in Vision and Ophthalmology Regulations and Standards (ARVORS) guidelines. Rabbits were anesthetized with subcutaneous ketamine (30 mg/kg). Ten minutes after anesthesia, the rabbit's head was held to keep the left eye horizontal and 50 µL of 0.1% dexamethasone a novel nanomicellar formulation (Vitamin E TPGS – 4.5% and Oc-40 – 2.0%) eye drops were instilled using a micropipette at the center of lower cul-de-sac. During the instillation, the lower eyelid was pulled slightly away from the globe and was returned to normal position immediately after instillation. After 60 min, rabbits were euthanized using 1 mL of intravenous injection of Fatal-Plus® (Vertech Pharmaceuticals Corporation, Dearborn, Mich) (39% sodium pentobarbital) into the marginal ear vein. Following euthanasia, the eye ball was enucleated immediately (on an average within 150 s) and transferred to a beaker containing ice-cold phosphate buffer (pH 7.4). Repetitive washings were carried out in cold phosphate buffer to remove any adsorbed drug on to the surface. Aqueous humor was withdrawn by limbal paracentesis and then vitreous humor was aspirated using a 1 mL tuberculin syringe after making a tiny incision at sclera–limbus junction. The enucleated eyeball was cut open and the following tissues were dissected: cornea, iris–ciliary body (ICB), lens, retina–choroid (RC) and sclera were all collected into pre-weighed eppendorfs. After dissection, the tissues were dried with Kimwipes® and weighed. Protein content in the aqueous and vitreous humor was measured by the method of

Bradford (Bio-Rad protein estimation kit, Hercules, CA). All tissue samples were stored at −80 °C until further analysis.

Preparation of samples

Tissues were homogenized in 500 L chilled (4 °C) phosphate buffer (pH 7.4) for about 4 min with a tissue homogenizer (Tissue Tearor, Model 985-370; Dremel Multipro, Racine, WI) in an ice bath, with the exception of sclera, which required 1.5 mL. One hundred microliters of aqueous humor (AH) and vitreous humor (VH) were collected for analysis without further processing. Subsequently 100 L of the tissue homogenates (cornea, iris–ciliary body, lens, retina–choroid and sclera), aqueous humor and vitreous humor were collected for further sample processing.

Dexamethasone ocular tissue sample extraction

Dexamethasone was extracted from ocular tissue homogenates by a simple liquid–liquid extraction as described previously. All tissue samples were analyzed with freshly prepared calibration curve and quality control standards. Calibration curve (2.70–617.60 ng/mL) and QC standards were prepared by spiking appropriate abounds in seven different blank ocular matrices (control tissues) with varying concentrations of dexamethasone with PD as an IS. All standards and samples were analyzed with LC–MS/MS.

Statistical Analysis

The experimental design and the data analysis were performed by student version of JMP® 9.0 software. Standard least squares were used to fit the models. Data for *in vitro* experiments were conducted at least in quadruplicate (n = 4) and the results were expressed as mean ± standard deviation (SD). Statistical comparison of mean values was performed with Student's t-test. A P-value of <0.05 was considered to be statistically significant.

Results

Nanomicellar formulations of DEX were prepared following solvent evaporation and rehydration method. Statistical design of experiments was used to optimize the NMF with respect to entrapment efficiency, size and polydispersity index. However, size and polydispersity index had no significant effect on the formulation optimization. Therefore, were negated from optimization parameters. The optimal blend ratio of Vit. E TPGS and Oc-40 were 4.5 wt% and 2.0 wt%, respectively which had the lower CMC (0.012 wt%) relative to individual polymers (Vit. E TPGS = 0.022 wt% and Oc-40 = 0.108 wt%). This polymeric ratio had lower CMC and was used to entrap DEX (0.1%). *In vitro* studies on rPCEC cells demonstrated DEX NMF to be safe, well-tolerated and results were comparable to that of negative control.

Quantitative determination of DEX in different ocular tissues after topical administration showed higher concentrations in anterior ocular tissues. DEX was identified in cornea, iris-ciliary body, sclera and retina-choroid. Aqueous humor

had small amounts of DEX. However, no DEX identified (below limit of quantitation i.e., less than 2.7 ng/mL) in lens and vitreous humor.

Discussion

Selection of critical (or meaningful) factors based on experimental design

In this study we selected full factorial design of experiments (DOE) to screen essential independent factors for outcomes (entrapment, size and PDI). All the formulations were subjected to other characterizations such as loading efficiency, CMC, optical absorbance, osmolality, pH, dissociation temperature, regeneration time, osmolality, viscosity and surface potential (**Table 19** and **Table 20**). The results for dependent variables (Y1, Y2 and Y3) from 9 sets of NMFs are presented in **Table 19**. The standard least square fit analysis *via* JMP® 9.0 software (331) was performed to identify the most influencing factors for each dependent variable. The model fit was significant when one of the formulations (F8 in **Table 19)** was excluded from the analysis. Therefore eight sets of formulations were considered for formulation optimization following standard least square fit analysis. The main effects of one-factor and two factor interaction effects were taken into consideration. The rationale behind this selection was higher interactions are less significant. The parameters that exhibited most significant outcome were selected and processed with standard least square regression model to fit those parameters.

Table 19. Results of full factorial design

Formulation code/number	NMF code pattern[a]	Vit. E TPGS (wt%)	Oc-40 (wt%)	% Entrapment efficiency	NMF effective diameter (nm)	NMF PDI	Loading efficiency	CMC (wt% X 10^{-3})
F1	++	4.5	2.0	99 ± 5.5	10.5	0.086	1.50	12
F2	+0	4.5	1.05	92 ± 2.3	11.3	0.099	1.64	59
F3	+-	4.5	0.1	86 ± 3.4	12.2	0.078	1.85	90
F4	0+	3.5	2.0	93 ± 2.7	10.1	0.057	1.66	103
F5	00	3.5	1.05	82 ± 5.8	11.9	0.123	1.79	127
F6	0-	3.5	0.1	26 ± 3.5	10.2	0.078	0.70	420
F7	-+	2.5	2.0	82 ± 3.2	11.0	0.132	1.79	218
F8	-0	2.5	1.05	81 ± 4.2	12.2	0.085	2.25	172
F9	--	2.5	0.1	23 ± 5.7	13.4	0.089	0.86	620
Vit. E TPGS		4.5	0.0	67± 3.7	10.0	0.069	1.45	25
Oc-40		0.0	2.0	N.D	N.D	N.D	N.D	107

[a]NMF code pattern: (+) high, (0) medium, (-) low; NMF = Nanomicellar Formulation; PDI = Polydispersity Index; CMC = Critical Micellar Concentration; nm = nanometer; wt% = weight percent; N.D =Not Determined

Table 20. Characterization of nanomicellar formulation

Formulation code/ number	Absorbance at 400 nm ± S.D	D.T (° C) ± S.D	R.T (sec) ±S.D	Osmolality (mOsm/kg)		Viscosity (cP)	Zeta potential (mV)
				Before	After		
F1	0.040 ± 0.001	A.D.T	N.D	205	299	1.79	-2.26
F2	0.013 ± 0.002	84 ± 0.87	9 ± 1.00	218	307	1.68	-1.67
F3	0.020 ± 0.001	76 ± 1.49	40 ± 1.70	219	315	1.72	-2.92
F4	0.046 ± 0.001	93 ± 0.87	16 ± 2.31	253	289	1.59	-1.63
F5	0.025 ± 0.001	76 ± 0.76	28 ± 1.73	203	315	1.74	-1.32
F6	0.044 ± 0.001	74 ± 0.87	42 ± 12.0	222	308	1.65	-2.30
F7	0.046 ± 0.001	71 ± 0.81	18 ± 2.31	201	295	1.69	-3.41
F8	0.044 ± 0.001	91 ± 0.30	15 ± 1.00	214	301	1.75	-2.47
F9	0.025 ± 0.001	71 ± 0.79	40 ± 5.00	216	298	N.D	-1.89

D.T = Dissociation Temperature; R.T = Regeneration Time; mOsm/kg = milliOsmols/kilogram; cP = centipoise; mV = millivolts; A.D.T. = above detection point (> 100 ºC); N.D = Not determined. In osmolality columns “before” means before addition of tonicity enhancing agent and “after” means improved tonicity after addition of tonicity enhancer.

Table 21. Summary showing fit to the model prediction of entrapment, size and PDI.

	Entrapment efficiency (%Y1)	**NMF Size (nm) (Y2)**	**NMF PDI (Y3)**
R square	0.88032	0.413733	0.228791
R square adjusted	0.790559	-0.020597	-0.34962
Root mean square error	13.91169	1.154439	0.028684
Mean of Response	72.85	11.29625	0.09275
Observations	8	8	8

NMF = Nanomicellar formulation; PDI = Polydispersity index

We could fit the model for percent entrapment efficiency but not for size and PDI. The summary for fit model for entrapment efficiency is presented in **Table 21**. Further, analysis of variance (ANOVA) for entrapment efficiency showed a significant effect with F ratio (probability > F) of 0.026.

Master formula (Prediction Equation)

The fit model developed the following polynomial equations for the output: entrapment efficiency (Eq 4), NMF size (Eq 5) and PDI (Eq 6):

$$Y1 = -24.46 + 20.3X1 + 22.80X2 + (-12.08)(X1-3.625)(X2-1.0375) \quad \textit{Eq. 11}$$

$$Y2 = 13.33 - 0.354X1 – 0.723X2 + (-0.198)(X1-3.625)(X2-1.0375) \quad \textit{Eq.12}$$

$$Y3 = 0.126 - 0.010X1 – 0.00367X2 + (-0.009421)\ (X1-3.625)(X2-1.0375) \quad \textit{Eq 13}$$

(where X1 = Vit. E TPGS level/experimental code; X2 = Oc-40 level/experimental code and X1X2 are the interaction levels/experimental code of Vit. E TPGS and Oc-40).

After interpreting the data obtained (Eqs. 11, 12 and 13), polynomial equation for the response variable (Y1, Y2 and Y3) for three level, two factor variables was developed. Since the polynomial equations for Y1 fit well (R^2 = 0.880), it was used for optimization process. The other two polynomial equations for Y2 and Y3 did not fit (R^2 = 0.41 and 0.23). The possible reasons for low fit may be due to extreme small size range of nanomicelles. Results show that there

is no significant difference in nanomicellar size and PDI (**Table 19**). Therefore, the obtained polynomial equation for entrapment efficiency (Y1) was applied to predict entrapment efficiencies of NMFs by adjusting the levels of input variables. Of all the predicted entrapment efficiencies, NMF F1 was predicted to be (102.33 %) when both polymers are set at high levels.

Pareto chart was developed for each individual outcome. It is used to determine which factors and interactions are relevant. These charts are developed using the absolute value obtained from the half the value of main effects. The bars in the chart that extend past the line indicate values reaching statistical significance ($\alpha = 0.05$). In the case of entrapment efficiency both factors, Vit. E TPGS and Oc-40, are found to pass the line indicating their statistically significant effect on entrapment efficiency (**Figure 47A**). But, interactions between these two input factors did not cross the line and was not significant for DEX entrapment efficiency. Similarly, effects of input variables on the NMF size and PDI outcomes were determined with Pareto chart and found to have negligible effect (**Figure 47B and C**). These results indicate that only DEX entrapment was dependent on individual input variables (Vit. E TPGS and Oc-40). As said earlier, we were unable to fit the model for nanomicellar size and PDI. Other models have to be tried to fit the model. From the obtained results in **Table 19** there appeared no significant difference in nanomicellar size and PDI. Therefore, we did not make any attempts to use the fit model results. Also, the results obtained from the standard least square fit model for nanomicellar size and PDI revealed that

there is no statistically significant difference in the outcome (data not shown). Prediction profiler for entrapment efficiency, size and PDI was developed (**Figure 48**). Prediction profiler helps to determine the levels of input variables to be adjusted in a combination where the outcome can be predicted. We found that when both the input variables (Vit. E TPGS and Oc-40) kept at high levels (4.5:2.0) resulted in high entrapment efficiency (98.7 ± 5.5), which is evident from the results. The prediction profiler results and the experimental results are in agreement. Therefore, the combination of variables at high level with high entrapment efficiency was assumed to be the better formulation. To further determine the effects of the input variables on the entrapment efficiency a contour plot analysis was developed (data not shown). A contour plot is a three dimensional representation for the outcome when the input variables are adjusted. From the contour plot one can estimate the levels of the input variables and determine the outcome (present on the surface of the box). The shaded region in contour plot indicates the lower entrapment region of DEX. On the other hand, the unshaded region represents the higher entrapment. We observed that when both variables (Vit. E TPGS) set at high level, high entrapment efficiency was predicted. Experimental design results and our experimental outcome suggest that when the polymer combination is kept at high level results in higher entrapment. The results appear to be in agreement with the outcome.

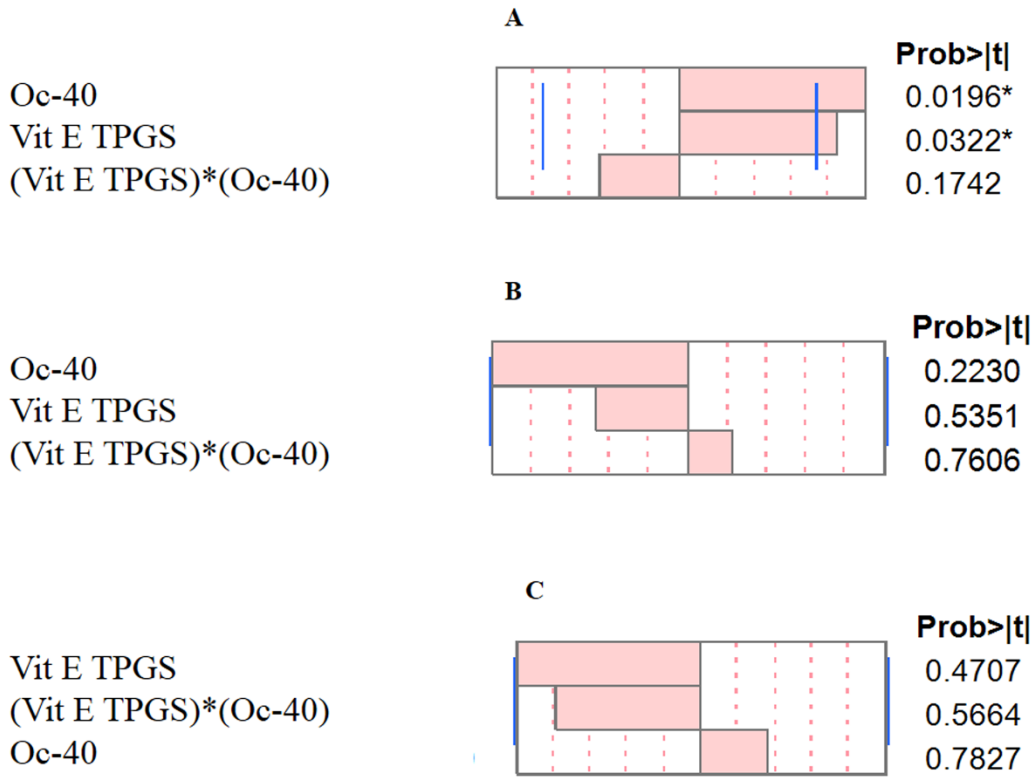

Figure 47. Pareto charts (A) Entrapment efficiency for DEX (B) nanomicellar size (C) Polydispersity Index.

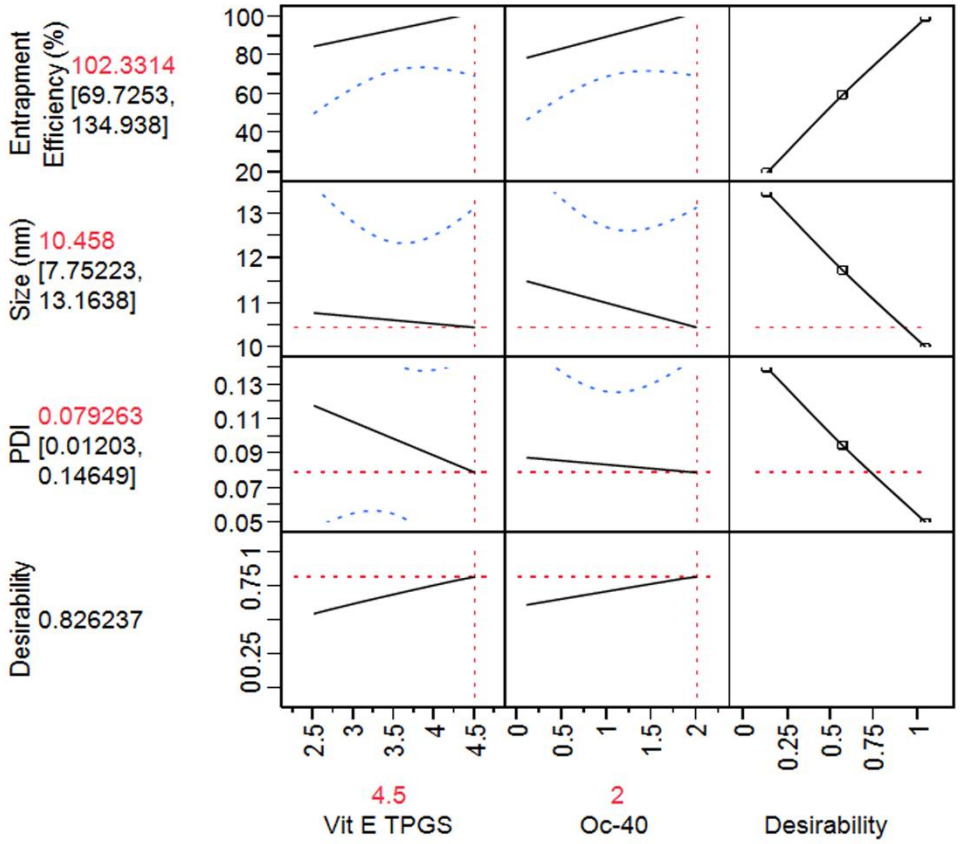

Figure 48. Prediction profiler for optimal nanomicellar formulation

From the prediction equation and contour plot high entrapment efficiency was predicted when input variables were set at high levels. Taking input levels at high levels, entrapment efficiency was predicted to be 101.44%. We conducted NMF preparation following the procedure described earlier and the entrapment efficiency was determined according to the RP-HPLC method. Results confirmed that percent DEX entrapment into NMF to be 97.5 ± 2.5, which is in agreement with the DOE.

Entrapment and loading efficiency

DEX entrapment and loading into the nanomicelles was determined with RP-HPLC method described earlier. All the NMFs showed excellent drug entrapment and loading efficiencies, which are summarized in **Table 19**. Among the formulations prepared and from the experimental design results it can be concluded that formulation F1 has the highest entrapment efficiency with optimal drug loading. Before conducting further characterization for F1 formulation, all the formulations were commonly subjected to appearance, viscosity, osmolality, size, PDI, surface charge, dissociation temperature and regeneration time tests (**Table 20**).

Micellar size, polydispersity, surface charge and morphology

Nanomicellar size and polydispersity indices were determined for all the prepared formulations. Results show a size range between 10 and 40 nm (**Table 19**). Polydispersity indices were observed to be in the range of 0.080 – 0.135 (**Table 19**). DEX loaded NMF are slightly larger than blank NMF. Blank NMF (Vit. E

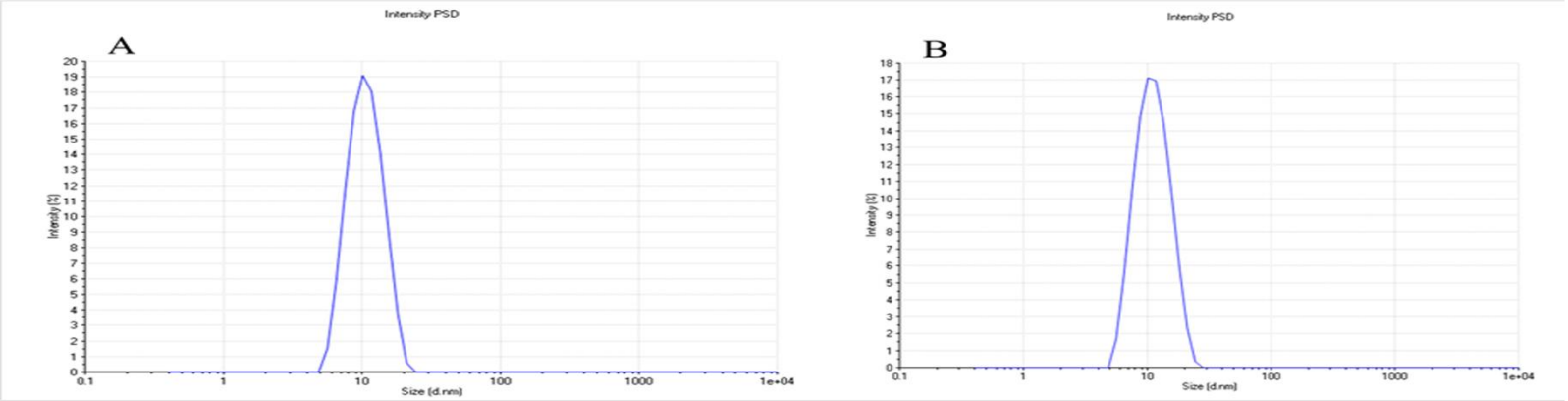

Figure 49. Size distribution for nanomicelles (A) Blank nanomicelles effective diameter 10.2 ± 0.3 nm (B) DEX loaded nanomicelles effective diameter 10.46 ± 0.3 nm.

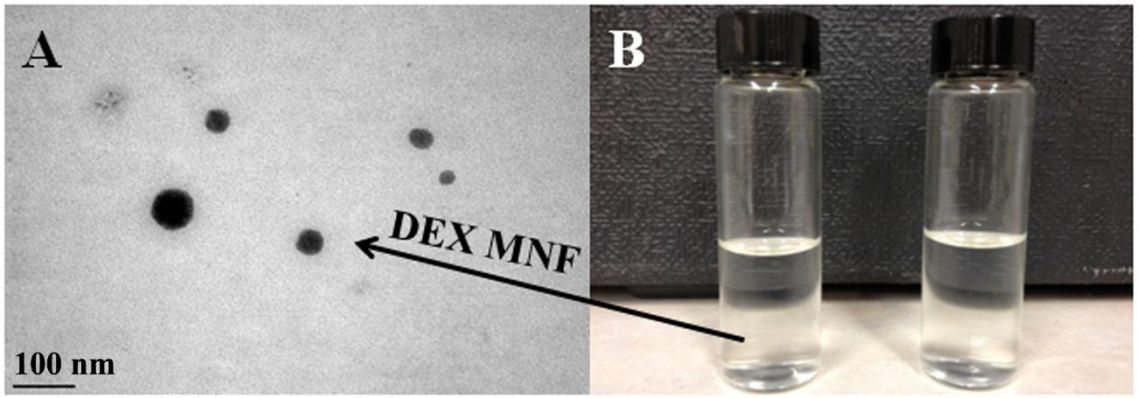

Figure 50. TEM image of DEX encapsulated nanomicellar formulation, A) TEM picture of DEX encapsulated nanomicelles (scale bar = 100 nm) and B) 0.1% DEX nanomicellar formulation on the left compared with DI water on right.

TPGS: Oc-40; 4.5:2.0) and optimally DEX loaded NMF (F1) exhibited a size of 10.2 ± 0.3 nm and 10.46 ± 0.3 nm respectively (**Figure 49**). We assume that the size of NMF to be sufficiently suitable to traverse across aqueous scleral channels/pore that have a size range between 20 and 80 nm (63). Also, these micelles display a narrow and unimodal particle size distribution. However, no significant changes in micelle size or size distribution were noted. Since these NMF's are in the same size range as membrane receptors, proteins, and other biomolecules, such carriers may have the ability to bind with cellular barriers. Surface charge of NMFs was found to carry a slight negative charge (**Table 20**). Surface morphology of DEX loaded NMFs was studied with TEM and results revealed that the NMFs are spherical in shape with smooth surface architecture without any aggregation (see **Figure 50**). The particle size visualized by TEM were in agreement with the size obtained by DLS.

Optical clarity / Appearance

One of the major objective of this study was to prepare an aqueous clear solution of DEX. Optical clarity/appearance refers to 90% or greater transmission of light of 400 nm wavelength in a 1.0 cm path. Micelle size, typically smaller than the smallest wavelength of a visible light radiation (about 350 nm), denotes clarity of the solution. In general, light scattering occurs when any particle interferes with the visible light wavelengths. Due to extremely small size of the nanomicelles light is not scattered, which denotes

a transparent/clear aqueous solution. Ophthalmic compositions of the present DEX formulations are substantially clear with an absorption units below 0.05 measured at 400 nm (data not shown). The low absorbance of the formulation indicates the clarity of the formulation which is devoid of any particulate matter. For example, absorbance data for the formulation (F1) used for the characterization studies was (0.040 ± 0.001). The optical clarity of the formulation was compared with distilled deionized water as blank. This study indicates that all the NMFs are similar to water with no particulate matter present.

Viscosity

Viscosity of the formulation is another critical factor that needs to be maintained. Optimal viscosity helps to increase the mean residence time of NMF at the administration site (precorneal and under eye lid pocket). Therefore, bioadhesive polymers such as PVP-K-30, hydroxypropyl methyl cellulose, hydroxyethyl cellulose or polycarbophil could be used. The high concentrations of these polymers were required to improve viscosity which resulted in undesirable outcomes like increase in NMF size, PDI or reduced NMF dissociation temperature (data not shown). However, PVP-K-90 polymer had negligible effect on the NMF and raised the dissociation temperature. Therefore, PVP-K-90 was selected as a bioadhesive and viscosity enhancing excipient/agent. Formulation viscosity was adjusted to be less than 2.0 centipoise (cP) (well below critical point of 4.4 cP) to hold formulation in the cul-de-sac and which does not affect rate of tear drainage (285).

Thermal dissociation and regeneration time

The NMF has to be robust and the parameters used, in general, include thermal dissociation and regeneration time. DEX loaded NMF with very high thermal dissociation temperature (DT) indicates the formulation is stable at high temperature. Following thermal dissociation when NMFs are allowed to cool to room temperature under ambient conditions, micelles were regenerated within less than one minute resulting in optically clear solutions. In general micelles are unstable structures possessing two characteristic relaxation times i.e., fast (τ_1) and slow (τ_2). The results show the time taken to regenerate the micelles is in seconds (**Table 20**), because both surfactants are non-ionic in nature. This peculiar behavior of the formulation indicates that the hydrophobic DEX is entrapped in the nanomicellar core even after being subjected to harsh conditions. Thermal dissociation/dissociation temperature of the blank NMF is about 20-40 ^{o}C higher than the formulation containing drug. With temperature rising above DT, micelles appear to dissociate into individual monomer units. Such disruption of micelle structures causes drug release in surrounding aqueous medium. Such destabilization of nanomicelles results in the formation of a cloudy or milky white solution. DT of the optimized formulation appears to be extremely high (>100 ^{o}C) which provides maximal stability to the formulation at normal room temperature. The results clearly show that increase in concentration of Oc-40 raises the DT at constant Vit. E TPGS.

Critical micellar concentration

Ocular drug delivery is impeded from delivering therapeutic concentrations of drug due to ocular static and dynamic barrier which includes tear/tear dilution (332). CMC is a critical factor that regulates premature release of drug due to tear dilution after topical drop administration. Of the total volume applied, only 20% of the formulation is available for absorption (14). The applied formulation occupies the space in pre-corneal pocket by replacing lacrimal fluid. The total volume of tear that pre-corneal pocket can hold without overflowing is 10 µl (333). Tear turnover rate is ~0.7 µl/min (333). The formulation applied will be continuously diluted by tears. This tear dilution may disrupt the micelles and release the drug at the site of application. To prevent the disruption of micelles by dilution a low CMC of the formulation is desired (334). To reduce the CMC of the polymeric surfactants a blend of non-ionic polymers is used. This low CMC provides the DEX entrapped NMF with high stability after topical drop application. In the current study, CMC was determined for Vit. ETPGS, Oc-40 and for the blend of polymer mixtures (see **Table 19**) with iodine as a probe. A lowering in CMC is an indicator of stable formulation at low surfactant concentrations. The results obtained were plotted for iodine intensity *versus* log wt% of polymer or blend of polymers was plotted to determine the intersection, which is CMC. CMC of Vit. ETPGS was found to be approximately 0.025 wt%, which is in agreement with the literature value. The other polymer, Oc-40, generated a CMC value of 0.107 wt% which is greater than the CMC of Vit. ETPGS. A combination of the surfactants in varying ratio decreased the CMC value to 0.012 wt% (Formulation F1). The obtained individual

results were subjected to student t-test. The obtained CMC values are significant at $p < 0.05$ level.

^{1}H NMR characterization

^{1}H NMR analysis is used to determine the presence of drug molecules in solution at parts per million (ppm) levels. NMFs were prepared in different media such as $CDCl_3$ and D_2O. ^{1}H NMR spectroscopy studies were conducted for DEX (

Figure **51**), mixture of polymers dissolved in $CDCl_3$ (

Figure **52**) and entrapped drug in $CDCl_3$ and D_2O. The concentration of DEX entrapped in the NMF is ~6.3 times higher than its aqueous solubility (0.159 mg/mL) (326). Addition of higher concentration of DEX in the aqueous environment leads to drug precipitation at the bottom of the vial due to insolubility. In our studies, we did not observe any precipitate at the bottom of the vial. Also, due to DEX aqueous solubility a small amount of unentrapped DEX may be present in the outer aqueous environment (D_2O), which may not be identified visually or with naked eye. Results show that in $CDCl_3$, the resonance peaks corresponding to DEX and nanomicelles are present (

Figure **53**). In D_2O, peaks corresponding to nanomicelles are only detected and no peaks for DEX were evident (

Figure **54**). These results clearly indicate, DEX was entrapped into the inner

hydrophobic microenvironment/core of nanomicelles. Also, study suggests that no free/unentrapped DEX was present in the NMF. These results are similar to earlier shown results for paclitaxel loaded mixed polymeric micelles in D_2O (280, 284).

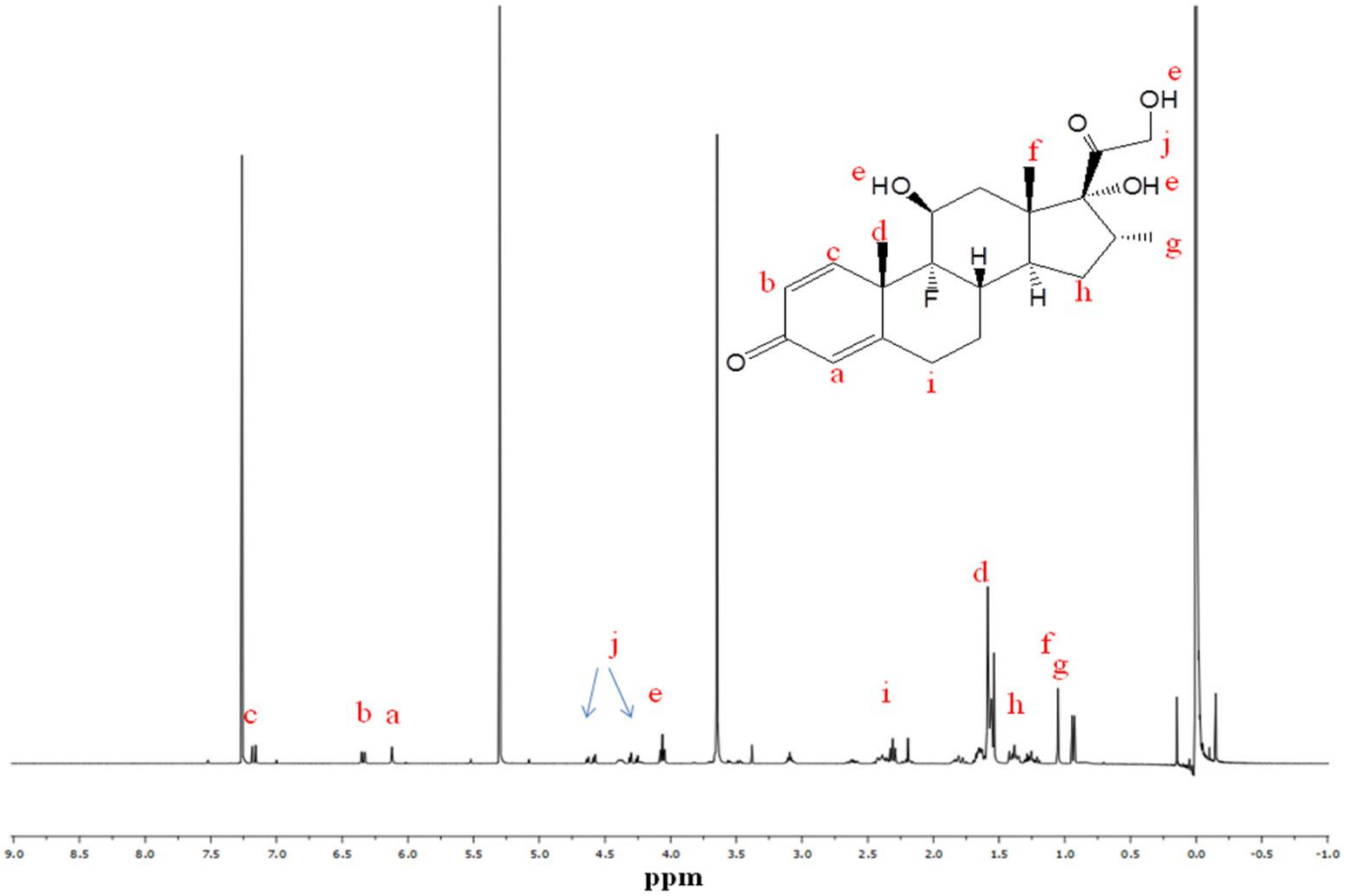

Figure 51. ^{1}H NMR for DEX and nanomicellar formulation. (A) ^{1}H NMR dexamethasone in $CDCl_3$

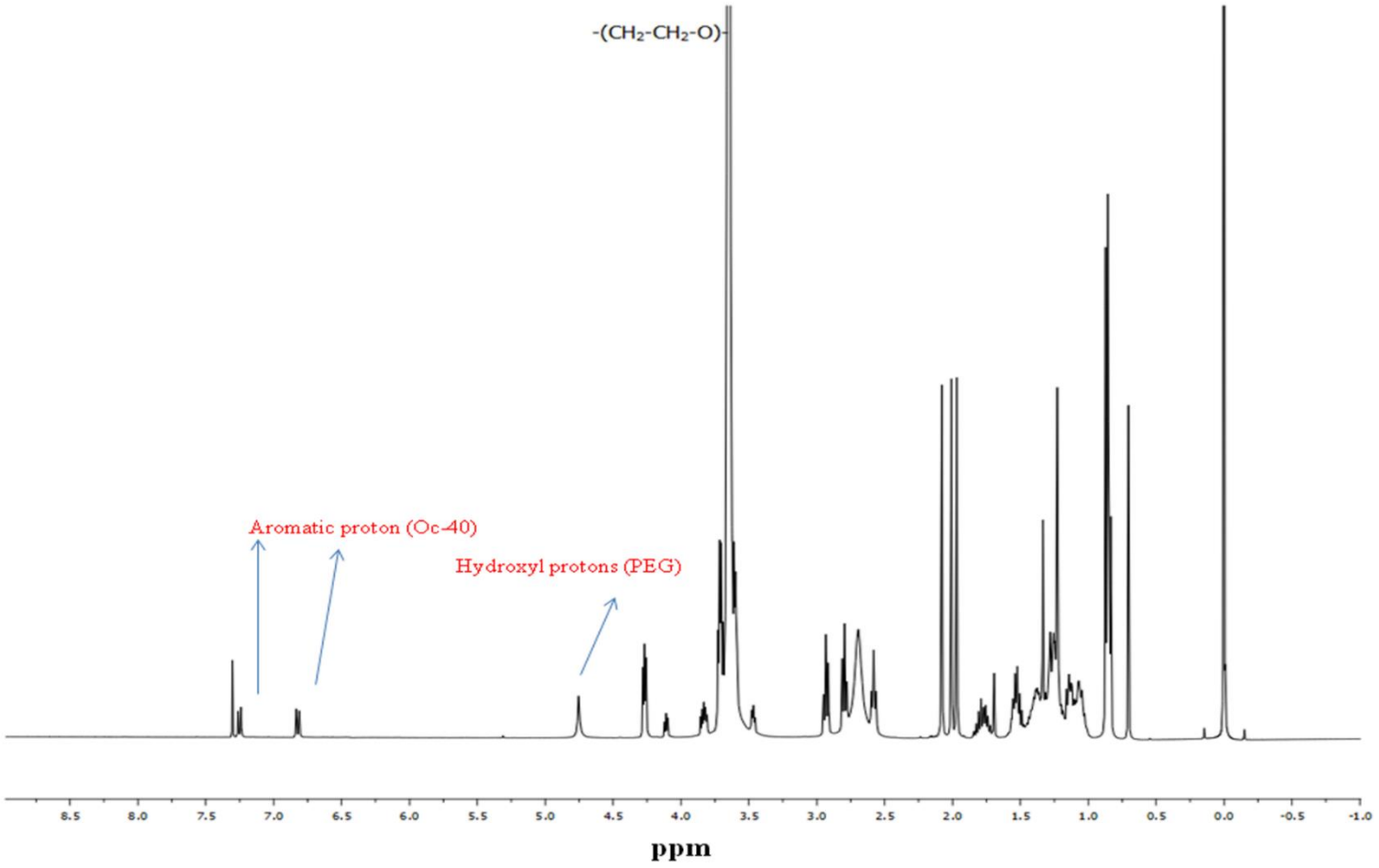

Figure 52. ^{1}H NMR blank nanomicelles in $CDCl_3$

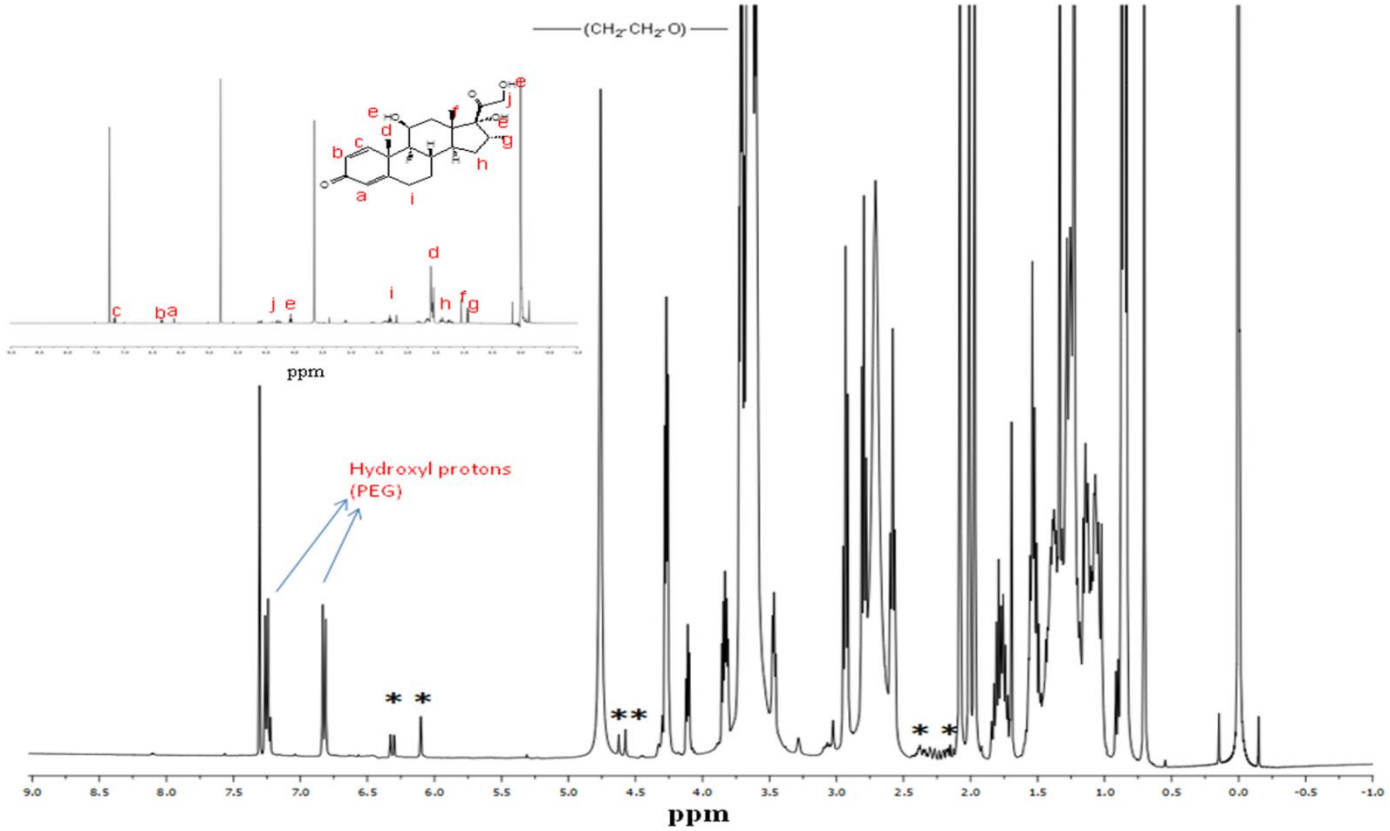

Figure 53. ^{1}H NMR nanomicellar formulation of dexamethasone in $CDCl_3$. The symbol "*" indicates the resonance peaks corresponding to dexamethasone

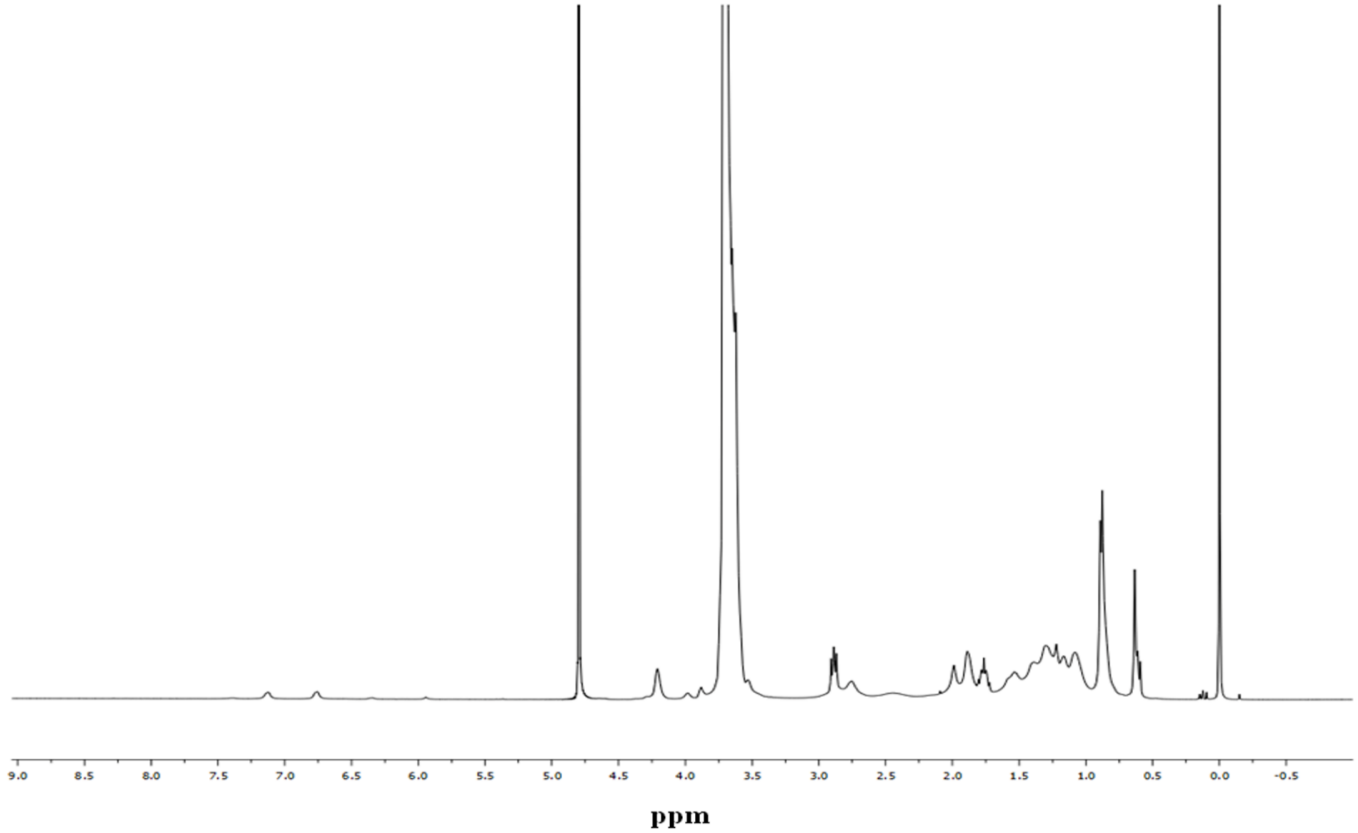

Figure 54. ^{1}H NMR dexamethasone entrapped nanomicellar formulation in D_2O

In vitro cytotoxicity

To evaluate the cytotoxic effect of NMFs (blank and DEX loaded), MTS and LDH assays were performed on rPCEC cells. Since eye drops are rapidly cleared from the pre-corneal pocket (335, 336) MTS assay was performed for 1 h. It was assumed that a 1 h incubation period would be sufficient to evaluate any toxicity. Percent viable cells for all the NMFs were comparable to that of negative control (culture medium) (**Figure 55A**). Triton-X 100 served as positive control and reduced the percent cell viability to 10% of the total cell number. In another set of studies, cell plasma membrane damage test (LDH assay) studies were conducted following manufacturer's protocol for 2 h, 6 h and 24 h incubation and examined for LDH release. The amount of LDH released in the culture media directly correlates with cytotoxicity. Triton-X 100 caused significant toxicity/membrane damage. Percentage cytotoxicity to rPCEC cells post exposure to NMFs (blank and DEX loaded) appeared to be negligible (**Figure 55B**) indicating NMFs did not cause cell membrane damage. Results from these assays clearly suggest that our NMFs do not cause cell death or damage to plasma membrane and are safe for topical ocular application.

In vitro DEX release

In vitro release kinetics of DEX from Vit. ETPGS and nanomicelles (F1) were investigated at a physiological pH of 7.4 at 37 ^{o}C. An equal quantity of DEX (1 mg) was dissolved in 1 mL of absolute ethanol that served as a control. DEX release from ethanolic solution was much more rapid than DEX in Vit. ETPGS and

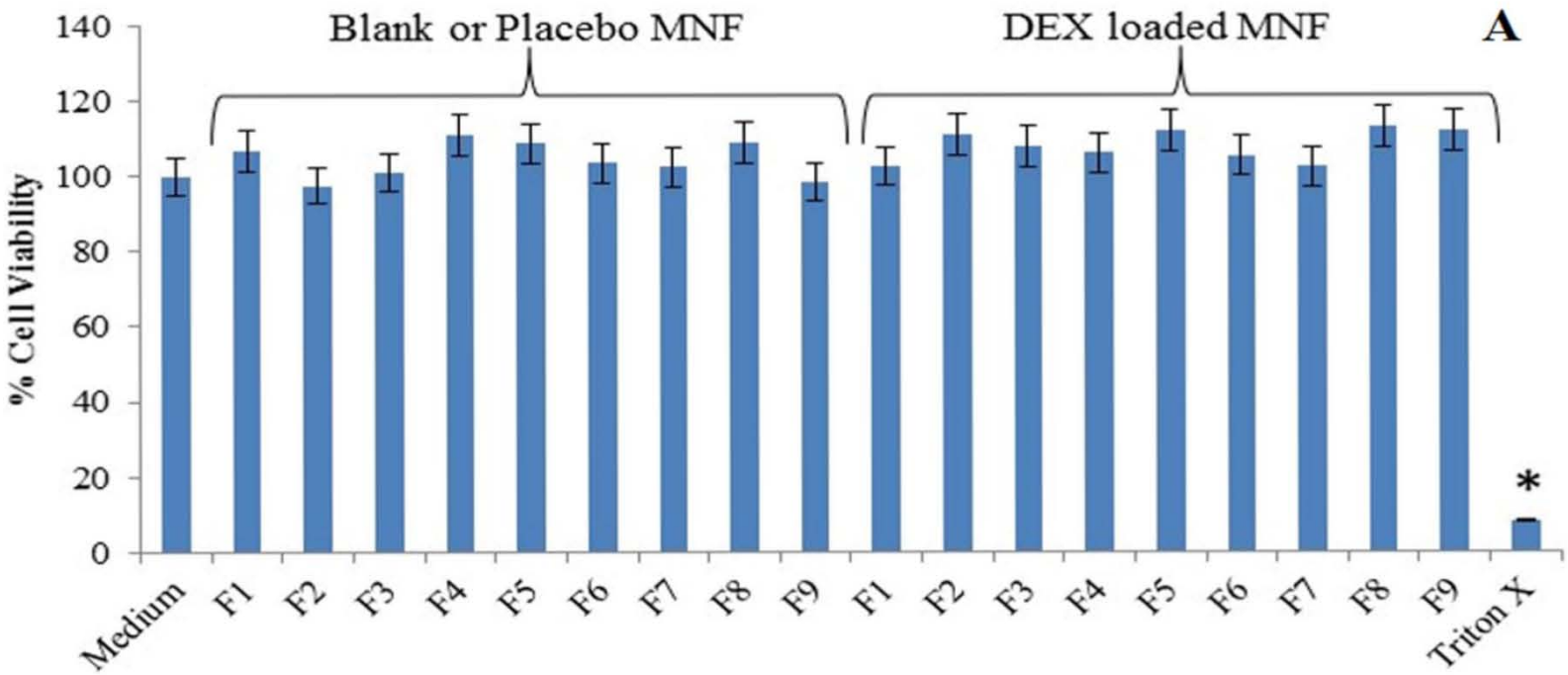
Blank or Placebo MNF
DEX loaded MNF
A
% Cell Viability
140
120
100
80
60
40
20
0
*
Medium
F1
F2
F3
F4
F5
F6
F7
F8
F9
F1
F2
F3
F4
F5
F6
F7
F8
F9
Triton X

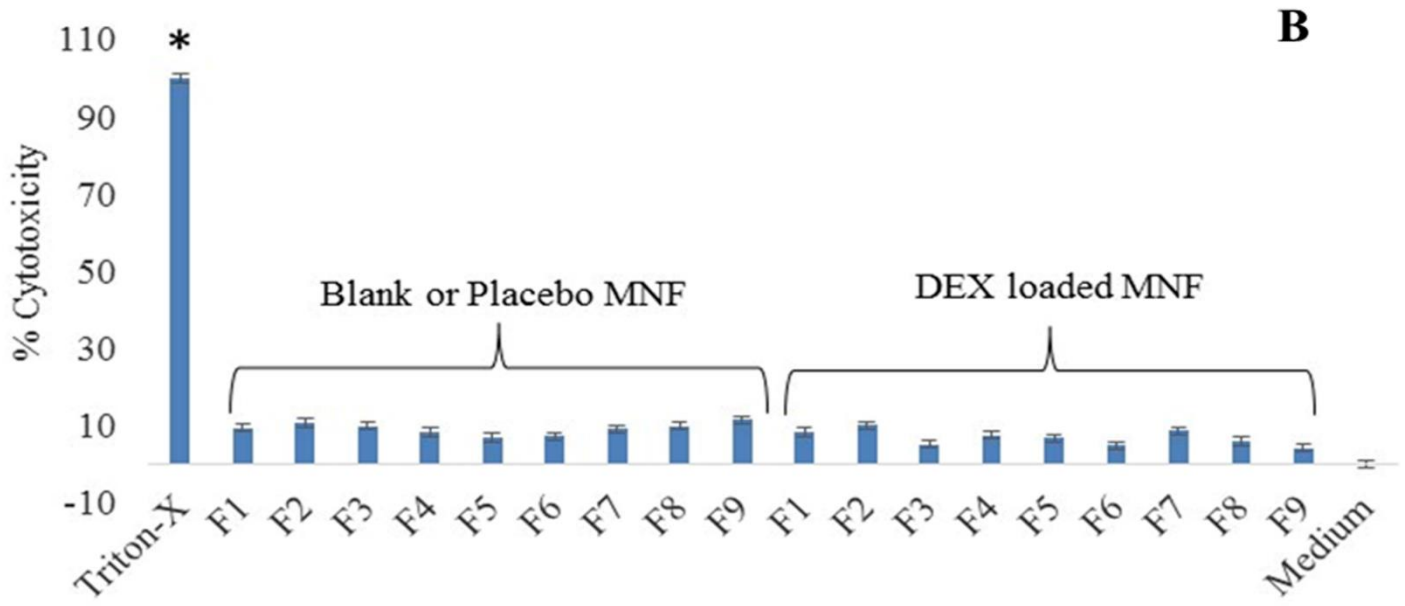

Figure 55. Cytotoxicity of blank and 0.1% DEX loaded nanomicellar formulations on rabbit primary corneal epithelial cells (rPCEC). (A) Cytotoxicity of blank and DEX loaded nanomicellar formulations on rabbit primary corneal epithelial cells (rPCEC), 1 h exposure time, Triton-X 100 positive control and culture medium negative control; (B) Cell membrane damage (LDH assay) studies on rPCEC cells, 24 h incubation time, Triton-X 100 positive control and culture medium negative control (Formulation abbreviation are described in Table 19). Data are shown as mean ± S.E.M (n = 4). *$p < 0.05$ versus control (paired t-test).

nanomicelles. Almost 100 % DEX release occurs in approximately four hours for ethanolic DEX. The release kinetic profiles of ethanolic and encapsulated DEX from the nanomicelles have been depicted in **Figure 56**. Nanomicellar DEX release half-lives were slow and not associated with any significant burst effect. The results suggest a sustained release of DEX from the core of nanomicelles over a period of 4.2 days. Results suggest that under physiological conditions, topical administration of DEX NMF helps to sustain release of DEX. As a result it aids in achieving therapeutic concentrations of DEX in ocular tissues thereby reducing dosing frequency.

Nanomicelle stability

The stability of NMFs is a very important segment in the formulation development process. In order to determine the stability of the novel NMF, we selected F1 formulation for long term stability studies. NMF F1 has low CMC, high entrapment efficiency, small size, narrow polydispersity index and high dissociation temperature. Formulation F1 was stored at 40 ^{o}C, 25 ^{o}C and 4 ^{o}C for 6 months. Samples were monitored for time-dependent changes in nanomicellar size and drug content during the storage period. At predetermined time points, NMF sample was collected, centrifuged at 10,000 rpm for 10 mins at 4 ^{o}C, supernatant was collected and analyzed for DEX with RP-HPLC. Analysis shows that the drug concentration was low (**Figure 57**). A plot of ln [DEX] *versus* time (h) was used to determine the shelf and half-lives of NMF. The formulation stored at

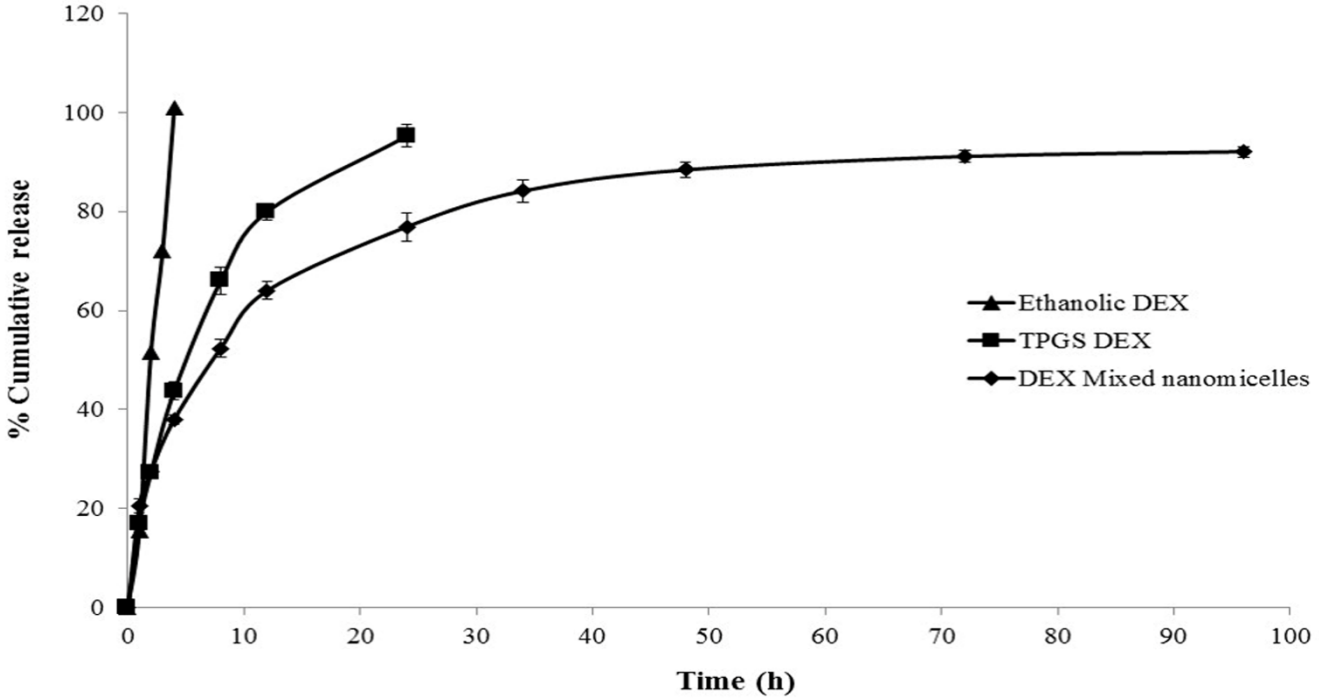

Figure 56. *In vitro* dexamethasone release studies. Graph showing dexamethasone release under *in vitro* conditions (N = 4). (▲) dexamethasone release from ethanolic solution. Dexamethasone was completely released in 4 h (■) dexamethasone release from Vit. ETPGS alone. Dexamethasone release was sustained up to ~22 h and (♦) dexamethasone release from blend of Vit. ETPGS and Oc-40 (4.5:2.0) mixture for more than 100 h.

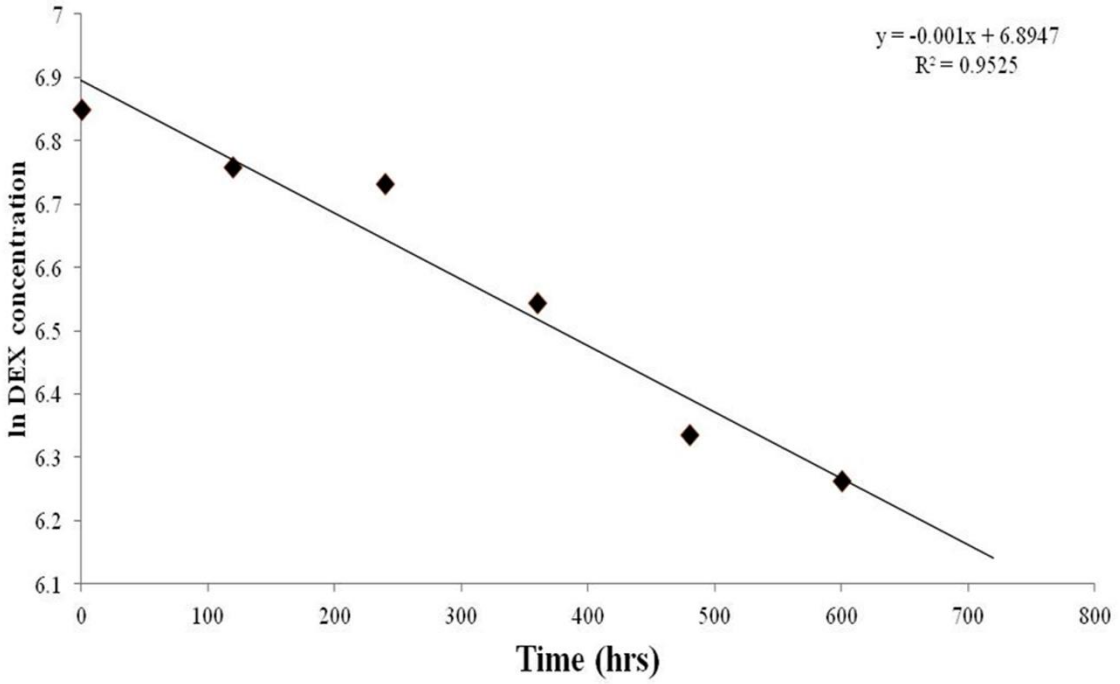

Figure 57. Formulation stability studies (N= 4) at 40 ºC.

40 ^{o}C exhibited a shelf life (t_{90}) of 4.2 days and half-life of 27.7 days respectively (**Figure 57**). Simultaneously, nanomicellar size determination studies were conducted. No difference in micellar size for the samples was observed (data not shown). The micellar size for the formulation remained the same in the stability studies conducted at 40 ^{o}C, room temperature (25 ^{o}C) and 4 ^{o}C. NMF of DEX stored at 25 ^{o}C and 4 ^{o}C are stable for more than three and six months respectively (data not shown). Quantitative estimation of remainder DEX in the aqueous NMF was conducted with RP-HPLC as described earlier. At high temperature the formulation showed decreasing DEX concentration with time. Free drug precipitated out of the formulation and settled at the bottom of the vial, which was confirmed by RP-HPLC after separation of precipitate from the aqueous NMF.

In vivo studies

Quantitative determination of DEX in different ocular tissues after topical administration is shown in

Concentration (ng/g tissue)	Set 1	Set 2	Set 3	Set 4	Average ± SD
Cornea	1415.01	1459.60	652.73	675.58	**1051 ± 446.8**
ICB	922.2	630.27	265.98	299.76	**530 ± 309.1**
Sclera	180.2	77.49	54.06	---	**104 ± 67.1**

RC	27.36	80.15	50.29	36.27	**49 ± 23.1**
AH (ng/mg protein)	464.8	401.05	314.94	195.13	**344 ± 117**
Lens	BLOQ	BLOQ	BLOQ	BLOQ	**BLOQ**
VH (ng/mg protein)	BLOQ	BLOQ	BLOQ	BLOQ	**BLOQ**

Table **22**. Sixty minutes after topical application to a rabbit eye, DEX concentration in the anterior segment (cornea, aqueous humor, iris ciliary bodies and lens) and posterior tissues (sclera, vitreous humor, and retina-choroid) was determined. DEX concentrations of 1415.01, 1459.60, 652.73 and 675.58 ng/g (four times dilution factor was applied to those cornea samples, values are 353.75 × 4, 364.90 × 4, 163.18 × 4 and 168.90 × 4 ng/g respectively) of tissue and 464.80, 401.05, 314.94 and 195.13 ng/mg protein were quantified in the cornea

Table 22. DEX drug levels in ocular tissues from 0.1% nanomicellar formulation after topical administration.

Concentration (ng/g tissue)	Set 1	Set 2	Set 3	Set 4	Average ± SD
Cornea	1415.01	1459.60	652.73	675.58	**1051 ± 446.8**
ICB	922.2	630.27	265.98	299.76	**530 ± 309.1**
Sclera	180.2	77.49	54.06	---	**104 ± 67.1**
RC	27.36	80.15	50.29	36.27	**49 ± 23.1**
AH (ng/mg protein)	464.8	401.05	314.94	195.13	**344 ± 117**
Lens	BLOQ	BLOQ	BLOQ	BLOQ	**BLOQ**
VH (ng/mg protein)	BLOQ	BLOQ	BLOQ	BLOQ	**BLOQ**

BLOQ: Below limit of quantification; LOQ: limit of quantification (2.70 ng/mL). [a] Dilution factors: cornea (4X) and ICB (2X); "—" tissue lost due to experimental error.

and aqueous humor respectively. For the posterior segment, DEX concentrations in the sclera, retina-choroid and iris ciliary bodies were observed to be 180.20, 77.49 and 54.06 ng/g of tissue, and 27.36, 80.15, 50.29 and 36.27 ng/g of tissue, and 922.20, 630.27 ng/g (two times dilution factor is applied values are 461.10 × 2 and 315.14 × 2 ng/g), 265.98 and 299.76 ng/g of tissue respectively. DEX concentration in the lens and vitreous humor were below LLOQ (LLOQ = 2.7 ng/mL). Mean concentration and standard deviations of DEX in various ocular tissue matrices are summarized in

Table **22**. A novel 0.1% nanomicellar formulation of DEX showed high concentration levels in back-of-the-eye (retina-choroid = 49 ng/g of tissue) suggesting conjunctival scleral (trans-corneal) pathway of nanomicelles carrying

Concentration (ng/g tissue)	Set 1	Set 2	Set 3	Set 4	Average ± SD
Cornea	1415.01	1459.60	652.73	675.58	**1051 ± 446.8**
ICB	922.2	630.27	265.98	299.76	**530 ± 309.1**
Sclera	180.2	77.49	54.06	---	**104 ± 67.1**
RC	27.36	80.15	50.29	36.27	**49 ± 23.1**
AH (ng/mg protein)	464.8	401.05	314.94	195.13	**344 ± 117**
Lens	BLOQ	BLOQ	BLOQ	BLOQ	**BLOQ**
VH (ng/mg protein)	BLOQ	BLOQ	BLOQ	BLOQ	**BLOQ**

the payload to back-of-the-eye tissues (retina-choroid).

Conclusion

A clear, stable, aqueous DEX loaded NMF was prepared and optimized with full factorial statistical DOE. Results indicate that DEX entrapment efficiency was dependent on two input factors Vit. ETPGS and Oc-40. A specific blend of Vit. ETPGS and Oc-40 at a particular wt% ratio (4.5:2.0) produced excellent drug entrapment, loading and small nanomicellar size as well as narrow PDI. This method of drug entrapment can minimize drug loss during large scale production. Since this aqueous DEX NMF is highly stable for prolonged period and it appears from the *in vitro* cytotoxicity results that it may not be very toxic. *In vivo* ocular tissue distribution demonstrates high DEX levels in anterior ocular tissues. Moreover, therapeutic drug concentrations were detected in retina-choroid. No drug was detected in lens and vitreous humor suggesting a transscleral (conjunctival-scleral) pathway of drug delivery to retina-choroid.

Chapter 6

TOPICAL AQUEOUS CLEAR RAPAMYCIN (SIROLIMUS) NANOMICELLAR FORMULATION: DEVELOPMENT AND IN VIVO TISSUE DISTRIBUTION

Rationale

Rapamycin is extremely hydrophobic with an octanol/water partition coefficient (log P) of 5.77 and an aqueous solubility of 2.6 µg/mL (337). Also, rapamycin is pH and light sensitive (338). Oral or intravenous administration of rapamycin for back-of-the-eye delivery is not medically acceptable. Rapamycin, an immunosuppressant, may severely compromise immune function if administered through systemic route (339). To deliver rapamycin locally to the eye, various strategies such as route of administration (periocular, subconjunctival, intravitreal implants/injections), and formulations (nanoparticles, liposomes) based have been implemented (11, 337, 340). Strategies such as periocular, subconjunctival and intravitreal implants/injections of rapamycin are invasive and associated with side effects such as retinal detachment or damage, endophthalmitis, and pseudoendophthalmitis. Polyethylene glycol-b-poly(Ɛ-caprolactone) micelles have been previously developed to improve solubility. This micellar formulation resulted in an improvement of solubility up to a concentration of 1 mg/mL (341).

Among the ocular delivery routes topical drop instillation is the most patient acceptable route of drug administration. Static and ocular barriers impede drug permeation from front to the back-of-the-eye tissues (retina-choroid). Therefore, the objectives of this work are to improve rapamycin aqueous solubility, develop a

novel clear, aqueous, nanomicellar formulation (NMF) and deliver therapeutic rapamycin levels in back-of-the-eye tissues with topical drop instillation. To achieve this objective we have employed a blend of polymers Vit. E TPGS and Oc-40. Vit. E TPGS is a FDA approved amphiphilic polymer. In pharmaceutical industry it is employed as an emulsifier, solubulizer, absorption enhancer and a vehicle for hydrophobic drugs (342). This HLB value of Vit. E TPGS renders it to be a more lipophilic (343) polymer relative to the second polymer (Oc-40, HLB = 18.0). Also, Vit. E TPGS is a potent inhibitor of multi-drug efflux pumps (P-glycoprotein, P-gp), facilitates drug translocation across cell membrane, modulates drug pharmacokinetics and improves bioavailability (344, 345). Another polymer, Oc-40 employed in this study is also FDA approved for human use. A unique ratio of these polymeric blend (4.5:2.0, for Vit. E TPGS and Oc-40) was selected due to their low critical micellar concentration (0.012 wt%) of the combination relative to individual polymers (**Table 19**) (278, 346).

Materials and Methods

Materials

Rapamycin and erythromycin were purchased from LC laboratories USA and Sigma Chemicals (St. Louis, MO), respectively. HPLC grade methanol, acetonitrile, triethylamine, and formic acid were procured from Fisher Scientific (New Brunswick, NJ). Ultrapure water from MilliQ-system (Millipore, Molshecin France) was used through the study. All chemicals were of HPLC grade and used as received without further purification. An Xterra reverse phase HPLC column

procured from Waters Corporation USA.Vitamin E TPGS was purchased from the Peboc division of Eastman Company, UK Limited, UK. Igepal (Oc-40) was obtained from Rhodio Inc, New Jersey, USA. Kollidon(R) 90F (povidone K 90) Ph. Eur., USP was procured from Mutcher, Inc., Pharmaceutical ingredients, Harrington Park, New Jersey, USA. HPLC grade methanol and acetonitrile were procured from Fisher Scientific, USA. Ethanol was purchased from Aaper Alcohol and Chemical Co. Shelbyville, Kentucky, USA. For all the formulation preparations Hyclone cell culture water, Hyclone, USA, was utilized.

RP-HPLC method

To determine concentration of entrapped drug within the core of NMF RP-HPLC analysis was performed utilizing C8 column (Phenomenex C8, 5 µm; 150 mm X 2.1 mm), an autosampler (Alcott, model 718 AL), a column heater (Flatron CH-30 column heater, Flatron Systems Inc., USA) set at 40 ^{o}C, a pump (model SD 20, shimadzu) set to deliver 1.0 mL/min, a UV detector (Shimadzu, SPD 20A) set at 278 nm and an integrator to collect data. The mobile phase comprised of acetonitrile-methanol-water (30:35:35 v/v/v). Since the mobile phase contained higher organic phase it was prepared freshly before analysis. A 50 µL sample was injected into the HPLC system.

Method of preparation

Rapamycin loaded nanomicellar formulations (NMF) were prepared by a novel solvent evaporation method as described previously in Chapter 5 (278). A blank formulation was also prepared following a similar procedure without rapamycin.

Characterization of nanomicellar formulation

Rapamycin loaded nanomicellar formulations were subjected to characterization following procedures described in Chapter 3 for entrapment efficiency, loading efficiency, size, polydispersity index, surface potential and proton NMR studies. HPLC-UV was used for determining entrapment and drug loading efficiencies.

In vitro cytotoxicity

Cell viability and plasma membrane damage studies were conducted following the manufacturer's protocol described in Chapter 3 on rPCEC cell lines. Similarly, cell viability studies were conducted on D407 cells with NMF and placebo formulations.

LC-MS/MS method

Solutions and validation samples

Rapamycin and erythromycin as internal standard (IS) were dissolved in methanol to obtain, 1.0 mg/mL stock solutions, and were gradually diluted by the

serial dilution method using calibrated pipettes (2-20 µL, 10-100 µL and 100-1000 µL), in order to obtain working stock dilutions at decreasing concentrations (10, 8.5, 7.5, 5.0, 2.5, 1.0, 0.1 and 0.023 µg/mL). These solutions were used for the preparation of mass spectrometry optimization, calibration curve and quality control standards in methanol and ocular tissue homogenates. These stock solutions and stock dilutions were stored at below 10 ^{o}C, and at -20 ^{o}C, respectively. For the preparation of calibration curve standards, aliquots of 200 µL of blank ocular tissue homogenates were spiked with 20 µL of each of the rapamycin working stock dilutions in order to obtain eight calibration curve standards at decreasing concentrations (1000, 850, 750.0, 500.0, 250.0, 100.0, 10.0 and 2.3 ng/mL). Similarly, quality control (QC) samples were independently prepared at four levels of concentration (800.0, 480.0, 10 and 2.3 ng/ mL) in tissue homogenates from the working stock dilutions. Stock concentration was corrected by the formula below.

$$\text{Corrected conc.} = \frac{\text{Amount weighed (mg)} * \text{Mol. Weight (free form)} * \text{Potency (purity)}}{\text{Volume madeup (mL)} \ \text{Mol. Weight (salt form)}} * 100 \qquad \textit{Eq 14}$$

Mass spectrometry optimization

Mass spectrometry parameters optimization of rapamycin and erythromycin was carried out by a standard stock dilution (200.0 ng/mL) in methanol through direct infusion into the mass spectrometer with the inbuilt Harvard infusion pump. Data from rapamycin and erythromycin were first acquired in full scan from the range between m/z 50–1000 in order to identify the most suitable parent ion for

MS/ MS experiments. The sodium adduct $[M+Na]^+$ at m/z 936.6 was selected as the parent ion for rapamycin and fragmented. The MS/MS parent ion was still preserved as a parent in the MS2 spectrum and it was together with two other daughter ions at m/z 345.5 and 409.3. Erythromycin was also detected by using the proton adduct $[M+H]^+$ ion at m/z 734.4 as the parent (under the same instrumental parameters), daughter ions at m/z 158.2 and 576.5 were optimized.

LC-MS/MS chromatographic separation

LC-MS/MS chromatographic separation was achieved on reversed phase C8 silica gel material. The column oven temperature was maintained at 40 ^oC. Extracted calibration and QC samples were reconstituted in 200 μL of mobile phase. Twenty microliters was injected on LC-MS/MS. Ionspray source temperature 350 ^oC and ionspray voltages 5500V were optimized. Mass spectrometry data was acquired in positive ion mode and processed using Analyst software (version 1.4.2, AB Sciex). An LC-MS/MS analysis, rapamycin was determined at retention time 3.011 min and erythromycin, as IS was at 1.318 min. The curtain gas (CUR) was at 40.0 psi, the nebulizer source gas 1 at 40.0 psi, and the turbo ion source gas 2 at 45.0 psi was utilized. Declustering potential 105.0 V, and entrance potential 10.0 V were optimized. Rapamycin fragmentation was induced by collisionally activated dissociation (CAD) with nitrogen gas. The collision gas pressure was set at 2.0 psi for multiple reaction monitoring (MRM) quantitation. The collision energy 75.0 V for rapamycin and 30.0 V for erythromycin and the collision cell exit potential 10.0 V for rapamycin and 8.0 V

for erythromycin were utilized. The erythromycin scan was optimized by the proton adduct [M+H]+ ion at m/z 734.4 as parent ion. The daughter ion at m/z 576.5 was selected. Dwell time 200 ms was employed.

Sample preparation and extraction

Homogenates of rabbit ocular blank tissue were used for calibration curve and QC standards. A simple, clean and easy protein precipitation extraction technique was developed. Two hundred microliter aliquot of tissue homogenate sample was mixed with 25 µL (5 µg/mL) of internal standard. The mixture was vortex-mixed for 30 seconds, then 25 µL of a 50% triethyl amine in methanol was added, and the solution was vortex mixed for additional 2.0 min. One mL of methanol was added and this mixture was again vortex-mixed for 2 min in order to precipitate tissue protein. The final mixture was centrifuged at 10000 rpm for 30 min at 40 ^{o}C. The supernatant was collected and dried under speed vacuum (Genevac DD-4X evaporator, Genevac Inc., 815 Route 208, Gardiner, NY 12525 USA) at 37 ^{o}C for 90 min. Dried samples were stored at -80 ^{o}C until further analysis. Samples were reconstituted in 200 µL of mobile phase and analyzed by LC-MS/MS.

The Specificity and selectivity of rapamycin

The specificity and selectivity of the method were tested by analyzing six ocular blank samples. We processed LLOQ (n=6) in order to assess the blank interference at the peak of interest. The percentage of blank interference was

calculated by comparing mean peak area of LLOQ of the analyte for peak response obtained from the blank samples. Peak areas of blanks co-eluting with the analyte should not be more than 20% of the mean peak area at the LLOQ.

Precision and accuracy of rapamycin

Intra-day and inter-day precision and accuracy experiments were performed by analyzing extracted calibration curve and QC standards. The standard samples were prepared based on the procedure described in our previously published LC-MS/MS method (347). Accuracy was reported as the percentage difference between the mean concentrations divided by the nominal concentration multiplied by 100. Accuracy of the method must be between 85 - 115% of the nominal value in all the standards, except at the lower limit of quantitation (LLOQ) level, which is 80-120 % according to the guidance for industry bioanalytical method validation in Food and Drug Administration guidelines of May 2001 (www.fda.gov). Precision was calculated using the coefficient of variation (CV) (standard deviation/mean concentration) multiplied by 100. Precision of the method should be within 15% of the nominal concentration except at the LLOQ, which is within 20%.

Matrix effect

Matrix effect was evaluated by analyzing six replicates of each two sets at low, middle and high quality control standards of post-spiked (extracted blank tissue homogenates), and spiked in aqueous samples (represents no matrix effect) at the same concentration for rapamycin. One concentration of IS spiked in both

the sets. Ion suppression was calculated by comparing mean peak area ratios of analyte and IS generated from the post-spiked quality controls of ocular tissue homogenate samples to aqueous spiked quality control standards. A relative matrix effect was estimated by comparing mean peak area ratios of the analytes to internal standard obtained from the post-spiked QC (blank ocular matrix samples versus aqueous standards). Thirty-six blank ocular matrix samples were processed and extracted for low, middle, and high QC standards according to the sample preparation and extraction procedure. Quality control standards, LQC, MQC and HQC were prepared in a blank reconstitution solution to obtain the same concentrations (800.0, 480.0 and 10.0 ng/mL).

Recovery

Extraction recovery of rapamycin was estimated by analysis of two sets of six replicates of each at three quality control standards of spiked and post-spiked (representing 100% recovery) samples with the IS. Extraction recovery was measured by comparing mean peak area ratios of analyte and IS of ocular tissue/fluid homogenates to unextracted (post-spiked) quality control standards. Recovery quality control samples were made in a blank matrix and were extracted to get equal concentrations (800.0, 480.0 and 10.0 ng/ mL).

Stability in ocular matrix

Stability samples were prepared in tissue homogenates and were stored at −80 ºC and −20 ºC for several weeks to estimate the degradation of analyte in the

matrix. Stability QC samples were extracted along with the freshly spiked calibration curve standards and were tested on the same day. The extracted QC samples were stored for 2 days at 4 ^{o}C, and analyzed with the freshly spiked and processed calibration standards for in-injector and post-processed stability. The stability samples were frozen and stored for the next 6 weeks at −80 ^{o}C. Freeze–thaw stability QC samples were freeze-thawed for three cycles, and the analysis were conducted.

Stability experiments have shown that rapamycin had an adequate stability in matrix. These samples were stored for 6 weeks to anticipate the original samples storage conditions (Bench top, freeze storage, freeze thaw and processed storage stability) (347).

HPLC chromatographic separation conditions

Chromatographic separation was carried out on a UFLC Shimadzu prominence system consisting of LC-20AD liquid chromatography low pressure gradient pump, SPD-M20A diode array detector, SIL-20AST auto sampler, and DGU-20As degasser (Shimadzu USA manufacturing Inc., 3111 Lomita Boulevard, Torrance, California 90505, USA) with a reverse phase Xterra MS C8 column 50 x 4.6 mm, i.d, 5µm (Waters Corporation, 32 Maple Street, Massachusetts 01757-3696, USA). Isocratic mobile phase composed of 80% acetonitrile in water mixture containing 0.05 % of formic acid at a flow rate of 0.25 mL/min was used. As sample injection volume of 20.0 µL was used, and total analytical run time was 6.0 min.

In vivo studies

Animals: New Zealand white male rabbits weighing between 2.0 to 2.5 kg were employed for *in vivo* studies. Animals were obtained from Myrtle's rabbittry (Thompson, TN) and acclaimed for 24 h in the animal care facility. Animal care and treatment in this investigation was in compliance with the Association for Research in Vision and Ophthalmology (ARVO) statement for the use of animals in ophthalmic and vision research.

Ocular tissue dissection

Animals were anesthetized prior to an experiment with ketamine HCl (35 mg/kg) and xylazine (3.5 mg/kg) administered intramuscularly. For the treatment, N=10 eyes were utilized. Anesthesia was maintained throughout the experiment. A 50 µL of 0.2% rapamycin NMF was instilled into each conjunctival sac. After a period of 60 minutes, euthanasia was performed under deep anesthesia with an intravenous injection of sodium pentobarbital through the marginal ear vein. Following euthanasia, the globe was immediately enucleated within a period of 2 minutes and was transferred to the ice cold Dulbecco's phosphate buffer saline (DBPS, pH = 7.4). Enucleated eyes were rinsed twice in the ice cold DPBS to remove any traces of drug adsorbed onto the surface of the tissue. The sample of aqueous humor was withdrawn using 27 guage needle by limbal paracentesis. A small incision was made at the back of the globe and the vitreous humor was aspirated with the tuberculin syringe. Care was taken to avoid contamination by other tissues such as lens. The lens was carefully separated and collected. The iris-

ciliary body was removed and cornea was excised by incision along the sclera-limbus junction. Retina-choroid layer was removed and separated from the sclera. All the collected tissues were dried with Kimwipes®. Dissected posterior ocular tissues (sclera and retina-choroid) transferred to preweighed eppendorf tubes and stored at -80 ºC until further extraction and analysis. Vitreous humor was transferred to a 15 mL falcon tube and stored at -80 ºC until further analysis.

*Drug extractio*n*:* For rapamycin extraction, a volume of 200 µL of tissue homogenate was used. For vitreous humor a volume of 100 µL was aspirated. Rapamycin was extracted from eye tissues following a previously described protocol from our laboratory (348). Briefly, to extract rapamycin protein precipitation method was used. Erythromycin was selected as an internal standard (IS). To all the tissue homogenates, except blank, 25 µL of IS at a concentration of 5.0 µg/mL was added and vortexed for one minute. Twenty five microliters of 50% triethylamine in methanol (v/v) was added to all the samples and then vortexed vigorously for 2 minutes. Proteins were precipitated by addition of 800 µL of methanol. All the tissue homogenate samples were vortexed for another 2 minutes. Samples were centrifuged at 10,000 rpm for 30 mins at 4 ºC. A volume of 500 µL supernatant was separated and evaporated using SpeedVac® (Savant Instruments, Inc, Holbrook, NY). A 100µL of HPLC mobile phase was added to the dry residue and reconstituted by vortexing for 2 mins. This solution was centrifuged for 1 minute at 1000 rpm and the supernatant was injected into HPLC for rapamycin quantification.

Statistical Analysis

Data for *in vitro* experiments were conducted at least in quadruplicate and the results were expressed as mean ± standard deviation (SD). Statistical comparison of mean values was performed with Student's t-test. A *p-value* of <0.05 was considered to be statistically significant.

Results

In the present study rapamycin (0.1% and 0.2%) loaded NMFs were successfully prepared. The NMF particles were optically clear and were comparable to that of distilled deionized water. Viscosity of the aqueous clear NMF was similar to water. However, the viscosity of the formulation was improved by adding PVP-K90 (0.6%). Osmolality was adjusted to physiological range of ~300 mOsm/kg with sodium chloride solution. Blank NMF (Vit. E TPGS/Oc-40; 4.5:2.0) exhibited an average nanomicellar size of 10.98 ± 0.089 nm. However, the size of 0.1% and 0.2% were 10.54 ± 0.089 and 10.84 ± 0.11 respectively (**Table 23**) (**Figure 58A and B**). Entrapment efficiency for both formulations was also > 90 %. Surface potential was found be slight negative and architecture was found to be smooth surface, spherical in shape and devoid of aggregation (**Figure 59A**). Qualitative ^{1}H NMR study demonstrated that no free rapamycin was available in the aqueous environment of NMF (**Figure 60** through **Figure 63**). Results were comparable to that of formulations prepared in earlier chapters. Dilution studies were conducted

Table 23. Characteristics of the nanomicellar formulation.

Sample	Entrapment Efficiency (%) ± S.D	Loading Efficiency (%) ± S.D	Micelle size (nm) ± S.D	Polydispersity index	Surface potential (mV)	Appearance (400 nm)
Placebo	-	-	10.98 ± 0.09	0.08	-0.812	0.036
0.1%	98 ± 1.5	1.5 ± 0.02	10.54 ± 0.09	0.07	-0.580	0.042
0.2%	100 ± 1.2	3.0 ± 0.03	10.84 ± 0.11	0.05	-0.789	0.041

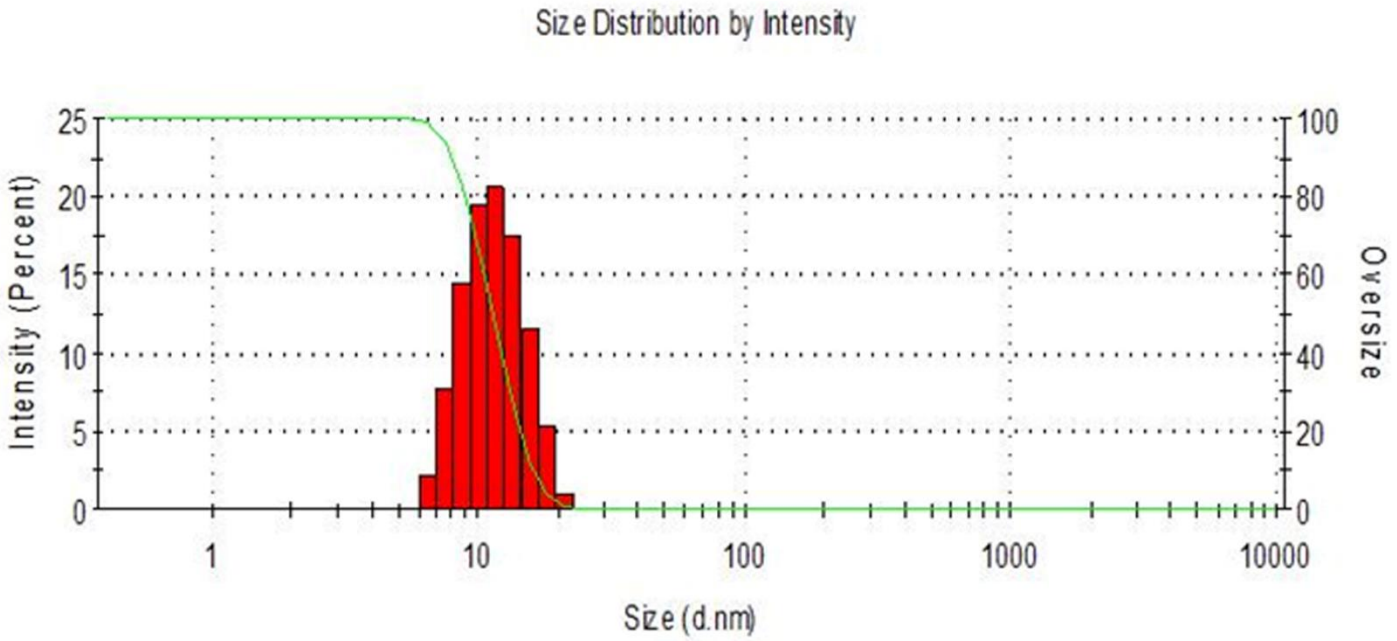

(A) Nanomicellar size distribution for placebo NMF.

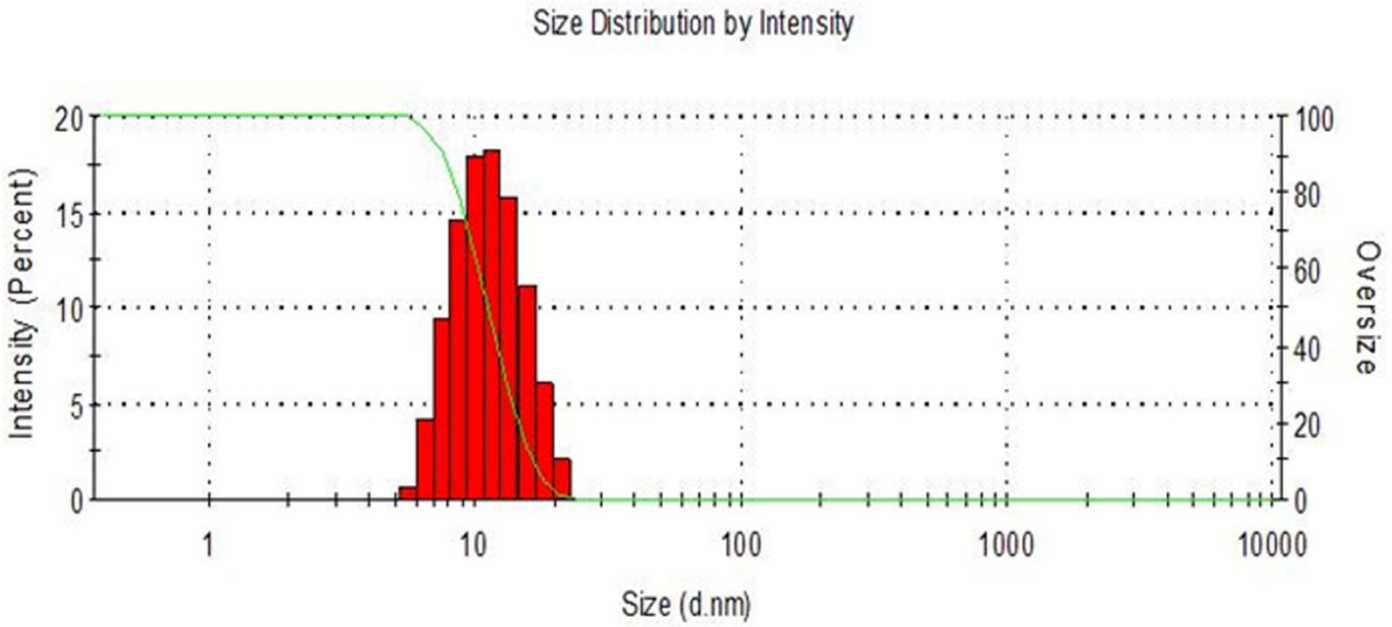

(B) Nanomicellar size distribution for 0.2% rapamycin loaded MNF

Figure 58. Nanomicellar size distribution for (A) placebo and (B) 0.2% rapamycin loaded NMF.

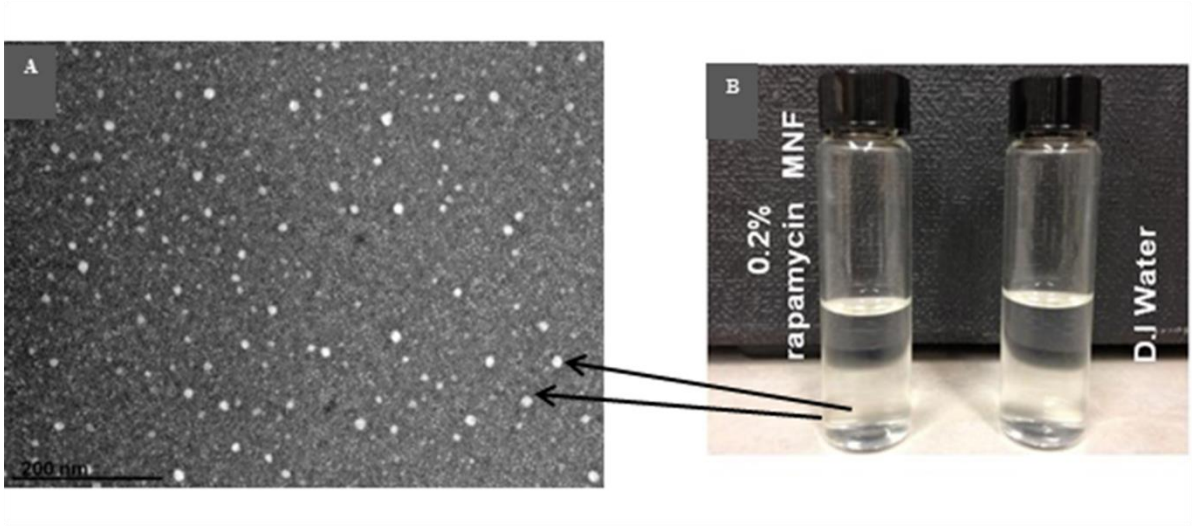

Figure 59. (A) Real time Scanning Transmission Electron Microscope (STEM) image of 0.2% rapamycin loaded nanomicellar formulation (x147,000). Scale bar 200 nm. (B) Image showing visual appearance 0.2% rapamycin loaded NMF on left side in comparison to water on right side.

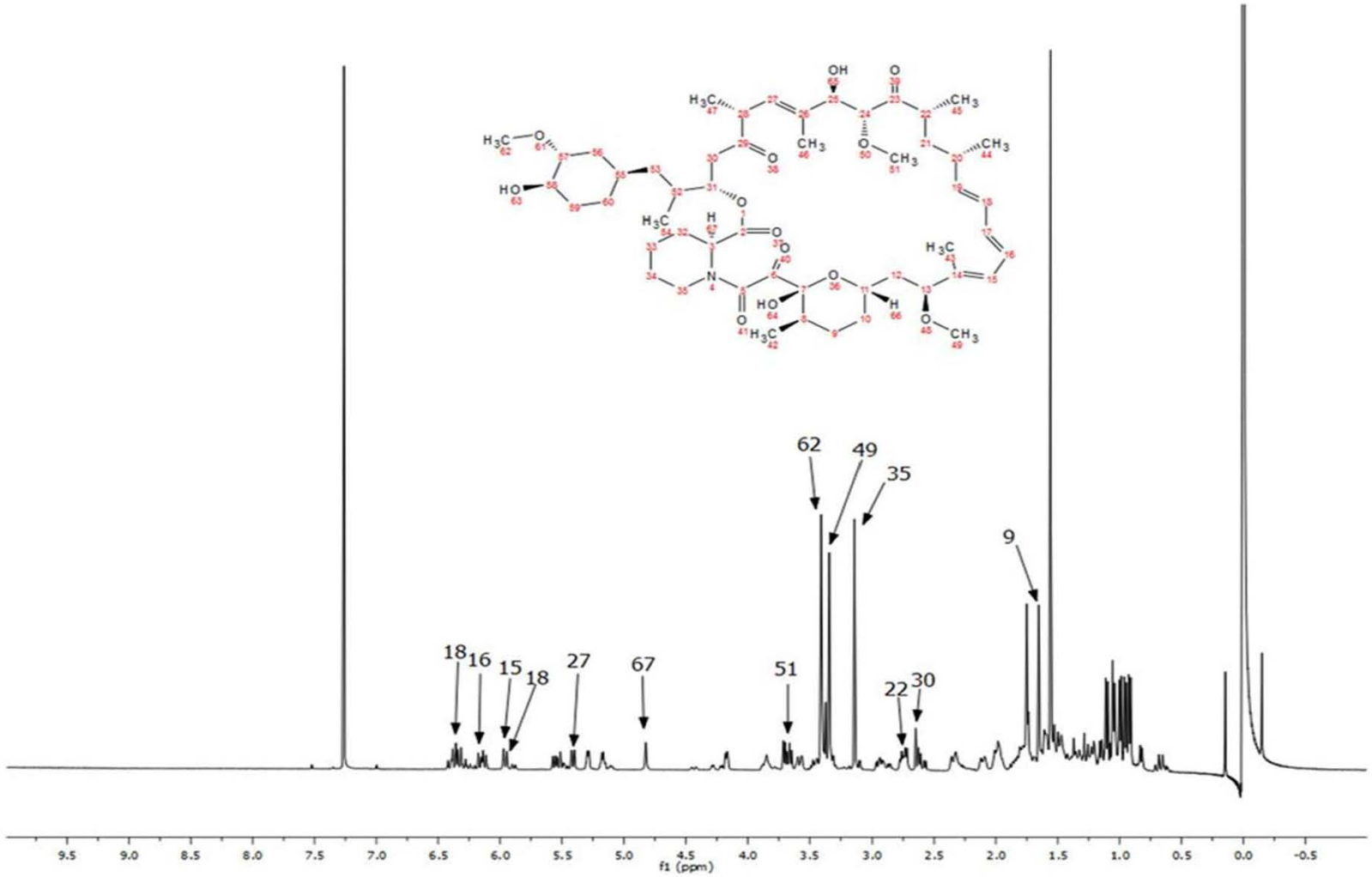

Figure 60. ^{1}H NMR spectral studies; ^{1}H NMR for pure rapamycin in $CDCl_3$

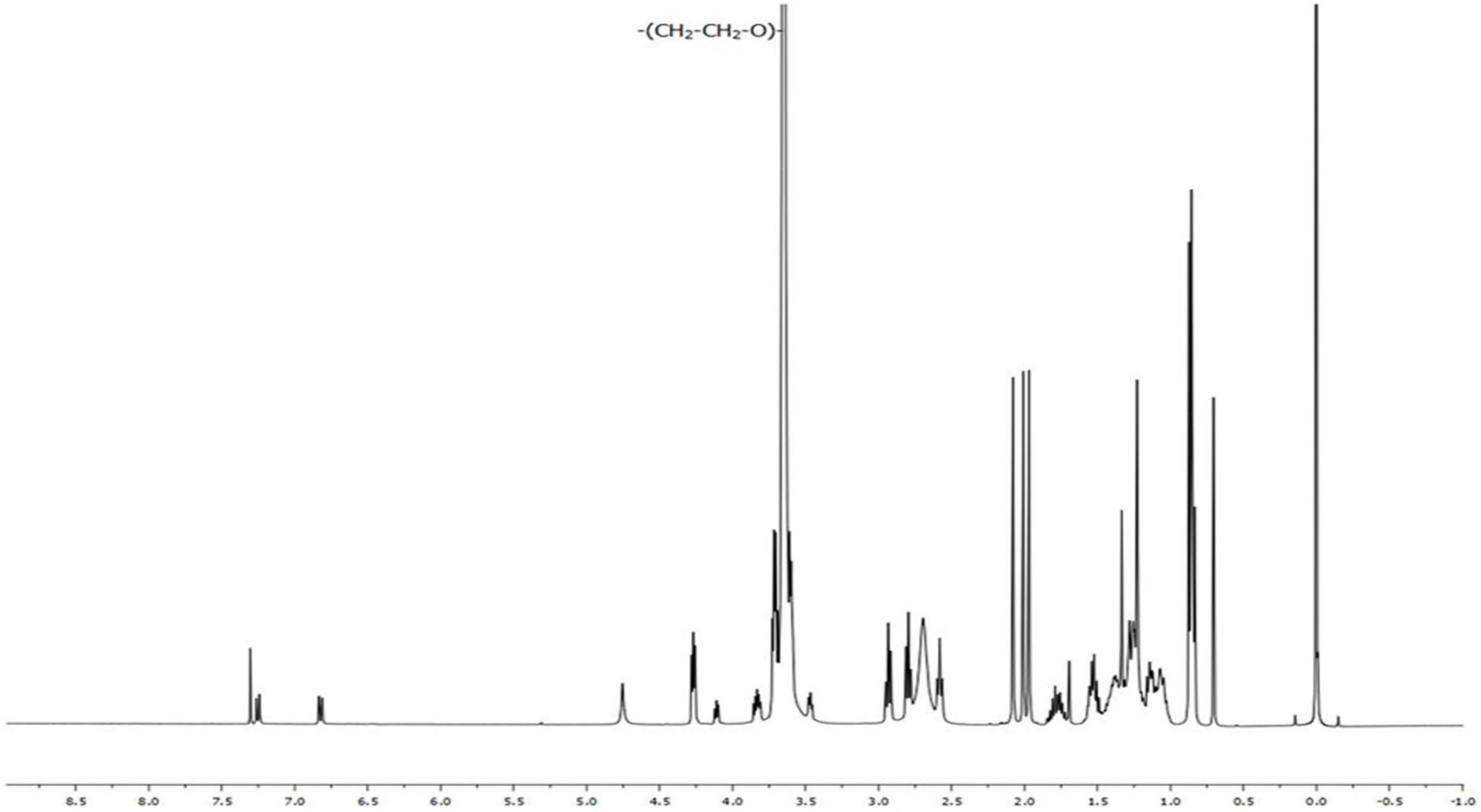

Figure 61. ^{1}H NMR for placebo nanomicelles in $CDCl_3$.

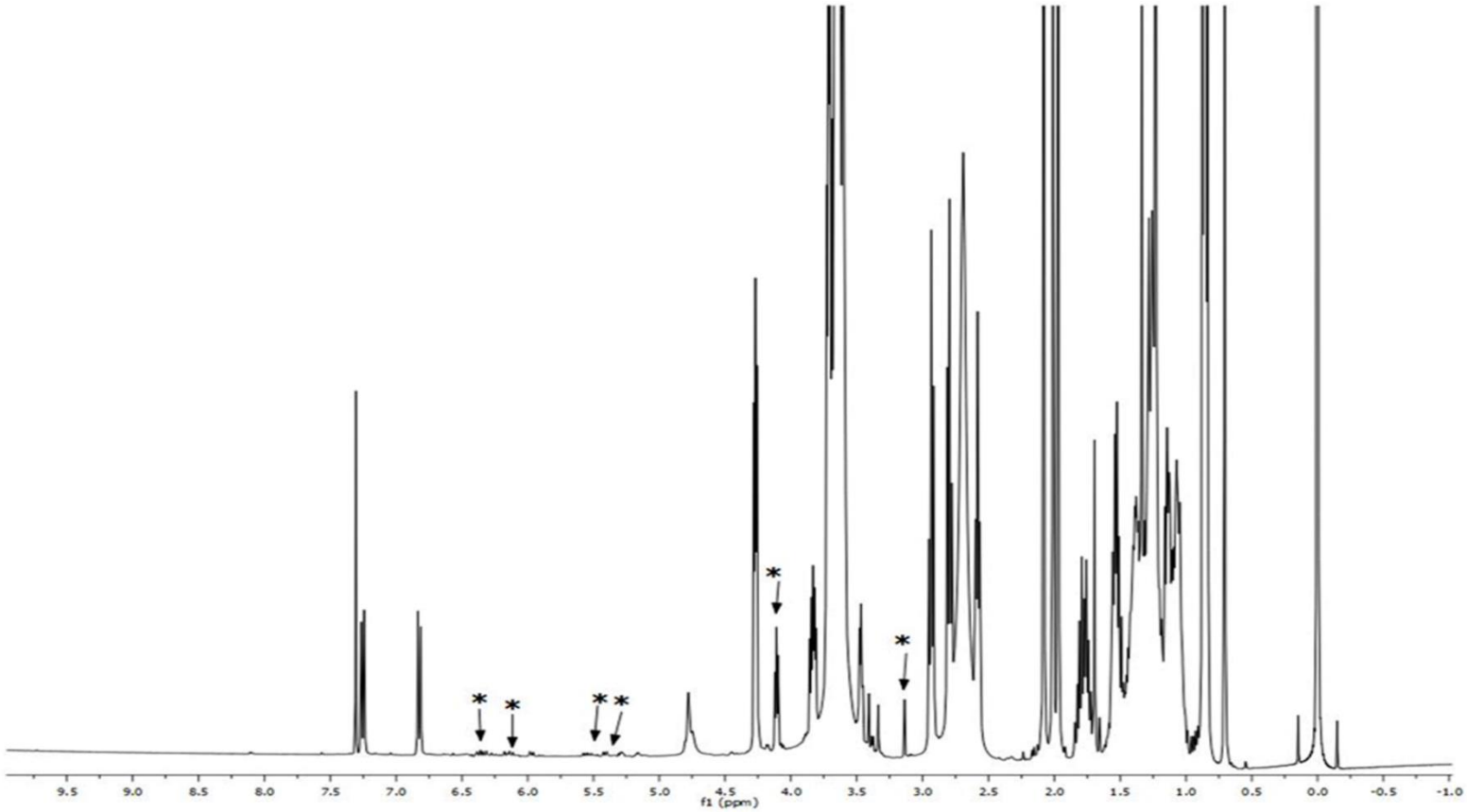

Figure 62. ^{1}H NMR for rapamycin loaded nanomicelles in $CDCl_3$. The symbol "*" indicates rapamycin

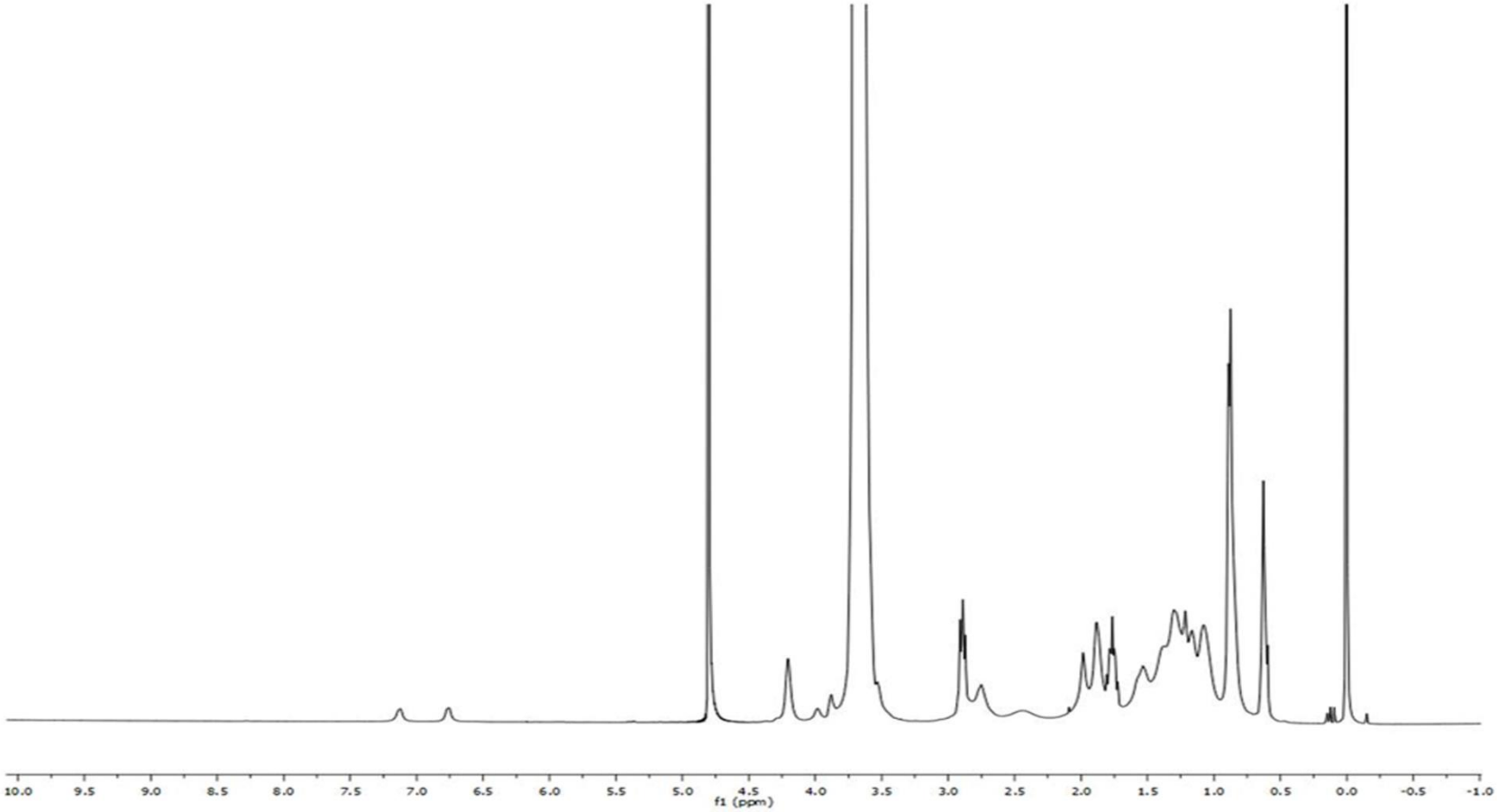

Figure 63. ^{1}H NMR for rapamycin loaded nanomicelles in deuterated water (D_2O).

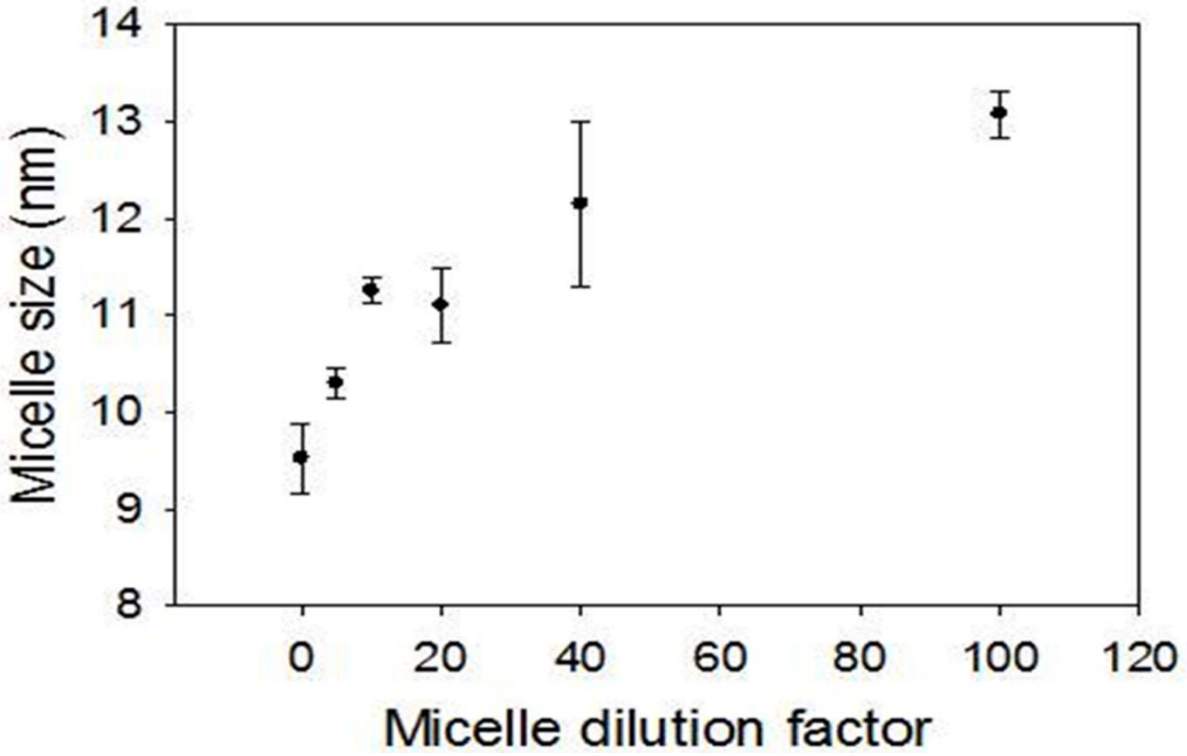

Figure 64. Effect of dilution on nanomicellar size.

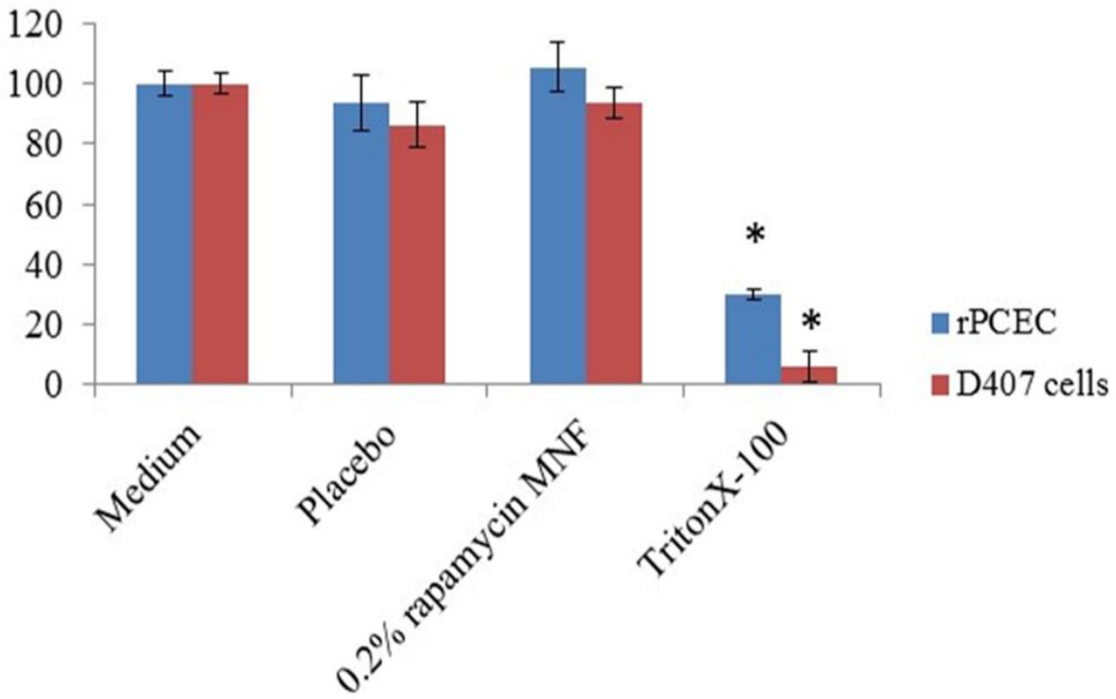

Figure 65. Cell proliferation assay demonstrating percent cell viability for blank and 0.2% rapamycin NMF on rPCEC and D407 cells after 1h exposure time. Triton-X 100 (10%) is positive control and culture medium is negative control. Data are shown as mean ± S.E.M (n = 4). *$p < 0.05$ versus control (paired t-test).

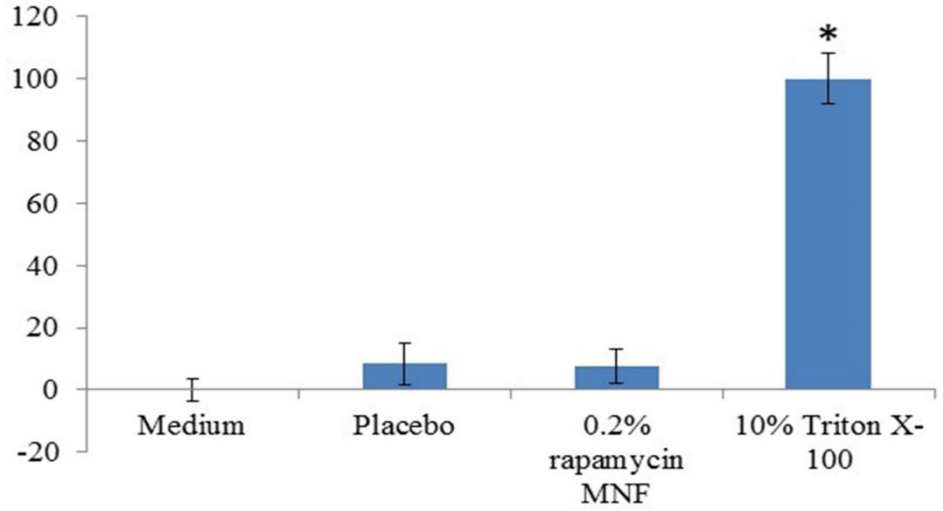

Figure 66. LDH assay results for placebo and 0.2% rapamycin NMF on rPCEC cells indicating negligible LDH release upon 2h NMF exposure. Triton-X 100 (10%) is positive control and culture medium is negative control. Data are shown as mean ± S.E.M (n = 4). *$p < 0.05$ versus control (paired t-test).

for NMF. Mean micelle increased with dilution without any significant impact. The reason may be attributed to decrease in concentration of monomers in the NMF with dilution (**Figure 64**). *In vitro* studies with MTT and LDH assay on rPCEC cells demonstrated to be safe and well-tolerated (**Figure 65** and **Figure 66**).

Bioanalytical Rapamycin Analysis

Specificity, selectivity, limit of quantification and linearity of calibration standards

Rapamycin and erythromycin (**Figure 67**) both were clearly extracted and separated from endogenous peaks originating from the blank matrix. The mass spectrums corresponding to rapamycin and erythromycin are provided in **Figure 68** and **Figure 69.** The total ion count spectrum is obtained for rapamycin and erythromycin (**Figure 70**). The assay condition had adequate specificity for rapamycin, while no interfering peaks were observed at its retention times as shown in **Figure 70** and **Figure 71**. Erythromycin was used as an IS in this method because it is readily available in our laboratory and has structural similarity. It is also economical compared to other drugs which were used as IS such as deuterated rapamycin (rapamycin 13Cd3), 27-demethoxy-sirolimus, 32-demethoxy rapamycin, tacrolimus and secomycin. However, it also shows consistent recovery and served our purpose of research. The lower limit of quantitation (LLOQ) for rapamycin was set to 2.3 ng/mL. Modifying mobile phase composition and column heater temperature have increased chromatographic resolution significantly. The chromatogram represents that the peak response of rapamycin was proportional to the concentration from LLOQ to ULOQ. In **Figure 72** and **Figure 73,** we have

shown one of the best illustrations of an extracted chromatogram at both the LLOQ and ULOQ level with IS along with the extracted blank. The signal to noise ratio (S/N) of rapamycin was determined at LLOQ level, and it was greater than 50. The S/N ratio explains the extraction efficiency and capability that removes all interfering endogenous components which are usually present in the biological matrix.

Accuracy and Precision

The best linear fit and least-square residuals for the calibration curve were achieved with a $1/X_2$ weighing factor, giving a mean linear regression equation for the calibration curve. The assay was linear over the range 2.3 -1000 ng/mL with r^2 (n=6) $\geq$ 0.993 with a mean and standard deviation (s.d.). A regression equation for rapamycin, y = 0.0208(0.0016) x + 0.0043(0.0073) was obtained. Inter-and intra-day performance of validation quality control results are summarized in **Table 24**, showing both accuracy and precision for the drug concentrations of 2.3 to 800 ng/mL. The lower limit of quantitation (LLOQ) with inter-day coefficients of variation ranged between 0.3–17.2% for cornea, iris ciliary body, lens, aqueous humor, sclera, vitreous humor, and retina choroid as shown in **Table 24**. The regression constant describes the relationship between expected results and analyzed results and was linear, $r^2 \geq 0.9998$ for rapamycin, in the entire tissue matrix (**Table 24**). **Figure 72** and **Figure 73** represents an example of extracted validation quality control of LLOQQC (2.5 ng/mL), LQC (10 ng/mL), MQC (480 ng/mL) and HQC (800 ng/mL) chromatogram peak responses in ocular matrix. The

chromatogram result explains the methods robustness and accuracy. **Figure 72** and **Figure 73** shows the correlation of results for all the tissue homogenates derived by the method. **Figure 70** and **Figure 71** MRM chromatogram demonstrates the total ion (TIC) counts and extracted ion (XIC) counts in positive mode. These figures have shown the peak response with two different transitions (i) with the same retention times for rapamycin and erythromycin but with varying response.

Mass spectrometry characterization MS/MS

Most reported LC-MS/MS methods have used ammonium acetate or formate buffers in the mobile phase system. Eventually, ammonium adducts of rapamycin were selected for analysis. Usually, ammoniated buffer mobile phase systems will enhance ionization of analytes, but at the same time which may generally clog the peak tubes, pump seals, and rapamycin might also degrade faster at high buffer concentrations at pH 7.4. Therefore, we optimized rapamycin with a sodium adduct $[M+Na]^+$ in positive ion mode in a formic acid mobile phase system. Formic acid containing mobile phase mixtures has the advantage that they never clog the peak tubes and the seals.

The instrument parameters were determined monthly on a routine basis as per our in-house protocol by calibration with polypropylene glycol standards as recommended by the manufacturer. The orifice voltage was adjusted to obtain maximum signal intensity and CAD experiments were carried out after obtaining maximum signal intensity using the orifice voltage as described in the experiment section before. High pure liquid nitrogen gas was employed as CAD and collision

gas with the collision energy. Molecular ion full-scan spectrums were acquired for both the rapamycin and erythromycin in positive ion mode as shown in **Figure 68** and **Figure 69**. The MS2 spectrum with sodium adducts were also matched with the previously reported method (349). The two most abundant fragment ions $[M+Na]^+$ m/z at 409.3 and 345.3 were selected for MRM analysis. In which, the m/z 936.3→409.3 transition has shown higher intensity and reproducible results than the 936.3→345.5 ion pair. Eventually, the 936.3→409.3 ion was selected for entire MRM quantitative analysis as shown in **Figure 70**. Earlier reports also described how rapamycin sodium adduct $[M+Na]^+$ show relatively greater response than the proton adduct$[M+H]^+$ in positive mode with the electrospray ionization (350, 351). We also observed that sodium adducts of rapamycin has exhibited minimal matrix effect with the optimal response in all the ocular tissue matrices. Transition pairs were selected for erythromycin in which 734.4→158.5 have higher intensity than 734.4→576.5 in MRM **Figure 70**.

Recovery

Recovery of rapamycin was high and reproducible in this extraction method. Several extraction techniques such as protein precipitation, liquid–liquid extraction and its combination of procedures with different solvent and solvent systems such as ethyl acetate, methyl (t)-butyl ether (MTBE), dichloromethane, chloroform, cyclohexane, hexane, ether, ethanol, 2-propanol, perchloric acid, triethylamine, acetonitrile and methanol were tested. All the tissue proteins were precipitated with

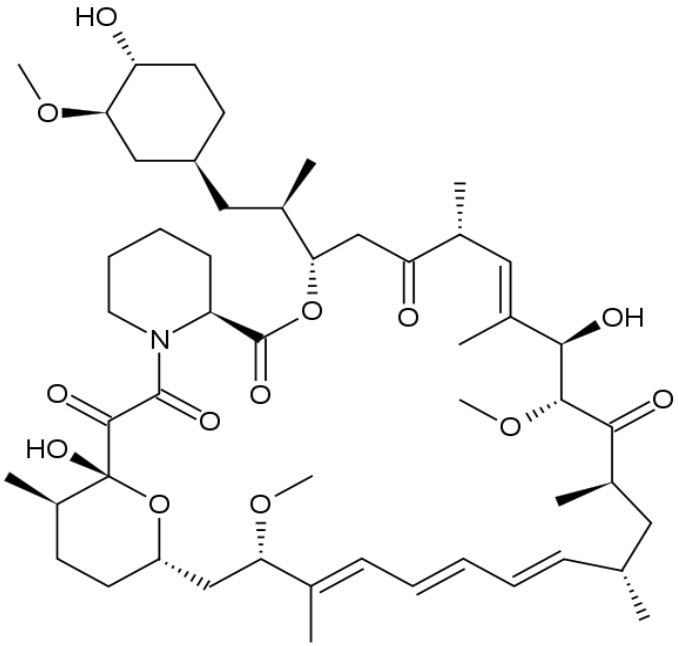

Rapamycin (sirolimus)
Formula: $C_{51}H_{79}NO_{13}$
Mol. Mass: 914.172 g/mol

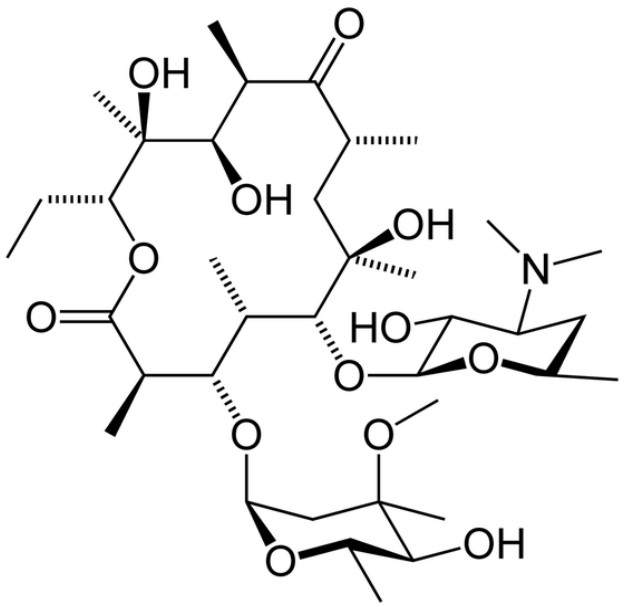

Erythromycin
Formula: $C_{37}H_{67}NO_{13}$
Mol. Mass:733.93 g/mol

Figure 67. Chemical structures, formulas and molecular masses of rapamycin and erythromycin.

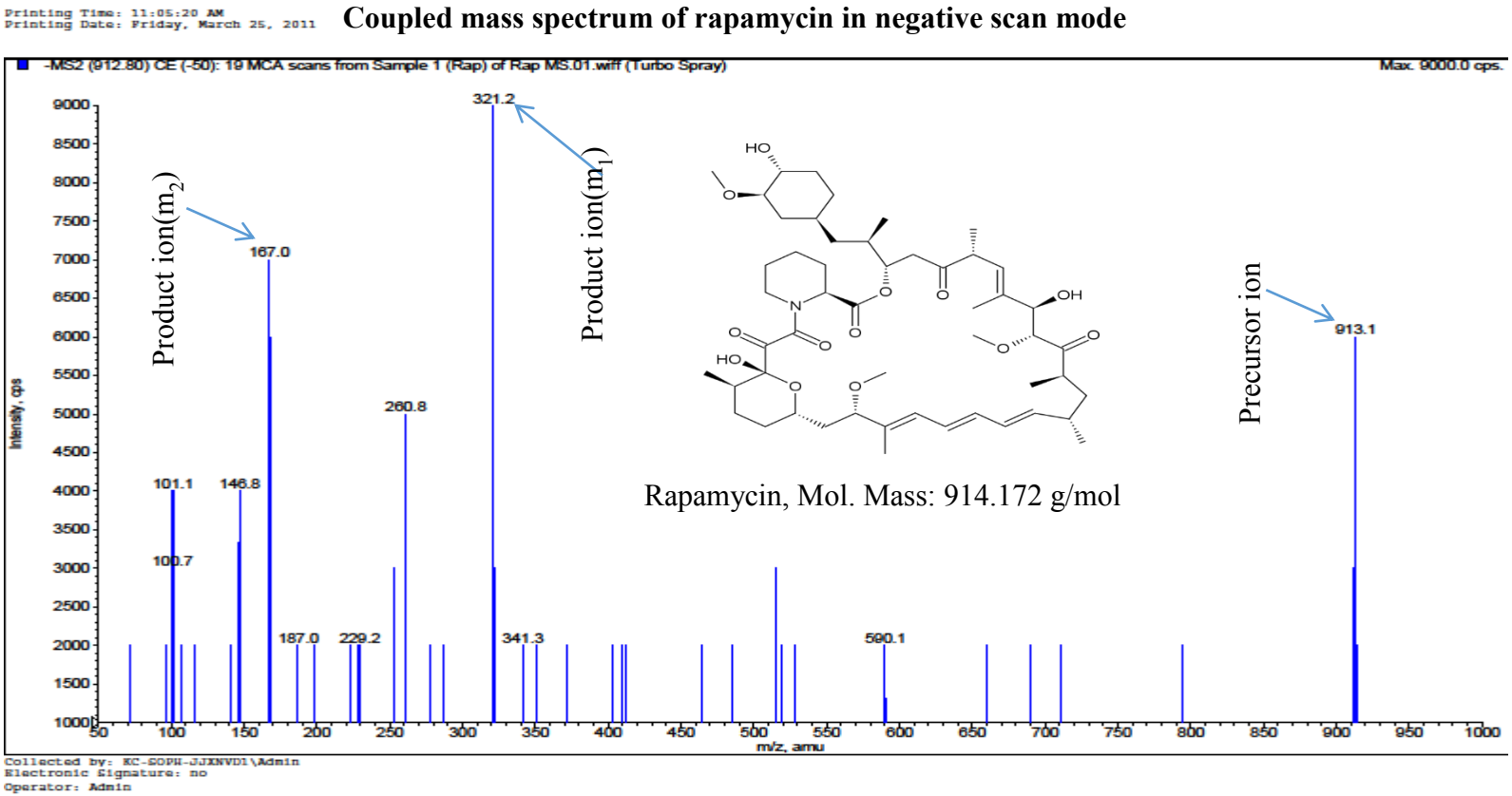

Figure 68. Coupled mass spectrum of rapamycin in electrospray ionization (ESI) positive scan mode with sodium adduct, precursor ion *mass* to *charge* ration (*m/z*) $[M + Na]^+$: 936.6 Da, product ions *m/z* (m1) 409.3 and (m2) 345.3 Da

Coupled mass spectrum of erythromycin in positive scan mode

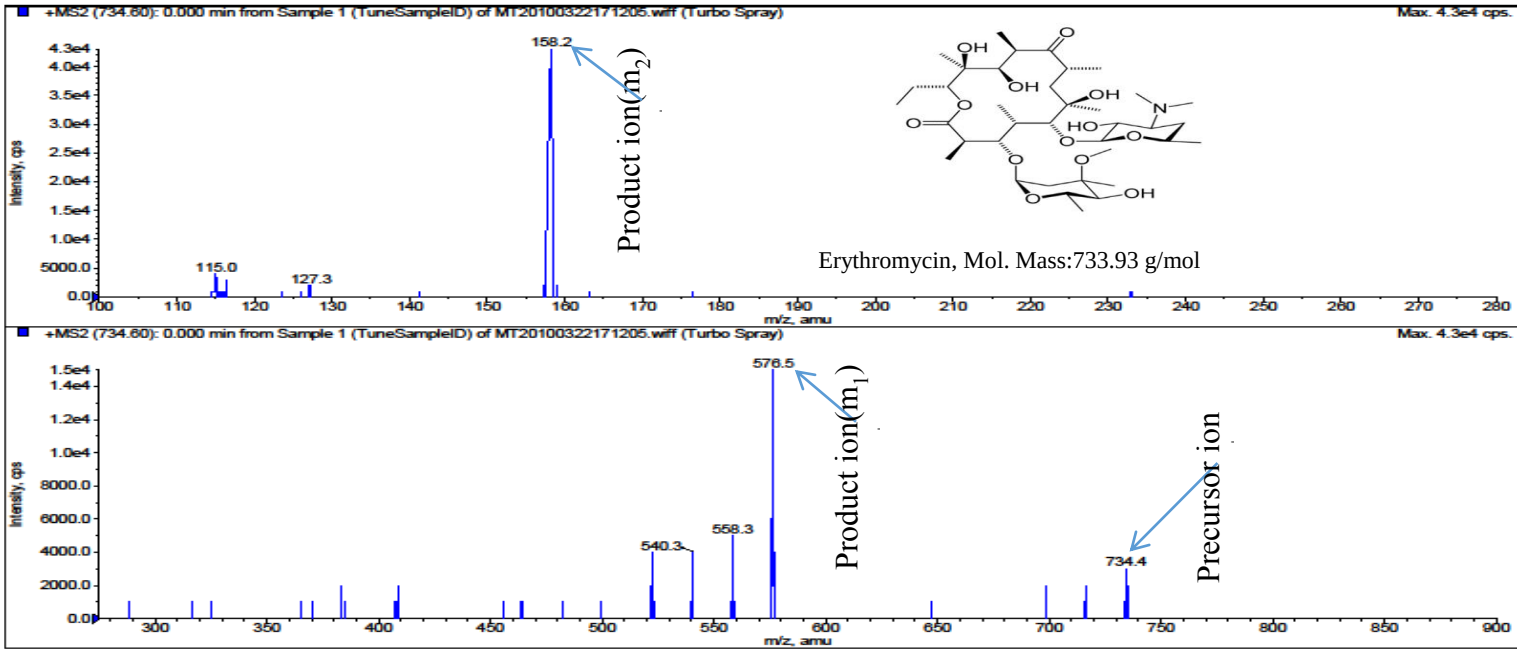

Figure 69. Coupled mass spectrum of erythromycin in Electrospray Ionization (ESI) positive scan mode with proton adduct, precursor ion *mass* to *charge* ration (*m/z*) $[M-H]^-$: 734.4, product ion *m/z* (m1) 576.3 and (m2) 158.2 Da.

Total ion counts (XIC) of positive MRM Chromatograms

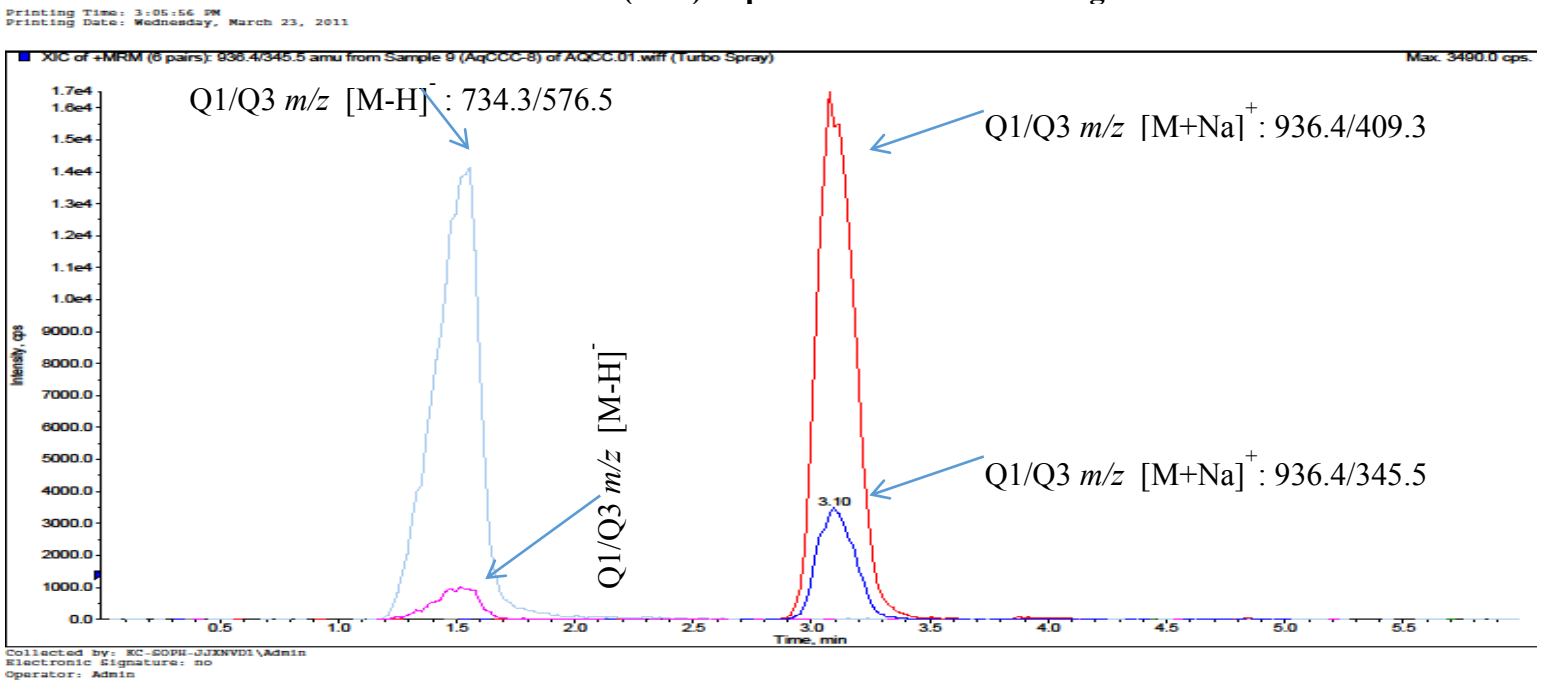

Figure 70. Total ion count (XIC) of positive scan MRM chromatograms of rapamycin with precursor ion $[M + Na]^+$ product ion (m1) Q1/Q3 *m/z* : 936.6/409.3 and precursor ion $[M + Na]^+$ product ion (m2) Q1/Q3 *m/z* : 936.6/345.3 (right side peaks at retention time 3.1 min), Erythromycin with precursor ion $[M + H]^+$ product ion (m1) Q1/Q3 *m/z* : 734.4 /576.3 and precursor ion $[M +H]^+$ product ion (m2) Q1/Q3 *m/z* : 734.4 /158.2 (left side peaks at retention time 1.5 min) in ocular matrix.

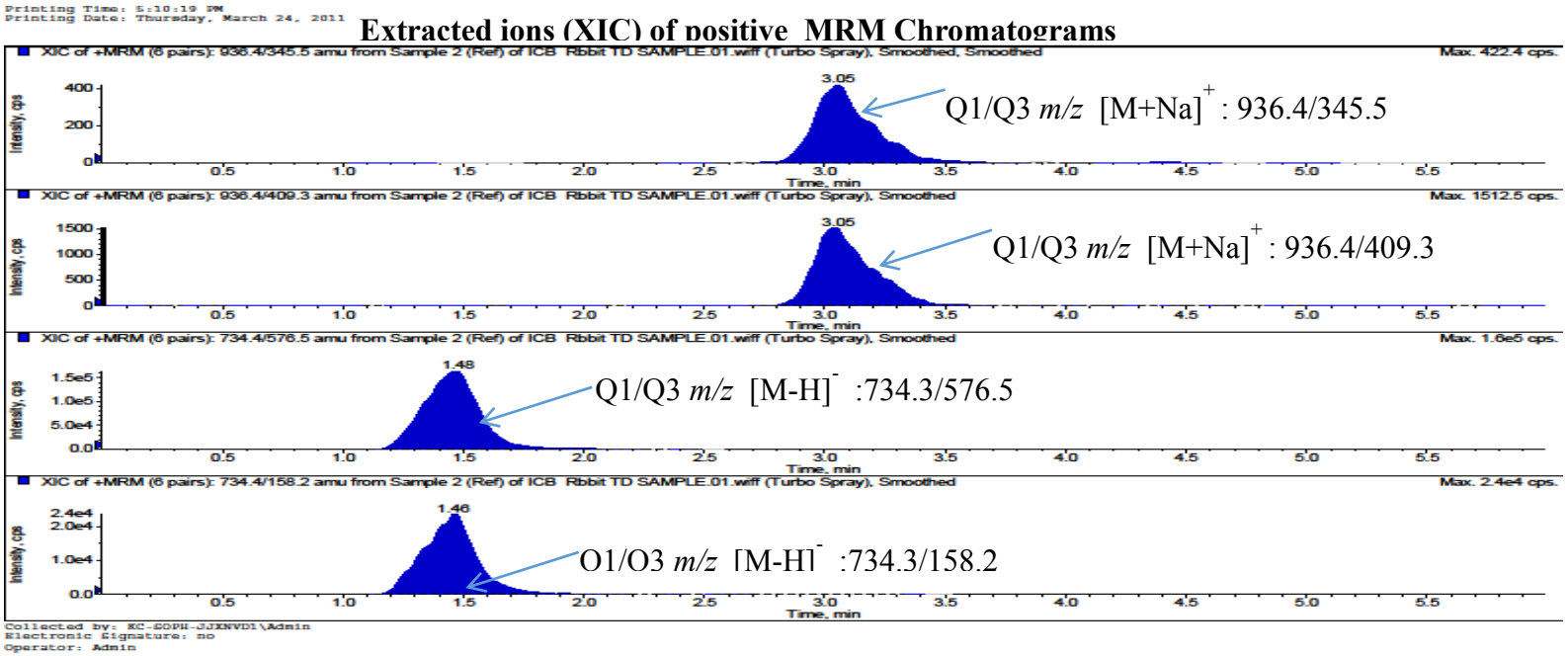

Figure 71. Extracted ion count (XIC) of positive scan MRM chromatograms of rapamycin with precursor ion $[M + Na]^+$ product ion (m1) Q1/Q3 *m/z* : 936.6/409.3 and precursor ion $[M + Na]^+$ product ion (m2) Q1/Q3 *m/z* : 936.6/345.3 (top two columns); Erythromycin with precursor ion [M +H]+ product ion (m1) Q1/Q3 *m/z* : 734.4 /576.3 and precursor ion $[M +H]^+$ product ion (m2)Q1/Q3 *m/z* : 734.4 /158.2 (bottom two columns)

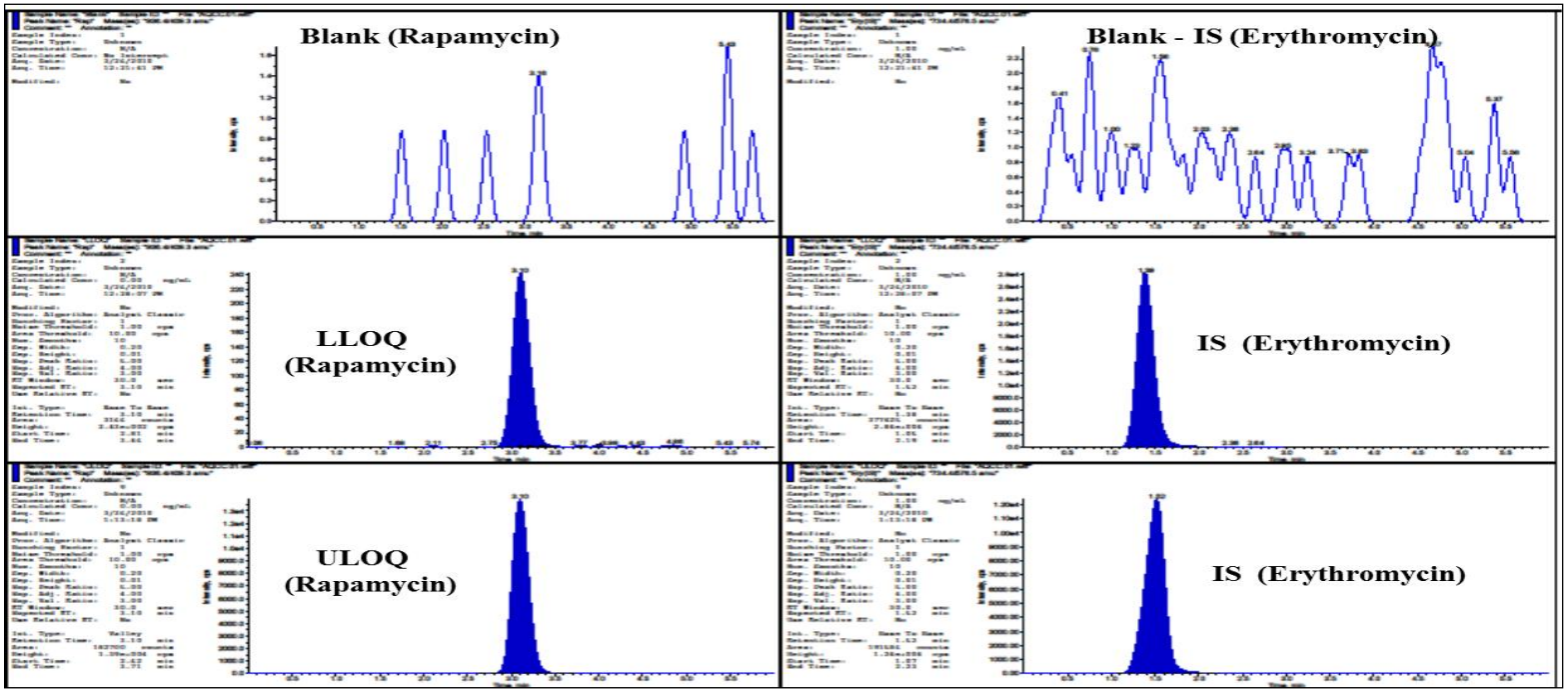

Figure 72. Integration algorithmic typical MRM chromatograms for selected extracted samples at lower and upper limit of quantitation (LLOQ and ULOQ) with IS. It shows endogenous peak in extracted blank sample (top). *Signal to noise ratio* (S/N) for rapamycin peak at LLOQ level was greater than 50. LLOQ, (2.3 ng/mL), and ULOQ, 800.0 ng/mL) in the left column from top to bottom, erythromycin as an internal standard (IS) blank, at LLOQ level and ULOQ level in the right column from top to bottom in ocular matrix.

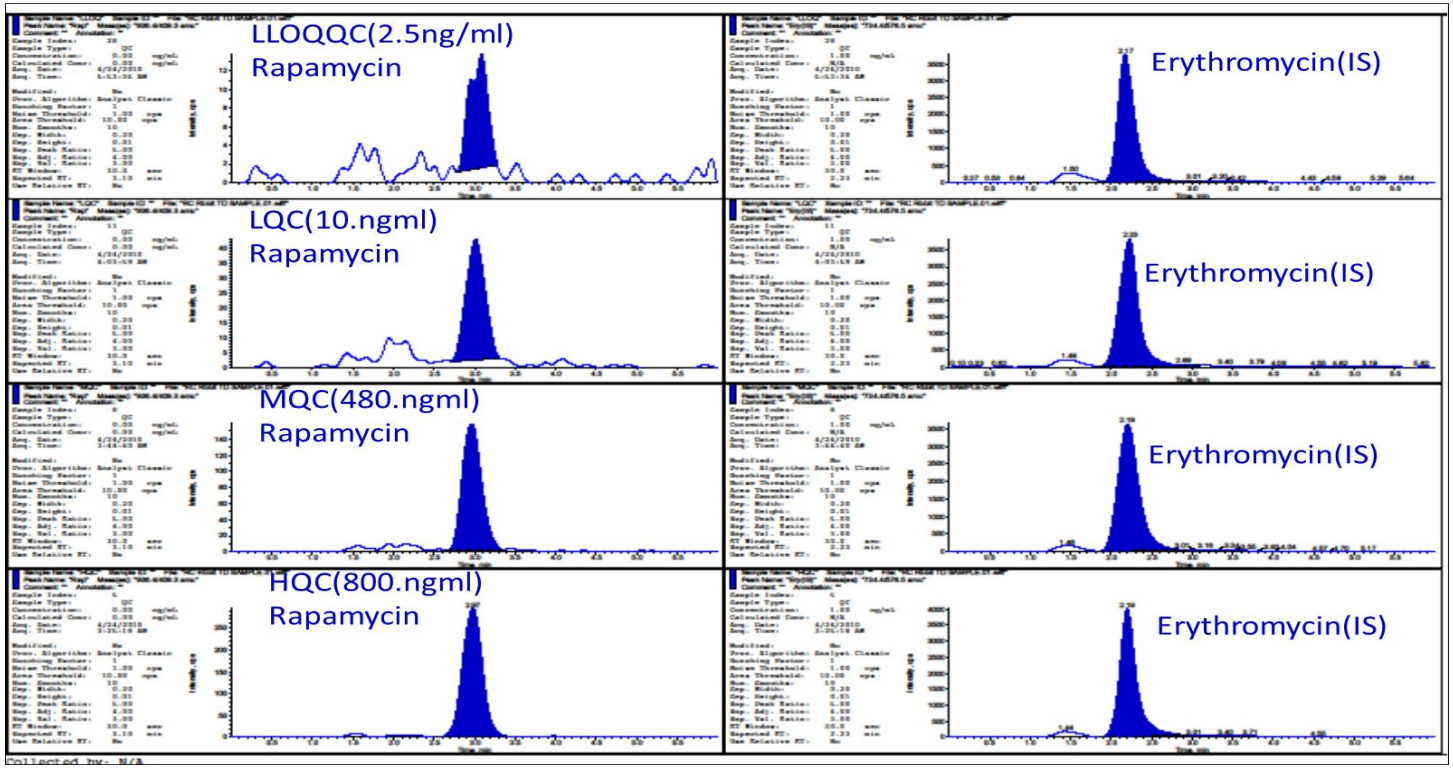

Figure 73. A typical example of extracted LLOQ (2.3 ng/ml), Low QC (10 ng/mL), middle QC (480 ng/mL) and high QC (800 ng/ml) Rapamycin (analyte) (*m/z*) $[M+Na]^+$: 936.6/409.3, Erythromycin (internal standard) : (*m/z*) $[M+H]^+$ 734.4/576.5 MRM quantitation chromatograms in ocular tissue matrices.

Table 24. Ocular tissue homogenate validation results , quality control each (n = 6 of 1 of 3 batches)

	Lower limit of quality control (2.3 ng/mL)	Low quality control (10 ng/mL)	Middle quality control (480 ng/mL)	High quality control (800 ng/mL)
		Cornea		
Mean concentration (ng/mL)	2.1	10.7	499.0	829.0
Inter run % CV	10.3	8.5	5.7	1.8
Inter run % Bias	-10.9	6.8	3.9	3.6
		Iris Ciliary Body		
Mean concentration (ng/mL)	2.0	10.3	472	847
Inter run % CV	10.9	3.8	2.0	2.8
Inter run % Bias	-15.2	2.9	-1.6	5.9

	Lower limit of quality control (2.3 ng/mL)	Low quality control (10 ng/mL)	Middle quality control (480 ng/mL)	High quality control (800 ng/mL)
			Lens	
Mean concentration (ng/mL)	2.1	9.8	562	807
Inter run % CV	17.2	7.9	1.0	4.0
Inter run % Bias	-10.9	-2.2	-3.7	0.9
			Aqueous humor	
Mean concentration (ng/mL)	2.0	10.3	495	824
Inter run % CV	7.1	4.0	4.6	3.0
Inter run % Bias	-13.0	2.8	3.1	3.0

	Lower limit of quality control (2.3 ng/mL)	Low quality control (10 ng/mL)	Middle quality control (480 ng/mL)	High quality control (800 ng/mL)
			Sclera	
Mean concentration (ng/mL)	2.2	9.7	432.1	797.4
Inter run % CV	9.9	8.2	10.9	2.3
Inter run % Bias	-6.5	-3.3	-10.0	-0.3
			Vitreous humor	
Mean concentration (ng/mL)	2.6	10.2	452	825
Inter run % CV	0.0	11	17	2.6
Inter run % Bias	13.0	2.4	-5.8	3.2

	Lower limit of quality control (2.3 ng/mL)	Low quality control (10 ng/mL)	Middle quality control (480 ng/mL)	High quality control (800 ng/mL)
			Retina-Choroid	
Mean concentration (ng/mL)	2.4	9.5	410	840
Inter run % CV	15.0	14.0	3.7	0.0
Inter run % Bias	2.2	-4.9	-14.7	5.0

the methanol, and triethylamine digested all the tissues and broke their integrity. By using this procedure we got the highest recovery of rapamycin. Mean recovery of rapamycin was found between 85-90% for the cornea, 89-91% for iris ciliary body, 81-93% for lens, 78-87% for aqueous humor, 82-93% for vitreous humor 81-94% for sclera and 86-90% for retina-choroid at LQC, MQC and HQC levels.

Matrix effect

Ion suppression expresses the matrix effect on ionization of analytes of interest. Usually, most results obtained from LC-MS/MS analysis are inconsistent because of ineffective sample preparation and extraction techniques. These problems may be overcome by modifying the sample extraction procedure (352). Liquid–liquid and solid-phase extraction are generally the most effective approach, but they are expensive and laborious. The elimination of undesirable water soluble compounds, including non-volatile materials like phosphates and sulfates are important in electro spray ionization. Reconstitution solution also plays a key role in ionization of analytes. Six replicates of LLOQ were processed and tested for its matrix effect. Found the ionization and peak response was increased when it was reconstituted in acetonitrile: water: formic acid mixture (80:20:0.05) compared to other reconstitution solutions such as acetonitrile, methanol and its mixtures. In this technique, triethylamine and methanol were able to generate clear and clean samples from the water-soluble compounds, such as phosphates and zinc sulfates. The zinc sulfate and phosphate were inhibiting the ionization of analytes during the

ESI (353, 354). The percentage of matrix was found 16%, 20 % and 26 % at HQC, MQC, and LQC levels, respectively.

Stability evaluation in ocular matrices

All stability experiments, linear regression, correlation coefficients with calibration curve and QC standards are presented in **Table 25** and **Table 26**. Accuracy and precision results of each stability experiment are also given in **Table 26**. Rapamycin was stable for three freeze-thaw cycles at -80 ^{o}C and six weeks at freezer storage temperature in all tissue homogenates. It was also stable for four hours on bench top at 25 ^{o}C 2 days for in-injector storage, and 15 days for post extracted storage at -80 ^{o}C. All the stability results of anterior and posterior tissue are presented in **Table 24**.

Quantitative determination of rapamycin in ocular homogenate

For an LC-MS/MS analysis, extraction procedure, pH, and reconstitution solvent are important parameters to obtain better chromatographic separation, reproducible and reliable results. Rapamycin was estimated in the anterior eye tissues such as cornea, lens, iris ciliary body and aqueous humor. The calibration curve accuracy and precision, retention times and linearity results of individual eye tissues are displayed in the **Table 26**.

Sample analysis of tissue distribution study in the rabbit eye

Rapamycin was measured in ocular tissues post 1hour of topical administration of 0.2% rapamycin nanomicellar formulation. Rapamycin was

found to be at 2260 ± 500 ng/g tissues in the cornea, and 585 ± 80 ng/g tissues in the iris ciliary body. Rapamycin concentration found by mass spectrometry analysis in the cornea, lens, and iris ciliary muscle was normalized with the volume (500 μL) used for homogenization and tissue (approx. 0.11 g) weight. In the lens and aqueous humor, rapamycin was found to be below the limit of quantitation (i.e. < 2.3 ng/mg protein). The results of rapamycin distribution in the eye tissues and fluids are shown in **Table 27**. The distribution coefficient between hydrophilic and lipophilic phases is also important for estimation of drug distribution in the eye. Rapamycin is practically insoluble in water (2.6 μg/mL), and has a high molecular weight (MW 914 Da) because it's more hydrophobic in nature. It contains no functional groups that are ionizable at pH range between 1 and 10 that easily penetrate the tissue (337).

Discussion

Rapamycin is a small molecule with poor aqueous solubility (2.6 μg/mL) (337). In the present study, we selected a blend of two FDA approved polymers (Vit. E TPGS and Oc-40) to entrap rapamycin into nanomicelles to improve its solubility. A weight percent ratio of 4.5:2.0 for Vit. E TPGS and Oc-40 was selected due to their low critical micellar concentration (CMC) value of 0.012 wt% relative to individual polymers (Vit. E TPGS (0.025%) and Oc-40 (0.107 wt%)) (278). Low CMC of this polymeric mixture allows to improve stability of NMF. We successfully prepared 0.1% and 0.2% rapamycin loaded NMFs with a blend of Vit. E TPGS/Oc-40 (4.5:2.0) in phosphate buffer. Although, rapamycin solubility was

Table 25. Ocular tissue homogenate stability results in anterior and posterior eye tissues

Nominal concentration (ng/mL)	**Cornea**		**Iris ciliary body**		**Lens**	
	LQC	HQC	LQC	HQC	LQC	HQC
	10	800	10	800	10	800
Freeze storage for 6 weeks at (−80 °C)						
Mean calculated concentration (ng/mL)	10.3	768	9.4	756	8.9	843
CV (%)	4.9	4	9.6	11.8	13.5	1.5
Bias(%)	2.9	−4.2	−6.4	−5.8	−12.4	5.1
Freeze thaw (−80 °C) stability (3 cycles)						
Mean calculated concentration (ng/mL)	9.2	876	9.1	698	8.9	856
CV (%)	5.4	3.5	9.9	12.8	13.5	1.5
Bias (%)	−8.7	8.7	−9.9	−14.6	−12.4	6.5
Autosampler in injector storage stability (2 days)						
Mean calculated concentration (ng/mL)	8.9	708	8.8	876	11.1	893
CV (%)	5.6	4.3	10.2	10.2	10.8	1.4
Bias (%)	−12.4	−13.0	−13.6	8.7	9.9	10.4
Post extracted samples storage stability (15 days) at (−80 °C)						
Mean calculated concentration (ng/mL)	8.5	850.9	9.1	688	8.4	890
CV (%)	5.9	3.6	9.9	12.9	14.3	1.4

Nominal concentration (ng/mL)	Cornea		Iris ciliary body		Lens	
Bias (%)	−17.6	6	−9.9	−16.3	−19.0	10.1
Bench top stability (4 h) at 25 °C						
Mean calculated concentration (ng/mL)	8.6	879	8.9	765	9.9	901
CV (%)	5.8	3.5	10.1	11.6	12.1	1.4
Bias (%)	−16.3	9	−12.4	−4.6	−1.0	11.2

Posterior chamber eye tissues

	Aqueous humor		Sclera		Vitreous humor		Retina-Choroid	
	LQC	HQC	LQC	HQC	LQC	HQC	LQC	HQC
Nominal Concentration (ng/mL)	10	800	10	800	10	800	10	800
Freeze storage for 6 weeks at (−80 °C)								
Mean calculated concentration (ng/mL)	9.7	867	9.1	679	9.3	847	11.2	893
CV (%)	4.9	2.7	9.4	11.8	13.5	1.5	16.5	2.9
Bias (%)	−3.1	7.7	−9.9	−17.8	−7.5	5.5	10.7	10.4
Freeze thaw (−80 °C) stability (3 cycles)								
Mean calculated concentration (ng/mL)	8.9	908	9.1	809	10.2	870	11	805
CV (%)	5.6	2.3	9.9	11	11.8	1.4	15.5	2.8
Bias (%)	12.4	11.9	−9.9	1.1	2	8	9.1	0.6

	Aqueous humor		Sclera		Vitreous humor		Retina-Choroid	
Autosampler in injector storage stability (2 days)								
Mean calculated concentration (ng/mL)	10.9	890	9.4	879	9.6	871	11.4	931
CV (%)	4.6	2.3	9.6	10.1	12.5	1.4	14.9	2.4
Bias (%)	8.3	10.1	−6.4	9	−4.2	8.2	12.3	14.1
Post extracted samples storage stability (15 days) at (−80 °C)								
Mean calculated concentration (ng/mL)	9.5	765	9.1	688	8.4	890	12.0	912
CV (%)	3.3	7.2	2.4	7.2	1.2	4.3	3.3	7.2
Bias (%)	−5.3	−4.6	−9.9	−16.3	−19.0	10.1	16.7	12.3
Bench top stability (4 h) at 25 °C								
Mean calculated concentration (ng/mL)	12	765	9.1	688	10.3	809	9.4	912
CV (%)	3.3	7.2	2.4	7.2	1.2	4.3	3.3	7.2
Bias (%)	16.7	−4.6	−9.9	−16.3	2.9	1.1	-6.4	12.3

Table 26. Table Anterior eye tissue sample analysis, calibration curve, and quality control (QC) standard (STD) results.

Name	Nominal conc .(ng/mL)	No. of replicate processed	No. of replicate injected	Retention time, min (mean , SD)	Calculated conc.(ng/mL) (Mean, SD)	(%) Accuracy	(%) Precision
			CORNEA				
Cornea STD-1	2.3	2	2	3.104, 0.016	1.9, 0.33	82.6	17.4
Cornea STD-2	10	2	2	3.017, 0.071	8.5, 1.37	85.0	16.1
Cornea STD-3	100	2	2	3.012, 0.019	91.5, 7.03	91.6	7.7
Cornea STD-4	250	2	2	3.018, 0.028	211.0, 26.0	85.6	12.7
Cornea STD-5	500	2	2	3.054, 0.047	432.9, 62.03	86.6	14.4
Cornea STD-6	750	2	2	3.030, 0.045	761.2, 123.0	101.5	16.2
Cornea STD-7	850	2	2	3.024, 0.036	801.0, 124.33	94.6	15.6
Cornea STD-8	1000	2	2	3.006, 0.011	899.9, 134.0	89.9	14.9
Cornea LLOQQC	2.3	4	8	3.024, 0.036	1.88, 0.24	81.6	12.8
Cornea LQC	10	4	8	3.016, 0.037	8.9, 1.31	89.0	14.7
Cornea MQC	480	4	8	3.022, 0.038	501.0, 71.33	104.3	14.2
Cornea HQC	800	4	8	3.041, 0.03	721.9, 81.33	90.1	7.4
Cornea 10 samples (mean± SD) = 2260.74 ± 507.11 ng/g of tissue , the value obtained by LC-MS/MS was normalized with the tissue volume(mL) and weight(g)							

Name	Nominal conc .(ng/mL)	No. of replicate processed	No. of replicate injected	Retention time, min (mean , SD)	Calculated conc.(ng/mL) (Mean, SD)	(%) Accuracy	(%) Precision
IRIS CILIARY MUSCLE							
Iris cilairy body STD-1	2.3	2	2	3.002, 0.017	2.7, 0.36	117.4	13.3
Iris cilairy body STD-2	10	2	2	3.000, 0.061	9.5, 0.90	95.0	9.5
Iris cilairy body STD-3	100	2	2	3.102, 0.016	101.5, 5.6	101.5	5.5
Iris cilairy body STD-4	250	2	2	2.995, 0.005	267.0, 30.0	106.8	11.2
Iris cilairy body STD-5	500	2	2	3.007, 0.083	567.9, 32.03	113.6	5.6
Iris cilairy body STD-6	750	2	2	3.028, 0.043	679.2, 102.0	90.5	15.0
Iris cilairy body STD-7	850	2	2	3.012, 0.043	900.9, 125.0	105.6	13.9
Iris cilairy body STD-8	1000	2	2	3.022, 0.018	1100.0, 124.0	110.0	12.2
Iris cilairy body LLOQQC	2.3	4	8	3.024, 0.036	2.5, 0.21	108.7	8.4
Iris cilairy body LQC	10	4	8	2.989, 0.061	10.9, 1.31	110.0	11.9
Iris cilairy body MQC	480	4	8	2.992, 0.034	550.0, 71.00	114.3	12.2
Iris cilairy body HQC	1000			3.001, 0.01	908.0, 101.33	113.1	11.4

Iris cilairy body 10 samples (mean± SD) = 585.48 ±80.06 ng/g of tissue , the value obtained by LC-MS/MS was normalized with the tissue volume(mL) and weight(g)

Correlation coefficient equation (y=mx+c); coefficient of determination(r^2) =; Limit of quantitation (LOQ)= 2.3ng/mL ; Upper limit of quantitation (ULOQ)= 1000 ng/mL; LLOQQC= Lower LOQ quality control, LQC= Low QC, MQC= middle QC, HQC= high QC; STD= Standard

Name	Nominal conc .(ng/mL)	No. of replicate processed	No. of replicate injected	Retention time, min (mean , SD)	Calculated conc.(ng/mL) (Mean, SD)	(%) Accuracy	(%) Precision
AQUEOUS HUMOR							
Aqueous humor STD-1	2.3	2	2	32000,0.002	1.99, 0.22	86.5	11.1
Aqueous humor STD-2	10	2	2	3.042, 0.061	10.9, 0.80	109.0	7.3
Aqueous humor STD-3	100	2	2	3.012, 0.019	111.5, 10.60	111.5	9.5
Aqueous humor STD-4	250	2	2	3.018, 0.028	245.0, 12.0	98.0	4.9
Aqueous humor STD-5	500	2	2	3.024, 0.047	570.0, 23.03	114.0	4.0
Aqueous humor STD-6	750	2	2	3.031, 0.041	789.2, 102.0	105.5	12.9
Aqueous humor STD-7	850	2	2	3.024, 0.037	906.0, 111.00	106.6	12.3
Aqueous humor STD-8	1000	2	2	3.006, 0.011	1113.9, 104.0	111.3	12.1
Aqueous humor LLOQQC	2.3	4	8	3.004, 0.016	2.6, 0.32	89.0	10.1
Aqueous humor LQC	10	4	8	3.018, 0.039	8.9, 0.90	89.7	10.1
Aqueous humor MQC	480	4	8	3.032, 0.018	421.0, 2.60	87.3	0.6
Aqueous humor HQC	1000	4	8	3.045, 0.031	709.9, 65.00	88.6	9.2

Aqueous 10 samples (mean± SD) = Below limit of quantitation(BLOQ), the value obtained by LC-MS/MS was below limit of quantitation

Name	Nominal conc .(ng/mL)	No. of replicate processed	No. of replicate injected	Retention time, min (mean , SD)	Calculated conc.(ng/mL) (Mean, SD)	(%) Accuracy	(%) Precision
			LENS				
Lens STD-1	2.3	2	2	2.958,0.042	2.6, 0.11	113.0	4.2
Lens STD-2	10	2	2	2.958,0.048	9.9, 0.89	99.0	9.0
Lens STD-3	100	2	2	2.959, 0.014	114.0, 8.90	114.0	7.8
Lens STD-4	250	2	2	2.952, 0.023	230.0, 11.0	92.0	4.7
Lens STD-5	500	2	2	2.956, 0.024	532.0, 20.03	106.2	3.8
Lens STD-6	750	2	2	2.979, 0.016	700.2, 103.0	93.3	14.7
Lens STD-7	850	2	2	2.969, 0.055	768.9, 102.33	90.6	13.3
Lens STD-8	1000	2	2	3.009, 0.058	1089.9, 112.0	108.9	10.3
Lens LLOQQC	2.3	4	8	2.986, 0.065	2.03, 0.30	88.3	114.8
Lens LQC	10	4	8	2.949, 0.036	9.9, 1.10	99.0	11.1
Lens MQC	480	4	8	2.966, 0.019	521.0, 2.40	108.5	0.5
Lens HQC	1000	4	8	2.984, 0.050	721.9, 81.33	113.6	7.8

Lens 10 samples (mean± SD) = Below limit of quantitation(BLOQ), the value obtained by LC-MS/MS was below limit of quantitation

Correlation coefficient equation (y=mx+c); coefficient of determination(r^2) =; Limit of quantitation (LOQ)= 2.3ng/mL ; Upper limit of quantitation (ULOQ)= 1000 ng/mL; LLOQQC= Lower LOQ quality control, LQC= Low QC, MQC= middle QC, HQC= high QC; STD= Standard

improved with aqueous NMF, but topical drop instillation of aqueous drop may not retain the formulation in the pre-corneal pocket for longer period of time. A large portion (>90 %) of the topically applied formulations is lost due to tear drainage, induced lacrimation and tear dilution. Reflex blinking and loss of excess drop instillation may lead to spill over. Therefore, to improve NMF retention in the pre-corneal pocket viscosity enhancer with bio-adhesive properties is advisable. In the current study, we selected povidone K 90 as a viscosity and bio-adhesive property enhancing agent.

Dilution stability studies

Upon topical drop instillation rapamycin loaded nanomicelles may be rapidly hydrated causing increase in particle size and release of drug. To study the effect of dilution on the NMF, samples were diluted from 0 to 100 times. The concentrations at these dilutions of the monomers are well above the CMC. In general, tears are produced at an average flow rate of 1.2 µL/min. Any excessive tear production upon NMF instillation should not have an impact on NMF size. Therefore, we examined the dilution effect on nanomicellar size up to 100 fold dilution (way above tear dilution that is expected *in vivo*). The results of this dilution study are shown in **Figure 64.** Mean micelle increased with dilution without any significant impact. The reason may be attributed to decrease in concentration of monomers in the NMF with dilution. Our results are similar to the earlier studies. Xu, et al. hypothesized that the outer hydrophilic polyethylene oxide segment would form large and loose complex clusters in aqueous solution (288).

These new larger aggregates developed during dilution exhibit thermodynamically reversible association. Hydrophobic effect and hydrogen bonding may force the outer hydrophilic segment to cluster in aqueous solution. Clustering of outer hydrophilic segments may be the reason for increase in micelle size increase with dilution. The same reason is applicable to our studies. Upon dilution polymer concentration is lowered which leads to slight increase in micellar size (288). The prepared nanomicelles in this study sustained the dilution effect on their size and demonstrated negligible effect upon dilution indicating high stability upon dilution.

Cytotoxicity studies

After topical ophthalmic drop instillation into pre-corneal pocket, the formulations/solutions are rapidly cleared (within 5 to 10 minutes) (14, 355). Therefore, to determine the cytotoxic effect of NMF upon long time exposure to ocular tissues, LDH and cell proliferation assay were performed for one and two hour exposure. It was assumed that a 1h incubation period would be sufficient to evaluate any toxicity. Percent rPCEC viable cells for 0.2% rapamycin NMFs were comparable to that of positive control (culture medium) (**Figure 65**). Triton-X 100 served as negative control which reduced the percent cell viability to ~30% and ~6% for rPCEC and D407 cells. In another set of studies, cell plasma membrane damage tests (LDH assay) were studied with rPCEC cells. The amount of LDH released in the culture media directly correlates with membrane damage and cytotoxicity. Triton-X 100 caused significant toxicity/membrane damage. Percentage cytotoxicity to rPCEC cells post exposure to NMFs (blank and 0.2%

rapamycin) for 2 h appeared to be similar to negative control (**Figure 66**) indicating NMFs do not cause cell membrane damage. Results from these assays clearly suggest that NMF's are not cytotoxicity. Therefore these formulations appeared to be safe for topical ocular application.

In vivo ocular tissue rapamycin distribution studies

Delivery of drug to back-of-the-eye tissues is a major challenge. Diseases affecting the posterior segment ocular tissues, retina-choroid, require long term drug delivery. To determine whether the developed NMF can deliver the hydrophobic rapamycin, to back-of-the-eye tissues, an *in vivo* ocular tissue distribution study was conducted following topical (0.2% rapamycin) instillation into the pre-corneal pocket of rabbits.

Individual calibration curve were prepared for each ocular tissue and fluid. Multiple reactions monitoring (MRM) mode was utilized to detect the compound of interest. MRM transition for rapamycin m/z $[M+Na]^+$: 936.4/409.3 and for IS (erythromycin) m/z $[M+H]^+$: 734.4/576.5 were optimized. Specificity and selectivity of the method were tested by analyzing posterior ocular blank tissues and fluid. To assess blank interference with the peak of interest (rapamycin) we processed six replicates at lower limit of quantification (LLOQ). Peak areas of blanks co-eluting with the analyte was less than 20% of the mean peak area at LLOQ. Intra-day and inter-day precision and accuracy experiments were performed by analyzing extracted calibration curve and QC standards. Accuracy of the method was between 85% and 115% of the nominal value in all the standards, except at the

Table 27. Rapamycin levels in individual ocular tissues

Tissue	0.2% formulation Average amount of rapamycin (ng/g of tissue) Mean ±S.E.M
Retina-Choroid	362 ±56.17
Iris Ciliary Body	585 ±80.06
Cornea	2261 ±507.11
Sclera	486 ±89.99
Lens	BLOQ
Vitreous Humor	N.D
Aqueous Humor	BLOQ

S.E.M – Standard error of mean

BLOQ – Below limit of quantification

BLOQ for the first and the second set of experiment for all matrices except Retina-Choroid – 10.4 ng/mL

BLOQ for first set Retina-Choroid = 10.4 ng/mL

BLOQ for second set Retina-Choroid = 3.5 ng/mL

N.D – Not detectable

lower limit of quantitation (LLOQ) level, which was 80–120%. Precision was calculated using the coefficient of variation multiplied by 100. Precision of the method was less than 15% of the nominal concentration except at the LLOQ, which was below 20%. The interday precision validation was conducted at 3.5 ng/mL, 10 ng/mL, 480 ng/mL and 800 ng/mL. The LLOQ with inter-day coefficients of variation ranged between 2.3% and 16.7% for sclera, vitreous humor, and retina-choroid. The calibration curve was prepared from 3.5 ng/mL, 10.48 ng/mL, 29.5 ng/mL, 187.2 ng/mL, 312.0 ng/mL, 480 ng/mL and 800 ng/mL rapamycin doped in respective tissue sample extracts. The lower limit of quantitation (LLOQ) was determined to be 10.48 ng/mL for sclera and vitreous humor. LLOQ for retina-choroid was 3.5 ng/mL with a regression coefficient of 0.9984.

Topical drop instillation of 0.2% rapamycin NMF demonstrated detectable and quantifiable rapamycin levels in the back-of-the-eye tissues (sclera and retina-choroid). Rapamycin concentrations were quantified in anterior chamber eye tissues (cornea, iris-ciliary body) but not in lens and aqueous humor which was blow limit of quantitation (348). Rapamycin concentrations were also detected in back-of-the-eye tissues (sclera, retina-choroid) but not in fluid (vitreous humor) (**Table 27**). Results indicate that retina-choroid retained the drug at a concentration of 362.35 ± 56.7 ng/g tissue.

Topically administered drugs may follow corneal and/or conjunctival-scleral pathway to reach back-of-the-eye tissues (356). The current mode of drug delivery to posterior segment of the eye is primarily by invasive routes like subconjunctival, intravitreal injections or implants. These methods are also

associated with serious complications. Again, this method of drug delivery requires medical specialist to administer the drug, which makes treatment expensive. Also, these drugs are required to be administered for multiple times. Such invasive mode of delivery may provide treatment to back-of-the-eye disease but may cause serious ocular complications leading to vision loss. Therefore, to overcome such complications, patient compliant formulations like topical drops need to be developed. One of the major drawbacks with topically applied drug formulations is sub-therapeutic levels of drug reaching back-of-the-eye tissues. To address these problems and replace the current existing route of drug administration to retina-choroid, we have developed patient compliant clear, aqueous NMF topical drops that could deliver the drug non-invasively to the back-of-the-eye tissues. Most of the potent drug molecules suffer from two major barriers (i) sub-optimal physicochemical properties such as low aqueous solubility and (ii) ocular static and dynamic barriers. Ocular static barriers include sclera, RPE and multi-drug resistance efflux pumps. The dynamic barriers include conjunctival and choroidal blood and lymph vessels that wash drug out of ocular tissues into systemic circulation. Moreover, due to high lipophilicity, rapamycin may not be able to translocate across cornea (337), which is in agreement with our previously reported results (348).

The non-corneal route may be explored as a predominant route for back-of-the-eye delivery in comparison to corneal route. Aqueous solubility of the molecule is an important determinant for its transport across sclera but also for its ability to evade the conjunctival blood and lymph vessels mediated washout (357). Scleral

aqueous pore diameter varies between 20 and 80 nm (63), which facilitates the diffusion of small hydrophilic molecules. However, since rapamycin is highly hydrophobic, it undergoes partitioning to a larger extent into the lipophilic retinal tissue. In current formulation, rapamycin was sequestered into aqueous NMF with improved solubility (~800 times) relative to its aqueous solubility of 2.6 µg/mL (337). At the same time hydrophilic corona of the nanomicelles can be highly effective in utilizing scleral aqueous channels/pores (**Figure 74**). This alternative route may help permeation of nanomicelles to reach back-of-the-eye tissues (retina-choroid). Moreover, highly polar hydrophilic nanomicellar corona may minimize wash out into the systemic circulation from the conjunctival and choroidal blood and lymph vessels thus overcoming dynamic barriers. The rapamycin NMF present in sclera may act as a depot and slowly release the drug to deeper ocular tissues (**Figure 74**). On the other hand, we hypothesize that if the nanomicelles release rapamycin in scleral tissue, a constant rapamycin release to retinal tissues may be achieved which is an added advantage with NMF. NMF can follow the same route of drug transport (transscleral pathway) that was previously observed with sub-conjunctival injection of rapamycin (358).

Nanomicelles in the posterior ocular tissues release rapamycin to highly lipophilic retinal tissues (**Figure 74)**. However, rapamycin molecules do not appreciably partition into hydrophilic vitreous humor as evidenced by non-detectable rapamycin in vitreous humor. Hence, rapamycin accumulates in the lipoidal retinal layers. This drug is a substrate for efflux pumps like P-gp (23, 41).

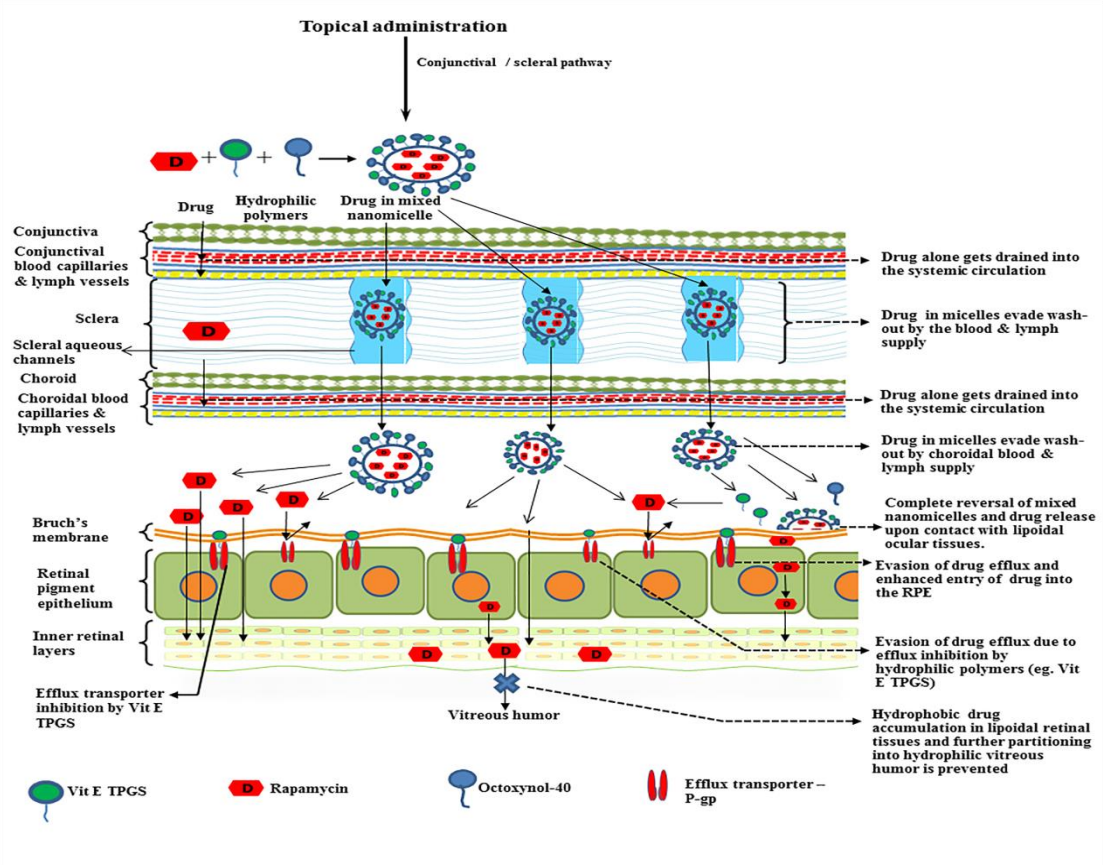

Figure 74. Hypothetical representation of rapamycin-loaded nanomicelles reaching the back-of-the-eye (retina-choroid) following conjunctival scleral pathway after topical drop administration. Vitamin E tocopherol polyethylene glycol succinate-1000 (Vit. E TPGS), P-glycoprotein (P-gp)

Vit. E TPGS is found to modulate P-gp efflux transport *via* P-gp ATPase inhibition (359). Upon disruption of micelles and release of rapamycin into back-of-the-eye lipid tissues, Vit. E TPGS monomers may help to inhibit P-gp (**Figure 74**). Thereby, higher rapamycin accumulation into the retina-choroid area may be achieved. Results from this study suggest that nanomicelles are novel carriers that can overcome both the static and dynamic ocular barriers and deliver therapeutic levels of rapamycin to back-of-the-eye tissue (retina-choroid). It is noted that much higher than presumably therapeutic levels of rapamycin (7 - 12 ng/mL) (337) were delivered to retina-choroid with a single topical drop instillation, indicating that the NMF should be safe and novel carriers for rapamycin.

Conclusion

A stable, clear aqueous 0.2% rapamycin loaded NMF has been prepared and characterized. Rapamycin loading in the NMF show excellent entrapment efficiency. Nanomicellar size was found to be ~10 nm with narrow polydispersity index. Surface potential studies demonstrated the formulations to carry slight negative charge. MNF were tested *in vitro* for their cytotoxicity on rPCEC cells and D407 cells following cell proliferation and LDH assays. Both cell assays demonstrated negligible cytotoxic effect with MNF relative to triton-x 100. Both studies demonstrated that placebo and 0.2% rapamycin loaded MNF are very safe and tolerable to eye. Bioanalytical, sensitive, robust LC-MS/MS method has been developed and validated. *In vivo* ocular tissue distribution studies with single topical drop instillation demonstrated rapamycin in anterior ocular tissues and to

reach retina-choroid. High levels of rapamycin were obtained in retina-choroid measured with sensitive LC-MS/MS. No rapamycin was present in vitreous body. These results indicate that MNF is able to deliver rapamycin to the retina-choroid tissues following topical drop administration to eye and rapamycin is sequestered into the lipid environment of RPE and Bruch's membrane and does not partition back to the aqueous environment of vitreous humor.

Chapter 7

SUMMARY AND RECOMMENDATIONS

Summary

Drugs like CsA, resolvin analog (RX-10045), dexamethasone and rapamycin are used to treat ocular conditions such as dry eye syndrome and uveitis. However, these drugs suffer from low oral and ocular bioavailability due to their lipophilicity and poor aqueous solubility. Moreover, topically administered dose to eye will be immediately diluted by excessive tear production, drained away into nasolacrimal duct and lost due to spillage over the cheeks. The small remainder amount of dose will be further prevented from ocular tissue penetration due to ocular static and dynamic barriers causing sub-therapeutic levels of drug in the tissue. Therefore, the broad long term objective of this dissertation is directed to improve solubility, drug stability, improve bioavailability and deliver therapeutic concentrations of drug to ocular tissues with topical drop. Chapter 3, the first part of the project (Chapter 3) is to develop and optimize aqueous solution of CsA, improve the ocular bioavailability with topical drop administration and minimize/avoid adverse effects that are observed with commercially available Restasis®. In this study, FDA approved amphiphilic polymers (hydrogenated castor oil-40 and Oc-40) for human use were used to encapsulate cyclosporine. Solvent evaporation rehydration method was used which generated 0.1% CsA aqueous solution. Further, blend of polymers (1.0:0.05 wt%) had lower critical micellar concentration (CMC) relative to individual polymers. Several NMF

physicochemical characterization studies were conducted. Studies revealed that no free drug was present in the aqueous NMF, nanomicelles were ~20 nm, spherical, devoid of aggregation and nanomicelles retained stability upon dilution. Cytotoxicity evaluation on rPCEC and human retinal pigment epithelial (D407) cells demonstrated the CsA loaded NMF to be safe and well-tolerated. *In vivo* biocompatibility and toxicological studies in rabbits demonstrated NMF to be safe and results were comparable to that of negative control (BSS). *In vivo* pharmacokinetic studies with topical ocular drop administration of Restasis (0.05% CsA emulsion), 0.05% CsA NMF, and 0.1% CsA NMF 4 times daily at 2-hour intervals for 7 days, revealed that CsA exposures followed 0.1% CsA NMF > 0.05% CsA NMF and Restasis® (0.05% CsA emulsion). Interestingly, negligible CsA concentrations were observed in vitreous and aqueous humor. The results suggest that NMF not only delivered therapeutic levels of CsA to anterior ocular tissues but also to back-of-the-eye tissues (retina-choroid). A corneal pathway may not be possible due to very low CsA concentrations in aqueous humor, lens and vitreous humor. Moreover the flow of aqueous humor is in opposite direction to that of molecular entry. Alternatively, ~12 nm nanomicelles efficiently permeate through 20 nm to 80 nm scleral pores and reach back-of-the-eye tissues (retina-choroid) following conjunctival-scleral (transscleral) pathway. In the lipoidal posterior ocular tissues, these nanoconstruct may release the cargo into Bruch's membrane/retina-choroid generating high drug levels. Moreover, hydrophobic CsA may not appreciably partition into hydrophilic vitreous humor. Chapter 4, the next aim (Chapter 4) was to (a) screen resolvin analog for efflux transporters and

(b) develop and aqueous clear resolvin NMF by improving aqueous solubility, stability and ocular bioavailability of yellow oily resolvin analog (RX-10045). Madin-Darby canine kidney (MDCK) cells transfected with the human MDR1 gene (MDCKII-MDR1), human MRP2 gene (MDCKII-MRP2), and human BCRP gene (MDCKII-BCRP) were employed to screen resolvin analog. From these studies resolvin analog was identified as substrate/inhibitor for efflux transporters (MRP and BCRP). Also, resolvin analog appears to be a strong inhibitor/substrate of OCT-1. Moreover, encapsulation of resolvin analog in NMF improved its aqueous stability, well-tolerated and had higher bioavailability. Ocular drug concentrations followed similar pattern as observed in earlier studies with CsA.

Next aim was to determine whether blend of Vitamin E TPGS and Oc-40 can entrap drugs with low and high lipophilicity. We selected DEX and RAP to entrap inside nanomicellar core. Solvent evaporation rehydration technique was used to develop formulation. NMF was optimized with statistical design of experiment. Physicochemical properties of nanomicelles were studied and observed to possess similar properties to that of NMF prepared in Chapter 3. These new blend of drug loaded NMF were safe and well tolerated by ocular cell lines. Sensitive, robust, rugged bioanalytical LC-MS/MS method was developed and validated for DEX and RAP in ocular tissues. Moreover, *in vivo* studies in rabbits with topical eye drops demonstrated surprisingly similar results as observed with earlier formulations. Drug was found in cornea, iris-ciliary body, sclera and retina-choroid. However, no drug was quantified in aqueous humor, lens and vitreous humor. Results repeatedly suggests that NMF utilize aqueous scleral pores (20 nm

to 80 nm), follow conjunctival-scleral pathway to reach back-of-the-eye lipoidal tissues (retina-choroid). Moreover, lipophilic drug is being released in the lipoidal tissues and further permeation of drug into hydrophilic stroma is prevented. Chapter 7, in summary, proper selection of surfactant/polymers, design and engineering techniques can produce nanomicelles which could be utilized to deliver drugs to both anterior and posterior ocular tissues i.e., retina-choroid, non-invasively in therapeutic levels. Such nanomicellar topical drop approach, in the near future, may replace the patient non-compliant routes of drug administration to posterior ocular tissues such as intravitreal and periocular injections into the globe.

Recommendations

The above studies were aimed at improving solubility, develop aqueous formulation of drug molecules and safely delivery to ocular tissues without any side effects. A few recommendations can be made to move further with this work based on the results obtained from the above studies.

First, investigations for DEX and RAP *in vivo* ocular tolerability and pharmacokinetic studies with single and multiple drop administration of NMF should be undertaken. Such studies allow to identify the best possible dose to treat ocular diseases such as dry eye syndrome, uveitis and ocular neovascularization.

Second, these drug molecules may be conjugated with targeting moieties and loaded into NMF. Such carriers may deliver the cargo non-invasively to back-of-the-eye tissues. Moreover, targeted drugs (constructs) helps to improve drug permeability and overcome efflux transporters. Peptide transporter and folate

receptor are expressed on the choroidal side of RPE. Conjugation of peptide and/or folate molecule to drug and simultaneous loading into NMF should be undertaken in order to come up with the best possible formulation.

Third, the concept of drug loaded NMF can be extended to delivery of other drug molecules such as ganciclovir and cidofovir to treat CMV retinitis, digoxin to treat choroidal/ retinal neovascularization and other back-of-the-eye diseases. Since, this novel nanomicellar design demonstrated higher drug concentrations in back-of-the-eye tissues, this approach may also result in higher permeability of macromolecules/peptides/protein therapeutics and other therapeutics such as genes, siRNA, antisense RNA and oligonucleotides.

Finally, in this dissertation project, a resolvin analog was for the first time screened for efflux transporters. NMF of hydrophobic drugs was successfully prepared, characterized and optimized. Results from these projects appeared to be very promising and laid a platform for posterior ocular delivery with topical drop. Interestingly and repeatedly similar results were achieved with different blends of polymers. Moreover, targeted delivery of drugs may be achieved by covalently conjugating targeting ligands to drug molecule (constructs). Topical drops of nanomicelles may deliver constructs to the retina-choroid. Constructs may reach into target tissue and cleaved to regenerate parent drug. Therefore, nanomicelles loaded with drug constructs may result in enhanced drug delivery and cellular uptake into target cells. Such novel nanocarriers may be used for enhanced delivery of poorly water soluble drugs to various diseased sites *via* variety of mechanisms.

Re: Re: Permission to reuse the manuscript content in my dissertation
DELETEREPLYREPLY ALLFORWARD
Mark as unread

Cholkar, Kishore (UMKC-Student)
Sun 1/4/2015 6:10 PM
Sent Items
To:
editorialoffice <editorialoffice@wjgnet.com>;
This message was sent with high importance.
Dear Editor,

Thank you for the permission.

Happy New Year - 2015.

Thanks & Regards,
Kishore Cholkar
Doctoral Candidate
Graduate Teaching and Research Assistant
Dr Ashim K Mitra's Group
University of Missouri Kansas City
Health Science Building, Room#5223,
2464 Charlotte Street, Kansas City,
Missouri, USA-64108.

From: editorialoffice <editorialoffice@wjgnet.com>
Sent: Sunday, January 4, 2015 6:07 PM
To: Cholkar, Kishore (UMKC-Student)
Subject: Re: Re: Permission to reuse the manuscript content in my dissertation

Dear Dr. Cholkar,
Thank you.

Yes, you can.

Best regards,

Jin-Lei Wang, Director, Editorial Office

Baishideng Publishing Group Inc

E-mail: j.l.wang@wjgnet.com
Help desk: http://www.wjgnet.com/esps/helpdesk.aspx
http://www.wjgnet.com

2015-01-05

Wang JL

发件人： Cholkar, Kishore (UMKC-Student)
发送时间： 2015-01-05 08:01:48
收件人： editorialoffice
抄送：
主题： Re: Permission to reuse the manuscript content in my dissertation

Dear Editor,

Can I take this email as "permission to reuse the content" in my dissertation writing ? Kindly confirm.

Thanks & Regards,
Kishore Cholkar
Doctoral Candidate
Graduate Teaching and Research Assistant
Dr Ashim K Mitra's Group
University of Missouri Kansas City
Health Science Building, Room#5223,
2464 Charlotte Street, Kansas City,
Missouri, USA-64108.

From: editorialoffice <editorialoffice@wjgnet.com>
Sent: Sunday, January 4, 2015 5:59 PM
To: Cholkar, Kishore (UMKC-Student)
Subject: Re: Permission to reuse the manuscript content in my dissertation

Dear Dr. Cholkar,
Thank you.

You can use the content with our permission.

Best regards,

Jin-Lei Wang, Director, Editorial Office

Baishideng Publishing Group Inc
E-mail: j.l.wang@wjgnet.com
Help desk: http://www.wjgnet.com/esps/helpdesk.aspx

http://www.wjgnet.com

2015-01-05

Wang JL

发件人： Cholkar, Kishore (UMKC-Student)
发送时间： 2014-12-31 10:44:49
收件人： editorialoffice@wjgnet.com
抄送：
主题： Permission to reuse the manuscript content in my dissertation

Dear Editor,

It was nice working with you on the following manuscript:

Ocular drug delivery systems: An overview
Ashaben Patel, **Kishore Cholkar,** Vibhuti Agrahari and Ashim K Mitra.
World J Pharmacol. 2013 June 9; 2(2): 47-64.

I am the co-author in this manuscript. I am here to request your permission to reuse the content in my dissertation writing.

I tried to find the application form on your website but unfortunately couldn't find one. Kindly provide me with permission to reuse the content.

Waiting for your response.

Thanks & Regards,
Kishore Cholkar
Doctoral Candidate
Graduate Teaching and Research Assistant
Dr Ashim K Mitra's Group
University of Missouri Kansas City
Health Science Building, Room#5223,
2464 Charlotte Street, Kansas City,
Missouri, USA-64108.

Copyright Clearance Center

Welcome, Kishore
Not you?

Log out | Cart (0) | Manage Account | Feedback | Help | Live Help

DIRECTPATH | GET PERMISSION | PRODUCTS & SOLUTIONS | EDUCATION | ABOUT US

Get Permission / Find Title
Publication Title or ISBN/ISSN
Go
Advanced Search Options

Order History

View Orders | View Order Details | View RIGHTSLINK Orders

View: Completed | Pending | Canceled | Credited | Denied

Sort orders by: Order Date ▾ Ascending Descending

LICENSE #: 3550850038756
Order Date: 01/16/2015

Elsevier Books

Title: Ocular Transporters and Receptors
Type of use: reuse in a thesis/dissertation

Fee: 0.00 USD

View printable order

LICENSE #: 3541530422129
Order Date: 01/03/2015

Journal of Chromatography B

Title: Bioanalytical method validation of rapamycin in ocular matrix by QTRAP LC–MS/MS: Application to rabbit anterior tissue distribution by topical administration of rapamycin nanomicellar formulation
Type of use: reuse in a thesis/dissertation

Fee: 0.00 USD

View printable order

Contd….

LICENSE #: 3541520892779 **Order Date:** 01/03/2015 View printable order	Journal of Pharmaceutical and Biomedical Analysis **Title:** Development and validation of a fast and sensitive bioanalytical method for the quantitative determination of glucocorticoids—Quantitative measurement of dexamethasone in rabbit ocular matrices by liquid chromatography tandem mass spectrometry **Type of use:** reuse in a thesis/dissertation	**Fee:** 0.00 USD
LICENSE #: 3541511043438 **Order Date:** 01/03/2015 View printable order	AAPS PharmSciTech **Title:** Optimization of Dexamethasone Mixed Nanomicellar Formulation **Type of use:** Thesis/Dissertation	**Fee:** 0.00 USD
LICENSE #: 3541510795574 **Order Date:** 01/03/2015 View printable order	AAPS PharmSciTech **Title:** Nanomicellar Topical Aqueous Drop Formulation of Rapamycin for Back-of-the-Eye Delivery **Type of use:** Thesis/Dissertation	**Fee:** 0.00 USD

LIST OF REFERENCES

1. McCannel CA, Holland GN, Helm CJ, Cornell PJ, Winston JV, Rimmer TG. Causes of uveitis in the general practice of ophthalmology. UCLA Community-Based Uveitis Study Group. Am J Ophthalmol. 1996;121(1):35-46.
2. Ueta M, Kinoshita S. Ocular surface inflammation is regulated by innate immunity. Prog Retin Eye Res. 2012.
3. Stein-Streilein J, Streilein JW. Anterior chamber associated immune deviation (ACAID): regulation, biological relevance, and implications for therapy. Int Rev Immunol. 2002;21(2-3):123-52.
4. Lapalus P, Moulin G, Bayer V, Fredj-Reygrobellet D, Elena PP. Effects of a new anti-allergic agent: the magnesium salt of N-acetyl-aspartyl-glutamic acid on experimental allergic inflammation of the rabbit eye. Curr Eye Res. 1986;5(7):517-22.
5. Ferguson VM, Spalton DJ. Recovery of the blood-aqueous barrier after cataract surgery. Br J Ophthalmol. 1991;75(2):106-10.
6. Abelson MB, Schaefer K. Conjunctivitis of allergic origin: immunologic mechanisms and current approaches to therapy. Surv Ophthalmol. 1993;38 Suppl:115-32.
7. Schaumberg DA, Dana R, Buring JE, Sullivan DA. Prevalence of dry eye disease among US men: estimates from the Physicians' Health Studies. Archives of ophthalmology. 2009;127(6):763-8.
8. Le Q, Ge L, Li M, Wu L, Xu J, Hong J, et al. Comparison on the vision-related quality of life between outpatients and general population with dry eye syndrome. Acta ophthalmologica. 2013.
9. Research in dry eye: report of the Research Subcommittee of the International Dry Eye WorkShop (2007). The ocular surface. 2007;5(2):179-93.
10. Gaffney EA, Tiffany JM, Yokoi N, Bron AJ. A mass and solute balance model for tear volume and osmolarity in the normal and the dry eye. Prog Retin Eye Res. 2010;29(1):59-78.
11. Nguyen QD, Ibrahim MA, Watters A, Bittencourt M, Yohannan J, Sepah YJ, et al. Ocular tolerability and efficacy of intravitreal and subconjunctival injections of sirolimus in patients with non-infectious uveitis: primary 6-month results of the SAVE Study. Journal of ophthalmic inflammation and infection. 2013;3(1):32.
12. Caspi R. Autoimmunity in the immune privileged eye: pathogenic and regulatory T cells. Immunologic research. 2008;42(1-3):41-50.
13. Gupta R, Murray PI. Chronic non-infectious uveitis in the elderly: epidemiology, pathophysiology and management. Drugs & aging. 2006;23(7):535-58.
14. Cholkar K, Patel SP, Vadlapudi AD, Mitra AK. Novel strategies for anterior segment ocular drug delivery. Journal of ocular pharmacology and therapeutics :

the official journal of the Association for Ocular Pharmacology and Therapeutics. 2013;29(2):106-23.
15. Bian ZM, Elner SG, Elner VM. Regulation of VEGF mRNA expression and protein secretion by TGF-beta2 in human retinal pigment epithelial cells. Experimental eye research. 2007;84(5):812-22.
16. Khurana RN, Do DV, Nguyen QD. Anti-VEGF therapeutic approaches for diabetic macular edema. International ophthalmology clinics. 2009;49(2):109-19.
17. Gunda S, Hariharan S, Mandava N, Mitra AK. Barriers in Ocular Drug Delivery. Ocular Transporters In Ophthalmic Diseases And Drug Delivery. In: Tombran-Tink J, Barnstable CJ, editors. Ophthalmology Research: Humana Press; 2008. p. 399-413.
18. Gueudry J, Roujeau JC, Binaghi M, Soubrane G, Muraine M. Risk factors for the development of ocular complications of Stevens-Johnson syndrome and toxic epidermal necrolysis. Archives of dermatology. 2009;145(2):157-62.
19. De Rojas MV, Dart JK, Saw VP. The natural history of Stevens Johnson syndrome: patterns of chronic ocular disease and the role of systemic immunosuppressive therapy. Br J Ophthalmol. 2007;91(8):1048-53.
20. Mandapati JS, Metta AK. Intraocular pressure variation in patients on long-term corticosteroids. Indian dermatology online journal. 2011;2(2):67-9.
21. Aswani Dutt Vadlapudi AP, Kishore Cholkar and Ashim K. Mitra Recent Patents on Emerging Therapeutics for the Treatment of Glaucoma, Age Related Macular Degeneration and Uveitis. Recent Patents on Biomedical Engineering 2013;6(3):83 - 101
22. Duvvuri S, Majumdar S, Mitra AK. Role of metabolism in ocular drug delivery. Curr Drug Metab. 2004;5(6):507-15.
23. Anglicheau D, Pallet N, Rabant M, Marquet P, Cassinat B, Meria P, et al. Role of P-glycoprotein in cyclosporine cytotoxicity in the cyclosporine-sirolimus interaction. Kidney international. 2006;70(6):1019-25.
24. accessed on 31st december 2013. Available from: http://www.fda.gov/drugs/developmentapprovalprocess/developmentresources/druginteractionslabeling/ucm093664.htm.
25. Xue Y, Yap CW, Sun LZ, Cao ZW, Wang JF, Chen YZ. Prediction of P-glycoprotein substrates by a support vector machine approach. Journal of chemical information and computer sciences. 2004;44(4):1497-505.
26. Schermer A, Galvin S, Sun TT. Differentiation-related expression of a major 64K corneal keratin in vivo and in culture suggests limbal location of corneal epithelial stem cells. J Cell Biol. 1986;103(1):49-62.
27. DelMonte DW, Kim T. Anatomy and physiology of the cornea. J Cataract Refract Surg. 2011;37(3):588-98.
28. Komai Y, Ushiki T. The three-dimensional organization of collagen fibrils in the human cornea and sclera. Invest Ophthalmol Vis Sci. 1991;32(8):2244-58.
29. Hogan MJ AJ, Weddell JE. Histology of the human eye. Philadelphia: WB Saunders; 1971.
30. Belmonte C, Acosta MC, Gallar J. Neural basis of sensation in intact and injured corneas. Experimental eye research. 2004;78(3):513-25.

31. Farjo AA MDM, Soong HK. Corneal anatomy, physiology and wound healing. Yanoff M DJ, editor: Edinburgh, Mosby Elsevier: Elsevier Inc.,; 2009.
32. Wiley L, SundarRaj N, Sun TT, Thoft RA. Regional heterogeneity in human corneal and limbal epithelia: an immunohistochemical evaluation. Invest Ophthalmol Vis Sci. 1991;32(3):594-602.
33. Roger W. Beuerman LP. Ultrastructure of the human cornea. Microscopy research and technique. 1996;33(4):320-35.
34. Freeman I. Collagen polymorphism in mature rabbit. Invest Ophthalmol in Visual Sciences. 1978;17:171-7.
35. Jaleh Barar MA, Seyed Abdolreza Mortazavi-Tabatabaei, Yadollah Omidi. Ocular drug delivery; Impact of in vitro cell culture models. Journal of Ophthalmic Vision Research. 2009;4(4):238-52.
36. Matthias Böhnke BRM. Confocal microscopy of the cornea. Progress in Retinal and Eye Research. 1999;18(5):553-688.
37. Boote C, Dennis S, Newton RH, Puri H, Meek KM. Collagen fibrils appear more closely packed in the prepupillary cornea: optical and biomechanical implications. Invest Ophthalmol Vis Sci. 2003;44(7):2941-8.
38. Gipson IK JN. Anatomy and cell biology of the cornea, superficial limbus, and conjunctiva. Albert DM JF, ed,, editor. Philadelphia2008.
39. Fini ME SB. How the cornea heals; cornea-specific repair mechanisms affecting surgical outcomes. Cornea.24(suppl 1):S2-S11.
40. Geroski DH, Matsuda M, Yee RW, Edelhauser HF. Pump function of the human corneal endothelium. Effects of age and cornea guttata. Ophthalmology. 1985;92(6):759-63.
41. Roger W. Anatomy of the Eye and Orbit. 7 ed. Wolff E, editor. Philadelphia: WB Saunders; 1976.
42. Moore J, Trkola A. HIV type 1 coreceptors, neutralization serotypes, and vaccine development. AIDS Res Hum Retroviruses. 1997;13(9):733-6.
43. Watsky MA, Jablonski MM, Edelhauser HF. Comparison of conjunctival and corneal surface areas in rabbit and human. Curr Eye Res. 1988;7(5):483-6.
44. Bron AJ TR, Tripathi BJ. The ocular appendages: eyelids, conjunctiva and lacrimal apparatus. Wolff's, editor. London: Chapman & Hall Medical; 1997.
45. Gormley PD, Powell-Richards AO, Azuara-Blanco A, Donoso LA, Dua HS. Lymphocyte subsets in conjunctival mucosa-associated-lymphoid-tissue after exposure to retinal-S-antigen. Int Ophthalmol. 1998;22(2):77-80.
46. Knop NKaE. Conjunctiva-Associated Lymphoid Tissue in the Human Eye. Investigative Ophthalmology & Visual Science. 2000;41(6):1270-9.
47. Pabst R, Westermann J. Which steps in lymphocyte recirculation are regulated by interferon-gamma? Res Immunol. 1994;145(4):289-94.
48. Gowans JL. The recirculation of lymphocytes from blood to lymph in the rat. J Physiol. 1959;146(1):54-69.
49. Chastain JE. General Consideration in Ocular Drug Delivery. 2 ed. Mitra AK, editor. New York, Basel: Marcel Dekker, Inc; 2003.
50. TF F. Shifting the paradigm of the blood-aqueous barrier. Experimental eye research. 2001;73:581.

51. H D. The aqueous humor and the introcular pressure. Davson H e, editor. New York: Pergamon Press; 1990.
52. Fielder AR RA. Immunoglobulins of normal aqueous humor. Trans Ophthalmol Soc UK. 1979;99:120.
53. A B. Uveoscleral drainage of aqueous humor in human eye. Experimental eye research. 1971;12:275.
54. Pederson JE TC. Uveoscleral outflow: diffusion or flow? Invest Ophthalmol Visual Sciences. 1987;28:1022.
55. Danysh BP, Duncan MK. The lens capsule. Experimental eye research. 2009;88(2):151-64.
56. Fischbarg J, Diecke FP, Kuang K, Yu B, Kang F, Iserovich P, et al. Transport of fluid by lens epithelium. Am J Physiol. 1999;276(3 Pt 1):C548-57.
57. Fisher RF. Changes in the permeability of the lens capsule in senile cataract. Trans Ophthalmol Soc U K. 1977;97(1):100-3.
58. Friedenwald JS. The Permeability of the Lens Capsule to Water, Dextrose, and Other Sugars. Trans Am Ophthalmol Soc. 1930;28:195-211.
59. Friedenwald JS. Permeability of the lens capsule with special reference to the etiology of senile cataract. Arch Ophthalmol. 1930b;3:182-93.
60. Christina J. Lee, Jonathan A. Vroom, Harvey A. Fishman, Bent SF. Determination of human lens capsule permeability and its feasibility as a replacement for Bruch's membrane. Biomaterials. 2006;27(8):1670-8.
61. Fisher RF, Pettet BE. Presbyopia and the water content of the human crystalline lens. J Physiol. 1973;234(2):443-7.
62. Norman RE, Flanagan JG, Rausch SM, Sigal IA, Tertinegg I, Eilaghi A, et al. Dimensions of the human sclera: Thickness measurement and regional changes with axial length. Experimental eye research. 2010;90(2):277-84.
63. Chopra P, Hao J, Li SK. Iontophoretic transport of charged macromolecules across human sclera. Int J Pharm. 2010;388(1-2):107-13.
64. Alm A BA. Ocular and optic nerve blood flow at normal and increased intraocular pressures in monkeys (Macaca iris): A study with radioactively labelled microspheres including flow determinations in brain and some other tissues. Experimental eye research. 1973;15:15.
65. A B. Blood circulation and fluid dynamics in the eye. Physiol Rev. 1975;55:383.
66. Friedman E KH, Smith TR. Retinal and choroidal blood flow determined with krypton-85 in anesthetized animals. Invest Ophthalmol Visual Sciences. 1964;3:539.
67. WS F. The choroidal circulation and retinal metabolism-an overview. Eye. 1990;4:243.
68. A B. Some aspects of the ocular circulation (Friedenwald Lecture). Invest Ophthalmol Visual Sciences. 1985;26:410.
69. LM P. Temperature modulating action of choroidal blood flow. Eye. 1991;5:181.
70. Guymer R, Luthert P, Bird A. Changes in Bruch's membrane and related structures with age. Prog Retin Eye Res. 1999;18(1):59-90.

71. Panda-Jonas S, Jonas JB, Jakobczyk-Zmija M. Retinal pigment epithelial cell count, distribution, and correlations in normal human eyes. Am J Ophthalmol. 1996;121(2):181-9.
72. Boulton M, Dayhaw-Barker P. The role of the retinal pigment epithelium: topographical variation and ageing changes. Eye (Lond). 2001;15(Pt 3):384-9.
73. Thumann G, Hoffmann, S., Hinton, D.R. Cell biology of the retinal pigment epithelium. Ryan SJ, editor. Mosby, St Louis: Elsevier; 2006.
74. Strauss O. The retinal pigment epithelium in visual function. Physiol Rev. 2005;85(3):845-81.
75. Hendrickson A, Possin D, Vajzovic L, Toth CA. Histologic development of the human fovea from midgestation to maturity. Am J Ophthalmol. 2012;154(5):767-78 e2.
76. La Cour M. The retinal pigment epithelium. Kaufmann P.L. A, A (eds), editor. Mosby, St Louis2003.
77. Thumann G, Hoffmann, S., Hinton, D.R. Cell biology of the retinal pigment epithelium. Ryan SJ, editor. St. Louis: Elsevier-Mosby; 2006.
78. Strauss O. The retinal pigment epithelium in visual function. Physiol Rev. 2005;85:845-81.
79. Oyster C. Retinal III: regional variation and spatial organization (Chapter 15). . Oyster Ce, editor. Sunderland, Massachusetts Sinauer Associates; 1999.
80. Curcio CA, Sloan, K.R., Kalina, R.E., Hendrickson, A.E. Human photoreceptor topography. J Comp Neurol. 1990;292:497-523.
81. Harris A, Gingaman, D.P., Ciulla, T.A., Martin, B.J. Retinal and choroidal blood flow in health and disease. Ryan SJe, editor. St Louis Mosby; 2001.
82. Provis JM. Development of the primate retinal vasculature. Prog Ret Eye Res. 2001;20:799–821.
83. Mann I. The development of the human eye, 3rd edition. Travistock square, London1964.
84. Sulik K, Wright, K.W. Embryology. Wright KW, Spiegel, P.H.(eds), editor. Berlin: Springer; 2003.
85. Levin LA. Optic nerve. Kaufman PL, Alm, A(eds), editor. St Louis: Mosby; 2003.
86. Tessier-Lavingne M. Visual processing by the retina. Kandel ER, Schwartz, J.H., Jessel, T.M. (eds), editor. New York: McGraw-Hill; 2000.
87. Wurtz RHK. Kandel ER, Schwartz, J.H., Jessel, T.M. (eds), editor. New York McGraw-Hill; 2000.
88. Lee B, Litt M, Buchsbaum G. Rheology of the vitreous body: part 3. Concentration of electrolytes, collagen and hyaluronic acid. Biorheology. 1994;31(4):339-51.
89. Lee B, Litt M, Buchsbaum G. Rheology of the vitreous body: Part 2. Viscoelasticity of bovine and porcine vitreous. Biorheology. 1994;31(4):327-38.
90. Edelhauser HF, Rowe-Rendleman CL, Robinson MR, Dawson DG, Chader GJ, Grossniklaus HE, et al. Ophthalmic drug delivery systems for the treatment of retinal diseases: basic research to clinical applications. Invest Ophthalmol Vis Sci. 2010;51(11):5403-20.

91. Hamalainen KM, Kananen K, Auriola S, Kontturi K, Urtti A. Characterization of paracellular and aqueous penetration routes in cornea, conjunctiva, and sclera. Invest Ophthalmol Vis Sci. 1997;38(3):627-34.
92. Yi X, Wang Y, Yu FS. Corneal epithelial tight junctions and their response to lipopolysaccharide challenge. Invest Ophthalmol Vis Sci. 2000;41(13):4093-100.
93. F. J. The Corneal Endothelium. J F, editor: Elsevier; 2005.
94. Stefano Bonini RS, Marco Coassin, and Sergio Bonini. Allergic Conjunctivitis: Update on Its Pathophysiology and Perspectives for Future Treatment. Ruby Pawankar STH, Lanny J. Rosenwasser,, editor. Tokyo: Springer; 2009.
95. Trocme SD, Kephart GM, Allansmith MR, Bourne WM, Gleich GJ. Conjunctival deposition of eosinophil granule major basic protein in vernal keratoconjunctivitis and contact lens-associated giant papillary conjunctivitis. Am J Ophthalmol. 1989;108(1):57-63.
96. Udell IJ, Gleich GJ, Allansmith MR, Ackerman SJ, Abelson MB. Eosinophil granule major basic protein and Charcot-Leyden crystal protein in human tears. Am J Ophthalmol. 1981;92(6):824-8.
97. Montan PG, van Hage-Hamsten M, Zetterstrom O. Sustained eosinophil cationic protein release into tears after a single high-dose conjunctival allergen challenge. Clin Exp Allergy. 1996;26(10):1125-30.
98. Leonardi A, Borghesan F, Faggian D, Secchi A, Plebani M. Eosinophil cationic protein in tears of normal subjects and patients affected by vernal keratoconjunctivitis. Allergy. 1995;50(7):610-3.
99. Leonardi A, Borghesan F, DePaoli M, Plebani M, Secchi AG. Procollagens and inflammatory cytokine concentrations in tarsal and limbal vernal keratoconjunctivitis. Experimental eye research. 1998;67(1):105-12.
100. Leonardi A, Brun P, Tavolato M, Plebani M, Abatangelo G, Secchi AG. Tumor necrosis factor-alpha (TNF-alpha) in seasonal allergic conjunctivitis and vernal keratoconjunctivitis. Eur J Ophthalmol. 2003;13(7):606-10.
101. Fujishima H, Takeuchi T, Shinozaki N, Saito I, Tsubota K. Measurement of IL-4 in tears of patients with seasonal allergic conjunctivitis and vernal keratoconjunctivitis. Clin Exp Immunol. 1995;102(2):395-8.
102. Li Q, Fukuda K, Lu Y, Nakamura Y, Chikama T, Kumagai N, et al. Enhancement by neutrophils of collagen degradation by corneal fibroblasts. J Leukoc Biol. 2003;74(3):412-9.
103. Trocme SD, Leiferman KM, George T, Bonini S, Foster CS, Smit EE, et al. Neutrophil and eosinophil participation in atopic and vernal keratoconjunctivitis. Curr Eye Res. 2003;26(6):319-25.
104. Fini ME, Parks WC, Rinehart WB, Girard MT, Matsubara M, Cook JR, et al. Role of matrix metalloproteinases in failure to re-epithelialize after corneal injury. Am J Pathol. 1996;149(4):1287-302.
105. Fukuda K, Chikama T, Nakamura M, Nishida T. Differential distribution of subchains of the basement membrane components type IV collagen and laminin among the amniotic membrane, cornea, and conjunctiva. Cornea. 1999;18(1):73-9.

106. Saha P, Kim KJ, Lee VH. A primary culture model of rabbit conjunctival epithelial cells exhibiting tight barrier properties. Curr Eye Res. 1996;15(12):1163-9.
107. Kompella UB, Kim KJ, Lee VH. Active chloride transport in the pigmented rabbit conjunctiva. Curr Eye Res. 1993;12(12):1041-8.
108. Shi XP, Candia OA. Active sodium and chloride transport across the isolated rabbit conjunctiva. Curr Eye Res. 1995;14(10):927-35.
109. Huang AJ, Tseng SC, Kenyon KR. Paracellular permeability of corneal and conjunctival epithelia. Invest Ophthalmol Vis Sci. 1989;30(4):684-9.
110. Hopkins GA PRe. General pharmacological principles. Butterworth-Heinemann, editor. Oxford, UK1998.
111. Sasaki H YKNKea. Delivery of drugs to the eye by topical application. Progr Retinal Eye Res. 1996;15:583-620.
112. Horibe Y, Hosoya K, Kim KJ, Ogiso T, Lee VH. Polar solute transport across the pigmented rabbit conjunctiva: size dependence and the influence of 8-bromo cyclic adenosine monophosphate. Pharm Res. 1997;14(9):1246-51.
113. Gunda S, Hariharan S, Mitra AK. Corneal absorption and anterior chamber pharmacokinetics of dipeptide monoester prodrugs of ganciclovir (GCV): in vivo comparative evaluation of these prodrugs with Val-GCV and GCV in rabbits. Journal of ocular pharmacology and therapeutics : the official journal of the Association for Ocular Pharmacology and Therapeutics. 2006;22(6):465-76.
114. Chien DS, Sasaki H, Bundgaard H, Buur A, Lee VH. Role of enzymatic lability in the corneal and conjunctival penetration of timolol ester prodrugs in the pigmented rabbit. Pharm Res. 1991;8(6):728-33.
115. Gukasyan HJ, Yerxa BR, Pendergast W, Lee VH. Metabolism and transport of purinergic receptor agonists in rabbit conjunctival epithelial cells. Adv Exp Med Biol. 2002;506(Pt A):255-9.
116. Freddo TF. Shifting the paradigm of the blood-aqueous barrier. Experimental eye research. 2001;73(5):581-92.
117. Cunha-Vaz JG. The blood-ocular barriers: past, present, and future. Doc Ophthalmol. 1997;93(1-2):149-57.
118. Urtti A. Challenges and obstacles of ocular pharmacokinetics and drug delivery. Adv Drug Deliv Rev. 2006;58(11):1131-5.
119. Mannermaa E, Vellonen KS, Urtti A. Drug transport in corneal epithelium and blood-retina barrier: emerging role of transporters in ocular pharmacokinetics. Adv Drug Deliv Rev. 2006;58(11):1136-63.
120. Schoenwald RD. Ocular drug delivery. Pharmacokinetic considerations. Clin Pharmacokinet. 1990;18(4):255-69.
121. Mishima S, Gasset A, Klyce SD, Jr., Baum JL. Determination of tear volume and tear flow. Invest Ophthalmol. 1966;5(3):264-76.
122. Chrai SS, Patton TF, Mehta A, Robinson JR. Lacrimal and instilled fluid dynamics in rabbit eyes. J Pharm Sci. 1973;62(7):1112-21.
123. Ahmed I, Patton TF. Importance of the noncorneal absorption route in topical ophthalmic drug delivery. Invest Ophthalmol Vis Sci. 1985;26(4):584-7.

124. I. A. The noncorneal route in ocular drug delivery Mitra AK, editor. New York: Marcel Dekker, Inc.; 2003.
125. Robinson MR, Lee SS, Kim H, Kim S, Lutz RJ, Galban C, et al. A rabbit model for assessing the ocular barriers to the transscleral delivery of triamcinolone acetonide. Experimental eye research. 2006;82(3):479-87.
126. Lee SJ, He W, Robinson SB, Robinson MR, Csaky KG, Kim H. Evaluation of clearance mechanisms with transscleral drug delivery. Invest Ophthalmol Vis Sci. 2010;51(10):5205-12.
127. Ghate D, Brooks W, McCarey BE, Edelhauser HF. Pharmacokinetics of intraocular drug delivery by periocular injections using ocular fluorophotometry. Invest Ophthalmol Vis Sci. 2007;48(5):2230-7.
128. Hornof M, Toropainen E, Urtti A. Cell culture models of the ocular barriers. Eur J Pharm Biopharm. 2005;60(2):207-25.
129. Mariko Okada KS. The continuous and quantitative observation of permeability changes of the blood aqueous barrier in allergic inflammation of the eye. Association for Research in Vision and Ophthalmology. 1980;19(2):169-75.
130. Kong X, Liu X, Huang X, Mao Z, Zhong Y, Chi W. Damage to the blood-aqueous barrier in eyes with primary angle closure glaucoma. Mol Vis. 2010;16:2026-32.
131. Fujiwara T, Imamura Y, Margolis R, Slakter JS, Spaide RF. Enhanced depth imaging optical coherence tomography of the choroid in highly myopic eyes. Am J Ophthalmol. 2009;148(3):445-50.
132. Booij JC, Baas DC, Beisekeeva J, Gorgels TG, Bergen AA. The dynamic nature of Bruch's membrane. Prog Retin Eye Res. 2010;29(1):1-18.
133. Spraul CW, Lang GE, Grossniklaus HE, Lang GK. Histologic and morphometric analysis of the choroid, Bruch's membrane, and retinal pigment epithelium in postmortem eyes with age-related macular degeneration and histologic examination of surgically excised choroidal neovascular membranes. Surv Ophthalmol. 1999;44 Suppl 1:S10-32.
134. Hewitt AT, Newsome DA. Altered synthesis of Bruch's membrane proteoglycans associated with dominant retinitis pigmentosa. Curr Eye Res. 1985;4(3):169-74.
135. Hewitt AT, Nakazawa K, Newsome DA. Analysis of newly synthesized Bruch's membrane proteoglycans. Invest Ophthalmol Vis Sci. 1989;30(3):478-86.
136. Usha Chakravarthy JE, Philip J Rosenfeld. Age related macular degeneration. BMJ Clinical Review. 2010;340:526-30.
137. Cunha-Vaz J, Bernardes R, Lobo C. Blood-retinal barrier. Eur J Ophthalmol. 2010;21(S6):3-9.
138. Cunha-Vaz JG. The blood-retinal barriers system. Basic concepts and clinical evaluation. Experimental eye research. 2004;78(3):715-21.
139. Gardner TW, Lieth E, Khin SA, Barber AJ, Bonsall DJ, Lesher T, et al. Astrocytes increase barrier properties and ZO-1 expression in retinal vascular endothelial cells. Invest Ophthalmol Vis Sci. 1997;38(11):2423-7.
140. Zhang Y, Stone J. Role of astrocytes in the control of developing retinal vessels. Invest Ophthalmol Vis Sci. 1997;38(9):1653-66.

141. Olsen TW, Edelhauser HF, Lim JI, Geroski DH. Human scleral permeability. Effects of age, cryotherapy, transscleral diode laser, and surgical thinning. Invest Ophthalmol Vis Sci. 1995;36(9):1893-903.
142. Ambati J, Canakis CS, Miller JW, Gragoudas ES, Edwards A, Weissgold DJ, et al. Diffusion of high molecular weight compounds through sclera. Invest Ophthalmol Vis Sci. 2000;41(5):1181-5.
143. Nicoli S, Ferrari G, Quarta M, Macaluso C, Santi P. In vitro transscleral iontophoresis of high molecular weight neutral compounds. Eur J Pharm Sci. 2009;36(4-5):486-92.
144. Alm A, Bill A, Young FA. The effects of pilocarpine and neostigmine on the blood flow through the anterior uvea in monkeys. A study with radioactively labelled microspheres. Experimental eye research. 1973;15(1):31-6.
145. Alm A, Bill A. Ocular and optic nerve blood flow at normal and increased intraocular pressures in monkeys (Macaca irus): a study with radioactively labelled microspheres including flow determinations in brain and some other tissues. Experimental eye research. 1973;15(1):15-29.
146. Steuer H, Jaworski A, Elger B, Kaussmann M, Keldenich J, Schneider H, et al. Functional characterization and comparison of the outer blood-retina barrier and the blood-brain barrier. Invest Ophthalmol Vis Sci. 2005;46(3):1047-53.
147. Kennedy BG, Mangini NJ. P-glycoprotein expression in human retinal pigment epithelium. Mol Vis. 2002;8:422-30.
148. Greenwood J. Characterization of a rat retinal endothelial cell culture and the expression of P-glycoprotein in brain and retinal endothelium in vitro. J Neuroimmunol. 1992;39(1-2):123-32.
149. Tagami M, Kusuhara S, Honda S, Tsukahara Y, Negi A. Expression of ATP-binding cassette transporters at the inner blood-retinal barrier in a neonatal mouse model of oxygen-induced retinopathy. Brain Res. 2009;1283:186-93.
150. Mannermaa E, Vellonen KS, Ryhanen T, Kokkonen K, Ranta VP, Kaarniranta K, et al. Efflux protein expression in human retinal pigment epithelium cell lines. Pharm Res. 2009;26(7):1785-91.
151. Chaine G, Imbs, J.L. Rappel anatomo-physiologique des particularites de la circulation oculaire. Flament J, Storck, D. (eds), editor. Paris Masson,; 1997.
152. Lee SJ, Kim ES, Geroski DH, McCarey BE, Edelhauser HF. Pharmacokinetics of intraocular drug delivery of Oregon green 488-labeled triamcinolone by subtenon injection using ocular fluorophotometry in rabbit eyes. Invest Ophthalmol Vis Sci. 2008;49(10):4506-14.
153. Bourlais CL, Acar L, Zia H, Sado PA, Needham T, Leverge R. Ophthalmic drug delivery systems--recent advances. Prog Retin Eye Res. 1998;17(1):33-58.
154. Gulsen D, Chauhan A. Ophthalmic drug delivery through contact lenses. Invest Ophthalmol Vis Sci. 2004;45(7):2342-7.
155. Gaudana R, Ananthula HK, Parenky A, Mitra AK. Ocular drug delivery. The AAPS journal. 2010;12(3):348-60.
156. Gaudana R, Jwala J, Boddu SH, Mitra AK. Recent perspectives in ocular drug delivery. Pharm Res. 2009;26(5):1197-216.

157. Bochot A, Fattal E. Liposomes for intravitreal drug delivery: a state of the art. Journal of controlled release : official journal of the Controlled Release Society. 2012;161(2):628-34.
158. Kim SH, Lutz RJ, Wang NS, Robinson MR. Transport barriers in transscleral drug delivery for retinal diseases. Ophthalmic research. 2007;39(5):244-54.
159. Vaka SR, Sammeta SM, Day LB, Murthy SN. Transcorneal iontophoresis for delivery of ciprofloxacin hydrochloride. Curr Eye Res. 2008;33(8):661-7.
160. Tirucherai GS, Dias C, Mitra AK. Corneal permeation of ganciclovir: mechanism of ganciclovir permeation enhancement by acyl ester prodrug design. Journal of ocular pharmacology and therapeutics : the official journal of the Association for Ocular Pharmacology and Therapeutics. 2002;18(6):535-48.
161. Gallarate M, Chirio D, Bussano R, Peira E, Battaglia L, Baratta F, et al. Development of O/W nanoemulsions for ophthalmic administration of timolol. Int J Pharm. 2012.
162. Tirucherai GS, Mitra AK. Effect of hydroxypropyl beta cyclodextrin complexation on aqueous solubility, stability, and corneal permeation of acyl ester prodrugs of ganciclovir. AAPS PharmSciTech. 2003;4(3):E45.
163. Vulovic N, Primorac M, Stupar M, Brown MW, Ford JL. Some studies on the preservation of indometacin suspensions intended for ophthalmic use. Pharmazie. 1990;45(9):678-9.
164. Meseguer G, Buri P, Plazonnet B, Rozier A, Gurny R. Gamma scintigraphic comparison of eyedrops containing pilocarpine in healthy volunteers. Journal of ocular pharmacology and therapeutics : the official journal of the Association for Ocular Pharmacology and Therapeutics. 1996;12(4):481-8.
165. Gebhardt BM, Varnell ED, Kaufman HE. Cyclosporine in collagen particles: corneal penetration and suppression of allograft rejection. Journal of ocular pharmacology and therapeutics : the official journal of the Association for Ocular Pharmacology and Therapeutics. 1995;11(4):509-17.
166. Saettone MF, Chetoni P, Cerbai R, Mazzanti G, Braghiroli L. Evaluation of ocular permeation enhancers: in vitro effects on corneal transport of four beta-blockers, and in vitro/in vivo toxic activity. International Journal of Pharmaceutics. 1996;142(1):103-13.
167. van der Bijl P, van Eyk AD, Meyer D. Effects of three penetration enhancers on transcorneal permeation of cyclosporine. Cornea. 2001;20(5):505-8.
168. Burgalassi S, Chetoni P, Monti D, Saettone MF. Cytotoxicity of potential ocular permeation enhancers evaluated on rabbit and human corneal epithelial cell lines. Toxicol Lett. 2001;122(1):1-8.
169. Keister JC, Cooper ER, Missel PJ, Lang JC, Hager DF. Limits on optimizing ocular drug delivery. J Pharm Sci. 1991;80(1):50-3.
170. Hornof MD, Bernkop-Schnurch A. In vitro evaluation of the permeation enhancing effect of polycarbophil-cysteine conjugates on the cornea of rabbits. J Pharm Sci. 2002;91(12):2588-92.
171. Kurz D, Ciulla TA. Novel approaches for retinal drug delivery. Ophthalmol Clin North Am. 2002;15(3):405-10.

172. Cholkar K, Patel SP, Vadlapudi AD, Mitra AK. Novel Strategies for Anterior Segment Ocular Drug Delivery. Journal of ocular pharmacology and therapeutics : the official journal of the Association for Ocular Pharmacology and Therapeutics. 2012.
173. Shen J, Gan L, Zhu C, Zhang X, Dong Y, Jiang M, et al. Novel NSAIDs ophthalmic formulation: flurbiprofen axetil emulsion with low irritancy and improved anti-inflammation effect. Int J Pharm.412(1-2):115-22.
174. Vandamme TF. Microemulsions as ocular drug delivery systems: recent developments and future challenges. Prog Retin Eye Res. 2002;21(1):15-34.
175. Liang H, Brignole-Baudouin F, Rabinovich-Guilatt L, Mao Z, Riancho L, Faure MO, et al. Reduction of quaternary ammonium-induced ocular surface toxicity by emulsions: an in vivo study in rabbits. Mol Vis. 2008;14:204-16.
176. Tajika T, Isowaki A, Sakaki H. Ocular distribution of difluprednate ophthalmic emulsion 0.05% in rabbits. Journal of ocular pharmacology and therapeutics : the official journal of the Association for Ocular Pharmacology and Therapeutics.27(1):43-9.
177. Liu Y, Lin X, Tang X. Lipid emulsions as a potential delivery system for ocular use of azithromycin. Drug Dev Ind Pharm. 2009;35(7):887-96.
178. Karasawa F, Ehata T, Okuda T, Satoh T. Propofol injection pain is not alleviated by pretreatment with flurbiprofen axetil, a prodrug of a nonsteroidal antiinflammatory drug. J Anesth. 2000;14(3):135-7.
179. Yamaguchi M, Ueda K, Isowaki A, Ohtori A, Takeuchi H, Ohguro N, et al. Mucoadhesive properties of chitosan-coated ophthalmic lipid emulsion containing indomethacin in tear fluid. Biol Pharm Bull. 2009;32(7):1266-71.
180. Scoper SV, Kabat AG, Owen GR, Stroman DW, Kabra BP, Faulkner R, et al. Ocular distribution, bactericidal activity and settling characteristics of TobraDex ST ophthalmic suspension compared with TobraDex ophthalmic suspension. Advances in therapy. 2008;25(2):77-88.
181. Kinoshita S, Awamura S, Oshiden K, Nakamichi N, Suzuki H, Yokoi N, et al. Rebamipide (OPC-12759) in the Treatment of Dry Eye: A Randomized, Double-Masked, Multicenter, Placebo-Controlled Phase II Study. Ophthalmology. 2012;119(12):2471-8.
182. Sasaki H, Yamamura K, Mukai T, Nishida K, Nakamura J, Nakashima M, et al. Enhancement of ocular drug penetration. Critical reviews in therapeutic drug carrier systems. 1999;16(1):85-146.
183. Fukuda M, Hanazome I, Sasaki K. The intraocular dynamics of vancomycin hydrochloride ophthalmic ointment (TN-011) in rabbits. Journal of infection and chemotherapy : official journal of the Japan Society of Chemotherapy. 2003;9(1):93-6.
184. Eguchi H, Shiota H, Oguro S, Kasama T. The inhibitory effect of vancomycin ointment on the manifestation of MRSA keratitis in rabbits. Journal of infection and chemotherapy : official journal of the Japan Society of Chemotherapy. 2009;15(5):279-83.

185. Pouliquen Y, Patey A, Foster CS, Goichot L, Savoldelli M. Drug-induced cicatricial pemphigoid affecting the conjunctiva. Light and electron microscopic features. Ophthalmology. 1986;93(6):775-83.
186. Ishibashi T, Yokoi N, Kinoshita S. Comparison of the short-term effects on the human corneal surface of topical timolol maleate with and without benzalkonium chloride. Journal of glaucoma. 2003;12(6):486-90.
187. Whitson JT, Ochsner KI, Moster MR, Sullivan EK, Andrew RM, Silver LH, et al. The safety and intraocular pressure-lowering efficacy of brimonidine tartrate 0.15% preserved with polyquaternium-1. Ophthalmology. 2006;113(8):1333-9.
188. Ayaki M, Yaguchi S, Iwasawa A, Koide R. Cytotoxicity of ophthalmic solutions with and without preservatives to human corneal endothelial cells, epithelial cells and conjunctival epithelial cells. Clinical & experimental ophthalmology. 2008;36(6):553-9.
189. Ayaki M, Iwasawa A, Yaguchi S, Koide R. Preserved and unpreserved 12 anti-allergic ophthalmic solutions and ocular surface toxicity: in vitro assessment in four cultured corneal and conjunctival epithelial cell lines. Biocontrol science. 2010;15(4):143-8.
190. Cholkar Kishore **PA,** Dutt Aswani, Mitra Ashim,. Novel Nanomicellar Formulation Approaches for Anterior and Posterior Segment Ocular Drug Delivery. Recent Patents on Nanomedicine. **2012**;2(2):82-95.
191. Civiale C, Licciardi M, Cavallaro G, Giammona G, Mazzone MG. Polyhydroxyethylaspartamide-based micelles for ocular drug delivery. Int J Pharm. 2009;378(1-2):177-86.
192. Liaw J, Chang SF, Hsiao FC. In vivo gene delivery into ocular tissues by eye drops of poly(ethylene oxide)-poly(propylene oxide)-poly(ethylene oxide) (PEO-PPO-PEO) polymeric micelles. Gene therapy. 2001;8(13):999-1004.
193. Tong YC, Chang SF, Liu CY, Kao WW, Huang CH, Liaw J. Eye drop delivery of nano-polymeric micelle formulated genes with cornea-specific promoters. The journal of gene medicine. 2007;9(11):956-66.
194. Ashim K. Mitra PRV, Subramanian Natesan, inventorOphthalmic Compositions. USA2013.
195. Ideta R, Yanagi Y, Tamaki Y, Tasaka F, Harada A, Kataoka K. Effective accumulation of polyion complex micelle to experimental choroidal neovascularization in rats. FEBS Lett. 2004;557(1-3):21-5.
196. Ideta R, Tasaka F, Jang WD, Nishiyama N, Zhang GD, Harada A, et al. Nanotechnology-based photodynamic therapy for neovascular disease using a supramolecular nanocarrier loaded with a dendritic photosensitizer. Nano letters. 2005;5(12):2426-31.
197. Bu HZ, Gukasyan HJ, Goulet L, Lou XJ, Xiang C, Koudriakova T. Ocular disposition, pharmacokinetics, efficacy and safety of nanoparticle-formulated ophthalmic drugs. Curr Drug Metab. 2007;8(2):91-107.
198. Bhatta RS, Chandasana H, Chhonker YS, Rathi C, Kumar D, Mitra K, et al. Mucoadhesive nanoparticles for prolonged ocular delivery of natamycin: In vitro and pharmacokinetics studies. Int J Pharm. 2012;432(1-2):105-12.

199. Musumeci T, Bucolo C, Carbone C, Pignatello R, Drago F, Puglisi G. Polymeric nanoparticles augment the ocular hypotensive effect of melatonin in rabbits. Int J Pharm. 2012.
200. Amrite AC, Kompella UB. Size-dependent disposition of nanoparticles and microparticles following subconjunctival administration. The Journal of pharmacy and pharmacology. 2005;57(12):1555-63.
201. Amrite AC, Edelhauser HF, Singh SR, Kompella UB. Effect of circulation on the disposition and ocular tissue distribution of 20 nm nanoparticles after periocular administration. Mol Vis. 2008;14:150-60.
202. Zhang L, Li Y, Zhang C, Wang Y, Song C. Pharmacokinetics and tolerance study of intravitreal injection of dexamethasone-loaded nanoparticles in rabbits. International journal of nanomedicine. 2009;4:175-83.
203. Bourges JL, Gautier SE, Delie F, Bejjani RA, Jeanny JC, Gurny R, et al. Ocular drug delivery targeting the retina and retinal pigment epithelium using polylactide nanoparticles. Invest Ophthalmol Vis Sci. 2003;44(8):3562-9.
204. Koo H, Moon H, Han H, Na JH, Huh MS, Park JH, et al. The movement of self-assembled amphiphilic polymeric nanoparticles in the vitreous and retina after intravitreal injection. Biomaterials. 2012;33(12):3485-93.
205. Kim H, Robinson SB, Csaky KG. Investigating the movement of intravitreal human serum albumin nanoparticles in the vitreous and retina. Pharm Res. 2009;26(2):329-37.
206. Parveen S, Mitra M, Krishnakumar S, Sahoo SK. Enhanced antiproliferative activity of carboplatin-loaded chitosan-alginate nanoparticles in a retinoblastoma cell line. Acta biomaterialia. 2010;6(8):3120-31.
207. Nagarwal RC, Kumar R, Pandit JK. Chitosan coated sodium alginate-chitosan nanoparticles loaded with 5-FU for ocular delivery: In vitro characterization and in vivo study in rabbit eye. Eur J Pharm Sci.47(4):678-85.
208. Gupta H, Aqil M, Khar RK, Ali A, Bhatnagar A, Mittal G. Sparfloxacin-loaded PLGA nanoparticles for sustained ocular drug delivery. Nanomedicine.6(2):324-33.
209. Singh KH, Shinde UA. Development and Evaluation of Novel Polymeric Nanoparticles of Brimonidine Tartrate. Curr Drug Deliv.
210. Gupta H, Aqil M, Khar RK, Ali A, Bhatnagar A, Mittal G. Biodegradable levofloxacin nanoparticles for sustained ocular drug delivery. J Drug Target.19(6):409-17.
211. Agnihotri SM, Vavia PR. Diclofenac-loaded biopolymeric nanosuspensions for ophthalmic application. Nanomedicine. 2009;5(1):90-5.
212. Nair KL, Vidyanand S, James J, Kumar GSV. Pilocarpine-loaded poly(DL-lactic-co-glycolic acid) nanoparticles as potential candidates for controlled drug delivery with enhanced ocular pharmacological response. Journal of Applied Polymer Science.124(3):2030-6.
213. Ibrahim HK, El-Leithy IS, Makky AA. Mucoadhesive nanoparticles as carrier systems for prolonged ocular delivery of gatifloxacin/prednisolone bitherapy. Mol Pharm.7(2):576-85.

214. Pignatello R, Ricupero N, Bucolo C, Maugeri F, Maltese A, Puglisi G. Preparation and characterization of eudragit retard nanosuspensions for the ocular delivery of cloricromene. AAPS PharmSciTech. 2006;7(1):E27.
215. Bhagav P, Upadhyay H, Chandran S. Brimonidine tartrate-eudragit long-acting nanoparticles: formulation, optimization, in vitro and in vivo evaluation. AAPS PharmSciTech.12(4):1087-101.
216. Patravale VB, Date AA, Kulkarni RM. Nanosuspensions: a promising drug delivery strategy. The Journal of pharmacy and pharmacology. 2004;56(7):827-40.
217. Kassem MA, Abdel Rahman AA, Ghorab MM, Ahmed MB, Khalil RM. Nanosuspension as an ophthalmic delivery system for certain glucocorticoid drugs. Int J Pharm. 2007;340(1-2):126-33.
218. Ali HS, York P, Ali AM, Blagden N. Hydrocortisone nanosuspensions for ophthalmic delivery: A comparative study between microfluidic nanoprecipitation and wet milling. Journal of controlled release : official journal of the Controlled Release Society. 2011;149(2):175-81.
219. Kaur IP, Garg A, Singla AK, Aggarwal D. Vesicular systems in ocular drug delivery: an overview. Int J Pharm. 2004;269(1):1-14.
220. Natarajan JV, Chattopadhyay S, Ang M, Darwitan A, Foo S, Zhen M, et al. Sustained release of an anti-glaucoma drug: demonstration of efficacy of a liposomal formulation in the rabbit eye. PloS one. 2011;6(9):e24513.
221. Law SL, Huang KJ, Chiang CH. Acyclovir-containing liposomes for potential ocular delivery. Corneal penetration and absorption. Journal of controlled release : official journal of the Controlled Release Society. 2000;63(1-2):135-40.
222. Zhang J, Wang S. Topical use of coenzyme Q10-loaded liposomes coated with trimethyl chitosan: tolerance, precorneal retention and anti-cataract effect. Int J Pharm. 2009;372(1-2):66-75.
223. Alghadyan AA, Peyman GA, Khoobehi B, Milner S, Liu KR. Liposome-bound cyclosporine: clearance after intravitreal injection. Int Ophthalmol. 1988;12(2):109-12.
224. Gupta SK, Velpandian T, Dhingra N, Jaiswal J. Intravitreal pharmacokinetics of plain and liposome-entrapped fluconazole in rabbit eyes. Journal of ocular pharmacology and therapeutics : the official journal of the Association for Ocular Pharmacology and Therapeutics. 2000;16(6):511-8.
225. Zhang R, He R, Qian J, Guo J, Xue K, Yuan YF. Treatment of experimental autoimmune uveoretinitis with intravitreal injection of tacrolimus (FK506) encapsulated in liposomes. Invest Ophthalmol Vis Sci. 2010;51(7):3575-82.
226. Bressler NM, Treatment of Age-Related Macular Degeneration with Photodynamic Therapy Study G. Photodynamic therapy of subfoveal choroidal neovascularization in age-related macular degeneration with verteporfin: two-year results of 2 randomized clinical trials-tap report 2. Archives of ophthalmology. 2001;119(2):198-207.
227. Dausch D, Lee S, Dausch S, Kim JC, Schwert G, Michelson W. [Comparative study of treatment of the dry eye syndrome due to disturbances of the tear film lipid layer with lipid-containing tear substitutes]. Klinische Monatsblatter fur Augenheilkunde. 2006;223(12):974-83.

228. Lee S, Dausch S, Maierhofer G, Dausch D. [A new therapy concept for the treatment of dry eye--the usefulness of phospholipid liposomes]. Klinische Monatsblatter fur Augenheilkunde. 2004;221(10):825-36.
229. Fischer M, Vögtle F. Dendrimers: From Design to Application—A Progress Report. Angewandte Chemie International Edition. 1999;38(7):884-905.
230. Abdelkader H, Alany RG. Controlled and continuous release ocular drug delivery systems: pros and cons. Curr Drug Deliv.9(4):421-30.
231. Spataro G, Malecaze F, Turrin CO, Soler V, Duhayon C, Elena PP, et al. Designing dendrimers for ocular drug delivery. Eur J Med Chem.45(1):326-34.
232. Vandamme TF, Brobeck L. Poly(amidoamine) dendrimers as ophthalmic vehicles for ocular delivery of pilocarpine nitrate and tropicamide. Journal of controlled release : official journal of the Controlled Release Society. 2005;102(1):23-38.
233. Hathout RM, Mansour S, Mortada ND, Guinedi AS. Liposomes as an ocular delivery system for acetazolamide: in vitro and in vivo studies. AAPS PharmSciTech. 2007;8(1):1.
234. Abdelbary G. Ocular ciprofloxacin hydrochloride mucoadhesive chitosan-coated liposomes. Pharm Dev Technol.16(1):44-56.
235. Zhang J, Guan P, Wang T, Chang D, Jiang T, Wang S. Freeze-dried liposomes as potential carriers for ocular administration of cytochrome c against selenite cataract formation. The Journal of pharmacy and pharmacology. 2009;61(9):1171-8.
236. Lajavardi L, Bochot A, Camelo S, Goldenberg B, Naud MC, Behar-Cohen F, et al. Downregulation of endotoxin-induced uveitis by intravitreal injection of vasoactive intestinal Peptide encapsulated in liposomes. Invest Ophthalmol Vis Sci. 2007;48(7):3230-8.
237. Sasaki H, Karasawa K, Hironaka K, Tahara K, Tozuka Y, Takeuchi H. Retinal drug delivery using eye drop preparations of poly-l-lysine-modified liposomes. Eur J Pharm Biopharm.
238. Abrishami M, Zarei-Ghanavati S, Soroush D, Rouhbakhsh M, Jaafari MR, Malaekeh-Nikouei B. Preparation, characterization, and in vivo evaluation of nanoliposomes-encapsulated bevacizumab (avastin) for intravitreal administration. Retina. 2009;29(5):699-703.
239. Inokuchi Y, Hironaka K, Fujisawa T, Tozuka Y, Tsuruma K, Shimazawa M, et al. Physicochemical properties affecting retinal drug/coumarin-6 delivery from nanocarrier systems via eyedrop administration. Invest Ophthalmol Vis Sci.51(6):3162-70.
240. Habib FS, Fouad EA, Abdel-Rhaman MS, Fathalla D. Liposomes as an ocular delivery system of fluconazole: in-vitro studies. Acta ophthalmologica.88(8):901-4.
241. Shimazaki H, Hironaka K, Fujisawa T, Tsuruma K, Tozuka Y, Shimazawa M, et al. Edaravone-loaded liposome eyedrops protect against light-induced retinal damage in mice. Invest Ophthalmol Vis Sci.52(10):7289-97.
242. Fujisawa T, Miyai H, Hironaka K, Tsukamoto T, Tahara K, Tozuka Y, et al. Liposomal diclofenac eye drop formulations targeting the retina: formulation

stability improvement using surface modification of liposomes. Int J Pharm.436(1-2):564-7.
243. Shaunak S, Thomas S, Gianasi E, Godwin A, Jones E, Teo I, et al. Polyvalent dendrimer glucosamine conjugates prevent scar tissue formation. Nat Biotechnol. 2004;22(8):977-84.
244. Rajoria* G, Gupta A. In-Situ Gelling System: A Novel Approach for Ocular Drug Delivery. AJPTR. 2012;2(4):24-53.
245. Bonacucina G, Cespi M, Mencarelli G, Giorgioni G, Palmieri GF. Thermosensitive Self-Assembling Block Copolymers as Drug Delivery Systems. Polymers. 2011;3(2):779-811.
246. Gourav Rajoria AG. In-Situ Gelling System: A Novel Approach for Ocular Drug Delivery. American Journal of PharmTech Research. 2012;2(4):24-53.
247. Gao Y, Sun Y, Ren F, Gao S. PLGA-PEG-PLGA hydrogel for ocular drug delivery of dexamethasone acetate. Drug Dev Ind Pharm. 2010;36(10):1131-8.
248. Rieke ER, Amaral J, Becerra SP, Lutz RJ. Sustained subconjunctival protein delivery using a thermosetting gel delivery system. Journal of ocular pharmacology and therapeutics : the official journal of the Association for Ocular Pharmacology and Therapeutics. 2010;26(1):55-64.
249. Kang Derwent JJ, Mieler WF. Thermoresponsive hydrogels as a new ocular drug delivery platform to the posterior segment of the eye. Trans Am Ophthalmol Soc. 2008;106:206-13; discussion 13-4.
250. Gupta H, Aqil M. Contact lenses in ocular therapeutics. Drug discovery today. 2012;17(9-10):522-7.
251. Kim J, Chauhan A. Dexamethasone transport and ocular delivery from poly(hydroxyethyl methacrylate) gels. Int J Pharm. 2008;353(1-2):205-22.
252. Gulsen D, Li CC, Chauhan A. Dispersion of DMPC liposomes in contact lenses for ophthalmic drug delivery. Curr Eye Res. 2005;30(12):1071-80.
253. Gulsen D, Chauhan A. Dispersion of microemulsion drops in HEMA hydrogel: a potential ophthalmic drug delivery vehicle. Int J Pharm. 2005;292(1-2):95-117.
254. White CJ, Byrne ME. Molecularly imprinted therapeutic contact lenses. Expert opinion on drug delivery. 2010;7(6):765-80.
255. Hiratani H, Fujiwara A, Tamiya Y, Mizutani Y, Alvarez-Lorenzo C. Ocular release of timolol from molecularly imprinted soft contact lenses. Biomaterials. 2005;26(11):1293-8.
256. Tieppo A, White CJ, Paine AC, Voyles ML, McBride MK, Byrne ME. Sustained in vivo release from imprinted therapeutic contact lenses. Journal of controlled release : official journal of the Controlled Release Society. 2012;157(3):391-7.
257. Bourges JL, Bloquel C, Thomas A, Froussart F, Bochot A, Azan F, et al. Intraocular implants for extended drug delivery: therapeutic applications. Adv Drug Deliv Rev. 2006;58(11):1182-202.
258. Del Amo EM, Urtti A. Current and future ophthalmic drug delivery systems. A shift to the posterior segment. Drug discovery today. 2008;13(3-4):135-43.

259. Lee SS, Hughes P, Ross AD, Robinson MR. Biodegradable implants for sustained drug release in the eye. Pharm Res.27(10):2043-53.
260. Choonara YE, Pillay V, Danckwerts MP, Carmichael TR, du Toit LC. A review of implantable intravitreal drug delivery technologies for the treatment of posterior segment eye diseases. J Pharm Sci.99(5):2219-39.
261. Mohammad DA, Sweet BV, Elner SG. Retisert: is the new advance in treatment of uveitis a good one? Ann Pharmacother. 2007;41(3):449-54.
262. Jaffe GJ, McCallum RM, Branchaud B, Skalak C, Butuner Z, Ashton P. Long-term follow-up results of a pilot trial of a fluocinolone acetonide implant to treat posterior uveitis. Ophthalmology. 2005;112(7):1192-8.
263. Donnelly RF, Raj Singh TR, Woolfson AD. Microneedle-based drug delivery systems: microfabrication, drug delivery, and safety. Drug Deliv. 2010;17(4):187-207.
264. Jiang J, Moore JS, Edelhauser HF, Prausnitz MR. Intrascleral drug delivery to the eye using hollow microneedles. Pharm Res. 2009;26(2):395-403.
265. Patel SR, Lin AS, Edelhauser HF, Prausnitz MR. Suprachoroidal drug delivery to the back of the eye using hollow microneedles. Pharm Res. 2011;28(1):166-76.
266. Matsuda S, Koyasu S. Mechanisms of action of cyclosporine. Immunopharmacology. 2000;47(2-3):119-25.
267. Whitcup SM, Chan CC, Luyo DA, Bo P, Li Q. Topical cyclosporine inhibits mast cell-mediated conjunctivitis. Invest Ophthalmol Vis Sci. 1996;37(13):2686-93.
268. Kunert KS, Tisdale AS, Gipson IK. Goblet cell numbers and epithelial proliferation in the conjunctiva of patients with dry eye syndrome treated with cyclosporine. Archives of ophthalmology. 2002;120(3):330-7.
269. Mondon K, Zeisser-Labouebe M, Gurny R, Moller M. Novel cyclosporin A formulations using MPEG-hexyl-substituted polylactide micelles: a suitability study. Eur J Pharm Biopharm. 2011;77(1):56-65.
270. Gunduz K, Ozdemir O. Topical cyclosporin treatment of keratoconjunctivitis sicca in secondary Sjogren's syndrome. Acta Ophthalmol (Copenh). 1994;72(4):438-42.
271. Laibovitz RA, Solch S, Andriano K, O'Connell M, Silverman MH. Pilot trial of cyclosporine 1% ophthalmic ointment in the treatment of keratoconjunctivitis sicca. Cornea. 1993;12(4):315-23.
272. Rao SN. Topical cyclosporine 0.05% for the prevention of dry eye disease progression. Journal of ocular pharmacology and therapeutics : the official journal of the Association for Ocular Pharmacology and Therapeutics. 2010;26(2):157-64.
273. Toshida H, Nguyen DH, Beuerman RW, Murakami A. Neurologic evaluation of acute lacrimomimetic effect of cyclosporine in an experimental rabbit dry eye model. Invest Ophthalmol Vis Sci. 2009;50(6):2736-41.
274. Donnenfeld E, Pflugfelder SC. Topical ophthalmic cyclosporine: pharmacology and clinical uses. Surv Ophthalmol. 2009;54(3):321-38.
275. Sheppard JD, Scoper SV, Samudre S. Topical loteprednol pretreatment reduces cyclosporine stinging in chronic dry eye disease. Journal of ocular

pharmacology and therapeutics : the official journal of the Association for Ocular Pharmacology and Therapeutics. 2011;27(1):23-7.
276. Liang H, Baudouin C, Daull P, Garrigue JS, Brignole-Baudouin F. Ocular safety of cationic emulsion of cyclosporine in an in vitro corneal wound-healing model and an acute in vivo rabbit model. Mol Vis. 2012;18:2195-204.
277. Samik kumar Hait SPM. Determination of critical micellar concentration of non-ionic surfactants by donor-acceptor interaction with iodine and correlation of CMC with hydrophile-lipophile balance and other parameters of the surfactants. Journal of surfactants and detergents. 2001;4(3):303-9.
278. Cholkar K, Hariharan S, Gunda S, Mitra AK. Optimization of Dexamethasone Mixed Nanomicellar Formulation. AAPS PharmSciTech. 2014.
279. Saxena V, Hussain MD. Poloxamer 407/TPGS mixed micelles for delivery of gambogic acid to breast and multidrug-resistant cancer. International journal of nanomedicine. 2012;7:713-21.
280. Wei Z, Hao J, Yuan S, Li Y, Juan W, Sha X, et al. Paclitaxel-loaded Pluronic P123/F127 mixed polymeric micelles: formulation, optimization and in vitro characterization. Int J Pharm. 2009;376(1-2):176-85.
281. Samik kumar, Moulik SP. Determination of critical micellar concentration of non-ionic surfactants by donor-acceptor interaction with iodine and correlation of CMC with hydrophile-lipophile balance and other parameters of the surfactants. 2001;4(3):303-9.
282. Hariharan S, Minocha M, Mishra GP, Pal D, Krishna R, Mitra AK. Interaction of ocular hypotensive agents (PGF2 alpha analogs-bimatoprost, latanoprost, and travoprost) with MDR efflux pumps on the rabbit cornea. Journal of ocular pharmacology and therapeutics : the official journal of the Association for Ocular Pharmacology and Therapeutics. 2009;25(6):487-98.
283. Khurana V, Vadlapudi AD, Vadlapatla RK, Pal D, Mitra AK. Functional Characterization and Molecular Identification of Vitamin C Transporter (SVCT2) in Human Corneal Epithelial (HCEC) and Retinal Pigment Epithelial (D407) Cells. Curr Eye Res. 2014:1-13.
284. Lee SC, Huh KM, Lee J, Cho YW, Galinsky RE, Park K. Hydrotropic polymeric micelles for enhanced paclitaxel solubility: in vitro and in vivo characterization. Biomacromolecules. 2007;8(1):202-8.
285. Zhu H, Chauhan A. Effect of viscosity on tear drainage and ocular residence time. Optometry and vision science : official publication of the American Academy of Optometry. 2008;85(8):715-25.
286. Cholkar KP, Ashaben; Dutt Vadlapudi, Aswani; Ashim K. Mitra, . Novel Nanomicellar Formulation Approaches for Anterior and Posterior Segment Ocular Drug Delivery. Recent Patents on Nanomedicine, Volume 2, Number 2, October 2012 , pp 2012;2(2):82-95.
287. Moulik SKHSP. Determination of critical micellar concentration of non-ionic surfactants by donor-acceptor interaction with iodine and correlation of CMC with hydrophile-lipophile balance and other parameters of the surfactants. Journal of Surfactants and Detergents. 2001;4(3):303-9

288. Renliang Xu MAW, F. R. Hallett , Gerard Riess , Melvin D. Croucher. Light-scattering study of the association behavior of styrene-ethylene oxide block copolymers in aqueous solution. Macromolecules. 1991 24(1):87–93.
289. Jones CF, Grainger DW. In vitro assessments of nanomaterial toxicity. Adv Drug Deliv Rev. 2009;61(6):438-56.
290. Lai JY, Li YT, Wang TP. In vitro response of retinal pigment epithelial cells exposed to chitosan materials prepared with different cross-linkers. International journal of molecular sciences. 2010;11(12):5256-72.
291. Lang JC. Ocular drug delivery conventional ocular formulations. Advanced drug delivery reviews. 1995;16(1):39-43.
292. Järvinen K JT, Urtti A. Ocular absorption following topical delivery. Adv Drug Deliv Rev. 1995;16 3–19.
293. Acheampong AA, Shackleton M, Tang-Liu DD, Ding S, Stern ME, Decker R. Distribution of cyclosporin A in ocular tissues after topical administration to albino rabbits and beagle dogs. Curr Eye Res. 1999;18(2):91-103.
294. Di Tommaso C, Valamanesh F, Miller F, Furrer P, Rodriguez-Aller M, Behar-Cohen F, et al. A novel cyclosporin a aqueous formulation for dry eye treatment: in vitro and in vivo evaluation. Invest Ophthalmol Vis Sci. 2012;53(4):2292-9.
295. Maurice DM. Drug delivery to the posterior segment from drops. Surv Ophthalmol. 2002;47 Suppl 1:S41-52.
296. Loftsson T, Sigurdsson HH, Konradsdottir F, Gisladottir S, Jansook P, Stefansson E. Topical drug delivery to the posterior segment of the eye: anatomical and physiological considerations. Pharmazie. 2008;63(3):171-9.
297. Serhan CN, Hong S, Gronert K, Colgan SP, Devchand PR, Mirick G, et al. Resolvins: a family of bioactive products of omega-3 fatty acid transformation circuits initiated by aspirin treatment that counter proinflammation signals. J Exp Med. 2002;196(8):1025-37.
298. Arita M, Clish CB, Serhan CN. The contributions of aspirin and microbial oxygenase to the biosynthesis of anti-inflammatory resolvins: novel oxygenase products from omega-3 polyunsaturated fatty acids. Biochemical and biophysical research communications. 2005;338(1):149-57.
299. Serhan CN. Resolution phase of inflammation: novel endogenous anti-inflammatory and proresolving lipid mediators and pathways. Annual review of immunology. 2007;25:101-37.
300. Li N, He J, Schwartz CE, Gjorstrup P, Bazan HE. Resolvin E1 improves tear production and decreases inflammation in a dry eye mouse model. Journal of ocular pharmacology and therapeutics : the official journal of the Association for Ocular Pharmacology and Therapeutics. 2010;26(5):431-9.
301. Tian H, Lu Y, Sherwood AM, Hongqian D, Hong S. Resolvins E1 and D1 in choroid-retinal endothelial cells and leukocytes: biosynthesis and mechanisms of anti-inflammatory actions. Invest Ophthalmol Vis Sci. 2009;50(8):3613-20.
302. Settimio R, Clara DF, Franca F, Francesca S, Michele D. Resolvin D1 reduces the immunoinflammatory response of the rat eye following uveitis. Mediators of inflammation. 2012;2012:318621.

303. Resolvyx Announces Positive Data from Phase 2 Clinical Trial of the Resolvin RX-10045 in Patients with Dry Eye Syndrome 2013. Available from: http://www.resolvyx.com/news-pubs/releases/082409.asp.
304. Resolvins Inhibit Hypertonicity-Induced Proinflammatory Cytokine Release by Suppressing Mapk Pathway Activation in Human Corneal Epithelial Cells. Treating Dry Eye Disease; 1/6/20142008.
305. Hariharan S, Gunda S, Mishra GP, Pal D, Mitra AK. Enhanced corneal absorption of erythromycin by modulating P-glycoprotein and MRP mediated efflux with corticosteroids. Pharm Res. 2009;26(5):1270-82.
306. Cheng Y, Prusoff WH. Relationship between the inhibition constant (K1) and the concentration of inhibitor which causes 50 per cent inhibition (I50) of an enzymatic reaction. Biochemical pharmacology. 1973;22(23):3099-108.
307. Kwatra D, Vadlapatla RK, Vadlapudi AD, Pal D, Mitra AK. Interaction of gatifloxacin with efflux transporters: a possible mechanism for drug resistance. Int J Pharm. 2010;395(1-2):114-21.
308. Vellonen KS, Mannermaa E, Turner H, Hakli M, Wolosin JM, Tervo T, et al. Effluxing ABC transporters in human corneal epithelium. J Pharm Sci. 2010;99(2):1087-98.
309. Dey S, Patel J, Anand BS, Jain-Vakkalagadda B, Kaliki P, Pal D, et al. Molecular evidence and functional expression of P-glycoprotein (MDR1) in human and rabbit cornea and corneal epithelial cell lines. Invest Ophthalmol Vis Sci. 2003;44(7):2909-18.
310. Dey S, Gunda S, Mitra AK. Pharmacokinetics of erythromycin in rabbit corneas after single-dose infusion: role of P-glycoprotein as a barrier to in vivo ocular drug absorption. The Journal of pharmacology and experimental therapeutics. 2004;311(1):246-55.
311. Karla PK, Pal D, Quinn T, Mitra AK. Molecular evidence and functional expression of a novel drug efflux pump (ABCC2) in human corneal epithelium and rabbit cornea and its role in ocular drug efflux. Int J Pharm. 2007;336(1):12-21.
312. Karla PK, Earla R, Boddu SH, Johnston TP, Pal D, Mitra A. Molecular expression and functional evidence of a drug efflux pump (BCRP) in human corneal epithelial cells. Curr Eye Res. 2009;34(1):1-9.
313. Sikri V, Pal D, Jain R, Kalyani D, Mitra AK. Cotransport of macrolide and fluoroquinolones, a beneficial interaction reversing P-glycoprotein efflux. American journal of therapeutics. 2004;11(6):433-42.
314. Zhang S, Morris ME. Effect of the flavonoids biochanin A and silymarin on the P-glycoprotein-mediated transport of digoxin and vinblastine in human intestinal Caco-2 cells. Pharm Res. 2003;20(8):1184-91.
315. Agarwal S, Pal D, Mitra AK. Both P-gp and MRP2 mediate transport of Lopinavir, a protease inhibitor. Int J Pharm. 2007;339(1-2):139-47.
316. Polli JW, Wring SA, Humphreys JE, Huang L, Morgan JB, Webster LO, et al. Rational use of in vitro P-glycoprotein assays in drug discovery. The Journal of pharmacology and experimental therapeutics. 2001;299(2):620-8.

317. Tang F, Horie K, Borchardt RT. Are MDCK cells transfected with the human MRP2 gene a good model of the human intestinal mucosa? Pharm Res. 2002;19(6):773-9.
318. Minuesa G, Volk C, Molina-Arcas M, Gorboulev V, Erkizia I, Arndt P, et al. Transport of lamivudine [(-)-beta-L-2',3'-dideoxy-3'-thiacytidine] and high-affinity interaction of nucleoside reverse transcriptase inhibitors with human organic cation transporters 1, 2, and 3. The Journal of pharmacology and experimental therapeutics. 2009;329(1):252-61.
319. Xiang CD, Batugo M, Gale DC, Zhang T, Ye J, Li C, et al. Characterization of human corneal epithelial cell model as a surrogate for corneal permeability assessment: metabolism and transport. Drug metabolism and disposition: the biological fate of chemicals. 2009;37(5):992-8.
320. Cholkar K, Gunda S, Earla R, Pal D, Mitra AK. Nanomicellar Topical Aqueous Drop Formulation of Rapamycin for Back-of-the-Eye Delivery. AAPS PharmSciTech. 2014.
321. Kim DH, Martin DC. Sustained release of dexamethasone from hydrophilic matrices using PLGA nanoparticles for neural drug delivery. Biomaterials. 2006;27(15):3031-7.
322. Loftsson T, Stefansson E. Cyclodextrins in eye drop formulations: enhanced topical delivery of corticosteroids to the eye. Acta ophthalmologica Scandinavica. 2002;80(2):144-50.
323. Chang DT, Herceg MC, Bilonick RA, Camejo L, Schuman JS, Noecker RJ. Intracameral dexamethasone reduces inflammation on the first postoperative day after cataract surgery in eyes with and without glaucoma. Clinical ophthalmology. 2009;3:345-55.
324. Capone A, Jr., Singer MA, Dodwell DG, Dreyer RF, Oh KT, Roth DB, et al. Efficacy and safety of two or more dexamethasone intravitreal implant injections for treatment of macular edema related to retinal vein occlusion (Shasta study). Retina. 2014;34(2):342-51.
325. Sivaprasad S, McCluskey P, Lightman S. Intravitreal steroids in the management of macular oedema. Acta ophthalmologica Scandinavica. 2006;84(6):722-33.
326. Loftsson T, Hreinsdottir D. Determination of aqueous solubility by heating and equilibration: a technical note. AAPS PharmSciTech. 2006;7(1):E4.
327. Regina A, Romero IA, Greenwood J, Adamson P, Bourre JM, Couraud PO, et al. Dexamethasone regulation of P-glycoprotein activity in an immortalized rat brain endothelial cell line, GPNT. Journal of neurochemistry. 1999;73(5):1954-63.
328. Chen P, Chen H, Zang X, Chen M, Jiang H, Han S, et al. Expression of efflux transporters in human ocular tissues. Drug metabolism and disposition: the biological fate of chemicals. 2013;41(11):1934-48.
329. Sheu MT, Chen SY, Chen LC, Ho HO. Influence of micelle solubilization by tocopheryl polyethylene glycol succinate (TPGS) on solubility enhancement and percutaneous penetration of estradiol. Journal of controlled release : official journal of the Controlled Release Society. 2003;88(3):355-68.

330. Duong AD, Ruan G, Mahajan K, Winter JO, Wyslouzil BE. Scalable, semicontinuous production of micelles encapsulating nanoparticles via electrospray. Langmuir : the ACS journal of surfaces and colloids. 2014;30(14):3939-48.
331. Acharya G, Lee CH, Lee Y. Optimization of cardiovascular stent against restenosis: factorial design-based statistical analysis of polymer coating conditions. PloS one. 2012;7(8):e43100.
332. Kishore Cholkar AP, Aswani Dutt Vadlapudi, Ashim K Mitra Novel Nanomicellar Formulation Approaches for Anterior and Posterior Segment Ocular Drug Delivery. Recent patents on Nanomedicine. 2012;2(2): 82-95.
333. Mitra AK. Ophthalmic Drug Delivery Systems. Mitra AK, editor. New York,: Marcel Dekker; 2008.
334. Gao Y, Li LB, Zhai G. Preparation and characterization of Pluronic/TPGS mixed micelles for solubilization of camptothecin. Colloids and surfaces B, Biointerfaces. 2008;64(2):194-9.
335. JC L. Ocular drug delivery conventional ocular formulations. Adv Drug Deliv Rev. 1995;16:39- 43.
336. Järvinen K JT, Urtti A. . Ocular absorption following topical delivery. Adv Drug Deliv Rev. 1995(16):3-19.
337. Buech G, Bertelmann E, Pleyer U, Siebenbrodt I, Borchert HH. Formulation of sirolimus eye drops and corneal permeation studies. Journal of ocular pharmacology and therapeutics : the official journal of the Association for Ocular Pharmacology and Therapeutics. 2007;23(3):292-303.
338. Trepanier DJ, Gallant H, Legatt DF, Yatscoff RW. Rapamycin: distribution, pharmacokinetics and therapeutic range investigations: an update. Clinical biochemistry. 1998;31(5):345-51.
339. Yatscoff RW, Wang P, Chan K, Hicks D, Zimmerman J. Rapamycin: distribution, pharmacokinetics, and therapeutic range investigations. Therapeutic drug monitoring. 1995;17(6):666-71.
340. Zhaoliang Zhang LX, Hao Chen, Xingyi Li. Rapamycin-loaded poly(ε-caprolactone)-poly(ethylene glycol)-poly(ε-caprolactone) nanoparticles: preparation, characterization and potential application in corneal transplantation. Journal of Pharmacy and Pharmacology. In press.
341. Forrest ML, Won CY, Malick AW, Kwon GS. In vitro release of the mTOR inhibitor rapamycin from poly(ethylene glycol)-b-poly(epsilon-caprolactone) micelles. Journal of controlled release : official journal of the Controlled Release Society. 2006;110(2):370-7.
342. Mu L, Feng SS. Vitamin E TPGS used as emulsifier in the solvent evaporation/extraction technique for fabrication of polymeric nanospheres for controlled release of paclitaxel (Taxol). Journal of controlled release : official journal of the Controlled Release Society. 2002;80(1-3):129-44.
343. Eva-Maria Collnot, Christiane Baldes, Michael F. Wempe , John Hyatt , Lisa Navarro, Kevin J. Edgar, et al. Influence of vitamin E TPGS poly(ethylene glycol) chain length on apical efflux transporters in Caco-2 cell monolayers. Journal of Controlled Release. 2006;111(1-2):35-40.

344. Collnot EM, Baldes C, Wempe MF, Kappl R, Huttermann J, Hyatt JA, et al. Mechanism of inhibition of P-glycoprotein mediated efflux by vitamin E TPGS: influence on ATPase activity and membrane fluidity. Mol Pharm. 2007;4(3):465-74.
345. Khandavilli S, Panchagnula R. Nanoemulsions as versatile formulations for paclitaxel delivery: peroral and dermal delivery studies in rats. The Journal of investigative dermatology. 2007;127(1):154-62.
346. Vadlapudi AD, Cholkar K, Vadlapatla RK, Mitra AK. Aqueous Nanomicellar Formulation for Topical Delivery of Biotinylated Lipid Prodrug of Acyclovir: Formulation Development and Ocular Biocompatibility. Journal of ocular pharmacology and therapeutics : the official journal of the Association for Ocular Pharmacology and Therapeutics. 2013.
347. Earla R, Boddu SH, Cholkar K, Hariharan S, Jwala J, Mitra AK. Development and validation of a fast and sensitive bioanalytical method for the quantitative determination of glucocorticoids--quantitative measurement of dexamethasone in rabbit ocular matrices by liquid chromatography tandem mass spectrometry. Journal of pharmaceutical and biomedical analysis. 2010;52(4):525-33.
348. Earla R, Cholkar K, Gunda S, Earla RL, Mitra AK. Bioanalytical method validation of rapamycin in ocular matrix by QTRAP LC-MS/MS: application to rabbit anterior tissue distribution by topical administration of rapamycin nanomicellar formulation. Journal of chromatography B, Analytical technologies in the biomedical and life sciences. 2012;908:76-86.
349. Napoli KL. More on methanol-associated matrix effects in electrospray ionization mass spectrometry. Clinical chemistry. 2009;55(6):1250-2.
350. Streit F, Christians U, Schiebel HM, Napoli KL, Ernst L, Linck A, et al. Sensitive and specific quantification of sirolimus (rapamycin) and its metabolites in blood of kidney graft recipients by HPLC/electrospray-mass spectrometry. Clinical chemistry. 1996;42(9):1417-25.
351. Hallensleben K, Raida M, Habermehl G. Identification of a new metabolite of macrolide immunosuppressant, like rapamycin and SDZ RAD, using high performance liquid chromatography and electrospray tandem mass spectrometry. Journal of the American Society for Mass Spectrometry. 2000;11(6):516-25.
352. Jiang H, Cao H, Zhang Y, Fast DM. Systematic evaluation of supported liquid extraction in reducing matrix effect and improving extraction efficiency in LC-MS/MS based bioanalysis for 10 model pharmaceutical compounds. Journal of chromatography B, Analytical technologies in the biomedical and life sciences. 2012;891-892:71-80.
353. Clavijo C, Strom T, Moll V, Betts R, Zhang YL, Christians U, et al. Development and validation of a semi-automated assay for the highly sensitive quantification of Biolimus A9 in human whole blood using high-performance liquid chromatography-tandem mass spectrometry. Journal of chromatography B, Analytical technologies in the biomedical and life sciences. 2009;877(29):3506-14.
354. Bogusz MJ, Enazi EA, Hassan H, Abdel-Jawaad J, Ruwaily JA, Tufail MA. Simultaneous LC-MS-MS determination of cyclosporine A, tacrolimus, and

sirolimus in whole blood as well as mycophenolic acid in plasma using common pretreatment procedure. Journal of chromatography B, Analytical technologies in the biomedical and life sciences. 2007;850(1-2):471-80.
355. Kristiina Järvinena TJ, Arto Urtti. Ocular absorption following topical delivery. Adv Drug Deliv Rev. 1995;16(1):3-19.
356. Patrick M. Hughes OO, Joan-En Chang Lin, Clive G. Wilson. Topical and systemic drug delivery to the posterior segments. Adv Drug Deliv Rev. 2005;57(14):2010-32.
357. Aydemir O, Celebi S, Yilmaz T, Yekeler H, Kukner AS. Protective effects of vitamin E forms (alpha-tocopherol, gamma-tocopherol and d-alpha-tocopherol polyethylene glycol 1000 succinate) on retinal edema during ischemia-reperfusion injury in the guinea pig retina. Int Ophthalmol. 2004;25(5-6):283-9.
358. Dugel PU. Sirolimus in treatment of retinal diseases. Retina today. 2009(October):38-41.
359. Collnot EM, Baldes C, Schaefer UF, Edgar KJ, Wempe MF, Lehr CM. Vitamin E TPGS P-glycoprotein inhibition mechanism: influence on conformational flexibility, intracellular ATP levels, and role of time and site of access. Mol Pharm. 2010;7(3):642-51.

VITA

Kishore Cholkar was born on March 13, 1981, in Hyderabad, Telangana, India. He completed his B.Pharm in Pharmaceutical Sciences from Kakatiya University, Warangal, India and M.S in Chemistry (Chemical synthesis and kinetics) from Western Illinois University, USA. After completion of B.Pharm, he worked as an Assistant Quality Controller in Novasyn Organic Pvt. Ltd., Hyderabad, India. Mr. Cholkar joined the Interdisciplinary PhD program at UMKC in fall 2008. He served as a teaching assistant for Dr. Ashim K Mitra (Novel Drug Delivery Systems) and Dr. Johnston (Pharmacokinetics). He was nominated from the School of Pharmacy for the UMKC Chancellor's award in the year 2012 – 2013. He was awarded several travel awards to present his work at Association of Pharmaceutical Scientists (AAPS), Association of Research in Vision and Ophthalmology (ARVO) and Pharmaceutical Sciences Graduate Student Association (PSGSA) meetings from 2012 – 2015 by the School of Graduate Studies (SGS) and Interdisciplinary Doctoral Student Council (IDSC). Mr. Cholkar is a active member of AAPS, ARVO, PSGSA and Ophthalmology Group (OMICS). He received the First Best Poster Award from Ophthalmology Group in 2014 at Ophthalmology-2014 Conference, Baltimore, USA. He completed his doctoral studies in April 2015 under the guidance of Dr. Ashim K Mitra. He has authored/co-authored 22 peer reviewed publications. Moreover, he authored/co-authored six book chapters and presented his work (46 poster and one podia presentations) at several regional, national and international conferences.